MAY 1 0 [illegible]

D210.17/2: 986

Naval Research Laboratory

Washington, DC 20375-5000 NRL Publication 0104-2630 October 1987

1986 Review

COMPLETED

oa/RD

BEST COPY AVAILABLE

Cover:

NRL, a leader in the field of ultraviolet remote sensing, has demonstrated over recent years a technique to sense remotely the composition of the ionosphere and the upper atmosphere on a global scale. This technique uses passive observation from space of naturally occurring ultraviolet emission lines of ions, atoms, and molecules above 100 km. The ultraviolet wavelength bands include 30 to 400 nm (0.03 to 0.4 μ).

This artist concept illustrates a future Atmospheric and Ionospheric Remote Sensing (AIRS) system operating on a global scale. Images in spectrally pure light of selected ionospheric emissions will be processed and modeled to obtain global pictures of ionospheric conditions. Information on the electron density, ionospheric composition, morphology, and dynamics will be available from such data. Monitoring of "ionospheric weather" will lead to substantial improvement in Navy systems which rely on the propagation of electromagnetic radiation. A proof of concept program for AIRS, presently under development at NRL, is the Remote Atmospheric and Ionospheric Detection System (RAIDS) scheduled for 1990. (Dr. R. Meier, 4140)

REVIEWED AND APPROVED
September 1987

Commanding Officer

Approved for public release; distribution unlimited.

NAVAL RESEARCH LABORATORY

1986 Review

NRL presents in this Review *highlights of the unclassified research and development programs for calendar year 1986. This book fulfills a dual purpose: it provides an exchange of information among scientists, engineers, scholars, and managers; and it is used in recruiting science and engineering professionals. As you read this* Review, *you will become even more aware that the Laboratory is a dynamic team working together to promote the programs, progress, and innovations that will continue to foster discoveries, inventiveness, and scientific advances for the Navy of the future.*

BLANK PAGE

PREFACE

The most precious resource that NRL has to accomplish its research is its people whose diligence and devotion to science and engineering over the past 64 years have made NRL a respected laboratory possessing an enviable reputation. NRL is people engaged in creative enterprise. The Laboratory's success begins with a single scientist or a small group of researchers with ideas and goals fostered by the diverse scientific interactions that occur among our divisions. These ideas flourish with the backing of a well-managed scientific and support organization whose personnel put a premium on excellence and create a climate for inventiveness.

The NRL Review highlights this inventiveness. Published in its present form since 1967, the Reviews annually report NRL's unclassified research. Although not comprehensive in scope, the selected works described here demonstrate the broad base of research conducted at NRL.

As you read this *Review*, you will become even more aware that the laboratory is a dynamic family working together to promote the programs, progress, and innovations that will continue to foster discoveries, inventiveness, and scientific advances for the Navy of the future.

BLANK PAGE

√

CONTENTS

PREFACE iii

CAPT William C. Miller, Commanding Officer and
Dr. Timothy Coffey, Director of Research

MISSION v

THE NAVAL RESEARCH LABORATORY 3

NRL — Our heritage, NRL Today, NRL in the Future 3

Highlights of NRL Research in 1986 29

SCIENTIFIC ARTICLES 32

Inner and Outer Space 34

- Far Ultraviolet Imagery of Comet Halley from Sounding Rockets 35
- XLA—The X-ray Large Array for the Space Station 38
- Detection of Anti-Matter in the Galaxy 41
- The Coronae of Giant Stars 43
- Holograms Made with Laser Diodes for Use in a Satellite Communications Link 45

Sound and the Sea 50

- Active/Adaptive Noise Cancellation in a Liquid-Filled Pipe 51
- Steep and Breaking Deep Water Waves 53
- Rapid Three-Dimensional Ocean Acoustic Computations 56
- Inertial Wave Dynamics 58
- Nonlinear Salt-Finger Simulation 62
- Ship-Wake Experiment for Remote Sensing 64

Chemical Research 70

- Quantum Calculations of Chemical Chemical Reaction Pathways: The Methoxy Radical 71
- IR-Diode Laser Spectroscopy in the Study of the Vapor Phase Epitaxy Process 73
- Liposome-Encapsulated Hemoglobin: A Potential Blood Surrogate 74
- Two-Dimensional NMR Images in Solids 76
- Laser Studies of Flame Chemistry 78
- Advanced Fluorinated Polymers Meeting Navy Needs 79

Behavior and Properties of Materials 84

Constrained-Layer Damping of Structure-Borne Sound 85
Computer-Controlled Emissivity Measurement System 87
Measurement of Undercooling Effects in Gas-Atomized Metal Powders 89
Surface Modification for Improved Corrosion Resistance 92
Processing of High Critical Temperature Ceramic Superconductors 95
Computer Modelling of Anisotropic Elasticity and Piezoelectric Effects in Ceramics 97
Mechanisms of Interdiffusion in Coated Superalloys 102
Atomic Resolution Images 104

Electromagnetic Systems and Sensing 110

Radar Target Detection in Non-Gaussian, Correlated Clutter 111
Speckle in Space-Based Radar Images 112
Open Ocean Shipboard Radar Sea Clutter Experiments 114
Mark XV IFF Radar Mode 117

Electronics Research 122

Designing Systems with VHSIC Components 123
Surface Chemistry in Semiconductor Processing Using Laser Ionization 126
Ga Interstitials in AlGaAs Epitaxial Layers 128
Phase-Controlled Gyrotron Oscillators 130
β-SiC Transistor Development 133
Kinetic Inductance Microstrip Lines 136

Energetic Particles and Beams 140

Soft X-ray Laser Generation 141
Modulated Intense Relativistic Electron Beams 143
Charged-Particle Beam Propagation 145
Advanced Concepts in Radiation Sources and Particle Acceleration 147

Optical Systems 152

Optical Studies of Aerosols 153
Photoemitter Membrane Light Modulator Device for Optical Processing 155
Parametric Raman Gain Suppression 158
Fiber-Optic Magnetic Sensors 162
Development of Infrared Focal Plane Arrays for Advanced Navy Sensors 165

Numerical Simulation 170

Renormalized Inverse-Scattering Theory for Dielectric Profiles 171
Direct Numerical Simulation of Turbulent Channel Flow 173
Synthetic Line-of-Sight Simulations 175
Vortex Motions in Stratified Wakes 177
Analytic Representations of Viscoelastic Moduli 179

Information Technology 184

Integrated Battle Group Communications Networks 185
Single-Board Digital Signal Processor for Voice and Data Applications 188
SDI Mid-Course Battle Management 190

EXCELLENCE IN RESEARCH FOR TOMORROW'S NAVY 196

Special Awards and Recognition 197
Individual Honors 205
Alan Berman Research Publication Awards 215

PROGRAMS FOR PROFESSIONAL DEVELOPMENT 222

Programs for NRL People—University education and scholarships, continuing education, professional development, and other activities 223

Programs for Non-NRL People— Fellowships, exchange programs, and cooperative employment 232

PAPERS, REPORTS, AND PATENTS 238

Papers in Journals, Books, and Proceedings of Meetings 239
Formal Reports 278
Patents Granted 279

GENERAL INFORMATION 284

Organizational Charts, Key Personnel,
NRL Review Staff, Employment Opportunities,
Contributions by Divisions and Laboratories, Index, and Map 284

Established more than sixty years ago at the suggestion of Thomas A. Edison, the Naval Research Laboratory has exhibited through the years a firmly rooted tradition of contributions to science and technology. The scientists and engineers at the Laboratory are committed to the future in the interest of their country and mankind with ongoing research in physics, chemistry, electronics and mechanical engineering, computer sciences/mathematics, and materials sciences/engineering.

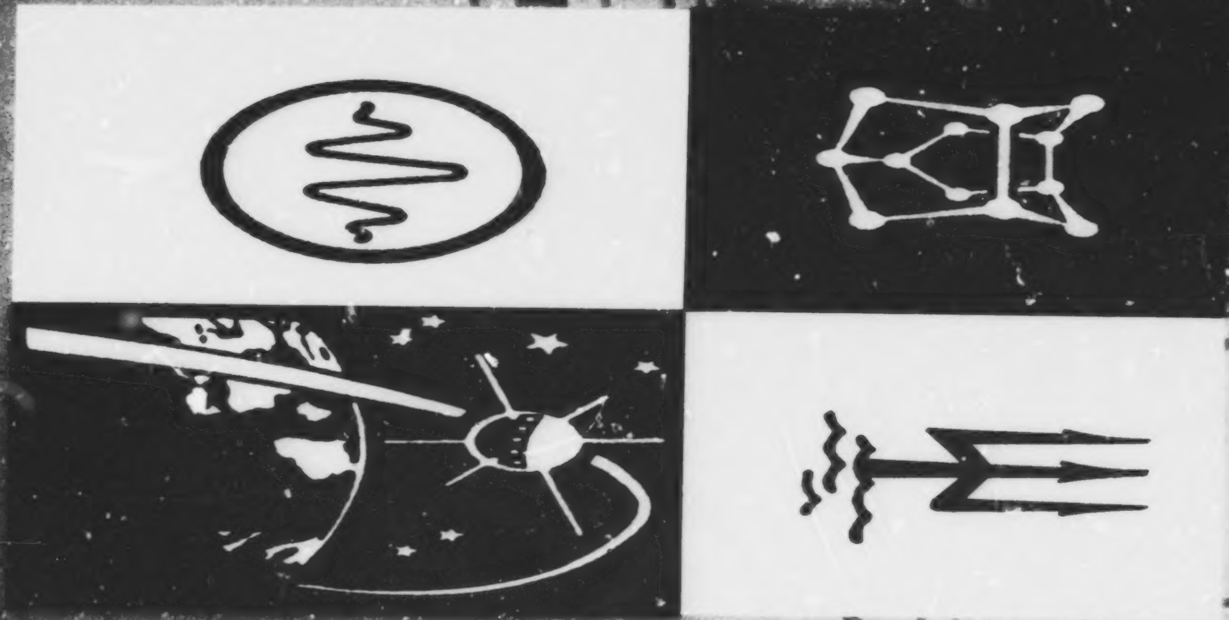

NAVAL RESEARCH LABORATORY

THE
NAVAL
RESEARCH
LABORATORY

3 NRL — Our Heritage, NRL Today, NRL in the Future

29 Highlights of NRL Research in 1986

THE NAVAL RESEARCH LABORATORY

Our Heritage

Today, when government and science seem inextricably linked, when virtually no one questions the dependence of national defense on the excellence of national technical capabilities, it is noteworthy that in-house defense research is relatively new in our Nation's history. The Naval Research Laboratory (NRL), the first modern research institution created within the United States Navy, began operations in 1923, just 64 years ago.

Thomas Edison's Vision: The first step came in May 1915, a time when Americans were deeply worried about the great European war. Thomas Edison, asked by a *New York Times* correspondent to comment on the conflict, argued that the Nation should look to science. "The Government," he proposed in a published interview, "should maintain a great research laboratory.... In this could be developed... all the technique of military and naval progression without any vast expense." Secretary of the Navy Josephus Daniels seized the opportunity created by Edison's public comments to enlist Edison's support. He agreed to serve as the head of a new body of civilian experts–the Naval Consulting Board–to advise the Navy on science and technology. The Board's most ambitious plan was the creation of a modern research facility for the Navy. Congress allocated $1.5 million for the institution in 1916, but wartime delays and disagreements within the Naval Consulting Board postponed construction until 1920.

The Laboratory's two original divisions, Radio and Sound, pioneered in the fields of high-frequency radio and underwater sound propagation. They produced communications equipment, direction-finding devices, sonar sets, and, perhaps most significant of all, the first practical radar equipment built in this country. They also performed basic research, participating, for example, in the discovery and early exploration of the ionosphere. Moreover, the Laboratory was able to work gradually toward its goal of becoming a broad-based research facility. By the beginning of World War II, five new divisions had been added: Physical Optics, Chemistry, Metallurgy, Mechanics and Electricity, and Internal Communications.

The War Years and Growth: Total employment at the Laboratory jumped from 396 in 1941 to 4400 in 1946, expenditures from $1.7 million to $13.7 million, the number of buildings from 23 to 67, and the number of projects from 200 to about 900. During the war, scientific activities necessarily were concentrated almost entirely on applied research. New electronics equipment–radio, radar, sonar–was developed. Countermeasures were devised. New lubricants were produced, as were antifouling paints, luminous identification tapes, and a sea marker to help save survivors of disasters at sea. A thermal diffusion process was conceived and used to supply some of the ^{235}U isotope needed for one of the first atomic bombs. Also, a host of new devices that developed from booming wartime industry were type-tested and then certified as reliable for the Fleet.

NRL Reorganizes for Peace: After the war, scientific research was widely recognized as a vital national resource, and the Laboratory had a major and continuing role to play in providing such research. When the Office of Naval Research was created in 1946, NRL was transferred to this office; NRL thus became the *corporate research laboratory* of the Navy.

The demands of this new position required substantial reorganization. Rapid expansion had met wartime demands but had left NRL improperly structured to address long-term Navy requirements. One major task-neither easily nor rapidly accomplished-was that of reshaping research. This was achieved by transforming a group of largely autonomous scientific divisions into a unified institution with a clear mission and a fully coordinated research program. The first attempt at reorganization vested power in an executive committee composed of all the division superintendents. This committee was impracticably large, so in 1949 a civilian director of research was named and given full authority over the program. Positions for associate directors were added in 1954.

The Breadth of NRL: During the 41 years since the war, the areas of study at the Laboratory have included basic research concerning the Navy's environment of sea, sky, and space. Investigations have ranged widely from monitoring the sun's behavior, to analyzing marine atmospheric conditions, to measuring parameters of the deep oceans. Detection and communication capabilities have benefited by research that has exploited new portions of the electromagnetic spectrum, extended ranges to outer space, and provided means of transferring information reliably and securely, even through massive jamming. Submarine habitability, lubricants, shipbuilding materials, fire fighting, along with the study of sound in the sea, have also been steadfast concerns.

The Laboratory has pioneered naval research into space, from atmospheric probes with captured V-2 rockets, through direction of the Vanguard project-America's first satellite program-up to involvement in such projects as the Navy Global Positioning System. Today, NRL is the Navy's lead laboratory in space research, fire research, tactical electronic warfare, microelectronic devices, and artificial intelligence. NRL has also evaluated new issues, such as the effects of intense radiation and various forms of shock and vibration on aircraft, ships, and satellites. In 1977, NRL studied and identified the source of the mysterious sonic boom heard along the east coast of the United States. And in 1983, NRL helped identify the reason for the failure of the first artificial heart and then improved its design. NRL has made and continues to make important nonmilitary contributions to science and technology: development of better composite materials, new numerical techniques, new and improved microelectronic devices, and high-energy sources.

Space science continues as an important part of NRL research. In 1984, NRL scientists used instruments aboard an astronomical satellite to map 842 celestial X-ray sources. Since then, researchers also made use of NASA's "get-away specials" program for space shuttle flights, sending aloft detectors that brought in an avalanche of data for analysis and use. Investigating new materials, NRL has produced new nonskid deck coatings for aircraft carriers. A free electron laser developed at NRL in 1985 produced radiation pulses 50 to 100 times longer than other models of similar power.

In 1986, investigations in material science helped produce new techniques for obtaining two-dimensional nuclear magnetic resonance images of solid specimens and for profiling the elemental composition in the near surface region of solid materials. NRL-designed erbium lasers and zirconium fluoride glass fibers were tested for potential use in microsurgery. On Earth, NRL researchers helped conduct a major geophysical study of an uncharted region of the Antarctic, and in space,

The original Naval Research Laboratory in 1923 as viewed from the Potomac River among the farmlands of Blue Plains

NRL today as viewed from the east

BEST COPY AVAILABLE

NRL-developed ultraviolet cameras launched aboard a NASA sounding rocket captured new and more detailed images of Halley's Comet.

One goal has guided NRL's diverse activities through the years–to conduct pioneering scientific research and development that will provide improved materials, equipment, techniques, systems, and operations for the Navy, for the Department of Defense (DoD), and for the U.S. Government.

NRL Today

ORGANIZATION AND ADMINISTRATION

The position of NRL within the Navy, illustrated on the organizational chart that appears on page 284 of this *Review*, is that of a field command under the Chief of Naval Research.

Heading the Laboratory with joint responsibilities are the naval commanding officer, Capt. William C. Miller, and the civilian director of research, Dr. Timothy Coffey. Line authority passes from the commanding officer and the director of research to five associate directors of research in the following areas:

- Technical services
- General science and technology
- Warfare systems and sensors research
- Material science and component technology
- Naval center for space technology.

The first of these provides centralized technical support; the other four are the research directorates responsible for executing NRL's research and development program. Further details of the organization of the Laboratory are given on the organizational chart that appears on page 284 of this *Review*.

Financially, NRL operates as a Navy Industrial Fund activity. This requires that all costs, including overhead costs, be charged to various research projects. Funding for scientific projects in 1986 came from the Chief of Naval Research, the Naval Systems Commands, and other government agencies, such as the Defense Advanced Research Projects Agency, the Department of Energy, and the National Aeronautics and Space Administration. NRL's relationship to its sponsoring agencies, both inside and outside DoD, is defined by a comprehensive policy on interagency support agreements.

Besides funding for scientific work, NRL receives Navy monies for general construction, maintenance, and operations. In fiscal year 1986, the Laboratory's total actual funds amounted to $348.2 million.

CHANGE of COMMAND
NRL

CAPT William C. Miller, USN (right), became the 27th military officer to head NRL in a change-of-command ceremony held October 30, 1986. He relieved CAPT James P. O'Donovan, USN, who served as Commanding Officer from October 26, 1984. Here they join in cutting the cake at the change-of-command celebration that followed the ceremony.

PERSONNEL DEVELOPMENT

At the end of 1986, NRL employed 3796 personnel–30 military officers, 61 enlisted men and women, and 3705 civilians. In the research staff there are 759 employees with doctorate degrees, 338 with masters degrees, and 662 with bachelors degrees. The support staff provides to the research staff administrative, computer-aided designing, machining, fabrication, electronic construction, publication, personnel development, information retrieval, large mainframe computer services, and contracting and supply management services.

BEST COPY AVAILABLE

Opportunities for higher education and other professional training for NRL employees are available through several programs offered by the Employee Development Branch. These programs provide for graduate work leading to advanced degrees, advanced training, college course work, short courses, continuing education, and career counseling. Graduate students, in certain cases, may use their NRL research for thesis material.

For non-NRL employees, several postdoctoral research programs exist. There are also cooperative education agreements with several universities, summer and part-time employment programs, and various summer and interchange programs for college faculty members, professional consultants, and employees of other government agencies.

NRL has active chapters of Women In Science and Engineering, Sigma Xi, Toastmaster's International, and the Federal Executive and Professional Association. Three personal computer clubs meet regularly—Edison Atari, NRL IBM-PC, and Edison Commodore. An amateur radio club, a wives' club, a musical drama group-the Showboaters, and several sports clubs are also active. NRL has a recreation club which provides swimming, sauna, whirlpool bath, gymnasium, and weight-room facilities. The recreation club also offers classes in karate, aerobics, swimming, and cardiopulmonary resuscitation.

A community outreach program at NRL provides tutoring for local students, science fair judging, participation in high school and college career day programs, an art and essay contest during Black History Month, and a Christmas party with donated gifts for disadvantaged children.

NRL has an active, growing Credit Union with assets of $107 million. Public transportation to NRL is provided by Metrobus.

More information on these programs can be found in the Review chapter entitled "Programs for Professional Development," page 223.

The Mall at NRL, with the Administration building in the background. The 50-ft dish of the radio telescope was identified by scientists as the first "accurately figured" radio telescope in the world.

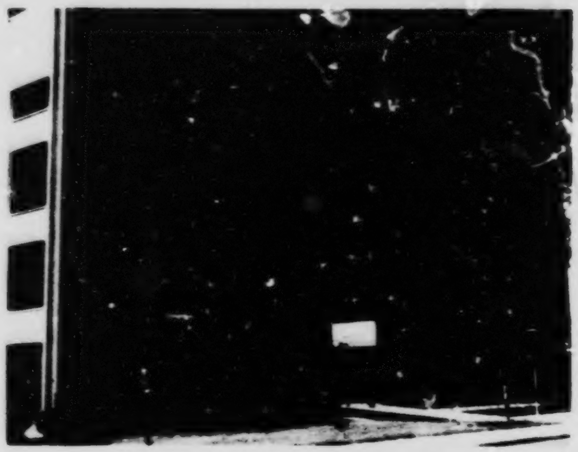

Building 207 houses the Chemistry Division

BEST COPY AVAILABLE

Looking from Building 207 toward Building 209, which houses the Space Science Division

Building 222 houses the Technical Information Division that provides centralized technical support to the Laboratory

Dr. John Davis transfers a substrate within the molecular beam epitaxy machine in preparation for growing a quantum well structure of gallium arsenide and aluminum gallium arsenide. Dr. Davis' research involves preparing novel device structures for use within the Electronics Technology Division and studies of the epitaxial growth process.

SCIENTIFIC FACILITIES

In addition to its main campus of about 130 acres and 152 buildings, NRL maintains 12 other research sites and a Flight Support Detachment. The many diverse scientific and technological research and support facilities are described in the following paragraphs.

Research Facilities

- Space Science

NRL is the Navy's main laboratory for conducting basic research and development in the space sciences. The Space Science Division has a number of commitments for space experiments in the areas of upper atmospheric, solar, and astronomical research aboard NASA, DoD, and foreign space projects. Division scientists are involved in major research thrusts that include remote sensing of the upper atmosphere by using ultraviolet sensing, studies of the solar atmosphere by using spectrographic techniques, and studies of astronomical radiation ranging from the ultraviolet through the cosmic rays. The Division maintains facilities to construct, assemble, and calibrate space experiments. A network of VAX computers, an array processor, image processing hardware, a PDS microdensitometer, and CRAY access are used to analyze and interpret space data. The Division also includes the Radio Astronomy Branch, which uses its radio telescope at the laboratory's Maryland Point site and its computational capability as represented by the Washington DC Correlator Facility, and the national radio astronomy facilities to conduct a broad program of radio astronomy.

- Space Systems

In its role as a center of excellence for space research, NRL establishes and supports the development of spacecraft and systems that use these

BEST COPY AVAILABLE

Lee M. Hammarstrom, Superintendent of the Space Systems Technolgoy Deparment, leads a broad range technology effort aimed at increasing the Navy's and DoD's use of space

spacecraft and their ground command and control stations. The Naval Center for Space Technology designs, builds, analyzes, tests, and operates spacecraft, as well as identifies and conducts promising research to improve spacecraft and their support systems. Division facilities that support this work include large and small anechoic radio frequency chambers, clean rooms, shock and vibration facilities, an acoustic reverberation chamber, large and small thermal vacuum test chambers, and model analysis test facilities. This Divison has a 31-m, computer-controlled wind and wave tank and special airborne instrumentation for developing electromagnetic remote sensing systems; a facility for long-term testing of satellite clock time frequency standards under thermal vacuum conditions linked to the Naval Observatory; a 5-m optical bench laser laboratory; and a hologram research laboratory to conduct research in support of the development of space systems.

Dr. Sidney L. Ossakow, superintendent of the Plasma Physics Division, is a recognized expert in space and Laboratory plasma physics

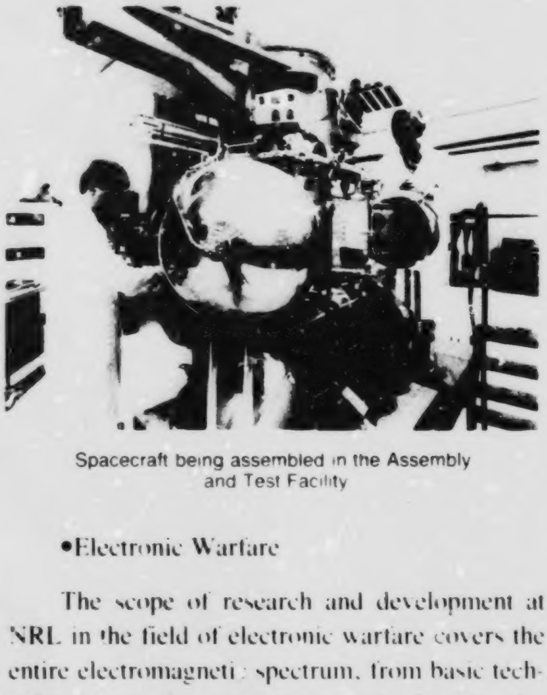

Spacecraft being assembled in the Assembly and Test Facility

•Electronic Warfare

The scope of research and development at NRL in the field of electronic warfare covers the entire electromagnetic spectrum, from basic technology research to component and subsystem development to system design and effectiveness evaluation. Major emphasis is placed on providing the method and means to counter enemy's hostile actions in all phases of battle from the beginning, when enemy forces are mobilized for an attack, to the final stages of the engagement. For this

BEST COPY AVAILABLE

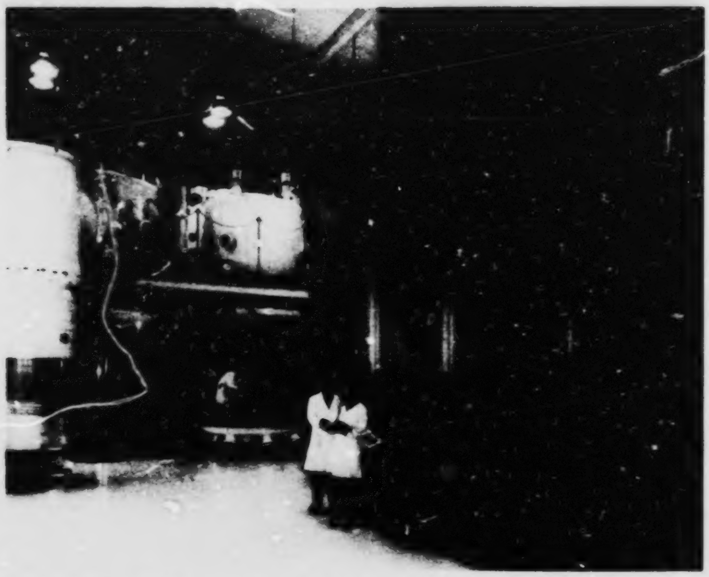

Exterior view of the thermal vacuum chamber in the Assembly and Test facility of the Naval Center for Space Technology

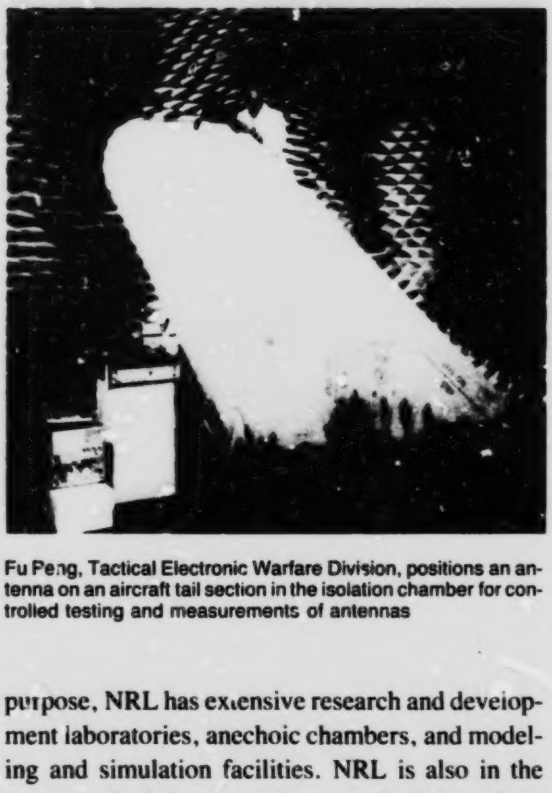

Fu Peng, Tactical Electronic Warfare Division, positions an antenna on an aircraft tail section in the isolation chamber for controlled testing and measurements of antennas

purpose, NRL has extensive research and development laboratories, anechoic chambers, and modeling and simulation facilities. NRL is also in the process of adding extensive new facilities where scientists can focus on the coordinated use of all organic defensive and offensive resources now present in the Fleet.

•Information Technology

The Information Technology Division, which includes the Navy Center for Applied Research in Artificial Intelligence, is at the forefront of DoD research and development in telecommunication, computer science, and artificial intelligence. The Division maintains a local area computer network to support its research.

The network comprises VAX 11/750s, 780s, a Gould 9005 UNIX machine, Symbolics, LMI and Xerox Dolphin LISP machines, SUN and ISI work stations, laser printers, network gateways, and terminal servers. A Butterfly 64-node parallel processor will become part of the computer's resources in the near future. The network is connected to NRL's Central Computing Facility and to the MILNET, ARPANET, and other university networks. The network will become part of the Strategic Defense Initiative (SDI) Battle Management Technology validation facility.

BEST COPY AVAILABLE

- Electronic Sciences

In addition to specific equipment and facilities to support individual technology-base programs in electronics, NRL operates two major central facilities that provide services to electronics programs throughout the Laboratory and to external organizations. The latter two facilities are the microelectronics processing facility and the high magnetic field facility.

Microelectronics Processing Facility-This facility provides support for NRL programs in electronics R&D design and process technology that require microelectronics processing skills and equipment. The facility supplies NRL programs with a range of items from discrete structures and devices to complete integrated circuits with very large scale integration (VLSI) complexity based on silicon metal oxide semiconductors (MOS) submicrometer technology.

Dr. Edward J. Cukauskas (background) and Dr. Clifford M. Krowne (seated), Electronic Technology Division, measure the a low-temperature behavior of a microwave slow-wave phase shifter, as Dr. Martin Nisenoff looks on.

High Magnetic Field Facility-This facility is used to support research projects throughout NRL, DoD, and, to a limited extent, the local scientific community. The facility provides the capability to determine the response of materials and devices to high magnetic fields up to 17 tesla with a variety of electrical, optical, and magnetic probes.

- Chemistry

NRL has been a major center for chemical research in support of Navy operational requirements since the late 1920s. The Chemistry Division continues its tradition with a broad spectrum of basic and applied research programs concerned with fuels and combustion, corrosion, advanced polymeric materials, ultrasensitive detection methods for chemical agents, special materials for electronic warfare applications, and biomolecular engineering research. Modern facilities for research include a wide range of the most modern optical, magnetic, and ion-based spectroscopic devices, a 325 m^3 (11,400 ft^3) fire research chamber (Fire I), multiple facilities for materials synthesis and physical/chemical characterization, high- and low-temperature equipment, and extensive surface-analytical instrumentation.

Ms. Elizabeth Twitchell, a laboratory technician from the University of Virginia, adds a chemical bonding agent to a "rusty bolt" in the testing device to monitor the agent's effects on reducing signal noise caused by the oxide on the metal surface. Looking on are Richard Steele (left), electronics engineer on contract from Locust Corporation and Drs. Ramanathan Panayappan, research chemist, and John C. Cooper, principal investigator, both of the Chemistry Division.

BEST COPY AVAILABLE

Nearfield acoustic hologram processed from a broadband hologram taken in the AARF (Advanced Acoustic Research Facility) at NRL. The different color shades represent the levels of pressure in the extreme nearfield, frozen at an instant in time, radiated from a point-driven submarinelike hull structure. The two colors represent opposite phases of the standing wave-like pressure field. The hull is vibrating at the frequency of this hologram with one-half wavelength axially and one wavelength circumferentially. (E. Williams)

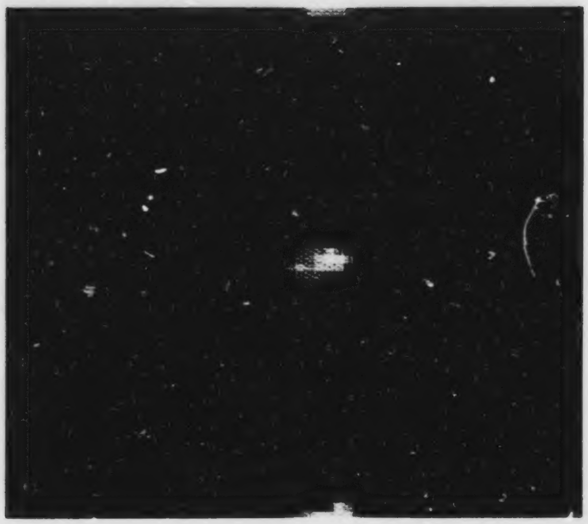

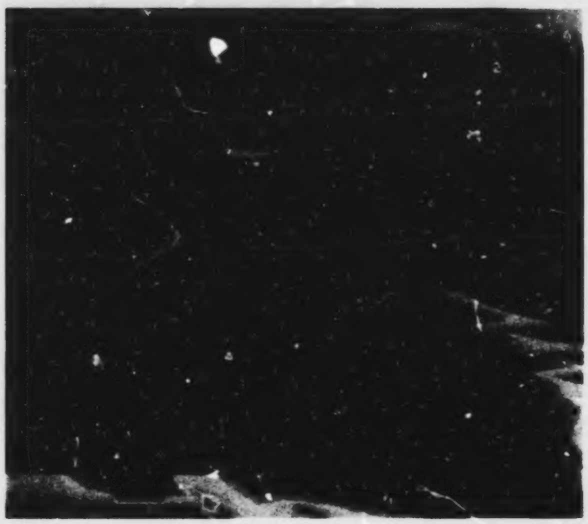

Numerical simulation of X-ray laser gain in the Defense Nuclear Agency "Double Eagle" pulsed power facility. Gain in the 172 Å line of neonlike krypton for a double-puff experiment is given as a function of radius (horizontal) and time (vertical). Gains in excess of 10 cm are calculated (pink) as the inward-propagating shock wave reaches the central axis, and several nanoseconds later as hot krypton, which has "bounced," stagnates with imploding material. (J. Davis)

BEST COPY AVAILABLE

Three different aspects are shown of the complex wake of a fluid flowing rapidly over a square-edged bluff body. This simulation of sound waves resonating with vortex shedding is typical of the fluid dynamics and other research simulations performed with the Cray X-MP and other advanced parallel processing computers at NRL, such as the Connection Machine, the Butterfly, and GAPS. The flow (from left to right in each panel) is constrained by rigid walls at the top and bottom of each panel, making a sort of organ pipe. The confined air is caused to vibrate in resonance with the vortex shedding, the recirculation zone behind obstacle flapping like the reed in musical instruments. (J. Boris, E. Oran, Code 4400)

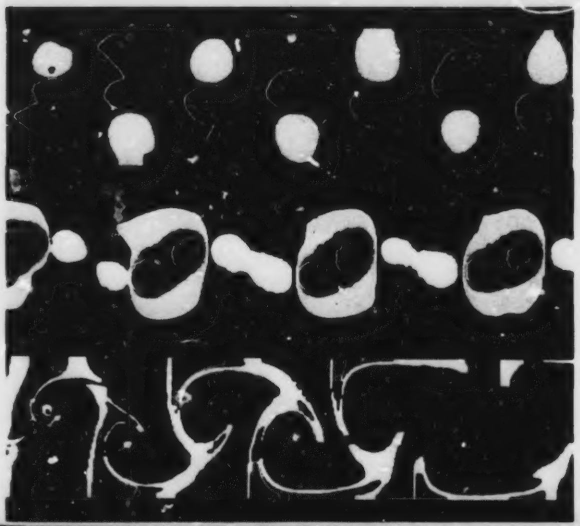

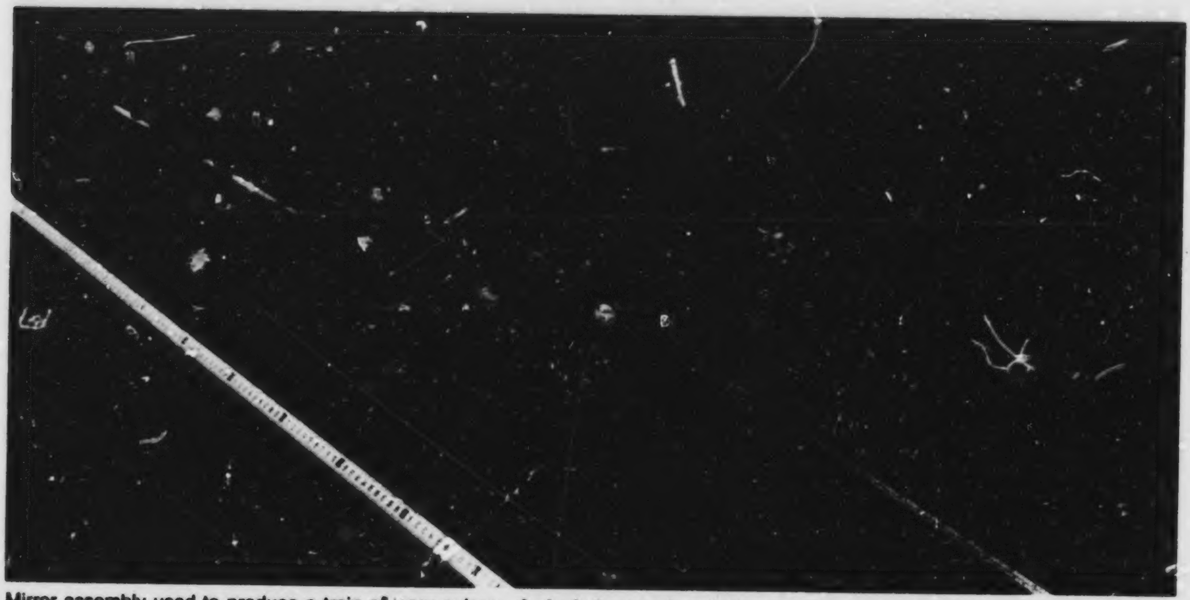

Mirror assembly used to produce a train of laser pulses. A single laser pulse of 40-ps duration enters from the left is reflected and delayed by beamsplitters and mirrors to produce a set of four equal intensity pulses, each spaced by 200 ps. (M. Duncan, Code 6540)

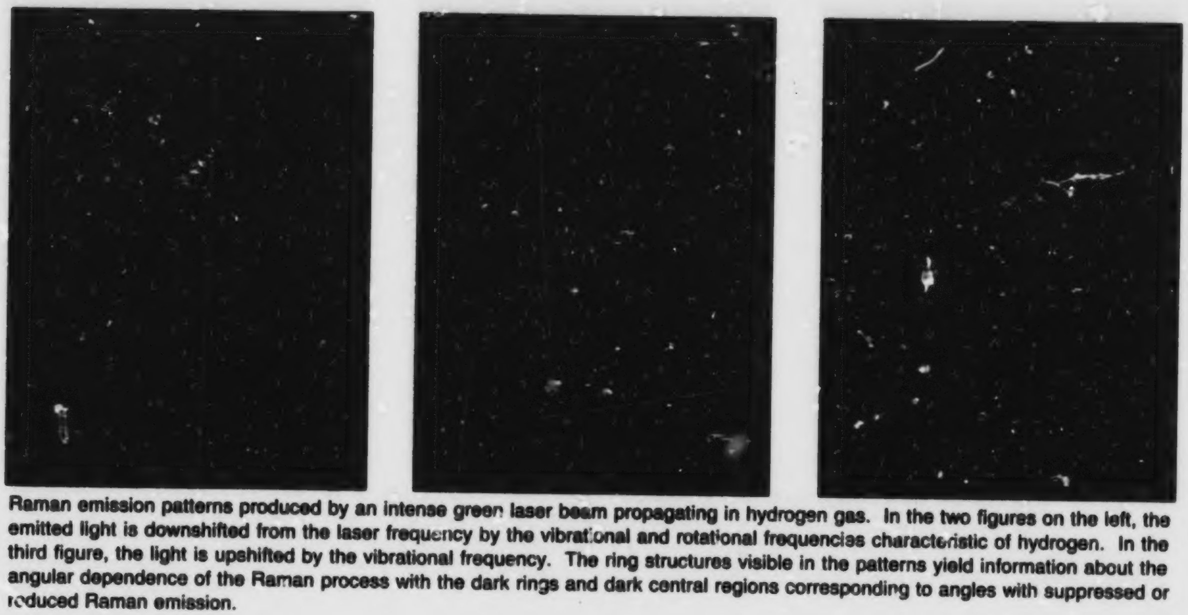

Raman emission patterns produced by an intense green laser beam propagating in hydrogen gas. In the two figures on the left, the emitted light is downshifted from the laser frequency by the vibrational and rotational frequencies characteristic of hydrogen. In the third figure, the light is upshifted by the vibrational frequency. The ring structures visible in the patterns yield information about the angular dependence of the Raman process with the dark rings and dark central regions corresponding to angles with suppressed or reduced Raman emission.

BEST COPY AVAILABLE

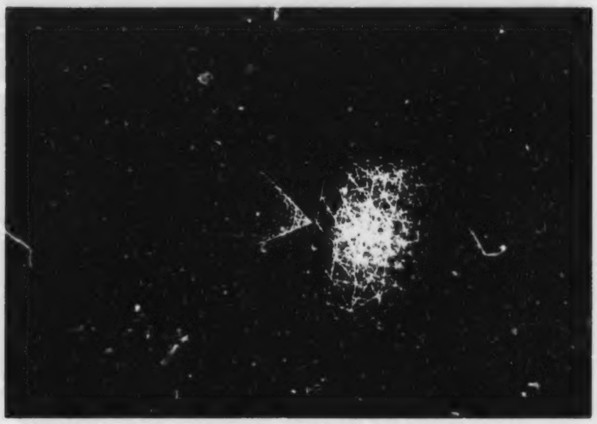

Partial view of the tetrahedral mesh for the engine intake. The surface triangulation is shown in blue, whereas sections of the mesh are shown in green, yellow, and red. (R. Löhner, Code 4410)

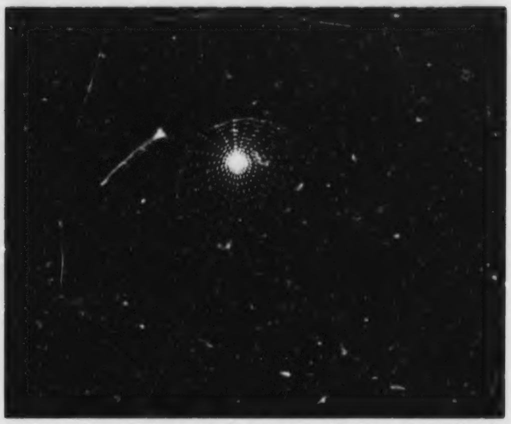

Engine intake (enlargement) showing the centerbody and outer walls of the nozzle (R. Löhner, Code 4410)

Surface triangulation of a manta ray showing the, wings-up configuration from above (R. Löhner, Code 4410)

BEST COPY AVAILABLE

Surface triangulation of a manta ray showing the <wings-down> configuration from below (R. Löhner, Code 4410)

BEST COPY AVAILABLE

Density field produced by a strong shock colliding with a missile launcher. Zones of high density are shown in blue, whereas zones of low density are shown in red. (R. Löhner, Code 4410)

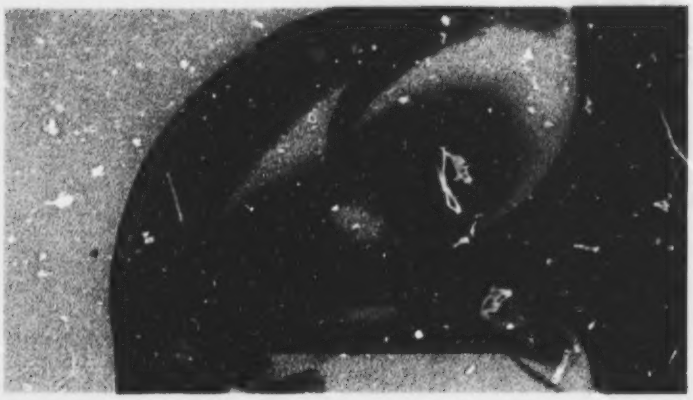

Surface triangulation (blue) and background grid used to construct a mesh of tetrahedrons for a missile launcher (R. Löhner, Code 4410)

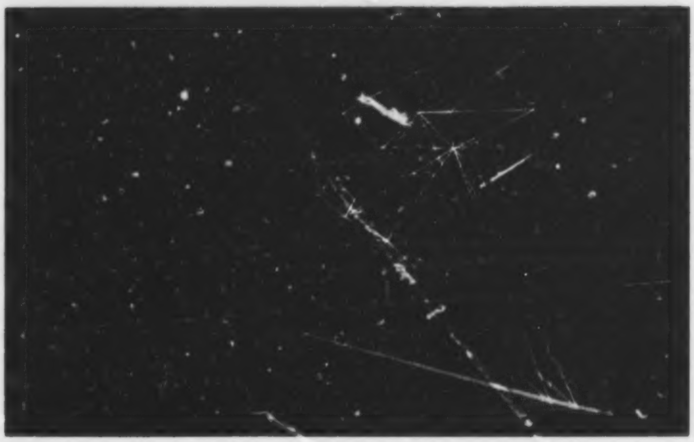

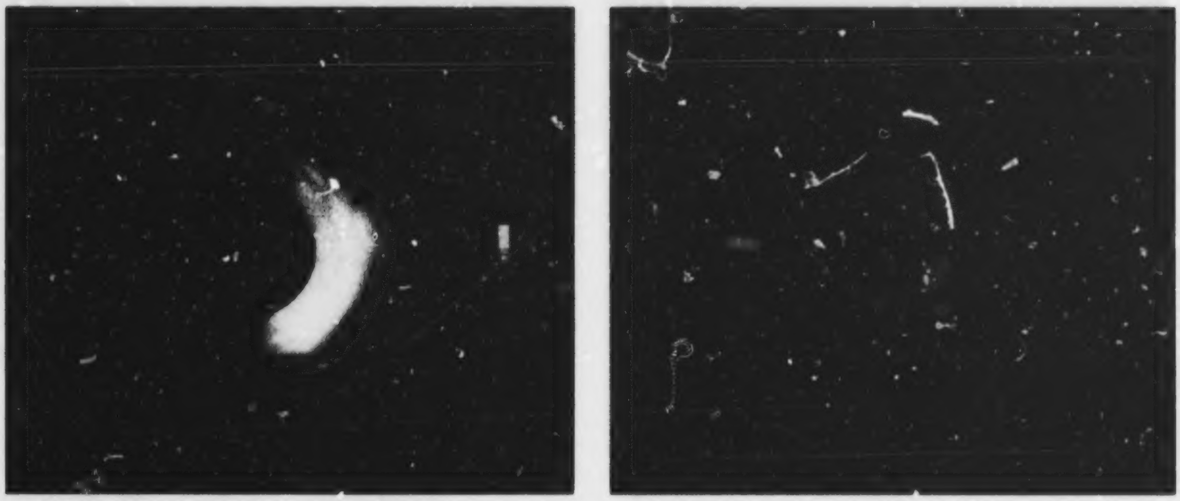

The Remote Atmospheric and Ionospheric Detection System (RAIDS) will image the ionosphere and provide the first comprehensive look at ionospheric weather. The two figures represent cross sections through Earth's ionosphere as seen in the light of O^+ ions. The figure at the left shows the southern lights or aurora australis, the other figure shows the northern lights, or aurora borealis. The large, bright features near the equator arise from the motion of O^+ ions along Earth's magnetic field as they are transported hundreds of miles up into the atmosphere by winds. This feature, visible for the first time in the extreme ultraviolet, is called the Appleton anomaly. (Dr. L. Paxton and Mr. S. Bailey)

Thomas Cosden, now retired from NRL, stands in front of the Optical Sciences Division's Large Optic, High-Precision Tracker. Mr .Cosden was instrumental in the creation of this multipurpose optical tracking system. With a 80-cm input aperture and TV correlation tracking capability, one task for this mobile system is to track and obtain infrared signatures of moving targets.

•Optics

Ultra-Low-Loss Fiber-Optic Waveguides-NRL has developed record-setting ultrahigh transparency infrared waveguides. These fluoride glass materials offer the promise of long-distance communications without the need of signal amplification.

Focal Plane Evaluation Facility-The facility has extensive capabilities to measure the optical and electrical characteristics of infrared focal plane arrays being developed for advanced Navy sensors. The facility includes electronics for clocking, video signal processing and digitization, and computer data reduction for arrays that use charge-coupled device (CCD), charge-injection device (CID), and charge-image matrix (C/M) technologies.

IR Missile Seeker Evaluation Facility-This facility performs open-loop measurements of the susceptibilities of infrared tracking sensors to optical countermeasures. The operation of the sources and rate table, as well as the data acquisition and reduction, is computer-controlled. Measurements are performed on modulation and image-based seekers.

Large Optic, High-Precision Tracker-NRL has developed a tracker system with an 80-cm primary for atmospheric transmission and target signature measurements. By using a quadrant detector, the servo system has demonstrated a 12-μrad tracking accuracy. An optical correlation tracker system has been added to facilitate tracking of objects without a beacon.

High-Energy Excimer Laser-NRL has constructed an X-ray preionized discharge excimer laser that has reliably produced 80 J of laser radiation at 308 nm in a 200-ns -long pulse. This represents the highest output energy achieved to date by any discharge-pumped excimer laser device. This facility is used to investigate a variety of research areas including Raman beam cleanup and combining nonlinear optical phase conjugation and high-energy laser-beam propagation.

Fiber Optics Sensors-The development and fabrication of fiber-optic sensor concepts, including acoustic, magnetic, and rate-of-rotation

BEST COPY AVAILABLE

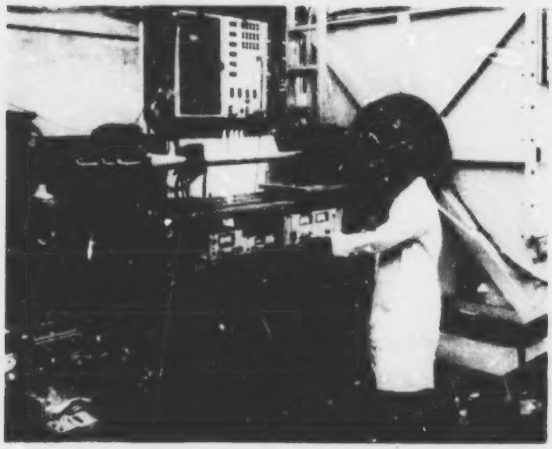

NRL's novel, high-power, free-electron laser oscillator is powered by a unique, long-pulse, induction linear accelerator. Dr. John Pasour, Plasma Physics Division, is the principal investigator and readies the tunable laser for a laboratory test.

sensors, are conducted in several facilities within the Laboratory's Optical Sciences and Acoustics Divisions. Equipment used for this research includes an automated system for fabricating fiber-optic couplers, facilities for evaluating optical fiber coatings, fiber splicers, an acoustic test cell, a three-axis magnetic sensor test cell, and a computer to model alternative sensor concepts.

Digital Processing Facility-This facility is used to collect, process, analyze, and manipulate infrared data and imagery from several sources. Digital Equipment Corporation VAX 11/780 and 11/750 computers are the heart of the system. Attached to the Central Processing Unit (CPU) are a Floating Point Systems AP-120B array processor, a CSPI mini-MAP array processor, and a Gould Deanza threecolor/256 intensity level image display. The Deanza system allows access to standard video signals. Extensive image processing software is installed and a high-speed interface to the NRL CRAY supercomputer is planned.

•Plasma Physics

The Plasma Physics Division is the major center for in-house Navy and DoD plasma physics research. The Division is involved in theoretical space plasma studies related to communications' effectiveness and in programs with experimental counterparts. These experimental programs include development of pulsed sources to generate electron and ion beams, powerful discharges, and various types of radiation. The largest of these pulsers, GAMBLE II, is used to study the production of megampere electron beams and for producing very hot, high-density plasmas. Other generators are used to produce particle beams that are injected into magnetic fields and/or cavities to generate intense microwave pulses. A new facility will soon be established to test advanced, charged particle beam propagation concepts. An extremely high power laser, PHAROS III, is used in inertial fusion research and in high-altitude nuclear explosion effects studies.

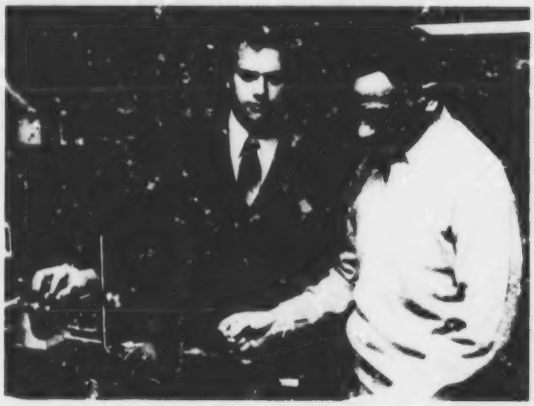

Dr. Leon Esterowitz (right), Optical Sciences Division, and Mark Strom, research physicist on contract from Sachs Freeman Associates, demonstrate an NRL-designed erbium laser that emits short , infrared light pulses through zirconium fluoride glass fibers. The unique laser holds great promise as a scalpel and for removing plaque from heart arteries without open heart surgery

•Computational Physics and Fluid Dynamics

The Laboratory for Computational Physics and Fluid Dynamics (LCP&FD) has been developing a Graphical and Array Processor System. The system centers around an Aptec I/O Computer that provides the necessary communications bandwidth and common memory for performing large simulations or processing graphical data from external sources on multiple integrated array processors and to immediately display the results from one or more sources on a high-resolution, high-speed graphics monitor. Specifically, the system is front ended by a VAX 11/780 that provides executive control and outside communication capability to other sites at NRL and outside laboratories; a 1.4 giga-byte high-speed this disk is incorporated for simulation storage and replay or review; the computational engines are two Numerix 4325 array processors at 30 mega-flops each and one floating point systems array processor rated at 12 mega-flops; the current graphics device is a Tektronix 4115B that has sixteen colors, 1024 × 1280 raster resolution, and high-speed block data transfer capability. The LCP&FD has plans to add a much faster graphics device. A general-purpose reactive flow model (RFM) has been written, debugged, and applied to a number of fluid dynamics problems.

The LCP&FD also maintains fluid dynamic laboratory facilities that include a 30-m wind/wave tank to study nonlinear ocean wave processes and fluid/structure interactions; a 20-m stratified tow channel to study geophysical flows jets and wakes; and blow-down water tunnels to study hydroacoustics, turbulent boundary layers, and non-Newtonion flows. Experimental efforts using these facilities are supported by flow measurement systems including multicomponent laser velocimeters and anemometers; digital image processing of flow visualization and of two-phase flows; hydrophones; imaging infrared radiometers; and in collaboration with other NRL organizations, a variety of microwave radar measurement systems for remote sensing studies of hydrodynamic processes. On-line experiment control, data acquisition and processing are achieved with a central HP1000 system or one of a number of smaller, portable units. Off-line data processing and analysis are available on a 3-CPU HP9000 system or any other LCP&FD or NRL system.

•Radar

NRL has gained worldwide renown as the "Birthplace of Radar" and has maintained its reputation as a leading center for radar-related research and development for a half century. An impressive array of facilities managed by NRL's Radar Division continues to contribute to this reputation. These include land-based, airborne, and laboratory radar cross section measurement systems; an airborne APS/116 radar with ISAR image processing; and an airborne adaptive array laboratory. Also, the division manages and maintains a radar display test bed, an IFF ground station, a digital signal processing facility, a digital image processing laboratory, and a radar cross section prediction facility. A radar research and development activity is located at the Chesapeake Bay Detachment (CBD), Randle Cliff, Maryland. It has separate facilities for specific types of systems that range from high-frequency, over-the-horizon systems to millimeter wave radars. The SENRAD radar test bed, a flexible and versatile system for demonstrating new developments in radar, is also located at CBD.

•Acoustics

NRL's facilities in support of acoustical investigations are located at the main Laboratory site and in Orlando, Florida at the Underwater Sound Reference Detachment (USRD). At the main Laboratory site, there are three research tanks instrumented to study echo characteristics and to develop devices; the largest tank is 9 m deep, 12 m long, and 8 m wide. There is also an underwater acoustic holography facility for research in acoustic fields, and a water tunnel having a large blow-down channel with a 15-m test section used for acoustic and flow-induced vibration studies of towed line arrays and flexible cables. For acoustic surveillance array processing and acoustic data processing, researchers have access to the multichannel, programmable, digital data processing system-a system of DEC computers, high-speed array processors, and peripherals

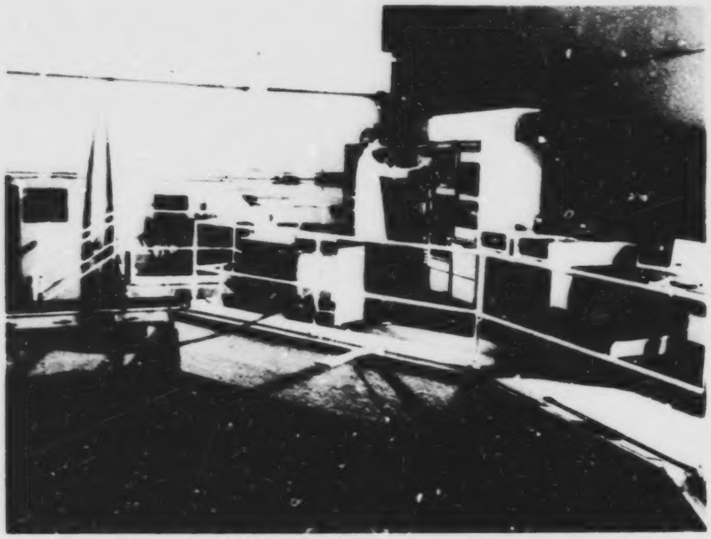

Brian Houston of the Acoustics Division is conducting research on scaled targets in the Target Acoustics Facility

for up to 256 channels. The USRD facilities are described with NRL's field stations.

•Materials

NRL has capabilities for X-ray and electron diffraction analysis, and for electron and Auger spectroscopy. It has a high-performance, secondary ion mass spectrometer for surface analysis and significantly extends the diagnostic capability of the technique. A high-resolution, high-performance, reverse-geometry mass spectrometer is used to probe reactions between ions and molecules. The Laboratory has fracture and fatigue testing machines with capacities to 272,000 kg, an ultrasonic gas atomization system that has a molten alloy capacity up to 5 kg, a gas inlet pressure capacity of up to 27.6 MPa, and hot isostatic press facilities.

The Laser-Materials Application Center has a high-energy, continuous wave (CW), 10.6 μm CO_2 electrical discharge laser that can output 12 kW or more of optical power. Both highly focusable and spatially uniform optics are available along with associated workpiece optics and fixtures. Facilities for recording the laser output characteristics and workpiece transducer outputs are available.

Dr. Kuntimaddi Sadananda, Materials Science and Technology Division, who is the principal investigator in the development of a technique to rework scrapped turbine blades from jet aircraft engines, adjusts the control board for a universal high-temperature machine that is used to test blade specimens

•Condensed Matter and Radiation Sciences

Ion Implantation Facility–The facility consists of a 200-keV ion implanter with specialized ultrahigh vacuum chambers and associated *in situ* specimen analysis instrumentation. The facility is used to develop advanced surface treatment of

Dr. Richard A Kant (left) and Bruce Sartwell, Condensed Matter and Radiation Sciences Division, are shown using an ion-assisted deposition system in a research experiment to produce adherent thin films

materials to modify their properties and improve corrosion and wear resistance.

3-MeV Tandem Van de Graaff—This facility is used to study charged particle radiation damage such as occurs in space, and to perform Rutherford backscattering spectroscopy and nuclear reaction analysis that produces high-sensitivity composition, depth profiles.

65-MeV Electron Linear Accelerator (LINAC)—The LINAC produces intense electron beams with 10 to 65 MeV energies. Pulse rates from 1 to 360/s and widths from 0.05 to 1.4 μs are selectable. This facility is used to study radiation effects on microelectronics and materials. Single beam pulses can be triggered on command, and the data from the target can be analyzed and stored in a fast multichannel digitizer system.

Epitaxial Growth of Metallic Films—NRL has two epitaxy facilities used to grow ultrathin, crystalline, metallic films for integrated circuit and basic quantum research. One uses a molecular beam, and the second uses an electron beam. Both have diagnostics to monitor the films while growing, and they both operate at 10^{-11} torr.

Hypervelocity Impact Facilities—Three facilities are used for ballistics research at speeds exceeding 9 km/s with toxic or explosive targets. The projectile velocity, orientation, and dynamic projectile-target interaction can be measured.

Synchrotron Radiation Facility—An intense monochromatic X-ray photon source, tunable from 4 to 12 keV, is available on the NRL-developed beam line at the National Synchrotron Light Source at Brookhaven National Laboratory. Environmental target chambers can span a pressure range from ambient to several hundred kbar and temperatures from 10 to 1500 K. A six-circle computer controlled goniometer is used to control and position targets.

Research Support Facilities

•Central Computing Facility

Recently NRL installed a Cray X-MP/24 Class VI supercomputer with VAX 11/785 front-end computer systems. This system provides balanced vector and very high-speed scalar processing. The Cray's peak processing speed is 210 million floating point operations per second (MFLOPS) with a sustainable speed of 105 MFLOPS. It has a central memory capacity of 4 million 64-bit words and an I/O subsystem with three interconnected I/O processors.

The Cray is accessed by VAX processors at the central computing site and through the Defense Data Network/Military Network from remote sites. The system has a network capability to link terminals, PCs, and minicomputers by means of DECNET and TCP/IP protocols. It also provides data-base management, document processing, and graphics support. FORTRAN, PASCAL and C languages are the primary programming languages for the Cray. A wide range of scientific, statistical, and mathematical software is also available. NASTRAN a finite element structural analysis program is available in the Cray.

A high-quality, high-performance pen plotter and a high-speed electrostatic plotter/printer are available. Plots can also be previewed on graphics terminals. Plotting software can generate tapes for the DICOMED system, located in the Technical Information Division.

•Technical Information Services

The Technical Library contains more than one million items including 2000 current journals. Much of the collection can be accessed by means of computerized search services. The Library also provides interlibrary loans, library of Congress stack passes, and a variety of reference services.

This area of the library at NRL holds over 2000 domestic and foreign journals in all fields of physical sciences and technology

Publication services include writing, editing, composition, phototypesetting, and publications consultation. The primary focus is on using computer-assisted publication techniques that produce scientific and technical information containing complex artwork and equations.

Graphic services include presentation and publications artwork.

Photography services include motion picture, video, and still-camera coverage for data documentation both at NRL and in the field.

Information specialists prepare written and visual display materials for media dissemination and for use at exhibitions and professional meetings and seminars.

The DICOMED computer graphics system produces high-resolution, high-quality color images on 35 mm slides, 8 × 10 in. viewgraphs, 16 mm movies, or microfiche. It is driven by tapes generated on many different computer systems.

•Engineering Services

The Engineering Services Division (ESD) provides NRL and other Navy laboratories with engineers/technicians and highly skilled mechanics to support research projects.

Elaine Snider, of the Engineering Services Division, designs a printed circuit board on a REDAC computer-aided design station

Aerial view of Pomonkey, MD, a field site south of NRL. At this site a free-space antenna range exists to develop and test a variety of antennas.

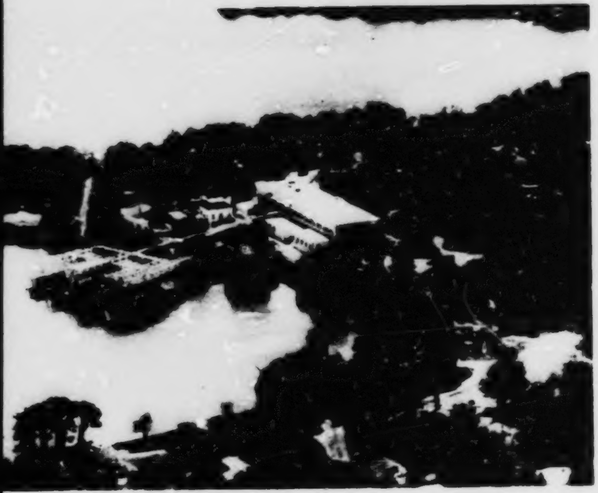

View overlooking the lake, piers, grounds, and buildings of NRL's Underwater Sound Reference Detachment (USRD), located in Orlando, Florida. NRL is the principal Navy activity that carries out the majority of acoustic calibration tests and evaluations at this location.

NRL FIELD SITES

USRD Anechoic Tank facility. Jim Momier and Keith Boyd show the electronic control system used to analyze the underwater sound signals coming from equipment being tested or evaluated in the tank.

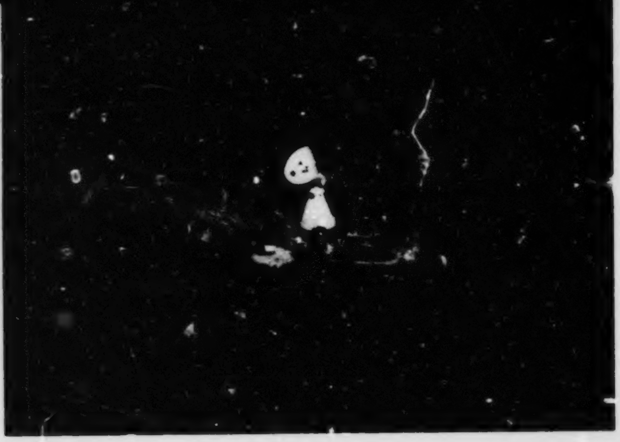

The Satellite Communication Facility, Waldorf, Maryland, is used as a transmit/receive site in the 2 to 20 GHz range

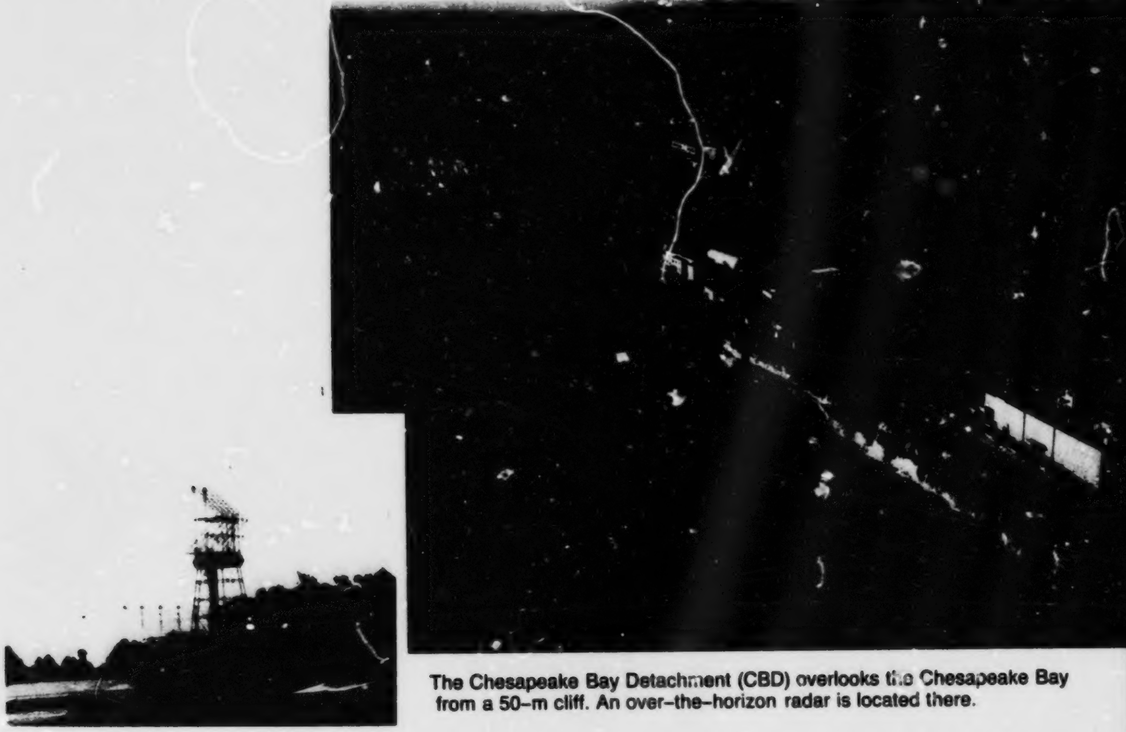

The Chesapeake Bay Detachment (CBD) overlooks the Chesapeake Bay from a 50-m cliff. An over-the-horizon radar is located there.

This 85-ft radio telescope is one of two antennas located at Maryland Point, Maryland that is used for high-precision radio astronomy measurements

ESD personnel work with the researchers on freehand sketches or detailed drawings according to MILSTD requirements and NASA standards. ESD's personnel perform a broad spectrum of tasks such as engineering analysis; fabrication of heavy structures; design and fabrication of original electronic devices and instruments; the computerized production of dense, printed circuit boards; and conventional/numerically controlled machining.

ESD has extensive shop capabilities for sheet metal fabrication, machining, and electroplating. It has a plastics shop where devices and forms are fabricated or molded from laminates, polymers, fiberglass, and plastics. ESD also operates a foundry where heat treating of metals, castings, and sand blasting jobs are performed.

FIELD STATIONS

NRL has acquired or made arrangements over the years to use a number of field sites or auxiliary facilities for research that cannot be conducted in Washington, DC. They are located in Maryland, Virginia, California, and Florida. The two largest facilities are the Chesapeake Bay Detachment (CBD) and the Underwater Sound Reference Detachment (USRD).

•CBD

CBD occupies 68.1 hectares near Chesapeake Beach, Maryland, and provides facilities and services for research in radar, electronic warfare, fire research, optical devices, materials, communications, and other subjects. Because of its location on the west shore of the Chesapeake Bay, unique experiments can be performed. Radar antennas 50 to 60 m above the water overlook the bay. Another site, Tilghman Island, is 16 km across the bay from CBD and in a direct line of sight from CBD. This creates a unique environment for low clutter and generally low background radar measurements. Experiments involving chaff dispensing over water and radar target characterizations of aircraft and ships are examples of military-oriented research. Basic research is also conducted in radar antenna properties, testing of radar remote sensing concepts, use of radar to sense ocean waves, and laser propagation.

•USRD

Located at Orlando, Florida, USRD functions in many ways like a standards bureau of underwater sound and also performs R&D for sonar transducers and related acoustic materials. Its semitropical climate and two clear, quiet lakes (the larger 11 m deep and nearly circular) are distinct assets to its research and development on sonar transducers and underwater reference standards and to its improvement of techniques to calibrate, test, and evaluate underwater acoustic devices. USRD has an anechoic tank for simulating ocean depths to 700 m and smaller pressure tanks for simulating depths to 7000 m. A spring-fed lake located in a remote area about 40 miles north of USRD, at the Leesburg Facility, provides a natural tank for water depths to 52 m with ambient noise level 10 dB below that for sea state zero, larger objects can be calibrated here. The detachment has provided acoustic equipment and calibration services not only to hundreds of Navy activities and their contractors but also to private firms and universities not engaged in DoD contracts.

•Marine Corrosion Test Facilities

Located on Fleming Key at Key West, Florida, these facilities offer clear, unpolluted quiescent of flowing seawater, and atmospheric environment to study salt atmosphere weathering; general corrosion and fouling resistance of metallic and nonmetallic materials and coatings; cathodic protection and other corrosion protection systems; and electrochemical corrosion.

•Other Sites

Some field sites have been chosen primarily because they provide favorable conditions to operate specific antennas and electronic subsystems and are close to NRL's main site. Maryland Point,

The skyline of NRL, viewed from the Potomac River, is changing as new buildings are added

south of NRL, operates two radio telescopes (25.6 and 26 m in diameter) for radio astronomy research. NRL's Waldorf Facility, south of NRL, operates 18.3 m, X-band and S-band antennas for space and communications research. Pomonkey, a field site south of NRL, has a free-space antenna range to develop and test a variety of antennas. The antenna model measurement range in Brandywine, Maryland, has a 4.6 m diameter turntable in the center of a 305-m diameter ground plane for conducting measurements on scale-model shipboard and other antenna designs. Blossom Point, Maryland is another NRL installation.

- Research Platforms

NRL uses ships and aircraft to conduct some of its research. Oceangoing research ships are obtained from a pool of vessels maintained by the Naval Oceanographic Office, Mississippi. For airborne research, NRL uses three four-engine turboprop P-3A Orions and one four-engine turboprop P-3B Orion. These airplanes annually log about 2000 hours of flying time on projects ranging from magnetic bathymetry and electronic countermeasure research to studies of radar signal reflections.

NRL in the Future

To continue its growth and provide preeminent research for tomorrow's Navy, NRL must maintain and upgrade its scientific and technological facilities at the forefront. Its physical plant to house these facilities must also be adequate. NRL recently embarked on a Corporate Facilities Investment Plan (CFIP) to renew its physical plant. This plan and future facility plans are described below.

THE CFIP - NEW SCIENTIFIC FACILITIES

The NRL Corporate Facilities Investment Plan (CFIP) is a 10-year program aimed at providing modern research facilities for advanced naval research by 1995. Phase I construction of the new Electro-Optics building is under way. When it is completed, the project will provide approximately 2323 m^2 (25,000 ft^2) of useable, isolated, optics space, and related office and computational areas.

The final phase of the Tactical Electronic Warfare Facility is under construction and is scheduled for completion in April 1989. This phase will yield 13,828 m^2 (148,841 ft^2) of space. The new building will provide a centrally managed system designed to fully assess the operational effectiveness of a wide variety of EW responses to various challenges.

The final design for the rehabilitation of Building 30 is under way. If approved, construction should begin by January 1988. The design for the renovation of Building 28 Auditorium has been completed; its construction is scheduled for completion by 21 September 1987. Moreover, Buildings 3, 28, 35, 46, 48, A52, and 56 will be completely or partially remodeled and reconfigured to meet today's research standards.

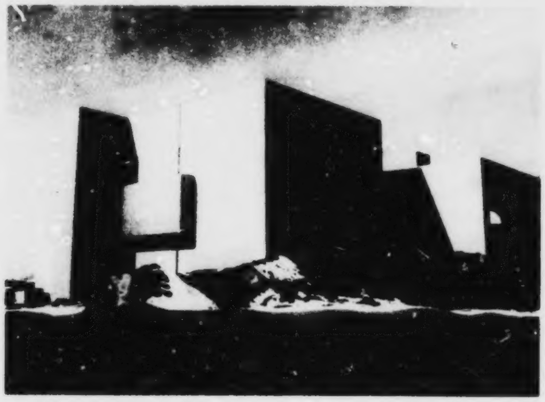

NRL's new electro-optics laboratory.
The building is near completion.

Electro-Optics Laboratory

Construction of a new electro-optics laboratory building (Phase I), has recently been completed. The new building provides 3359 m^2 (37,000 ft^2), of prime space for NRL. It includes structurally isolated vibration-free electro-optics laboratory rooms; class 100 clean suites; a 7.32-m fiber draw tower; electromagnetic shielding; vaults and computational facilities; and 24-h temperature, humidity, and pressure control.

•Plasma Physics Facilities

Two major facilities will be established in the Plasma Physics Division. A laboratory for studying the interaction of the intense electron beams with the atmosphere and their propagation properties will be completed during FY 87. A 5-MV generator will inject pulses of electron current into preheated ionization channel to study the effectiveness of propagation under various conditions. During the same year a KrF-laser facility will be initiated to provide intense radiation for studying the inertial confinement fusion target heating at short wavelengths.

•General-Purpose Laboratory

This environmentally controlled facility will provide stringently clean laboratories with carefully controllable temperature, humidity, ambient dust, and power for investigations in the rapidly evolving fields of electronic technology and composite materials synthesis and exploitation.

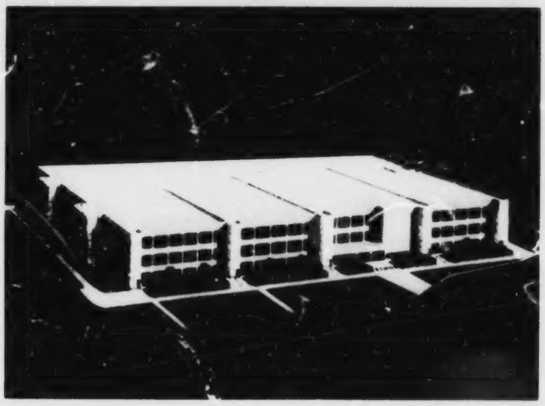

The future EW laboratory (to be completed in 1989) will permit coordinated use of resources to study the surveillance and force coordination phases of an enemy attack

•Electronic Warfare Laboratory

The electronic warfare program includes plans to develop, as part of the CFIP, a major simulation capability—the coordinated electronic warfare simulation laboratory (CEWSL)—to explore electronic countermeasure applications in all stages of naval combat.

•EW Optical Integration Laboratory

An optical integration laboratory facility will be incorporated into expanded Tactical Electronic

Warfare Division spaces. This facility will accommodate experimental optical and electronic capabilities that will enable the integration of critical technologies essential to enhanced electronic warfare capability. These spaces and the specialized optical assembly and electronic warfare evaluation equipment will be used as a staging facility providing for effective realistic evaluation early in the development cycle.

- Coordinated EW Simulation (CEWS) Laboratory

The CEWS Laboratory construction project (MILCON P- 380) began in FY-1986. It will provide the Navy with significant new force level simulation capabilities to assess and optimize the coordinated use of distributed U.S. EW systems in battle group engagement situations to oppose threat activities coupled across all combat stages, i.e., force coordination, surveillance, targeting, and terminal homing of missiles. EW decision nodes and EW system operators will be key elements in real-time closedloop simulations. The new R&D complex will permit simulated operational evaluation of new cooperative EW concepts, techniques, tactics, strategies, and the quantitative assessment of the contributions of individual EW systems' upgrades and improvement programs.

This new facility will also eliminate the need for much of the very expensive at-sea and in-air EW system tests and evaluations and will provide better focus and understanding for those that are conducted. It will support and expedite R&D by permitting evaluation of system concepts and techniques before actual hardware R&D is begun, as to optimize performance during development.

REHABILITATION OF SCIENTIFIC FACILITIES

Several of the research facilities at NRL will be upgraded in the near future. These are highlighted below.

- Central Computing Facilities

An NRL integrated communications network (NICENET) is being installed that provides access to the central site facilities from both terminals and other computers at NRL; other potential NICENET uses (for example video training and a campus-wide television network) are also under consideration. The ultimate goal of this network is to continue to expand and to provide universal access to common-shared computer resources, gateways to other networks (including satellite links) and graphics peripherals, and other noncomputer communications services.

- Other Facilities

Specialized facilities are being installed or upgraded in several of the research and support divisions.

Information Technology-An expanded computer network is being planned to provide each researcher in the division access to a computer from the office. Special test facilities are also being planned along with test-beds in support of specific R&D tasks.

Plasma Physics-Facilities, where established technology will be combined with new concepts, are under construction. The study methods for accelerating electrons to high energy at very high current levels will be facilitated, thus providing the technology needed to develop very compact and economical accelerators. A large inductive store is also being designed to provide a driver for an advanced plasma implosion facility to serve in a variaty of applications, including X-ray laser development.

Computational Physics-Work is continuing on the Graphical and Array Processing System, which the Laboratory for Computational Physics and Fluid Dynamics is developing on its VAX 11/780 computer. This facility couples multiple inexpensive array processors working asynchronously in parallel. Although the basic system is now in place and low-cost near-supercomputer performance has been demonstrated, scheduled upgrade to the graphics and computational engines will enhance its capabilities. This facility can be used for applied research on nuclear and environmental airblast effects; turbulence modeling for jets, wakes, and reactive flows; and for atmospheric turbulence predictions.

Engineering Services-An advanced technology and fabrication facility is being planned. It will be used to study fabrication methods by using new and/or unusual materials, processes, and techniques (such as powdered-metal mixtures, ion implantations, various composites, and laser machining of composites) developed by NRL research divisions or other Navy laboratories. Longer range plans call for new machines: both computer-controlled drives by our new computer-aided device/computer-aided manufacture (CAD/CAM) system, and human-controlled drives with enhanced precision capability using new and unusual material fabrication.

Radar-The Radar Division is installing a Computer-Aided Engineering (CAE) facility to aid in digital system design. The system has five full-color graphics workstations to provide capabilities for circuit designing and simulation, timing verification, and automated printed circuit board layout and gate array design.

The CAE facility will be used to design systems based on commercially available components as well as advanced systems incorporating VHSIC and gate array technologies. The CAE facility will become a valuable tool in evaluating new technologies for radar signal processing requirements.

Acoustics-Target Research Tank-Tank facilities for acoustic target research in the Acoustics Division will be significantly expanded to extend the range of target sizes. The expanded model tank is planned to contain a water volume of approximately 30,000 m^3.

High-Pressure Acoustic Test Facility-A new tank facility at NRL's Underwater Sound Reference Detachment (USRD) in Orlando, Florida, will be used for underwater acoustic-materials research, development, and test and evaluation of much larger objects at significantly increased pressures and lower frequencies. This new tank is patterned after the smaller, lower pressure anechoic tank that has been used to develop virtually every submarine and torpedo transducer in the fleet today. It will be operational in 1989.

Explosive Shock Test Facility for Sonar Transducers-Currently, some sonar transducers undergo explosive shock testing in open-water facilities and are often calibrated in USRD's Anechoic Tank Facility before and after undergoing shock tests. These will reduce the development time of transducers up to 12 months, substantially reduce the cost of shock tests, and provide basic research tools.

Further Information: The NRL Fact Book gives more details about the Laboratory and its operations. It lists major equipment, current fields of research, field sites, and outlying facilities, and it also presents information about the responsibilities, organization, key personnel, and funding of the divisions, detachments, and other major organization units.

Information on the research described in this *Review* may be obtained by contacting Mr. Richard Fulper, Jr., Head, Technology Transfer and Special Programs, Code 1005.4, (202) 767-3744. General information about NRL may be obtained from Information Services, Code 2610, (202) 767-2541. The sources of information on the various nonresearch programs at NRL are listed in the *Review* chapter entitled "Programs for Professional Development."

HIGHLIGHTS OF NRL RESEARCH IN 1986

Antimalarial Drugs

Structures were identified for a novel class of antimalarial drugs having a new type of silver coordination. This was a collaborative effort with the Walter Reed Army Research Institute, where the drug was synthesized.

***

Ultralow-Loss Optical Fiber

Glass fibers having an optical loss of 0.9 dB/km at 2.5 μm, with a potential for 0.01 dB/km, were produced from zirconium, barium, lanthanum, aluminum, and sodium fluorides as a replacement for silica glass in long-length glass communication links.

***

Tracking Algorithm

A new monotonic Lagrangian grid algorithm was developed to provide rapid access of computerized data on the near neighbors of any object in many-body systems ranging from battlefield scenarios to molecular dynamics simulations of biological arrays.

***

Radar Backscatter

Effects of the sea-air temperature differential and wind stress on radar backscatter were determined through both airborne and sea-surface measurements; the findings are important in radar imagery surveillance.

***

Aerogeophysical Sensing

NRL's airborne geophysical sensor suite, in collaboration with Columbia University and the governments of Chile and Argentina, was used in the remote detection of anomalies in magnetic and gravity fields caused by the earth's crustal variations beneath the ice-covered Weddell Sea in the Antarctic.

***

Star Tracker

A radiation-hardened star tracker has been developed. It uses a silicon charge injection device under microprocessor control to achieve a tracking accuracy of one part in ten thousand within its field of view.

***

Radiation Effects Satellite

A system was designed and tested for the measurement of radiation effects on integrated circuits. It will be flown on the Combined Release and Radiation Effects Satellite, where it will measure in-orbit total dose and single-event upset performance of devices planned for satellites of the 1990s.

***

Wideband Radar Modules

Power transistors and solid-state transmitter architectures for wideband high-power shipboard radars were developed. These highly reliable modules provide unprecedented flexibility in radar waveform selection in meeting specific operational needs.

***

Chemical Microsensor

Surface acoustic wave chemical microsensors were shown to discriminate between CW agents and benign species. Specific chemical selectivity is provided by arrays of the devices that have sensitivities exceeding 10 ppb and response times of seconds.

***

Diode-Pumped Holmium Laser

For the first time, a diode-pumped nonneodymium rare-earth laser based on the 2.1-μm holmium transition was demonstrated. Highly scalable infrared laser sources will have profound implications in a wide range of naval applications.

***

Pulsed-Power Generation

A high-energy density pulser (PAWN) was developed. It uses inductive (magnetic) energy storage with pulse compression by staged opening switches to drive loads at megaampere current levels. System size reduction by two orders of magnitude over conventional generators is anticipated.

***

Radiation-Hardened GaAs Devices

Undoped p-AlGaAs buffer layers grown by molecular-beam epitaxy were shown to reduce, by one order of magnitude, the long-term transient response resulting from 40 MeV electron and flash X-ray irradiation of GaAs field effect transistors.

***

Ultraviolet and X-Ray Charge-Coupled Imager

A charge-coupled device imager sensitive to short-wave radiation was designed and tested. Optimized backside layers resulted in an ultraviolet quantum efficiency of 20%; lightly doped silicon produced a ten-fold improvement in X-ray sensitivity.

***

Acoustic Propagation Scattering Model

The ocean-refraction bathymetric scattering (ORBS) model was developed as the first three-dimensional acoustic model that incorporates scattering caused by statistically described ocean bathymetry and refraction in the water column. The model has been used successfully to explain angular spreading in the mid-Atlantic Ridge area.

***

Electronic Ceramics with Ordered Voids

Techniques were developed to add to solids voids as small as 50 μm in a highly organized way. Both strength and toughness of PZT hydrophone materials were improved by the process. Finite difference modelling was used to explain the experimental results.

NRL maintains a strong interest in the regions far above the natural habitat of the Navy through research carried out by the Space Science Division in the fields of astrophysics and astronomy, atmospheric science, and solar-terrestrial physics. Results are important to radio communications, weather prediction, and understanding natural radiation and geophysical phenomena. Spacecraft engineering, spacecraft systems development, and ground command and control stations are among the concerns of the Naval Center for Space Technology.

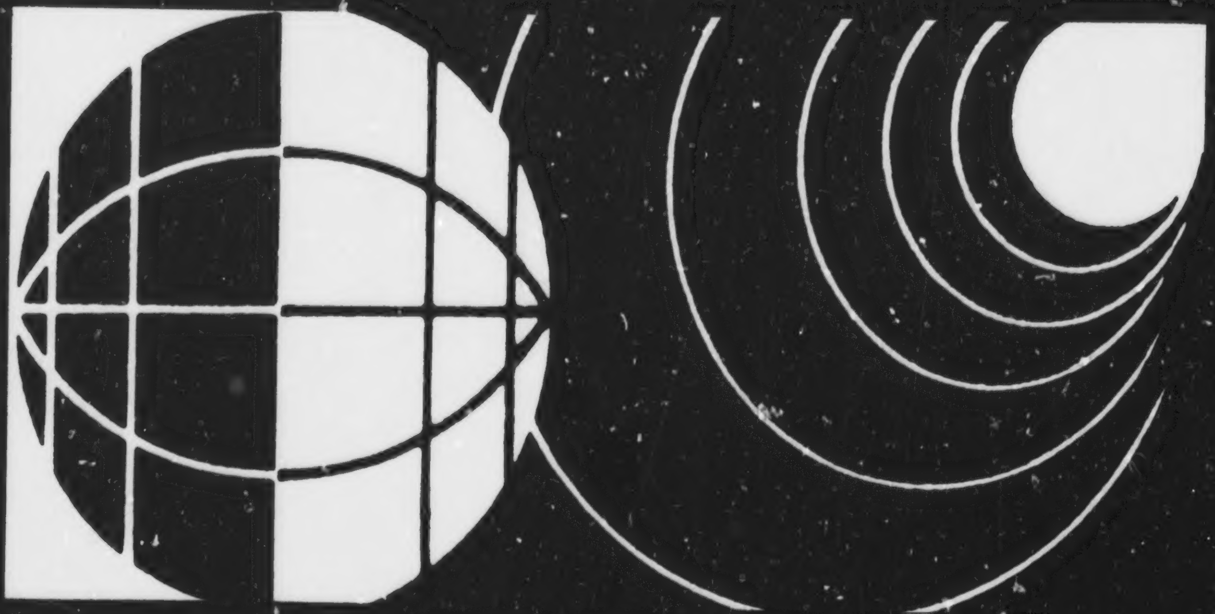

INNER AND OUTER SPACE

INNER
AND
OUTER
SPACE

35 **Far Ultraviolet Imagery of Comet Halley from Sounding Rockets**
Robert P. McCoy and George R. Carruthers

38 **XLA-The X-ray Large Array for the Space Station**
Kent Wood and Herbert Gursky

41 **Detection of Anti-Matter in the Galaxy**
Gerald H. Share and Robert L. Kinzer

43 **The Coronae of Giant Stars**
Spiro K. Antiochos

45 **Holograms Made with Laser Diodes for Use in a Satellite Communications Link**
G.C. Gilbreath and Anne E. Clement

Far Ultraviolet Imagery of Comet Halley from Sounding Rockets

R. P. McCoy and G. R. Carruthers
Space Science Division

No other comet in history has been more thoroughly studied than comet Halley. During its 1986 apparition, comet Halley was the focus of an unprecedented array of scientific investigations spearheaded by an international flotilla of six flyby spacecraft and supported by a multitude of observations from Earth-orbiting satellites, sounding rockets, aircraft, and mountaintop observatories. While undoubtedly most of this intense scientific activity was due to the notoriety of this most popular of all comets, it nonetheless provided a unique opportunity to study a rare natural phenomena exhibiting a wide range of chemical physical processes. Cometary nuclei, described as "dirty snowballs" by Fred Whipple, are believed to consist of frozen volatile materials (mainly water ice) and dust particles. Presumably, they represent leftover material from the formation of the solar system. Therefore, the study of comets provides an opportunity to examine the compositional and physical state of the material from which Earth and its planets were formed. As a comet nears the Sun, its frozen gases are warmed and sublimate to form an atmosphere, or coma, about the nucleus. A complex set of photochemical and plasma reactions take place that break down the original "parent" molecules into their elemental atomic constituents.

Observations of these "daughter" atoms can be used to infer the composition and production characteristics of the parent molecules. Most of the major daughter atoms in comets (H, C, O, and S) have strong resonance lines in the far ultraviolet (UV) and can be observed from above Earth's atmosphere with a satellite or sounding rocket.

The Rocket Observations: On February 24 and March 13, 1986 we launched a sounding rocket from White Sands Missile Range, New Mexico, to obtain far-UV spectral images of comet Halley. The February flight occurred at the first opportunity to observe the comet after perihelion, and the second flight was timed to match the flyby of the European *Giotto* spacecraft. The NRL rockets represented two of four rockets launched to observe the comet.

Both launches occurred before dawn to allow observations of the comet before sunrise. The rockets carried the far-UV imaging instrumentation to an apogee of 312 km, well above the ultraviolet absorbing layers of Earth's atmosphere. The science payload was recovered by parachute.

Instrumentation: The instrument payload shown in Fig. 1 consisted of two electrographic Schmidt cameras. Figure 2 shows the scientific payload. Similar versions of these cameras were on board the Apollo 16 mission, Skylab, and several

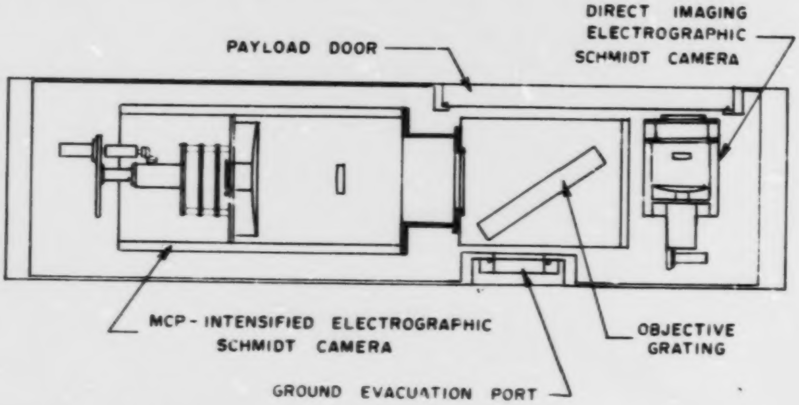
PAYLOAD DOOR
DIRECT IMAGING ELECTROGRAPHIC SCHMIDT CAMERA
MCP - INTENSIFIED ELECTROGRAPHIC SCHMIDT CAMERA
OBJECTIVE GRATING
GROUND EVACUATION PORT

Fig. 1 – Optical layout of the comet Halley far-UV sounding rocket payload

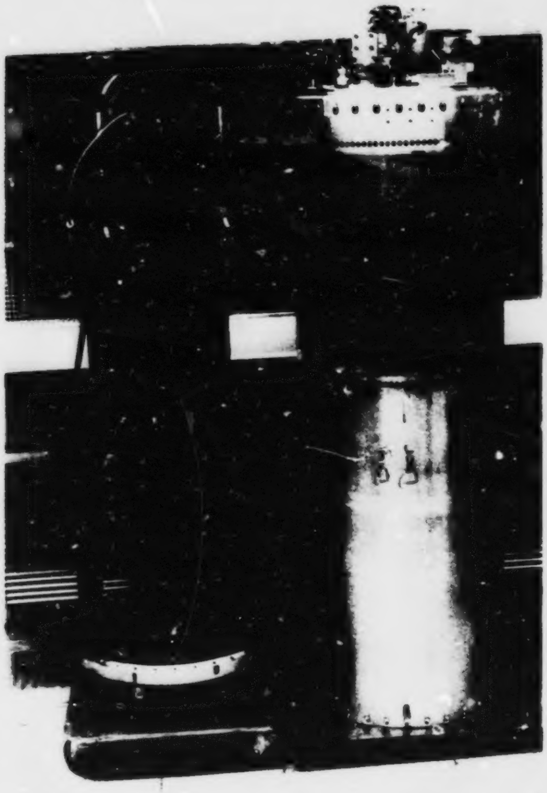

Fig. 2 – Scientific payload showing the internal instrument structure (left), and the exterior skin section with its opening door (right).

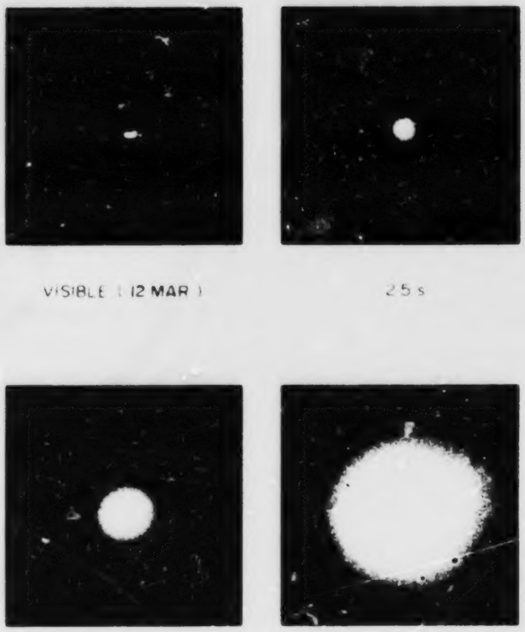

VISIBLE (12 MAR.) 2.5 s 9.5 s 29.5 s

Fig. 3 – Gray scale images of comet Halley at the hydrogen Lyman-alpha wavelength obtained with the direct imaging camera on March 13. Three different exposure times help reveal the structure of the emitting hydrogen cloud around the comet. A visible photograph (to the same scale) is included for comparison.

sounding rockets. One camera obtained direct images of the comet at the hydrogen Lyman-alpha (121.6 nm) line. The second camera was pointed at a plane grating to obtain objective spectra of the comet over the wavelength range 125.0 to 200.0 nm. This spectral range includes the bright cometary resonance lines of oxygen (130.4 nm), carbon (156.1 nm, 165.7 nm), and sulfur (181.4 nm).

Observations: Figure 3 shows the gray scale images of the comet obtained on March 13 with the direct imaging camera. This figure is a collage of images with three separate exposure times and a comparison with a ground based visible photograph (to the same scale) taken on the previous day. The Lyman-alpha images show an extensive cloud of hydrogen atoms surrounding the comet and extending tens of millions of kilometers from the nucleus. The large size of the hydrogen coma is due to the high velocity imparted to the lightweight hydrogen atoms in the photodissociation of water and other hydrogen compounds by ultraviolet sunlight.

The magnitude of the size of the hydrogen coma can be more easily visualized from Fig. 4, which is a false-color enhancement of a digitized version of one of the images in Fig. 3. The circle to the left that shows the direction of the Sun relative to the comet has been drawn to scale showing the actual size of the Sun for comparison. Even though the nucleus, as observed from the *Giotto* spacecraft, was only 15 km long, the hydrogen coma surrounding the comet and observed during this rocket flight was the largest object in the solar system. The distortion of the image from circular

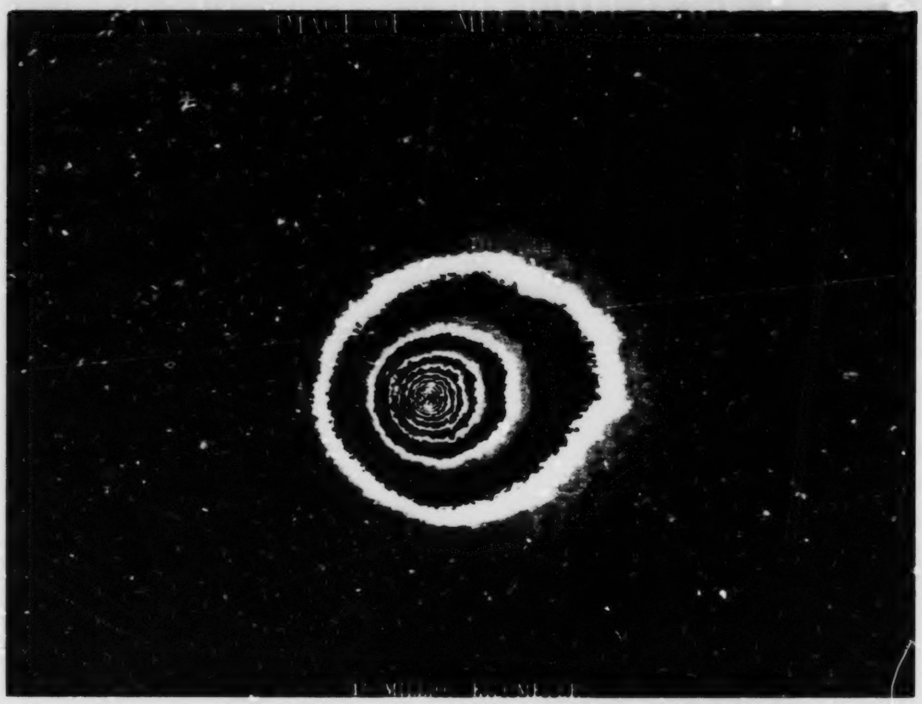

Fig. 4 – A false–color computer enhancement of the March 13 hydrogen Lyman–alpha image of comet Halley. This image is a composite of a 30–s exposure (outer regions) and a 10–s exposure (central region). The circle to the left shows the direction of the Sun'relative to the comet and has been drawn to scale to show the enormous size of the hydrogen cloud surrounding the comet.

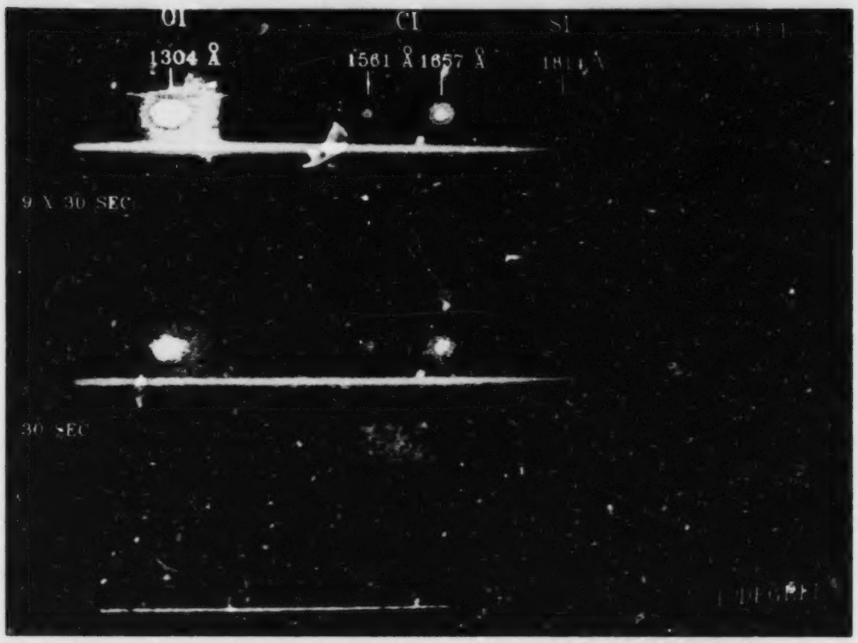

Fig. 5 – False–color computer enhancements of far–UV spectrograms of comet Halley obtained with the rocket flight on February 24. The three panels show a 9–s, 30–s, and sum of nine 30–s exposures. The spectrograms show images of the oxygen, carbon, and sulfur clouds surrounding the comet. The horizontal streaks are spectra of bright UV stars in the field.

BEST COPY AVAILABLE

Table 1 — Atomic and Molecular Production Rates Inferred from Sounding Rocket Observations on February 24 and March 13, 1987

Species	Production Rate (atoms/s)
H (Feb 24)	1.9×10^{30}
O	4.2×10^{29}
C	8.4×10^{28}
S	2.4×10^{27}
WATER	9.5×10^{29}
H (Mar 13)	1.4×10^{30}
O	1.0×10^{30}
C	1.0×10^{29}
WATER	7.0×10^{29}

symmetry is due to the strong influence of solar radiation pressure on the hydrogen atoms.

Samples of false-color computer enhancements of the objective spectra obtained on the February 24 flight are shown in Fig. 5. Three sets of exposure times are displayed, and the images of the coma of comet Halley at O, C, and S resonance lines are apparent. Because these atoms are more massive and therefore slower moving than the H atoms, their comas are not as extensive as that observed at Lyman-alpha. The horizontal streaks in the image are objective spectra of bright UV stars, and the individual spots are star images in zero order from the grating.

Interpretation: These images have been interpreted with a simple radial outflow model to calculate the production rates and outflow characteristics of each atomic species. More complex models will be used to analyze in detail the intensity distribution within each image. Table 1 gives the results of the analysis for the production rates of H, O, C, and S for the two flights. Since the major source of atomic hydrogen is water, these results can be used to infer water production rates of comet Halley for the two observation dates. These results are in general agreement with measurements obtained by other investigations, including rocket flights (by Johns Hopkins University), the Pioneer Venus Orbiting Ultraviolet Spectrometer, and in situ measurements made during the *Giotto* flyby. Analyses of these data sets will lead to a much greater understanding of comets in general and of comet Halley in particular.

[Sponsored by ONR and NASA] ■

XLA-The X-ray Large Array for the Space Station

K. Wood and H. Gursky
Space Science Division

Since the first V2 rockets were used for research purposes in the United States, the Naval Research Laboratory has been a leader in exploiting new space capabilities as they emerge. Now that the nation has committed itself to a space station, this tradition is likely to continue. This article describes the XLA (Fig.6), a large facility proposed for the space station by NRL scientists and scientists from Stanford University and the University of Washington. Engineering design studies are currently under way at NASA's Marshall Space Flight Center.

XLA will comprise an array of proportional counters designed to record X-ray photons from distant cosmic sources (Fig. 7). The use of such detectors was pioneered by Herbert Friedman at NRL, initially on sounding rockets, culminating in counters comprising 1 m^2 on NASA's HEAO-1

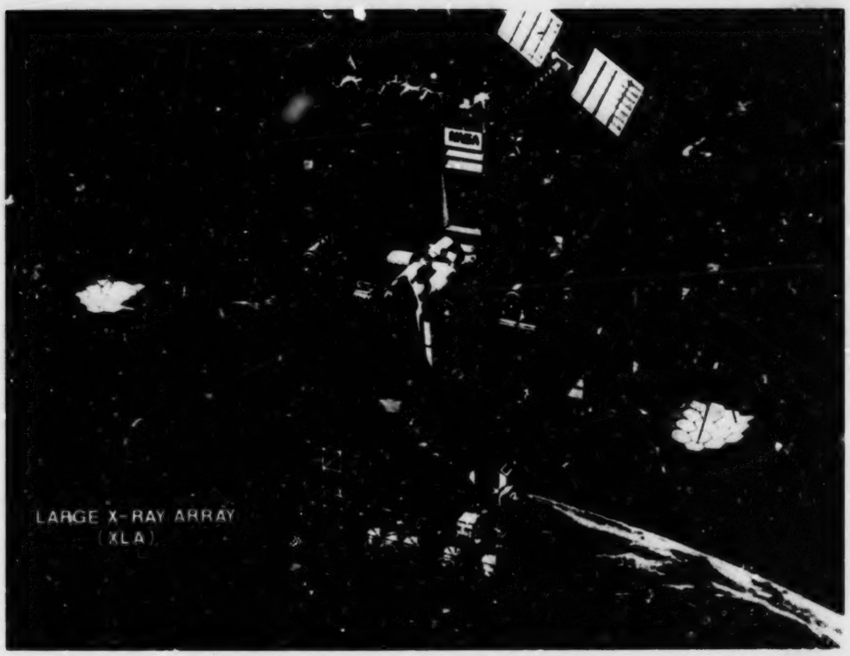

Fig. 6 – XLA mounted to double-keel version of NASA Space Station, courtesy NASA/MSFC

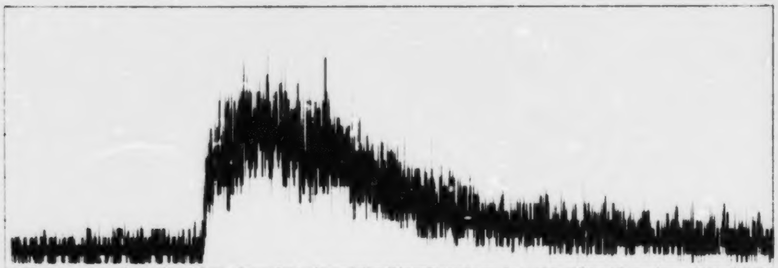

Fig. 7 – Time profile of an X-ray burst, from HEAO A-1. This phenomenon is a thermonuclear explosion on the surface of a neutron star. XLA would obtain many spectra during the rapid rise of the burst, which occurs in a few milliseconds.

spacecraft launched in 1977. XLA is intended to carry 100 m^2 of counters.

The discovery of cosmic X-ray sources occurred just 25 years ago. One of the authors (Herbert Gursky) was a member of the discovery team. The study of these objects has proven to be among the most fruitful of the space sciences and has led to the discovery of entirely novel objects in the sky, among which are neutron stars and black holes, ultrahigh density objects that test the limits of our understanding of the laws of physics. A key feature of these objects is the rapid time variability of their intensity–down to milliseconds–the study of which requires the large detection area of XLA (Fig.8).

Such variability is virtually the only information we have regarding the conditions near and even within these exotic objects. For example, the periodic emission seen from rotating neutron stars exhibits both short-term and long-term variations in periods that relate to the equation of state of the nuclear material in their interior and may even indicate the occurrence of earthquake-like phenomena on their surfaces.

BEST COPY AVAILABLE

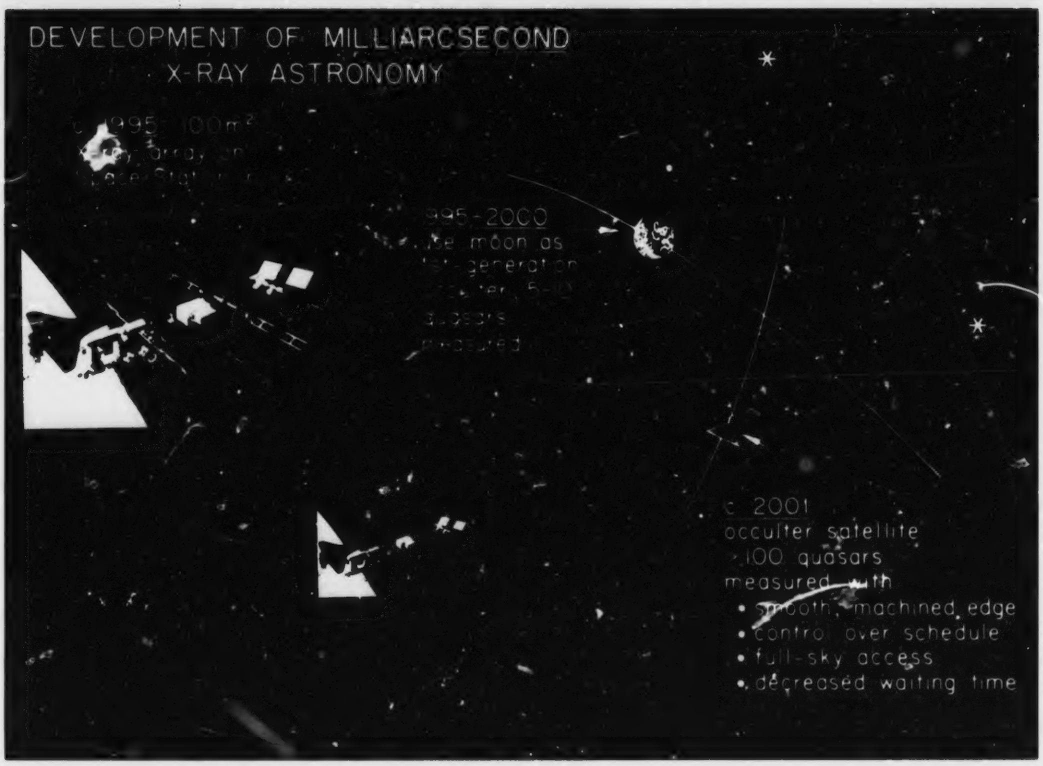
DEVELOPMENT OF MILLIARCSECOND
X-RAY ASTRONOMY
c. 1995 100m²
array on
1995-2000
use moon as
1st-generation
occulter, 5-10
quasars
measured
c. 2001
occulter satellite
>100 quasars
measured with
• smooth, machined edge
• control over schedule
• full-sky access
• decreased waiting time

Fig. 8 – Schematic showing use of XLA to develop milliarcsecond angular resolution in X rays

Variability occurs in every cosmic X-ray source on every time scale, presumably a reflection of the intrinsic instabilities that reflect underlying hydrodynamic and plasma processes. The range of physics and astronomical information that may yet be uncovered warrants the great interest in these measurements displayed by the scientific community.

An example is the millisecond binary X-ray pulsars, so far undetected, that are predicted as progenitors of millisecond pulsars seen at radio wavelengths. Such pulsars provide some of the best information we have on the general theory of relativity; for example, they have provided positive evidence for gravitational radiation, the gravitational analog of electromagnetic radiation. Several dozen candidates are in our galaxy, but detection of expected millisecond coherent pulsations is hampered by the high level of unpulsed flux from the source and by Doppler effects (frequency modulations) associated with orbital motions in binary systems. Detection of low levels of frequency-modulated pulsation requires short integration times, high signal-to-noise ratios, and new data reduction techniques, all of which mandate a large-area instrument such as XLA. The general principle is to search a large number of trial binary orbits that span the range of possible orbits. Computational cost becomes critical, and two strategies to minimize it were devised in 1986. One of these is to parametrize the orbit in such a manner that the dimensionality of the search is reduced from three orbit parameters to one. Another is to implement the search on an optical computer, incorporating the efficient parametrization. These methods improve sensitivity by as much as a factor of ten.

XLA represents an ideal use of the new capability created by the Space Station. It will be assembled at the station, its data will be gathered

BEST COPY AVAILABLE

there, and it will benefit from local, routine maintenance. One maintenance activity is data collection. The large aperture leads to photon rates exceeding several million counts per second that will result in data rates greater than 100 MB/s. Data will be accumulated on optical mass storage units that periodically are returned to Earth. Optical computations can also be used to preprocess data in orbit. XLA is a prime example of the kind of scientific payload that only becomes possible with the advent of the Space Station. The individual counters in the array are not the main novelty, since they are similar to and derive from those flown earlier by NRL on HEAO-1 and SPARTAN-1. XLA has roughly 500 such units. The new engineering challenges include low-cost replication of space hardware, inertial space pointing and control of a large structure attached to the Space Station, and optical data-handling in orbit.

The use of XLA is not restricted to fast timing applications. For example, whenever an X-ray source can be detected with good signal-to-noise in a millisecond, an orbiting occulting edge at a large distance from the XLA can be used to measure diameters of X-ray sources to milliarcseconds, comparable to the best resolution generally achievable in astronomy. The limb of the moon itself is a suitable edge, although it suffers from being fairly rough and from not accessing the full sky. In 1986, K. Wood of NRL and J. Breakwell of Stanford University proposed the creation of an artificial, steerable occulting edge with an orbiting satellite to provide occultations at any desired point on the sky.

The improvement in sensor capability represented by XLA and the engineering issues involved in it impact a variety of Navy interests. XLA type arrays provide for a qualitative improvement in space surveillance of radioactive material. Engineering concepts explored in the process of developing the XLA concept include optical computation and data handling in orbit, control and pointing of large structures in space, and high-precision satellite navigation in high orbits. There can be other navigational benefits. If fast X-ray pulsars indeed have the expected characteristics, they will themselves become ultraprecise clocks. More generally, use of the Space Station opens an entirely novel capability that can be exploited for the benefit of the Navy's space R&D effort.

[Sponsored by ONR] ■

Detection of Anti-Matter in the Galaxy

G. Share and R. Kinzer
Space Science Division

An instrument primarily designed to study high-energy emissions from the sun has recently been used to show that our Milky Way Galaxy emits a diffuse glow of gamma radiation with an energy of 511 keV. This is the characteristic energy of gamma rays emitted when electrons and their antimatter counterparts, known as positrons, annihilate one another (Fig. 9). The presence of a significant number of positrons distributed throughout the Galaxy has been suspected for a variety of reasons; this is the first definitive evidence of their existence.

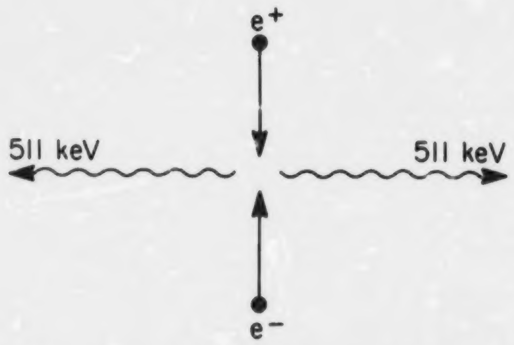

Fig. 9 – Interstellar electrons and positrons (antimatter electrons) annihilate each other and produce two 511 keV gamma rays. At least 90% of the time, the positron and electron first form a hydrogenlike atom called positronium before annihilating.

The instrument used in this analysis is a gamma-ray spectrometer on NASA's Solar Maximum Mission (SMM) satellite that has been in almost continuous operation since February 1980. A team of scientists at NRL, the University of New Hampshire, and the Max Planck Institute in Garching, Federal Republic of Germany (FRG), has been analyzing data contained on more than 2500 magnetic tapes thus far received from NASA. With this analysis significant advances have been made in the understanding of solar flares, cosmic gamma ray bursts, and production of radioactive materials in exploding stars. A description of the instrument and summaries of some of these discoveries can be found in earlier issues of the NRL Review [1-4].

The use of the SMM spectrometer as a tool for detecting antimatter in the interstellar medium results from a DoD need to determine the radioactive background in space. Unveiling the various sources of background has led to an improved understanding of the environment in which sensitive gamma-ray observations must be made. Detection of weak signals similar to the kind that are described here can be significant to our national security [5].

Galactic Emission: The galactic 511 keV gamma ray line is buried beneath an intense glow of radiation produced locally in the instrument, the spacecraft, and the atmosphere by bombardment of particles stored in Earth's radiation belts and energetic nuclei in cosmic radiation. A limiting feature of the SMM spectrometer is its broad field of view, about 120° at half maximum. This makes the task of separating the source from background quite difficult. The next generation of satellite instrumentation for gamma-ray astronomy addresses this problem; it is being developed by NRL for NASA's Gamma Ray Observatory (GRO). The GRO is currently scheduled for launch in early 1990.

Without the sophisticated systems soon to be available on the GRO, it has been necessary to understand the background in orbit to reveal the galactic emission. This has been done in very much the same way as was the discovery of galactic radio waves in the 1940's. That early discovery spawned the field of radio astronomy, which has provided the means for viewing the universe.

In December, each year, the sun passes within a few degrees of the center of our Galaxy. As the plane of the Galaxy traverses the aperture, the solar-oriented gamma-ray spectrometer can search for a coincident increase in the intensity of 511 keV annihilation radiation. This increase has, in fact, been observed in each of the years that the spectrometer was in operation, as illustrated in the lower plot of Fig. 10. The plot presents data obtained with the spectrometer pointed toward the sky. This annual increase is not observed when the spectrometer's aperture is blocked by Earth, as it is for the upper set of data. The gradual rise exhibited in both sets of data is due to the production in the instrument of the positron-emitting radioactive nucleus ^{22}Na (half-life 2.6 yr).

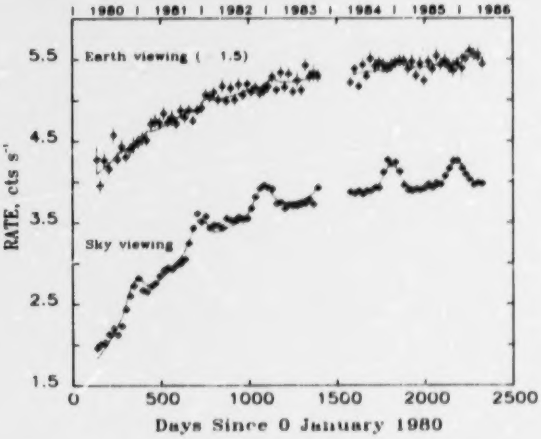

Fig. 10 – Time variation of the intensity of 511 keV gamma radiation measured by the gamma-ray spectrometer on SMM from launch until 1986. The lower plots show data accumulated with the spectrometer viewing the sky, and the upper plot is for data accumulated with Earth blocking the aperture. The annual increase in intensity in the sky-viewing data in December is due to emission from galactic 511 keV radiation entering the spectrometer's aperture.

One of the remarkable features of this galactic 511 keV radiation is that the variation is less than 30% over the 6 years during which the measurements have been made. This fact has been used along with measurements made with balloon-borne instruments having much

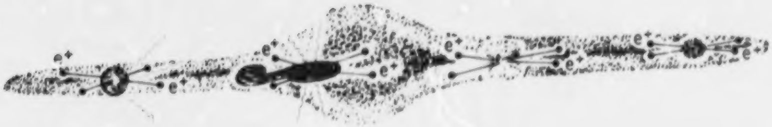

Fig. 11 – Galactic positrons can be produced in a variety of celestial objects, including supernovae, novae, pulsars, black holes, and massive stars. The positrons can live for over 10^5 years before capturing an electron and annihilating to form 511 keV radiation. This produces a diffuse glow of 511 keV radiation from the Galaxy.

narrower fields of view to infer that the radiation is broadly distributed in the Galaxy.

Emission Sources: We estimate that the mass of interstellar positrons responsible for the observed flux of annihilation line gamma rays is equivalent to about 8 times the mass of our planet Earth. Where these positrons come from is not known. Various sources have been suggested, including the most spectacular objects in the sky such as supernovae, novae, pulsars, and black holes, as well as more quiescent objects such as red giant and other massive stars (Fig. 11). Present theory suggests that supernovae may provide the bulk of the galactic positrons. Detailed measurements of the spatial distribution of these annihilation photons will assist in revealing their true origin and may, like the early measurements of galactic radio waves, mark the maturing of the fledgling field of gamma-ray astronomy.

[Sponsored by NASA]

References

1. G.H. Share, 1981 NRL Review, p. 106.
2. G.H. Share and P.L. Nolan, 1983 NRL Review, p. 117.
3. G.H. Share, 1984 NRL Review, p. 135.
4. G.H. Share, R.L. Kinzer, and J.D. Kurfess, 1985 NRL Review, p. 114.
5. G.H. Share et al., "Detection of Artificial Sources of Nuclear Radiation in Space," NRL Memorandum Report 4596 (1981). ■

The Coronae of Giant Stars

Spiro K. Antiochos
Space Science Division

One of the most interesting results of recent astronomical surveys with satellite-borne ultraviolet (UV) and X-ray telescopes is the discovery of a "dividing line" in the Hertzsprung-Russell diagram. In 1979, Linsky and Haisch [1] were the first to find that *cool* (photospheric temperatures less than 7000 K) giant and supergiant stars separate into two distinct groups: (a) a *solar-type* group to the left of the dividing line, manifesting both a chromosphere (plasma in the temperature range 5000 to 20,000 K) and a corona (plasma with temperatures greater than 100,000 K); and (b) a *nonsolar-type* group to the right of the dividing line, showing only a chromosphere. Stars in the first group are strong X-ray sources, like the Sun; whereas those in the second group have no detectable X-ray emission.

This result is puzzling because stars in the second group are believed to have all the necessary ingredients for producing a hot corona. The Sun's corona is due to the interaction of the solar magnetic field with the convective motions of the dense photospheric plasma. The bulk of the Sun's X-ray emission originates in small active regions that cover only about 3% of the solar surface and that have the strongest magnetic fields. The cool giants and supergiants also have convective motions and are expected to have strong magnetic fields as well. We propose that the explanation for the dividing line is that the giant stars have a much lower surface gravity g than the Sun.

The Theoretical Model: The fundamental structure of coronal plasma is known to be that of a loop; each loop corresponds to a magnetic flux tube that confines the hot plasma. The state of the plasma is determined by force balance between thermal pressure, magnetic pressure, and gravity, and by energy balance between radiation, conduction, and coronal heating. Recently we have found that under certain conditions, new cool solutions to the equilibrium equations appear in addition to the usual hot solutions [2]. The cool solutions are characterized by a maximum plasma temperature less than 100,000 K, whereas in the usual models the maximum temperature must be greater than 100,000 K. The reason for this critical temperature is that the radiative loss rate of solarlike plasma has a maximum at 100,000 K. For a particular loop, the physical parameter that determines whether the cool solution exists is the ratio of the gravitational scale height (~ $10^6/g$ km) of plasma at a temperature of 100,000 K to the loop height. If this ratio is less than unity, only the hot solution is possible, but if it is of order or greater than unity, the cool solution is possible.

The important conclusion of our work on the cool solutions is that a coronal active region divides naturally into two types of loops [2]. Those flux tubes, with heights greater than a critical height (5000 km in the case of the Sun), must be filled with hot, X-ray-emitting plasma, while those with lower heights will be filled with cool material, too cool to produce X rays.

Comparison with Observations: Let us now consider the implications of the cool solutions on observations. Figure 12 is a Hertzsprung-Russell (H-R) diagram showing all cool giant stars that have been detected in X rays and that are not known to be members of a binary or otherwise peculiar; also shown are some representative main sequence stars like the Sun. The size of each solid circle indicates the ratio of X ray to bolometric luminosity for that star; each broken circle indicates that no X rays were detected. The dividing line proposed by Linsky and Haisch [1] is shown as a straight dashed line. Contours of constant ϕ are shown by solid lines. Note that the main sequence runs along the bottom of the diagram.

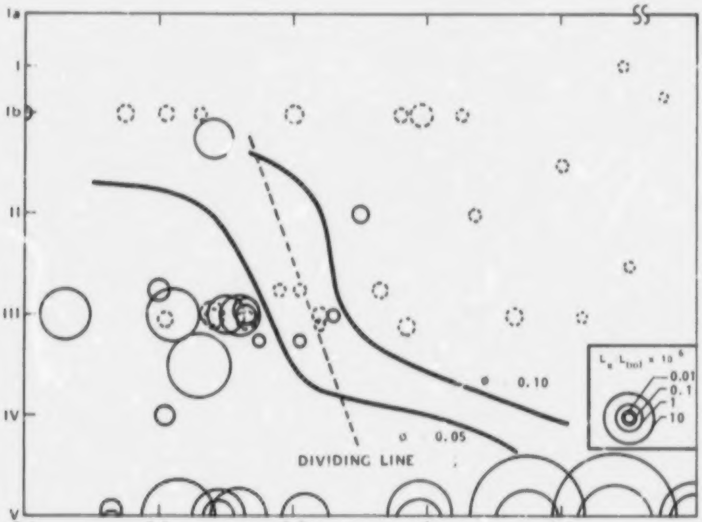

Fig. 12 – A Hertzsprung–Russell diagram showing the presence (solid circles) or absence (broken circles) of X-ray emission for all the cool, single stars observed by the EINSTEIN X-ray telescope. The ordinate indicates luminosity class (the stars' sizes increase upward), the abscissa indicates surface color (the stars' temperatures decrease to the right).

Also plotted in the figure is the theoretical dividing line predicted by our model, $\phi = 10^6/gR$. This assumes that the sizes of stellar magnetic regions scale linearly with stellar radius R, so that the height of a typical active region is given by ϕR. The Sun has a value of $\phi = 0.1$. There is a fair amount of uncertainty in the values for g and R, especially for the supergiant stars Also, variations in stellar evolution and abundances can result in differences in g and R at any given point on the H-R diagram. Hence we no longer expect a sharp dividing line based solely on spectral type or color. Because of these uncertainties, it is striking how well the curve $\phi = 0.1$ agrees with the observed separation of stars into those with and those without X-ray emission. It parallels the Linsky-Haisch dividing line in the giant and supergiant region of the diagram, and it also turns over at the main sequence in agreement with the observation that main-sequence stars of all types exhibit X-ray emission. We conclude from this result that the coronal dividing line can be understood simply in the terms of the static loop models once the effects of gravity are fully understood. This indicates that the fundamental processes of coronal heating and magnetic activity are likely to be the same in all cool stars and thereby emphasize the importance of understanding the solar corona.

[Sponsored by NASA and ONR]

References

1. J.L. Linsky and B.M. Haisch, "Outer Atmospheres of Cool Stars. I. The Sharp Division into Solar-Type and Nonsolar-Type Stars," *Astrophys. J. Lett.* **229**, L27 (1979).

2. S.K. Antiochos and G. Noci, "The Structure of the Static Corona and Transition Region," *Astrophys. J*, **301**, 440 (1986).

3. S.K. Antiochos, M. Haisch, and R.A. Stern, "On the Dividing Line for Stellar Coronae," *Astrophys. J.* **307**, L55-L59 (1986). ■

Holograms Made with Laser Diodes for Use in a Satellite Communications Link

G. C. Gilbreath and A. E. Clement
Naval Center for Space Technology

Holographic optical elements offer a compelling alternative to heavy and massive conventional optical solutions required to direct and correct a laser diode or diode array's beamfront for satellite communications applications. A hologram is compact, has low mass, and can enable solutions that cannot be achieved by using conventional optics. At present, however, no holographic recording medium is both sensitive at the wavelengths of interest (750 to 900 nm) and diffracts efficiently. A two-step construction, three-step reconstruction approach is being investigated whereby a "master" is made with the laser diode and an infrared (IR)-sensitive emulsion. This interference pattern is then transferred to a second hologram, which is a phase volume device made in a material that offers very high diffraction efficiencies [1].

A technique has been developed that enables construction of holograms made with laser diodes in IR-sensitive material that produces consistently good holographic recordings of a given interference pattern [2].

Modal instability resulting in radiation at different frequencies characterizes laser diode behavior. This precludes holographic recording and can cause unpredictable reconstruction. Consequently, temperature stabilization is required for a given current density to achieve radiation at a specific frequency. However, active mode-stabilization can cause environmental *noise* that would also preclude holographic construction. Our technique exploits the high power of the diode in combination with the extreme sensitivity of IR-sensitive material to circumvent the tendency of the laser to "mode-hop" when not actively cooled.

A 30-mW Sharp single-mode diode was initially characterized as wavefront quality and modal stability for a specific current density-temperature window. The diode was mode-stabilized through active cooling by using a thermoelectric cooler.

A Michelson interferometer determined the coherence length. With this type of interferometer, one of the mirrors is displaced and fringe visibility, $V(r)$, is monitored. $V(r)$ is defined by Michelson as:

$$V(r) = (I_{max} - I_{min}) / (I_{max} + I_{min}) \qquad (1)$$

where I_{max} and I_{min} are the irradiances measured at maximum and adjacent minimum fringes.

The limit to path displacement is $V(r)$ degraded so that it precludes meaningful holographic recording. Figure 13 illustrates the bench configuration used. This approach enabled us to monitor modal stability by using a Candela LS-1 spectrometer, beam quality by using a CCD field array camera, and fringe contrast by using a CCD linescan camera.

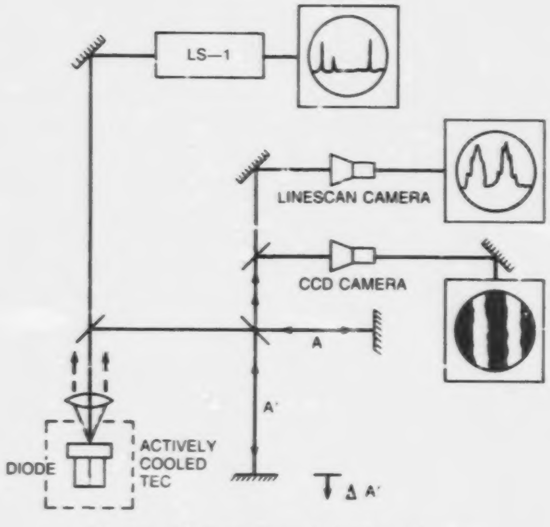

Fig. 13 - IR diode characterization using a Michelson Interferometer

The thermoelectric cooler (TEC) used to cool the laser was turned off, and the mode behavior was monitored as the diode warmed. The mode at which the diode had stabilized during active cooling began to lose amplitude in about 20 s and suffered a "mode-hop" in little more than a minute. This resulted in fringe "washout," thereby preventing meaningful holographic recording. This investigation enabled us to learn the time window for the exposure period when the diode was not actively cooled.

The resolution of the IR- sensitive emulsion is low (on the order of 100 to 200 line pairs/mm). Consequently, the angle of construction defined by Bragg's law must be small, and the relationship is defined as:

$$\theta = \sin^{-1} [\lambda / 2d] \qquad (2)$$

where λ is the wavelength, and d is the grating spacing that is the inverse of the resolution. Good control of small angles of construction can be achieved with a Mach-Zehnder interferometer. This type of interferometer was employed to construct the holograms. Part of the light was split off to allow monitoring of modal stability throughout the recording procedure. Figure 14 shows the optical bench configuration used to construct absorption plane wave gratings with the Sharp diode that was actively cooled with a TEC. Spectroscopic plates are typically used for infrared astronomy and are very sensitive. Energy densities of the plates were found experimentally to be on the order of 56 nJ/cm² at 842.4 nm. The high sensitivity in combination with the high power available from the laser diode allowed extremely short exposure times. Consequently, the cooler could be turned off during exposure periods. The modal stability was monitored by checking the output of the LS-1 spectrometer immediately prior to and just after exposure.

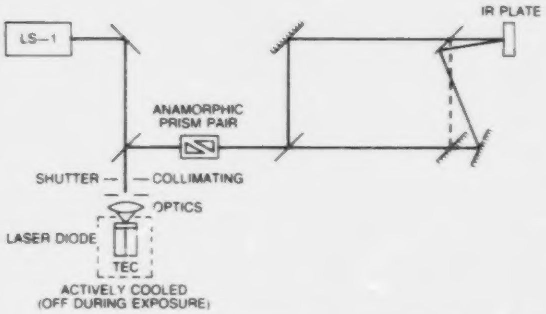

Fig. 14 - IR master construction configuration

Table 1—IR Master Visibility and Diffraction Efficiency* Measured with 632.8 nm

SAMPLE	$d(\mu)$	$V(r)$	$\eta_0(\%)$	$\eta_1(\%)$	O.D.†
3	8.0	0.296	66.0	0.81	0.324
5	16.2	0.673	70.1	3.36	0.398
8	71.6	0.930	69.7	14.60	0.194
10	11.4	0.549	82.1	1.90	0.287
15	7.2	0.097	68.8	0.54	0.375

*η_0 is diffraction efficiency out of zero order

*η_1 is diffraction efficiency into first order

†Specular

This procedure enhanced environmental stability during recording and ensured modal stability. Exposed plates were developed using standard D-19 processing techniques.

Diffraction efficiencies out of the zero order and into the first order were measured with a 632.8 nm helium neon source and a photodetector. Recorded fringe quality and visibility were examined and measured. Table 1 lists fringe spacing, *d*, diffraction efficiencies, optical densities, and visibility for selected samples. Gratings made by using smaller values for *d* yielded significantly lower diffraction efficiencies.

Selected masters are now being incorporated into the larger experiment wherein their recorded beamfronts are being transferred to a highly diffractive medium. At present, experimentation includes investigation with dichromated gelatin and photoresist.

References

1. C. Gilbreath-Frandsen, W.H. Carter, and J.W. Wagner, *SPIE Proc.* **600**, 81 (1985).
2. G.C. Gilbreath, A.E. Clement, and J.W. Wagner, *SPIE Proc.* **747** (1987). ■

Sound, sea, and the Navy are inextricably entwined. Sonar is seeing undersea. Acoustic and water waves are the signatures of ships. All of this and much more are the subjects of basic and applied research in the Acoustic Division and in NRL's Underwater Sound Reference Detachment in Orlando, Florida. Both depth and range are provided by their study of the ocean environment, target tracking, acoustically active materials, and physical acoustics. The vital technology of underwater sound measurement is one of the signal concerns of the Orlando facility.

SOUND AND THE SEA

BEST COPY AVAILABLE

SOUND AND THE SEA

51 **Active/Adaptive Noise Cancellation in a Liquid-Filled Pipe**
Eric W. Hendricks

53 **Steep and Breaking Deep Water Waves**
Owen M. Griffin and Steven E. Ramberg

56 **Rapid Three-Dimensional Ocean Acoustic Computations**
William A. Kuperman, Michael B. Porter, and Frank L. Ingenito

58 **Inertial Wave Dynamics**
Richard P. Mied, Gloria J. Lindemann, and Clifford L. Trump

62 **Nonlinear Salt-Finger Simulation**
Colin Y. Shen

64 **Ship-Wake Experiment for Remote Sensing**
Jack A.C. Kaiser, William D. Garrett, Steven E. Ramberg
and Rodney D. Peltzer

Active/Adaptive Noise Cancellation in a Liquid-Filled Pipe

E. W. Hendricks
Laboratory for Computational Physics and Fluid Dynamics

The reduction of low-frequency sound in pipes and piping systems is a problem of great practical importance. At NRL we are examining the potential utility of active sound cancellation in a liquid-filled pipe. Active sound cancellation ("anti-sound") has been recently applied to noise in air-filled pipes [1,2]. The "antisound" technique uses an acoustic signal generated by one or more sound sources placed in a system that destructively interferes with the unwanted noise field. Experiments conducted in air-filled pipes and ducts have shown the utility of active control for reducing noise consisting of pure tones, bandwidth-limited white noise, and transient pulses [3,4].

In our experiments with liquid-filled pipes, the dimensions and physical properties of the pipe employed were chosen to highlight the primary difference between typical air-filled and liquid-filled pipe applications. In the former the pipe wall acts as a rigid or nearly rigid structural element, whereas in the latter the finite loop stiffness of the pipe exerts a major influence on the propagation velocity of an acoustic disturbance in the pipe [5]. Our experiments were performed with "noise" generated by a sound source at one end of the liquid-filled pipe, with a second sound source located partway down the pipe serving as the cancellation source. We examined the extent to which this source could reduce the sound pressure level at the pipe outlet and in the liquid reservoir into which the pipe emptied. In all cases the cancellation source was driven by the output of a digital adaptive filter that continuously sampled the output of hydrophones located in the duct and reservoir.

Noise Reduction Apparatus: Figure 1 shows the experimental arrangement used in this work. It was composed of a long duct; two sound sources; three hydrophones; a large, water-filled reservoir; and a digital, adaptive electronic filter. Sound generated by the noise source propagated down the duct, past the detector hydrophone, the cancellation sound source, the performance (or error) hydrophone located at the pipe exit, and into the large water-filled reservoir.

The duct was an 8-in. (203.2 mm) diameter PVC pipe, as was the tee fitting used with the cancellation source. The duct wall was 0.5 in. (12.7 mm) thick. This duct rested on concrete blocks and wooden shims as shown in Fig. 1. Wooden cradles were constructed with rubber isolators to hold the brass-encased sound sources and to prevent noise from propagating through the concrete blocks and into the floor because of vibration of the sound sources. The pipe and

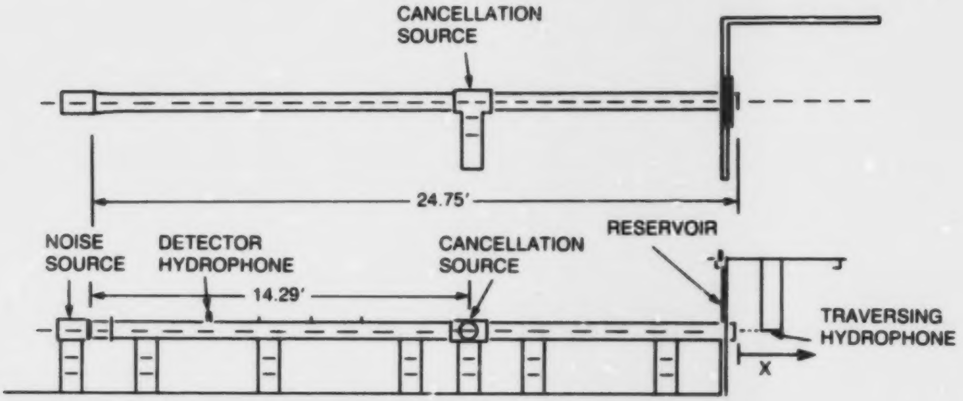

Fig. 1 – Experimental setup

reservoir were mechanically isolated by a flexible gasket to prevent transmission of vibrational energy between the two structures. The reservoir was 60 in. (1.52 m) in height, 20 ft. (6.1 m) in length, and 10 ft. (3.05 m) in width. The water level was 52 in. (1.32 m).

The digital, adaptive filter employed in the experiments was an implementation of the Wiener-Hopf least-mean-squares algorithm [6]. The filter was modified to allow external measurement of the difference between the performance and input signals, since the resulting error signal is formed in the duct itself by the linear superposition of the original unwanted noise and the output of the cancellation sound source. During our experiments it was determined that the filter performance was particularly sensitive to a time delay setting that accounted for the "time of flight" of an acoustic wave from the detector hydrophone to the cancellation source. We determined that the approximate value of this delay could be computed from a priori measurements of sound propagation velocity in the pipe.

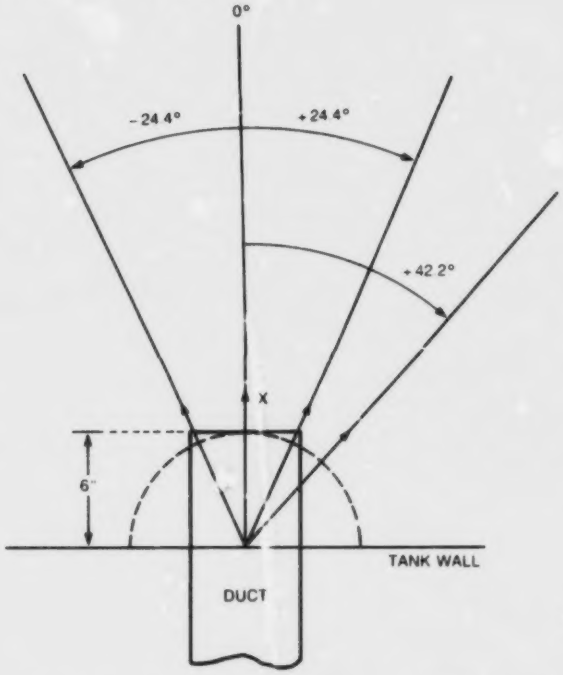

Fig. 2 – Coordinate system for measurements in the water reservoir (all coordinate lines lie in the horizontal plane passing through the pipe centerline)

Experiments were conducted in the duct system with the adaptive filter to determine the maximum possible attenuation of unwanted noise at the pipe exit duct and in the water reservoir, as well as the time required for adaptation to this condition. Figure 2 shows the coordinate system employed for hydrophone traverses in the liquid reservoir. These measurements were made on the horizontal plane through which the pipe centerline passes. The sound pressure level measurements were referenced to the ambient noise level in the tank with the sound sources turned off. (The ambient noise level was designated as 0 dB).

Results: Experimental results obtained at 100 Hz and 0° are shown in Fig. 3. At the open end of the pipe (X = 0.5), the uncancelled noise level was about 23 dB above the cancelled level. This differential decreases with increasing X because the sound pressure level in the tank, caused by the upstream noise source, decreases with X in the absence of cancellation, while the cancelled level at 100 Hz and 0° is essentially equal to the ambient noise level at all values of X. Filter adaptation times in the experiments were typically 0.33 to 0.38 s. Qualitatively similar results were obtained for sine waves of other frequencies and combinations of other frequencies along the 24.4° and 42.2° lines.

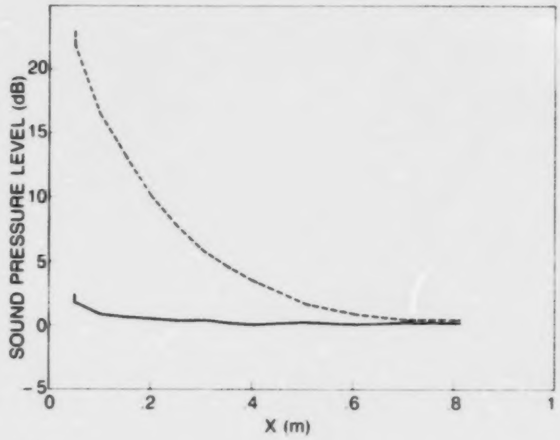

Fig. 3 – Measured sound pressure level in the water reservoir along the 0° coordinate line at 100 Hz (0, cancellation source off; x, cancellation source on)

BEST COPY AVAILABLE

Conclusions: Low-frequency noise at and emanating from the exit of a liquid-filled pipe is effectively reduced by active noise control. Reductions in the 20 dB range were observed. Moreover, the adaptation time of the digital, adaptive filter employed to control the active sound source was small. While improvements to the implementation employed herein can be incorporated, such as adaptive control of the time-delay setting for the adaptive filter, it is clear that active noise control is the only effective means of low-frequency noise control in liquid-filled pipes and piping systems.

This work was performed at NRL in collaboration with Robert J. Hansen, ONR Code 1215; and William G. Culbreth, American Society of Engineering Education Summer Faculty Member.

[Sponsored by ONR]

References

1. J.E. Ffowcs Williams, "Anti-Sound," *Proc. R. Soc. London, Ser. A* **395**, 63–88 (1984).
2. C.F. Ross, "Active Control of Sound," Dissertation, Queens' College, Cambridge, July 1980.
3. S.P. Klimov, A.A. Mazanikov, and V.V. Tyutekin, "Wideband Active System for the Suppression of Sound Fields in a Two Mode Waveguide," *Sov. Phys. Acoust.* **30**(5), 385–387 (1984).
4. J. Tichy, G.E. Warnaka, and L.A. Poole, "Active Noise Reduction Systems in Ducts," *ASME 84-WA/NCA-75*, 7 pp.
5. M.P. Horne and R.J. Hansen, "Sound Propagation in a Pipe Containing a Liquid of Comparable Acoustic Impedance," *J. Acoust. Soc. Am.* **71**(6), 1400–1405 (1982).
6. B. Widrow, J.R. Glover, Jr., et al., "Adaptive Noise Cancelling: Principles and Applications," *Proc. IEEE* **63**, 1692–1716 (1975). ■

Steep and Breaking Deep Water Waves

O. M. Griffin and S. E. Ramberg
Laboratory for Computational Physics
and Fluid Dynamics

The breaking processes associated with wave motions in deep water are poorly understood but have important naval applications. The interaction between waves (ship-generated and/or ambient) and surface currents often results in the production of waves that steepen to the point of breaking. Other applications include accurate descriptions of ocean surface dynamics, mixed layer dynamics, and remote sensing signatures obtained by a variety of both active and passive systems. These applications require a further basic understanding of the wave hydrodynamics up to and beyond the onset of breaking, and of the energy and momentum transfer processes during and after breaking.

Nonlinear wave flows such as these usually are considered to be irrotational up to the onset of breaking when turbulent flow and air entrainment processes are important. Breaking waves at sea also are three-dimensional, but many fundamental features can be determined by using simpler, two-dimensional approaches.

A computational and experimental study of deep-water wave-breaking is being made by the authors in collaboration with Professor William W. Schultz of the Department of Mechanical Engineering and Applied Mechanics at the University of Michigan. A numerical technique has been developed for the computation of steep asymmetric wave motions up to the incipient or onset stages of wave breaking [1], and it will be briefly described here. The computations are compared with recent measurements made at NRL and elsewhere of the limiting heights of deep-water waves [2].

Computational Model: Although formal analytical techniques have been developed for symmetric steep-gravity waves, unsteady and asymmetric steep-wave motions must be solved numerically. The most efficient of these algorithms are based on some form of boundary integral technique that has the advantage of requiring a solution only on the boundary of the computational domain instead of over the full domain. Thus the physical dimensions of the problem are reduced by one, which consequently reduces the complexity of the governing equations and reduces the computer resources required for an accurate solution. The method is valid for two-dimensional, steep, asymmetric waves in water of arbitrary depth. The complete formulation of the method and the assumptions on which it is based are described by Schultz et al. [1].

Wave Amplitude: Figure 4 shows a comparison between the computed wave crest profile results of two previous studies and the present one. The solved example problem had been given by McIver and Peregrine [3] in 1981. The results obtained in the NRL study have the advantages of being up to 50 times faster than one early approach [4] and of requiring a time step that is a factor of 10 to 20 larger than the time steps required by earlier methods. These reduced computing requirements will permit more extensive and realistic studies to be conducted. The initial wave amplitude of $a = 0.544$ in the example is sufficiently large to cause the forward face of the wave to form a jet, overturn, and to produce a plunging breaker. The three results are shown at a time just prior to the onset of breaking for this extreme condition. The onset of breaking in the computations is taken as that time when the implicit time integration fails to converge and the computed surface wave form becomes unstable.

The initial wave amplitude in Fig. 4 is always large enough to cause the wave to break. Two additional computations are shown in Figs. 5 and 6 for initial amplitudes of $a = 0.27$ and 0.28, respectively. A wave with initial amplitude $a = 0.27$ evolved in time and never broke, but a wave with an amplitude of $a = 0.28$ always broke after approximately 150 time steps. This represents the incipient stage of the breaking process.

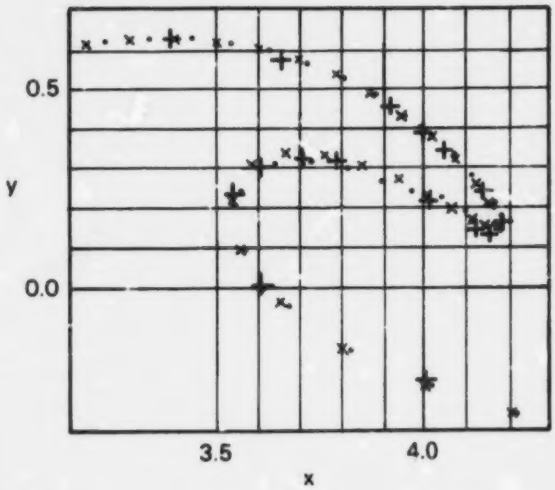

Fig. 4 – A comparison of recent NRL/U. of Michigan computations of a deep water plunging breaker profile (+) with the earlier computations of Longuet-Higgins and Cokelet [4] (.) and of Vinje and Brevig, 1981 (x). The initial wave amplitude was $a = 0.544$, and the profiles are shown at the time $t = 3.655$ just prior to breaking.

Limiting Wave Steepness: The limiting steepness or height of a progressive wave in deep water can be given simply by the relation $H = \alpha g T^2$, where H is the peak-to-trough wave height, T is the wave period, and g is the gravitational acceleration. The proportionality factor α is 0.27, based upon classical wave theory, and 0.21, based upon extensive recent experiments [2]. Thus the measured limiting wave height H is consistently less than the comparable prediction from classical wave theory by approximately 20%.

The value of α can also be estimated from the computations, with the result $\alpha = 0.020$, which is well within the experimental scatter shown by Ramberg and Griffin [2]. It needs to be emphasized that the concept of a limiting wave height or steepness applies to only the onset conditions for a wave breaking event. A breaking wave still can exist at a lower steepness after it has begun to break.

The results of these NRL computations and previous experiments conducted at NRL and elsewhere [2] have provided valuable guidance for future basic research on wave breaking while at the

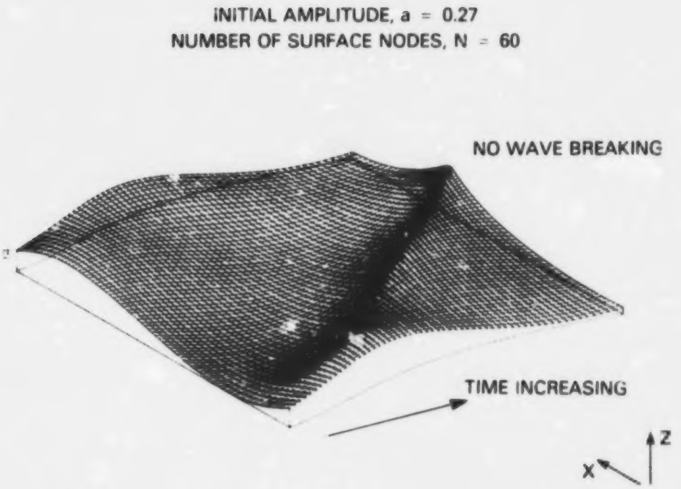

Fig. 5 – Computed time evolution of an asymmetric steep wave in deep water (NRL/U. of Michigan computations). The initial amplitude a = 0.27 was insufficient to cause wave breaking.

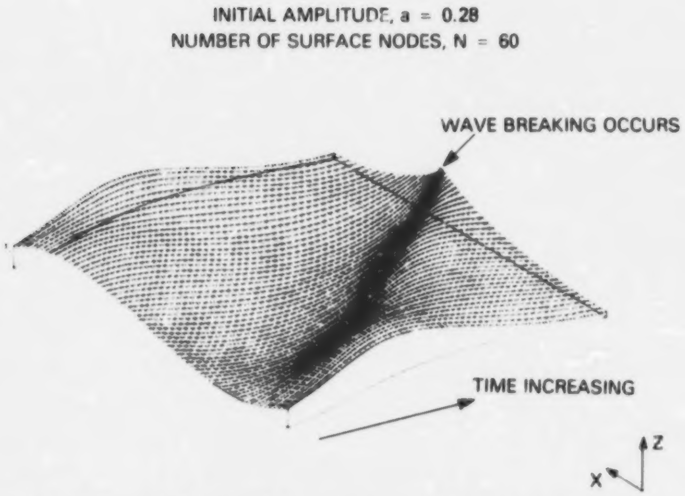

Fig. 6 – Computed time evolution of an asymmetric steep wave in deep water (NRL/U. of Michigan computations). The initial amplitude a = 0.28 caused wave breaking to occur after approximately 150 time steps.

BEST COPY AVAILABLE

same time yielding results for steep and breaking waves of immediate use to the Navy and to others.

[Sponsored by ONR]

References

1. W.W. Schultz, O.M. Griffin, and S.E. Ramberg, "Steep and Breaking Deep Water Waves," 16th Symposium on Naval Hydrodynamics Proc., University of California, Berkeley, July 1986, in press.

2. S.E. Ramberg and O.M. Griffin, "Laboratory Studies of Steep and Breaking Deep Water Waves," 1984 NRL Review, pp. 217-219.

3. P. McIver and D.H. Peregrine, "Comparison of Numerical and Analytical Results for Waves That are Starting to Break," Hydrodynamics in Ocean Engineering, Norwegian Institute of Technology, pp. 203-215 (1981).

4. M.S. Longuet-Higgins and E.D. Cokelet, "The Deformation of Steep Gravity Waves in Water. II. Growth of Normal Mode Instabilities," *Proc. R. Soc. London A* **364**, 128 (1978). ■

Rapid Three-Dimensional Ocean Acoustic Computations

W. A. Kuperman, M. B. Porter,
and F. L. Ingenito
Acoustics Division

Future sonar systems will use signal processing techniques that require rapid and accurate prediction of acoustic fields. These fields are finely gridded over large geographic areas and are range and time dependent. The resulting ocean acoustic description will basically be an acoustically illuminated picture of the ocean, analogous to a tomographic image. It will include mesoscale phenomena such as local ocean water masses and eddies drifting over the irregular ocean-bottom terrain. The terrain is layered and complex in shape and material. The production of this acoustic picture is an extremely intensive computational problem. It involves the solution of a nonseparable, three-dimensional acoustic wave equation whose parameters, coefficients, and boundary conditions are descriptive of the real ocean environment. In a future application, these parameters would be supplied by remote sensing devices. A composite of the resulting computation will provide a display of the coverage that a suite of acoustic sensors could provide over a large volume of ocean.

Acoustic modeling of the ocean can be broken down into two domains: ray theory and wave theory. Ray theory, though rapid, does not include diffraction and the other wave effects that are required for an accurate frequency-dependent description of sound channeling in the ocean and subbottom. The most accurate wave-theory models for range-dependent environments rely on numerical marching methods that must be repeated for any propagation computation in which part of the input information changes. For example, a new source/receiver configuration or a sound speed change over a limited portion of the propagation domain requires an entirely new computation. Hence, areawide acoustic propagation computations in a three-dimensional wave theoretic context has, until now, been computationally intractable.

Theoretical Model: A wave-theory model based on a precalculated boundary value, normal mode algorithm, combined with a horizontally gridded interpolation scheme, has been developed. A key feature of the model is that it takes advantage of the fact that most of the ocean below a certain depth is stable and that a significant portion of the local acoustic mode computation can be pre-calculated and stored. The final computation is only performed after the latest updated near-surface ocean environment is included. It is precisely this type of near-surface environmental input that lends itself to determination by satellite or other remote-sensing procedures. With the update of environmental data, the local mode calculation is performed and tabulated on a horizontal grid associated with the particular geographical location. The field resulting from acoustic transmission from a source to a receiver plane covering the gridded region can then be calculated by an 'adiabatic' mode algorithm that assumes that the modes adapt to the slowly changing ocean environment. A specially developed numerical scheme enables rapid field calculation that includes the effects of horizontal refraction. This three-dimensional model includes, therefore, ocean inhomogeneities in both the vertical and horizontal. Comparisons with previous wave theoretic methods for two-dimensional radial slices show excellent agreement. However, the computational speedup of the new model is so large that we now have the ability to produce fully three-dimensional acoustic tomographic slices of the ocean in any plane.

Results: Figures 7 and 8 display two acoustic images of a generic ocean. The ocean is constructed to encompass an extremely complex environment. The plot in Fig. 7 shows a plan view of the acoustic field (horizontal tomographic slice) at a receiver plane located at a depth of 160 m owing to a source located in the center of the plot and at a depth of 100 m. Looking first to the right (or east), we have a constant, range-independent ocean of 5000-m depth with a typical deep-water sound speed profile that acts as the acoustic index of refraction. The result is the well-known convergence-zone sound paths that periodically focus, as shown by the rings of high intensity in the eastern sector. The range depth slice shown in Fig. 8 displays this convergence-zone structure with the near surface refocusing about every 60 km. To the north in Fig. 7 there is an oceanic eddy, a mesoscale feature on the ocean that alters the sound speed because of its local temperature and density

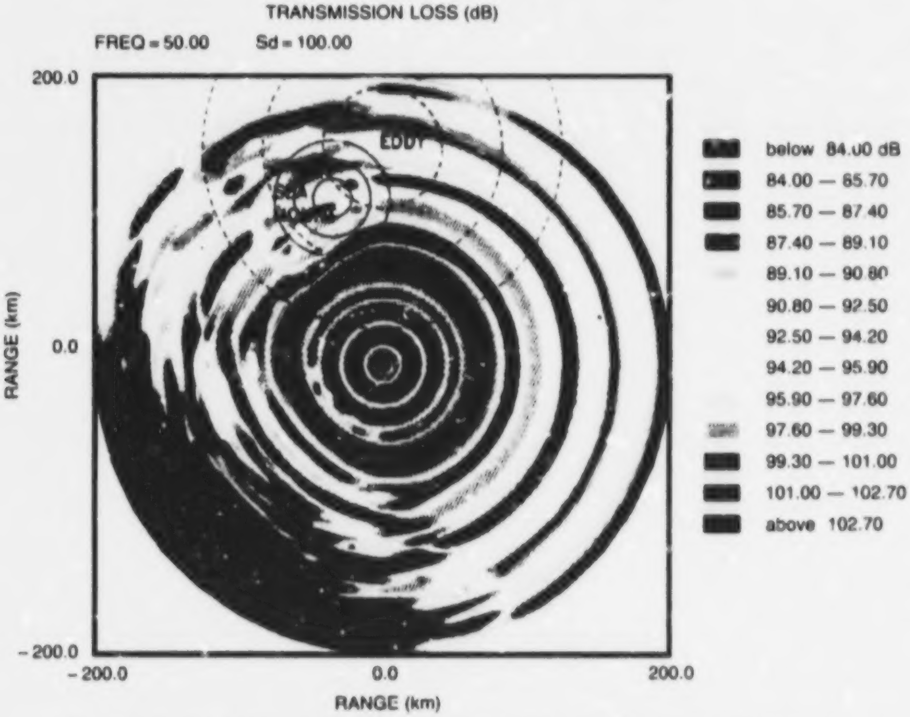

Fig. 7 – Contours of acoustic propagation loss over a large area of a complex generic ocean for a surface in the center at 100-m depth and a receiver plane at 160-m depth. The 5000-m deep region is range independent to the east, contains an oceanographic eddy due north, a seamount northwest, and a continental slope rising to a continental shelf of depth 1000 m to the southwest.

BEST COPY AVAILABLE

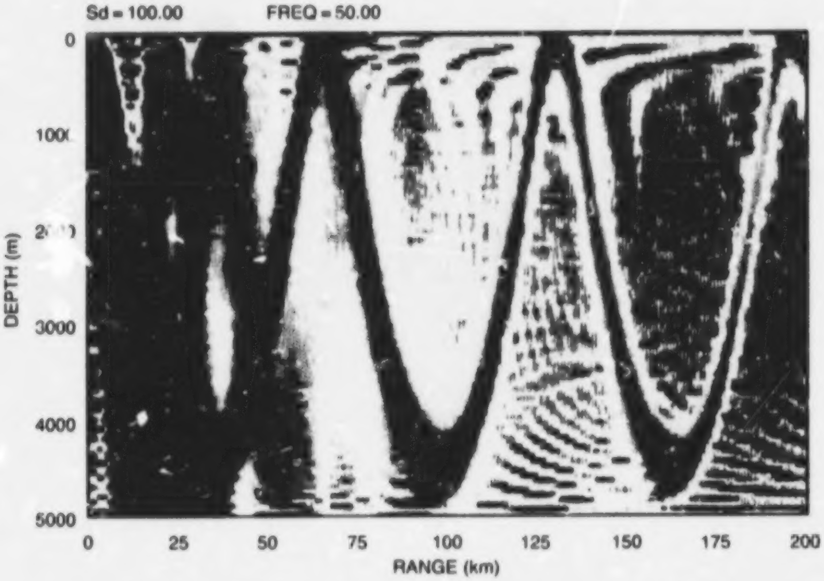

Fig. 8 – A vertical slice due to east shows the typical convergence-zone propagation emphasizing the vertical structure associated with the dark red rings at the 160-m receiver plane displayed in Fig. 7. The high intensity regions near the surface for ranges less than 50 km in both figures represent bottom-bounce returns.

structure. To the west of the eddy is a seamount rising 2000 m from the 5000-m deep ocean. This region of oceanographic and topographic complexity is highly visible in the acoustic picture of Fig. 7, strongly disturbing the regular convergence-zone ring structure existing to the east. Finally, to the southwest there is a continental slope at which the depth changes from 5000 to 1000 m in depth at the continental shelf. The convergence-zone structure disappears upslope because of the increasing sound interaction with the lossy ocean bottom.

Summary: The ability to perform three-dimensional sound propagation computations in a complex oceanic region permits us to examine for the first time the global physical processes occurring in large scale oceanographic acoustics. This new modeling capability will be an important tool to simulate and design future sonar systems incorporating new-generation, remote-sensing technology for optimal coverage of large oceanic regions.

[Sponsored by NOP and ONR] ■

Inertial Wave Dynamics

R. P. Mied, G. J. Lindemann,
and C.L. Trump
Acoustics Division

One of the objectives of the Advanced Research Initiative "Finescale Variability" is to understand the reasons for the geographical variation in the magnitude of temperature fluctuations with length scales of a centimeter to several meters. One of the working hypotheses is that energy put into the ocean by wind stress at the surface is propagated downward by near-inertial waves where it is dissipated into small-scale temperature fluctuations. An understanding of the dynamics of these waves in the ocean is thus essential for predicting the variability of the temperature fluctuations that influence high-frequency acoustics and nonacoustic antisubmarine warfare (ASW) phenomena. The restoring force for these waves is the local vertical component of the Coriolis force, although the waves are also affected by the background density

BEST COPY AVAILABLE

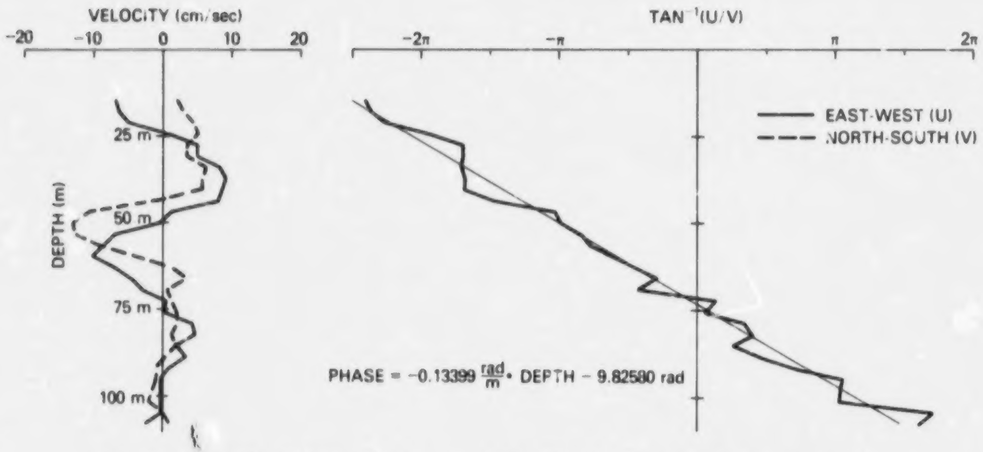

Fig. 9 — Velocities to the north (v) and east (u). The phase of the velocity vector with respect to north is shown. Increasing positive phase is clockwise.

stratification. Together, these forces yield a class of nearly horizontal rotary motions with periods near a half pendulum day (12 h/sin (latitude)).

In an attempt to determine the wavenumber, frequency, and spatial extent of a wave packet and to understand its physics, we performed an experiment in the North Atlantic Ocean with an acoustic doppler current profiler. In this experiment, the device yielded profiles of water velocity relative to the ship down to a depth of 115 m. Combining this information with LORAN-C navigation data, we obtain profiles of absolute velocity. A vertical profile of the horizontal velocity at one point within the ocean is shown in Fig. 9. The mean flow has been removed from the east-west (u) and north-south (v) components. The u component "leads" the v component with increasing depth, suggesting that the velocity vector twists clockwise with depth. The phase $\tan^{-1}(u/v)$, also plotted, shows that the phase does increase with depth, indicating the wave is carrying energy downward into the ocean. In Fig. 10(a), we show the ship track and the velocity vectors at a depth of 43.5 m. The peculiar sawtooth pattern results from an attempt to obtain many realizations of the wave motion by zigzagging across the path of a drogue that was deployed at the extreme western part of the frame and subsequently swept toward the east by the mean current.

Because the measurements took a day (about one wave period at this latitude) to perform, the observations of horizontal wave phase are severely contaminated by the passage of time. Since the current is strong, the locations where the measurements are made are continually advected downstream, giving a badly distorted spatial picture of the wave train as well. Together, these two effects mix the wave's temporal and spatial characters, which we must separate to understand the physics.

The velocity vectors indicate that the water follows a curved trajectory, being directed southeast where it enters in the west, and exiting in the east in a northeasterly direction. This average flow may be mapped by an objective analysis technique to obtain a smoothed streamline field. Figure 10(a) shows the track of the ship with respect to the Earth, but the point of the drogue-following experiment was to characterize an inertial wave by moving the ship relative to a specific parcel of water. By using the mean current stream function, the ship's motion can be reduced to a track relative to this piece of water at an arbitrarily selected reference time. For those portions of the ship track before time t_r, we advance the ship track to where it would have been at t_r. For times after t_r, we retard the track to where it was at t_r. This correction for the flow field produces the ship track that is shown in Fig. 10(b)

BEST COPY AVAILABLE

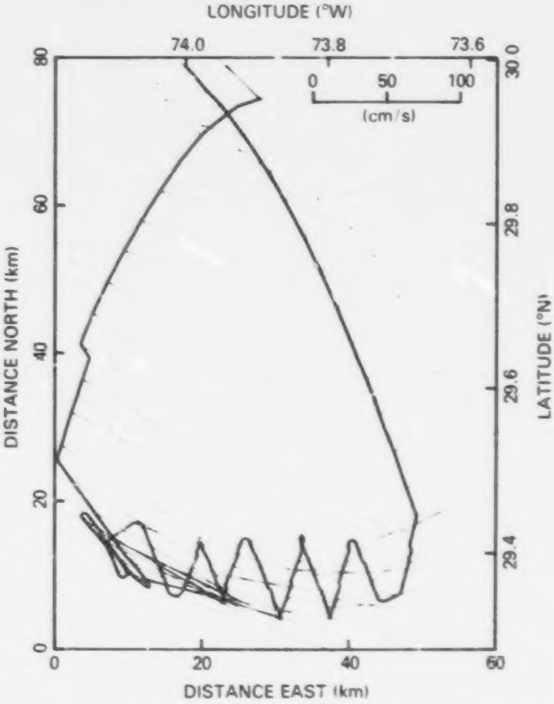

Fig. 10(a) — The ship track (bold line) with absolute current velocities (fine lines) at depth 43.5 m

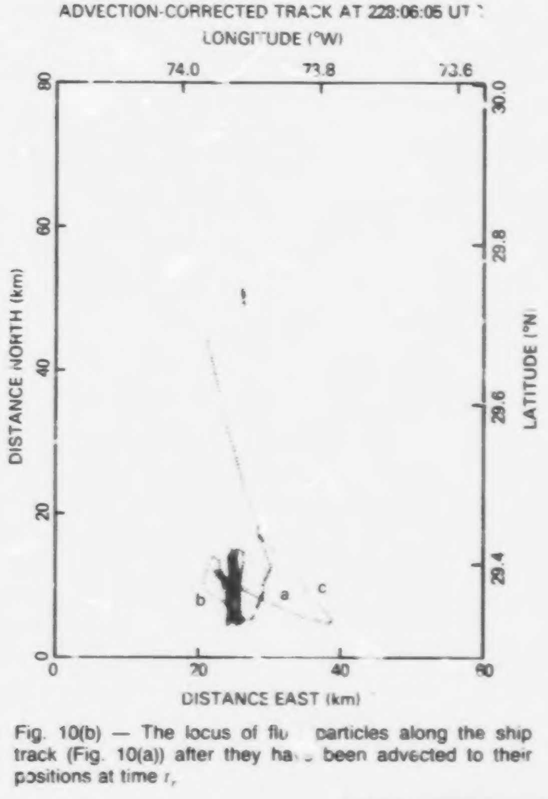

Fig. 10(b) — The locus of fluid particles along the ship track (Fig. 10(a)) after they have been advected to their positions at time t_r

BEST COPY AVAILABLE

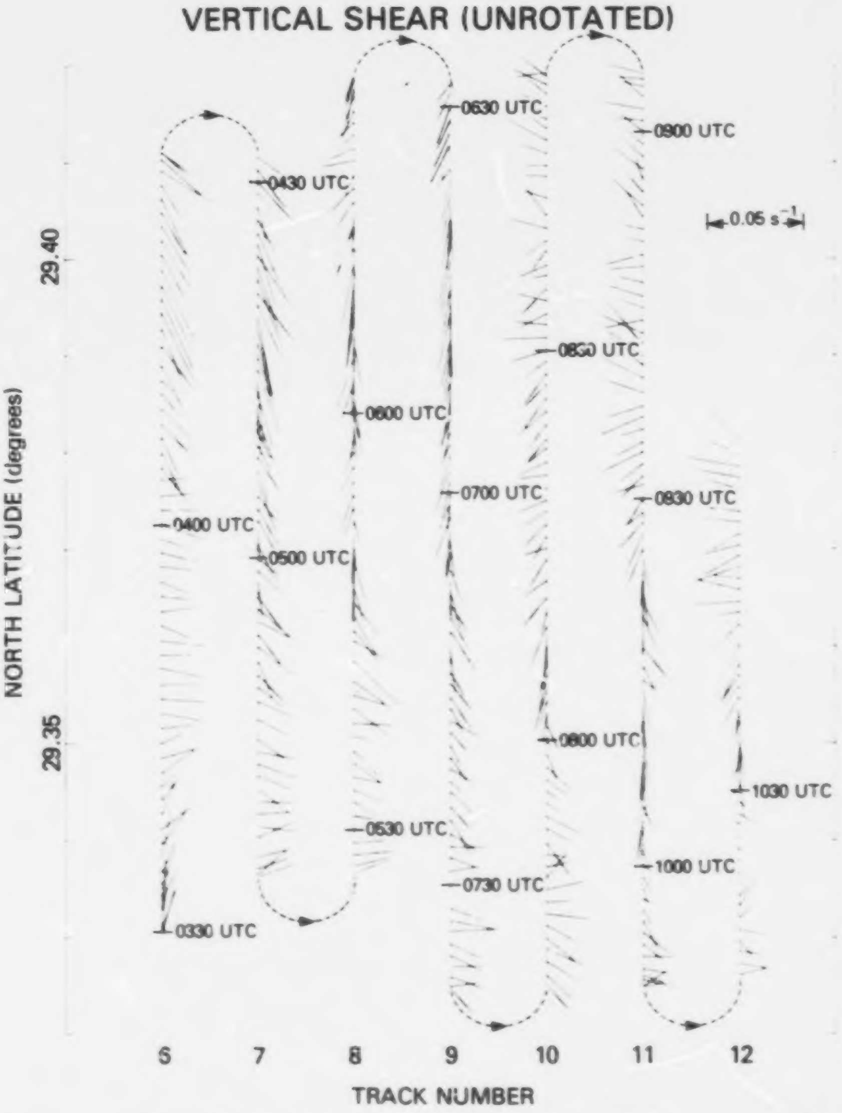
VERTICAL SHEAR (UNROTATED)

Fig. 11 – Vertical shear at 43.5 m depth along the seven tracks that collapse to a single north–south line in Fig. 10(b). Note the clockwise rotation at a constant latitude for successive tracks. Along any one track, the anticlockwise rotation as one moves south indicates propagation to the south.

for the time t_r. A number of legs in the zigzag pattern collapse to a single north–south section, so that the same body of fluid is repeatedly sampled. The results of this process are shown in Fig. 10(b). They indicate that several of the legs of the zigzag pattern do collapse to repeated north–south sections over the same body of fluid.

These overlying tracks are shown separately in Fig. 11. The vertical shear (the vertical derivative of the velocity vector) is shown along each track. Notice that at constant latitude the shear rotates clockwise in time, as we go from left to right. This clockwise rotation is a feature of all inertial oscillations in the northern hemisphere and the *rate* of rotation is the intrinsic frequency, or that following the mean flow. As we move from north to south along any of the seven tracks, the vector rotates anticlockwise, indicating energy

BEST COPY AVAILABLE

propagation to the south. Moreover, the north-south wavelength (20 km) is measured from the rate of this phase variation. The east-west wavelength can be estimated from similar tracks that have an easterly component; it is found to be 60 km.

Knowing the intrinsic frequency and the three components of the wavenumber at various times in the experiment allows comparison with the predictions of these quantities by using elementary ray-tracing methods. These calculations qualitatively reproduce the wave/mean flow interaction as it was observed.

[Sponsored by ONR]

References

1. R.P. Mied, C.Y. Shen, C.L. Trump, and G.J. Lindemann, "Internal-Inertial Waves in a Sargasso Sea Front," *J. Phys. Oceanogr.* **16**, 1751-1762 (1986). ■

Nonlinear Salt-Finger Simulation

C. Y. Shen
Acoustics Division

A fluid stratified in both heat and salt can evolve to become gravitationally unstable under certain conditions even though its initial overall density stratification is a stable one. One such condition is when both the temperature and the salt concentration in the fluid increase with height. In this case, the stable density stratification is maintained by the temperature, and the system evolves toward instability as the more rapidly diffusing heat weakens the stabilizing temperature stratification, causing the fluid to become top-heavy with salt. The ensuing unstable convection that occurs under this condition is commonly referred to as salt fingers. This name is given because the physical form of this convection is that of narrow columns of alternate upgoing and downgoing fluid; the width of the columns is on the order of a centimeter.

The condition described above for salt fingering is found in the upper part of the ocean in temperate regions. Presence of salt fingers in these regions has been detected. Salt fingers are of interest to both the Navy and ocean scientists because the vertical heat, and salt that fluxes from their convection can profoundly modify the ambient ocean environment. The scientific interest in the salt fingers and similar double diffusive processes, however, is not strictly limited to the ocean. The study of salt fingers is currently finding application in a wide variety of fluid systems, including liquid metals as well as magmas, all of which contain multiple density components with different molecular diffusivities [1] conducive to salt-finger formation.

Salt-finger convection involves complicated turbulent processes. The complexity of the processes has severely limited present theoretical understanding of the evolution of the finger convection. Direct numerical simulation provides an effective means for studying this complex phenomenon. Through the present simulation work, detailed information is obtained for the first time on the advanced stages of the evolution, including the transition of fingers to stratified turbulence [2].

Simulation: The model used for the simulation is a two-layer fluid system in which the upper warmer and salty layer is separated from the lower, colder and fresher layer by a sharp interface. This is a commonly used configuration in laboratory salt-finger experiments, with which the simulation can be compared. Salt fingers are simulated on a two-dimensional vertical plane to maximize the spatial resolution and are performed with the spatially accurate pseudospectral technique. Results are shown in Figs. 12 to 14 for the salt field. The temperature field has a similar structure, except for weaker fluctuations caused by its greater diffusivity. Fingers form at the interface, as observed in the laboratory experiments. Their initial structure has a smooth sinusoidal form that is described well by a small

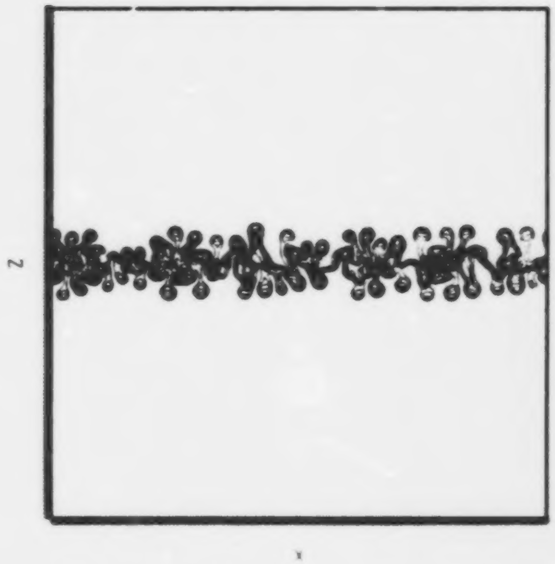
TOTAL S FIELD
(Time - 0.64 BVP.)

Fig. 12 — Finite amplitude salt finger before the onset of turbulent plumes. The time unit is given in terms of BVP, the fundamental oscillation period of the simulated fluid system. The simulation domain is approximately 1 m^2.

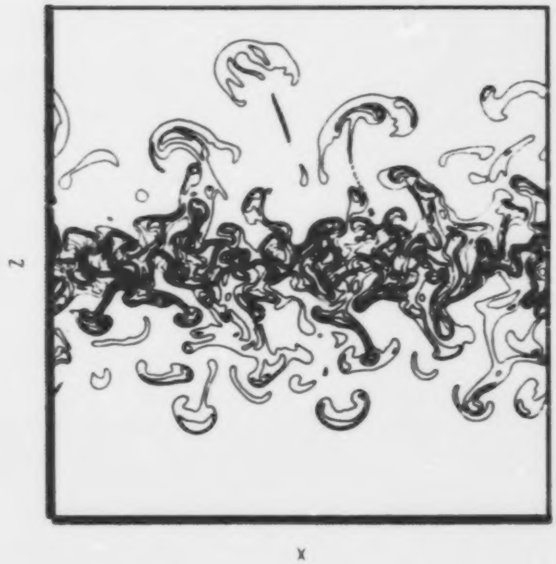
TOTAL S FIELD
(Time - 1.92 BVP.)

Fig. 13 - The onset of turbulent plumes as the salt-finger tips break away

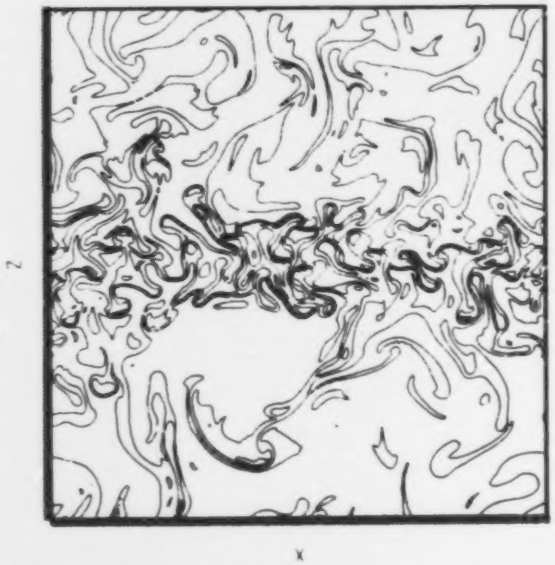
TOTAL S FIELD
(Time - 3.83 BVP.)

Fig. 14 - The final state of salt-finger convection where the fingering interface is bounded above and below by turbulent motions

amplitude linear theory. Finite amplitude fingers after the initial growth stage develop a nonuniform vertical structure, as shown in Fig. 12. The finger structure becomes increasingly irregular at a still larger amplitude, until finally the tips of the fingers break away from the fingering structure to form turbulent plumes (Fig. 13). The final state consists of a fingering interface and convecting motions above and below the interface (Fig. 14). A fingering interface is distinguished from the turbulent convection by its greater concentration of small-scale fluctuations.

Results: The final state shown in Fig. 14 is consistent with the laboratory observation [1]. The value of the simulation here is that it permits detailed analysis of the transition region between the fingers and the bounding turbulent motion. Analysis reveals that the transition to turbulence is a manifestation of another form of gravitational instability akin to that in the Rayleigh convection. It is also found that the transition determines the final buoyancy flux through the fingers. The thickness of the fingering interface is also determined by the

BEST COPY AVAILABLE

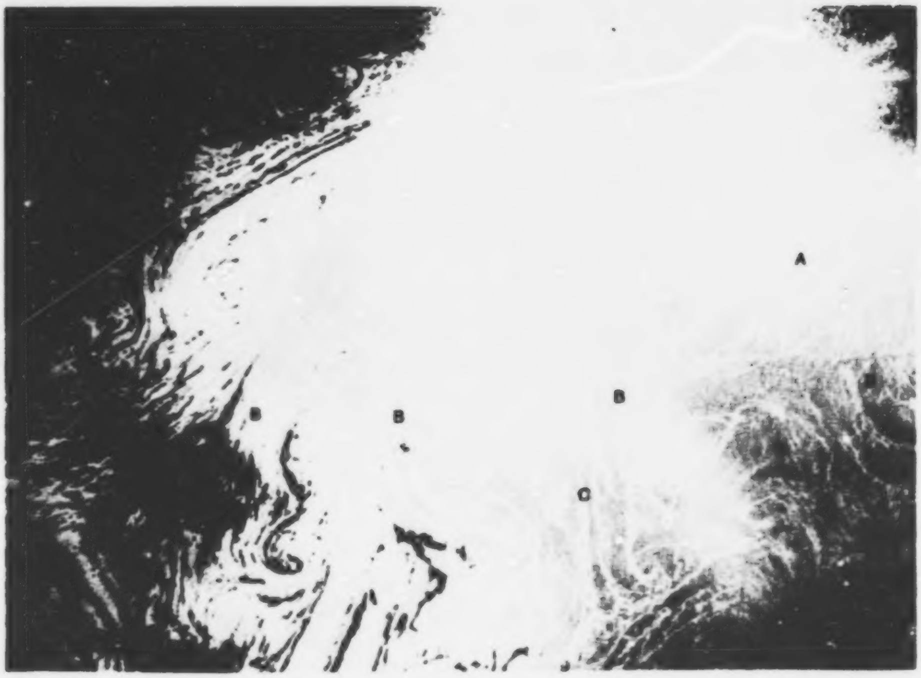

Fig. 15 – Photograph taken by Scully-Power from Challenger of the Mediterranean Sea surface shot into the reflected sun (glint) pattern. This photograph reveals eddylike circulations, but even more intriguing are the persistent ship wakes (at A, B, and C) that show up. The longest one (B) is at least 200 km long and may be 5 h old.

transition, but additionally, it depends on the vertical diffusion of heat and salt across the interface as well as the gradients of heat and salt fluxes. Identification of the transition condition makes it possible to obtain a finite amplitude salt-finger theory that allows prediction of various finger properties over a range of diffusivity parameters impossible to attain experimentally or with finite resolution simulation. Work is presently under way to study the details of motion within the fingering interface and effect of ocean internal wave motion on the salt fingers.

[Sponsored by ONR]

References

1. J.S. Turner, "Multicomponent Convection," *Ann. Rev. Fluid Mech.* **17**, 11–44 (1985).
2. C.Y. Shen, "The Finite Amplitude Growth of Salt Fingers," *EOS, Trans. Am. Geophys. Un.* **67** (44), 1046 (1986). ■

Ship-Wake Experiment for Remote Sensing

J. A. C. Kaiser*
Acoustics Division

W. D. Garrett**
Space Systems Technology Department

S. E. Ramberg and R. D. Peltzer
Laboratory for Computational Physics and Fluid Dynamics

A remarkable series of photographs of the ocean surface was taken from the Space Shuttle Challenger by Paul Scully-Power in 1984. Figure 15, one of the photographs, shows a very complex circulation pattern in the Mediterranean Sea, but even more fascinating are the surface ship wakes (at A, B, and C) that are visible from 100 km and persist for hours. Wake B is 200 km long and at least 5 h old.

---

*Presently with the Space Systems Technology Dept.

**Presently with Orincon Corp., Arlington, VA

BEST COPY AVAILABLE

Questions that arise are (a) what cause the increased reflectivity that produces the bright features? (b) what aspects of surface ship wakes cause them to persist for so long? The increased reflectivity is caused by chemical films on the water surface that are compacted by flow patterns in the water. These are particularly prevalent in light winds (18 km/h) and may appear as slicks. But the high persistence of the wakes is somewhat of a mystery. In September 1986, we conducted a surface ship film and wake experiment to explore this further.

Wake Processes: Compacted films increase the reflectivity of the ocean surface by damping the capillary and short gravity waves (1 mm to 10 cm wavelengths) [1]. One mechanism to produce this compaction in ship wakes has been proposed by Garrett and Smith [2], and has been further elaborated by Swanson [3]. They propose a vortexlike flow in the wake as illustrated in Fig. 16. These vortices (for a displacement hull) rotate to produce a velocity field *Vx* that produces a convergence band at the wake edge from *Vx* being blocked by the quiescent water outside the wake. However, our experiment in September suggested that the wave structure and bubble and foam formation around the ship's bow may produce wake bands in the convergence zone as shown in Fig. 16, and that the vortices maintain the bands.

The Experiment: We used two small boats, several commercial ships of opportunity (about 700 ft long), and two small high-wing aircraft (a Cessna 172 and a Cessna 180). Scientists in the aircraft identified and photographed interesting phenomena, observed the operations, and directed the small surface boats by two-way radio. (We also deployed artificial films and drove the small boats through them to observe the wake/film interaction.) The small boats crossed the wakes of the two commercial ships and measured the surface tension distribution; this allows us to determine the relative surface film distribution across the wake. We also distributed drifters in the wakes of the small boats and commercial ships and photographed them from the air with a 9-1/2-in. mapping camera to determine surface flow patterns.

During the experiment, the winds were less than 10 km/h, and the weather was mostly sunny to partly cloudy.

Results: Most of the major conclusions from our experiment are illustrated in Fig. 17, which shows the wake of a 45-ft boat at 10 knots. The two dark bands trailing behind the boat appear to be compacted surfactant material that has damped the shorter waves. As we follow these bands up to the boat, they appear to originate from the foam generated in the bow wave. This suggests the bow wave rather than the trailing vortex pair may form these *edge* bands. In fact, the foam and bubbles created below the bow wave probably scavenge dissolved surfactant material from the water column and, as they rise to the surface, bring this film-forming material into these bands.

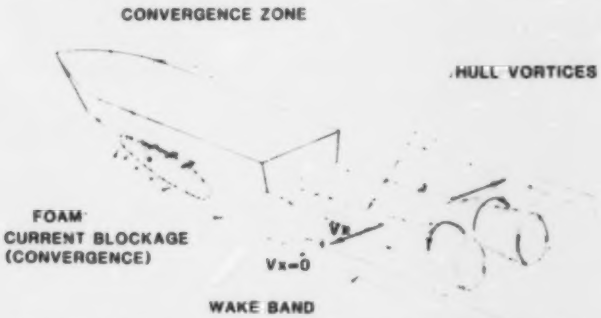

Fig. 16 – A displacement hull shedding a pair of vortices in the wake and also creating a bow wave and foam. The horizontal velocity fields at the water surface of the bow wave and the vortices can compact surface films in the convergence zone or region of current blockage.

BEST COPY AVAILABLE

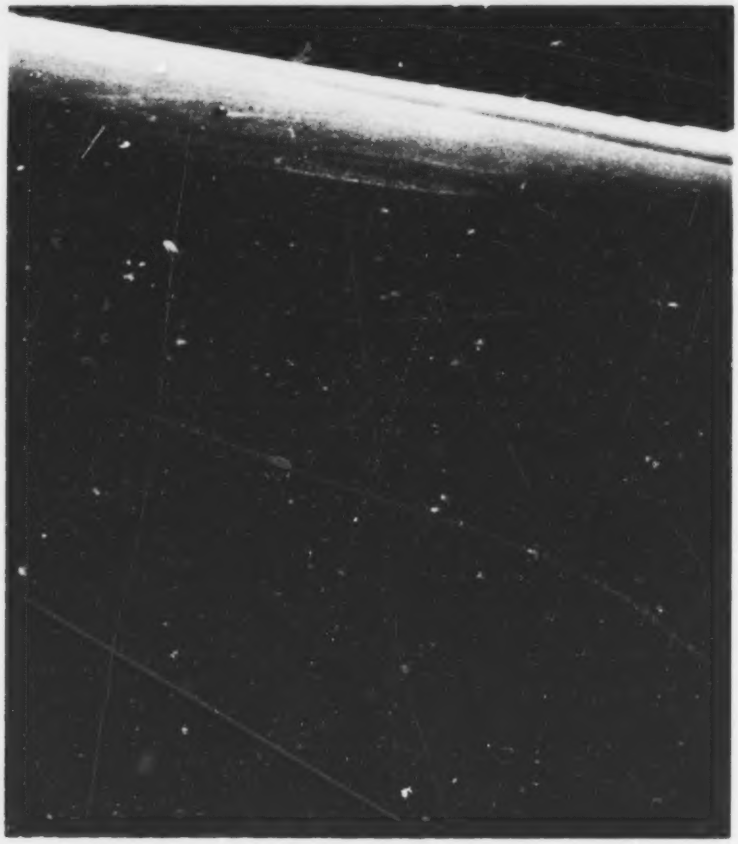

Fig. 17– Wake of a 45–ft displacement hull in light winds. The two bands trailing off the bow wave contain compacted surface film material and appear as slicks in the foreground because the compacted film has "smoothed" the small waves.

Figure 18 shows the surface tension (γ) distribution in the wake of a 750–ft tanker traveling at 12–1/2 knots. In the core of the wake, γ is greater than 72.5 mN/M; this high γ-value indicates a clean surface produced by water being brought up from below. In the *bands*, γ was about 68 mN/M and away from the wake γ varied from 69 to 71 mN/M. The lower γ-values in the bands indicate a compaction of the surface film and indeed these bands were visible as slicks. This γ-distribution is consistent with the wake vortex model.

Figure 19 is a slant photograph of drifters that were evenly distributed across the wake of a 700–ft container ship 12 min earlier. To make the drifters more visible in the printed copy, they were enhanced artistically. Notice how the drifters have aligned themselves into lines; these are near the edges of the wake. This shows that there is a divergent transverse velocity field in the wake at

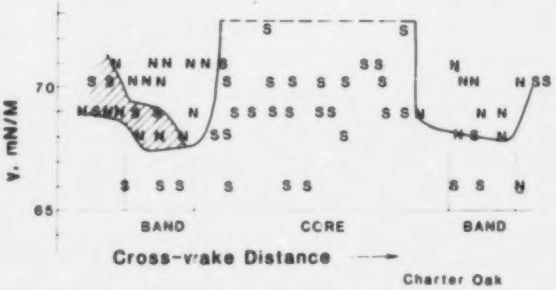

Fig. 18 — The transverse distribution of surface tension, γ, measured in the wake of a 750-ft tanker. The two regions of reduced γ correspond to the visible edge bands where the ambient surface film is compacted by transverse flows in the wake.

BEST COPY AVAILABLE

Fig. 19 — A slant photograph of surface markers that were evenly distributed in the wake of a large container ship 12 min earlier (the drifters were artistically enhanced). The markers have collected into bands near the wake edge because of the cross-wake flow at the water surface.

the water surface consistent with the vortex model illustrated in Fig. 16.

A more comprehensive description of all aspects of the experiment, data reduction, techniques, and results is given in Ref. 4.

Preliminary Conclusions: These simple experiments suggest that if film-forming material is present on the water surface, it can be compacted into bands to form the persistent pattern observed in ship wakes by Scully-Power. Two mechanisms may cause this. The bow wave initially organizes the film material into the bands, with the foam and bubbles generated in this bow wave contributing film material to these bands by scavenging in the water. A vortex pair is generated behind the hull, and its surface flow keeps the edge bands separated and compacted.

We have also demonstrated that a simple, inexpensive experiment such as this one can be a very cost-effective way to explore various mechanisms and phenomena, and also can be a test bed for new ideas and techniques. We found the high maneuverability of light aircraft and having scientists aboard them as observers generated a flexibility in operations that allowed rapid response to unexpected observations. Exercises like this can serve as an efficient trail for a more elaborate and expensive experiment.

[Sponsored by ONR]

References

1. W.D. Garrett, "Damping of Capillary Waves at the Air-Sea Interface by Oceanic Surface-Active Material," *J. Mar. Res.* **25**, 279-291 (1967).
2. W.D. Garrett and P.M. Smith, "Physical and Chemical Factors Affecting the Thermal IR Imaging of Ship Wakes," NRL Memorandum Report 5376 (1984).
3. C.V. Swanson, "The Effect of Persistent Ship Wake Currents on SAR Imagery," Appl. Phys. Tech. Report No. 6 (1986).
4. J.A.C. Kaiser, S.E. Rambert, R.D. Peltzer, M.D. Andrews, and W.D. Garrett, "WAKEX '86—A Ship Wake Film Interaction Experiment," NRL Memorandum Report in press. ■

BEST COPY AVAILABLE

Chemistry is one of the central sciences, and it plays a key role in a wide variety of NRL programs. A major focus is in the Chemistry Division itself, where emphasis is placed in broad areas of research ranging from polymeric materials, fuels and combustion, chemical diagnostics, surface and interface chemistry, synthesis of organic and inorganic materials to the burgeoning area of biomolecular engineering.
Dr. Jerome Karle, Head of the Laboratory for Structure of Matter, was winner of the Nobel Prize in Chemistry for 1985.

CHEMICAL RESEARCH

71 **Quantum Chemical Calculations of Chemical Reaction Pathways: The Methoxy Radical**
Michael Page

73 **IR-Diode Laser Spectroscopy in the Study of the Vapor Phase Epitaxy Process**
Nicholas Bottka, Roger S. Sillmon, David K. Gaskill, and James E. Butler

74 **Liposome-Encapsulated Hemoglobin: A Potential Blood Surrogate**
Alan S. Rudolph and Martha C. Farmer

76 **Two-Dimensional NMR Images in Solids**
Gerard C. Chingas, Joel B. Miller, and Allen N. Garroway

78 **Laser Studies of Flame Chemistry**
James W. Fleming, Louise R. Pasternack, and Herbert H. Nelson

79 **Advanced Fluorinated Polymers Meeting Navy Needs**
Robert L. Soulen, James R. Griffith, and Robert F. Brady, Jr.

Quantum Chemical Calculations of Chemical Reaction Pathways: The Methoxy Radical

M. Page
Laboratory for Computational Physics and Fluid Dynamics

The atoms in a molecule are perpetually vibrating and twisting about. When a molecule acquires a substantial amount of energy through collisions with other molecules, these internal twists, bends, and vibrations become so dramatic that the molecule either breaks apart into smaller fragments or permanently changes its shape in some way. If the original molecule or the fragments are short-lived transient species, experimental elucidation of the detailed sequence of these chemical reactions may not be feasible. However, understanding the detailed sequence of reactions is crucial for the prospect of predicting, and perhaps controlling, energy release from energetic materials for use in fuels, propellants, and explosives.

We describe here the theoretical prediction of chemical-reaction pathways. These are first-principle predictions. Beginning with the known laws of physics for the constituent particles, they are determined through a series of well-defined approximations and mathematical manipulations. There is no recourse or fitting to experimental data.

Potential Energy Surfaces: Central to the theoretical description of chemical phenomena is the Born-Oppenheimer approximation. This is the assertion that the rapid motion of the electrons in a molecule can instantaneously adjust to the changing position (motion) of the much heavier nuclei. The Born-Oppenheimer approximation leads to the concept of a potential energy surface (PES). For each set of positions of the nuclei in a molecule, a potential energy can be determined by solving the quantum mechanical equations of motion for the electrons. The PES is the function that describes how this potential energy changes as the nuclei move relative to one another. The PES is the multidimensional generalization of the familiar potential-energy curve for diatomic molecules.

The molecular PES has enormous significance in chemical physics. The stable configurations of a molecule are represented by local valleys or wells on this surface. Vibrational properties of a molecule are determined by the steepness of the walls in the vicinity of the local minimum, and the probability of chemical reaction is related to the energy of the highest point on the lowest energy pathway connecting two valleys, i.e., the saddle point. The most crucial step in the theoretical prediction of chemical reaction mechanisms is the location of the appropriate minima and saddle points on the PES and the reliable determination of their potential energy.

Two major developments in the last several years have significantly broadened our capabilities for exploring molecular PESs for reacting chemical systems. We have been involved, along with many others, in the development and implementation of both of these areas.

The first such area is the calculation of the electronic wavefunction. We solve the quantum mechanical equations of motion for the electrons in a molecule within a multiconfiguration self-consistent field (MCSCF) approximation. This variational principle-based technique significantly broadens our capabilities because unlike the Hartree-Fock method, the approximations are as valid for a molecule that is in the midst of breaking apart as they are for a molecule at its usual stable shape or configuration. The MCSCF wavefunction includes, in a consistent and well-defined manner, the instantaneous correlation in time of the motion of the electrons most involved in electronic structure changes during a chemical reaction. This wavefunction also provides a reference point for more accurate large-scale configuration interaction calculations.

The second recent advance is the analytical calculation of potential energy derivatives. The first derivatives, for example, are the slope on the many dimensional PES and represent the forces on the atoms in a molecule. They also make possible

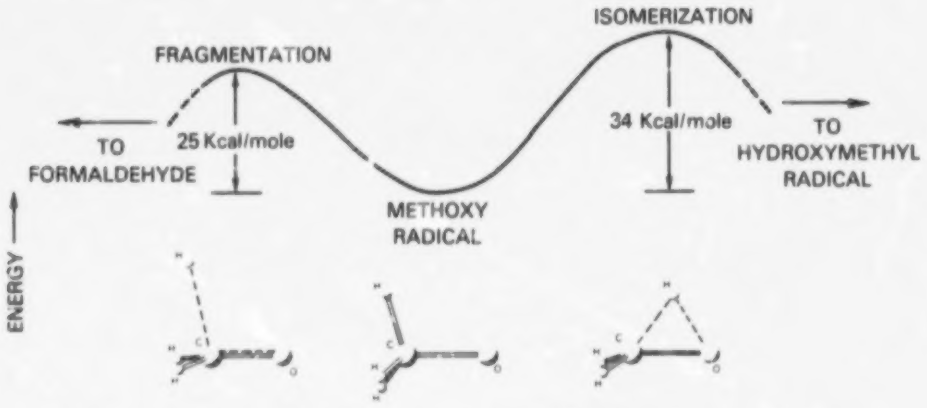

Fig. 1 – Potential energy profile for methoxy radical decomposition. The fragmentation pathway leading to formaldehyde has a lower activation energy and is the preferred mechanism of decomposition.

the evaluation of a model PES based on a local quadratic expansion of the potential energy about a reference reaction path [2]. These derivatives allow us to efficiently search the PES to locate the critical points.

Methoxy Radical Decomposition: An example of the utility of these techniques is found in our recent calculations on the methoxy radical (CH_3O). This prototype alkoxy radical is of considerable importance both in atmospheric chemistry and in the combustion of hydrocarbons. It is well established that this radical will not survive for long at reasonably high temperatures. A key question that has not been satisfactorily answered, however, is "What is the mechanism of decomposition?" Fragmentation leading to a hydrogen atom and the stable formaldehyde molecule (CH_2O) is expected to be an important path. Several recent theoretical and experimental studies indicate that there may be an alternative route that is competitive with this one: hydrogen atom migration to the oxygen yielding the hydroxymethyl radical (CH_2OH).

To address this alleged competition, we explored the PES for the methoxy system by using a MCSCF wavefunction capable of properly describing the CH bond breaking in methoxy and simultaneously, either the OH bond forming in hydroxymethyl or the pi-type bond forming in formaldehyde. The local minimum on the PES representing the methoxy radical and the saddle points representing the transition states for the two reaction channels were located by using a high-quality basis set (triple-zeta plus polarization). Figure 1 shows the resultant structures. Complete harmonic vibrational analyses were performed for each of these structures, enabling the computation of the vibrational zero-point energies. Best estimates for the energies of these critical points were found by performing multireference configuration interaction calculations with a triple-zeta plus polarization basis set.

Our best estimates of the activation energies for the fragmentation and isomerization processes are 24.5 and 33.7 kcal/mole respectively. Isomerization thus has an activation energy 9.2 kcal/mole higher than fragmentation. This result, further bolstered by the qualitative conjecture that the isomerization process is entropically unfavorable, leads us to conclude that the preferred mode of decomposition of the methoxy radical is fragmentation leading directly to formaldehyde.

[Sponsored by ONR]

Reference

1. M. Page, P. Saxe, G.F. Adams, and B.H. Lengsfield III, "Multireference CI Gradients and MCSCF Second Derivatives," *J. Chem. Phys.* **81**, 434 (1984).

2. M. Page and J.W. McIver, Jr., "On Evaluating the Reaction Path Hamiltonian," *J. Chem. Phys.* (in press).

IR-Diode Laser Spectroscopy in the Study of the Vapor Phase Epitaxy Process

N. Bottka, R. S. Sillmon, and D. K. Gaskill
Electronics Technology Division

J. E. Butler
Chemistry Division

Organometallic vapor phase epitaxy (OM-VPE) is an emerging crystal growth technology that has promise in the future to mass-produce complex artificial microelectronic structures that are essential to the electronics needs of the Navy and the nation [1]. NRL has been active in this field for the past four years and is a leader in the area of new organometal synthesis and in the area of diagnostic studies of the OM-VPE process. Because of the unique research facilities and talents available at NRL, an orchestrated effort has been made to address specific technological problems in OM-VPE, one of which is described here.

Recent experiments at NRL indicate that infrared (IR)-diode laser spectroscopy [2] is a powerful tool to study the reaction kinetics in the organometal vapor phase epitaxy (OM-VPE) process [3]. These real-time, in-situ measurements were able to identify for the first time the presence of metastable methyl radicals formed during the decomposition of metal alkyls such as trimethyl-aluminum, -gallium, and -indium. These findings have important implication to the growth of GaAs and related compounds by the OM-VPE process (Fig. 2).

The absorption IR-diode laser emission was used to monitor the vibrational frequencies of hot gaseous species within an OM-VPE reactor. Absorption lines associated with the metastable methyl radical were observed during the decomposition of trimethyl-aluminum, -gallium, and -indium. Results indicate that the decomposition of the metal alkyls proceeds by the removal of individual methyl radicals, and that there is a maximum methyl production at a temperature that increases with Group III metal-carbon bond strength, i.e., In-, Ga-, Al-C. It is also observed that the CH_3 radicals play a significant role in the decomposition of arsine and the formation of GaAs in OM-VPE. These results are important to the OM-VPE working community since it elucidates for the first time the importance of metastable radicals in the synthesis of new electronic materials.

Fig. 2 - The NRL organometallic vapor phase epitaxy reactor chamber during crystal growth. The RF-heated graphite susceptor holds the GaAs substrate upon which the thin epitaxial layers are grown. For the IR laser diode diagnostic experiments, a modified cell was used (not shown) that allowed for optical access to the volume immediately above the growth surface

In addition, the IR-diode laser system tuned to a methyl alkyl line can also serve as an on-line monitor of flow dynamics in a OM-VPE reactor. The effects of gas velocity, diffusion into or out of dead spaces, pressure variations, etc. can readily be identified and measured. This led to significant improvement of the NRL OM-VPE reactor. We

BEST COPY AVAILABLE

can now monitor abruptness changes in heterojunction and superlattice structures that are on the order of one atomic layer. This is a breakthrough for the OM-VPE technology.

Successful in-situ real-time monitoring in OM-VPE opens up a new area of research to study chemical reactions of new and unknown precursors and their usefulness as potential source materials in OM-VPE. This will be of particular importance in the future when OM-VPE enters large-scale production of electronic and electrooptic components. New and safer OM-sources are highly desirable. The chemical reaction pathways leading from starting precursors to crystalline solids will need to be determined. The above-mentioned diagnostic procedures will contribute to this understanding. Real-time monitoring of events has also a practical significance in anticipating and solving potential problems associated with reactor component failure. This can save time and money for the Navy and industry.

These monitoring aspects can be transferred to industrial facilities responsible for large-scale production of OM-VPE grown materials. Chemical reaction studies will be pursued in Navy and university laboratories and other institutions that have interest in OM-VPE related research.

[Sponsored by ONR]

References

1. M.J. Ludowise, *J. Appl. Phys.* **58** R31 (1985).
2. R.S. Eng and R.T. Ku, *Spectrosc. Lett.* **15**, 803 (1982).
3. J.E. Butler, N. Bottka, R.S. Sillmon, and D.K. Gaskill, *J. Cryst. Growth* **77**, 163 (1986). ■

Liposome-Encapsulated Hemoglobin: A Potential Blood Surrogate

A. S. Rudolph and M. C. Farmer
Chemistry Division

Blood surrogate research at NRL has led to the development of liposome-encapsulated hemoglobin (LEH) [1]. We have demonstrated that the biophysical criteria required for efficacy, including rapid gas exchange and appropriate oxygen-binding characteristics of the hemoglobin, could be attained with LEH. We have recently accomplished the first scale-up of LEH production. Recent efforts have been aimed at increasing the useful circulation lifetime of the liposomes, decreasing the cost of materials, and devising a means of scaled-up sterile production to support the extensive animal trials required before clinical trials can be considered.

The lipid formulations used successfully for production of LEH include roughly equivalent quantities of cholesterol and phosphatidylcholine, with 5 to 10% negatively charged lipid (such as phosphatidic acid, dicetyl phosphate, or dimyristoyl phosphatidyl glycerol (DMPG)). Our specific formulation uses a mixture of hydrogenated soy phosphatidylcholine (HSPC), cholesterol, DMPG, and alpha tocopherol in a molar ratio of 5:4:1:0.2.

The lipid/aqueous multilamellar vesicle (MLV) dispersion resulting from hydration of the mixture of dry lipid is pressure extruded through an emulsification apparatus. This causes shearing of the MLVs and forms large unilamellar vesicles (LUVs). Two liters of dispersion in less than 1 h are sufficient to provide a final liposome suspension roughly equivalent to 2 units of blood.

Small volumes of LEH have been tested in animals to determine circulation half-life. The method we have developed takes advantage of the difference in density between LEH and red blood cells (RBCs). After injecting a mouse with LEH,

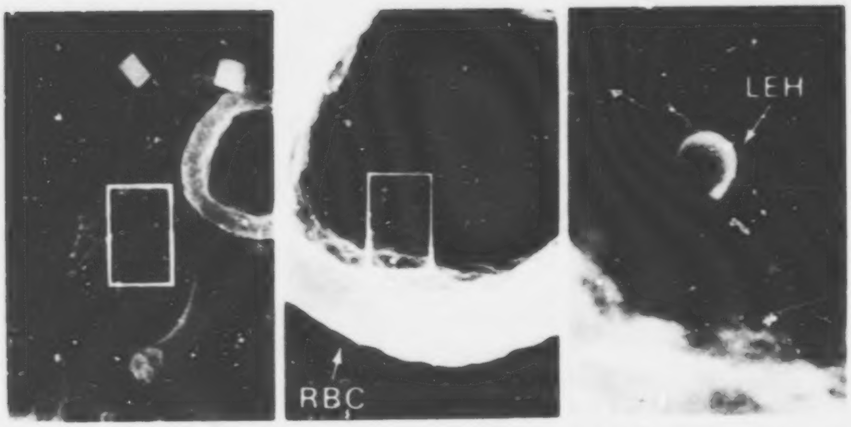

Fig. 3 - Scanning electron micrographs of a mixture of RBCs and LEH. Panels are of increasing magnification. RBCs average 8 μm in diameter compared to 0.2 μm for LEH.

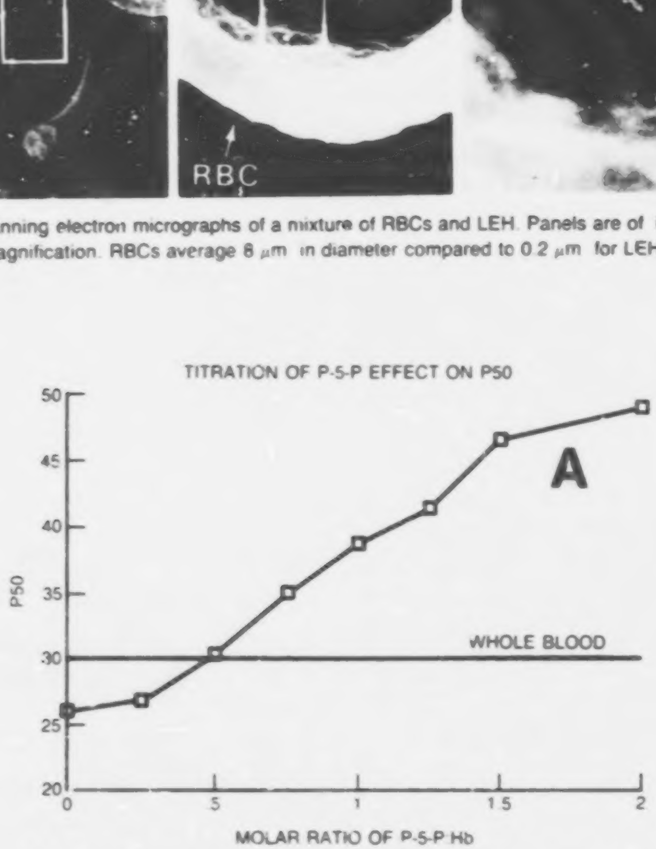

Fig. 4 – Impermeant organic phosphates can be coencapsulated to modulate the oxygen affinity (expressed as the partial pressure of O_2 at which hemoglobin is half saturated, or P50. The P50 of LEH containing 2,3-diphosphoglycerate (DPG), encapsulated with increasing molar ratio of DPG, gradually decreases.

50 μl blood samples were withdrawn at intervals from the eye sinus and centrifuged in microhematocrit tubes. The LEH forms a layer that packs above the RBC layer. The size of the "hemocrit" layer decreases as the LEH is removed by the reticuloendothelial system, and the circulation half-life can be calculated from the disappearance rate. The size relationship between the LEH and a RBC is shown in Fig. 3.

LEH can be physiologically altered by the addition of coencapsulated solutes. The partial pressure of O_2 at which the hemoglobin is half-saturated (P50) can be raised by coencapsulation of organic phosphates, thus lowering the oxygen affinity to that of fresh RBCs. As seen in Fig. 4, P-5-P (pyridoxal-5-phosphate) will actually maintain the high P50 of stored LEH for much longer than can be achieved with stored

RBCs. An increase in the concentration of P-5-P further shifts the P50, resulting in a significantly greater O_2 delivery.

The search for an inexpensive source of lipids for scale-up development led to the use of a soy lecithin that is comprised mainly (85%) of distearyl phosphatidylcholine (DSPC). Studies of liposome circulation half-life as a function of phospholipid indicate that synthetic DSPC, when mixed 1:1 with cholesterol, gives a circulation half-life several times that of synthetic dimyristyl phosphatidylcholine (DMPC). The soy lecithin gave identical results to DSPC, both in encapsulation efficiency and in circulation half-life. Since half-life is dose dependent, a constant dose equivalent to 25% of blood volume was injected in mice; all of the mice survived. The increase in LEH circulation half life in mice, from 4 hours with DMPC to at least 15 hours with HSPC, is shown in Fig. 5; this is a significant improvement over previously reported half-lives [2].

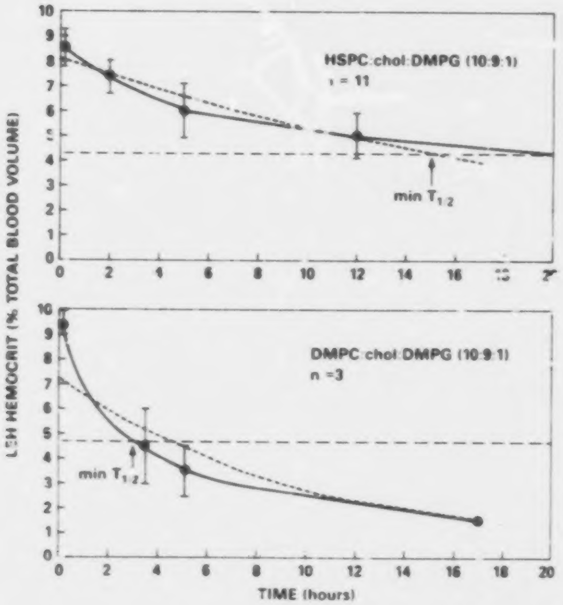

Fig. 5 — The time required for disappearance from circulation of half of the LEH, designated $T_{1/2}$, is estimated from the curves. The liposomal formulation that incorporates HSPC, the major component of soy lecithin, markedly increases the $T_{1/2}$ of LEH.

These results demonstrate that we have made significant improvements in two areas: extended half-life compared to DMPC and cost reduction. HSPC is approximately three orders of magnitude less expensive than the synthetic DMPC or DSPC. This allowed us to proceed with the scale-up feasibility study that required kilograms of the lipid. The scale-up capabilities will allow NRL to support extensive animal trials with LEH material. The practical question of long-term stability is also being addressed. We have initiated a study of natural cryoprotective agents to evaluate their efficacy in preserving LEH integrity and function during freeze/thaw and lyophilization events [3]. Long-term preservation of any blood substitute will be required for the stockpiling envisioned to be cost-effective, and for the vision of universal availability to become a reality.

Acknowledgment: Dr. Rudolph held a NRL/NRC Research Associateship while conducting this research.

[Sponsored by ONR]

References

1. M.C. Farmer and B.P. Gaber, "*Methods in Enzymology*" (1986) in press.
2. C.A. Hunt, R.R. Burnette, R.D. MacGregor, A.E. Strubbe, D.T. Lau, N. Taylor, and H. Kawada, *Science* **30**, 1165 (1985).
3. A.S. Rudolph and J.H. Crowe, *Cryobiology* **23**, 245 (1985).

Two-Dimensional NMR Images in Solids

G. C. Chingas, J. B. Miller,
and A. N. Garroway
Chemistry Division

As advanced organic matrix composites such as graphite-reinforced epoxies are introduced into naval service, the demands for nondestructive evaluation of these polymeric materials also increase. Many of today's methods are designed for metals that, on a coarse scale, are homogeneous and isotropic. By contrast, these organic matrix composites are inhomogeneous and anisotropic. To make matters worse, even the failure mechanisms in these polymer composites are presently poorly understood. New approaches to the nondestructive evaluation of organic matrix composites are sought. As a step towards this goal, we are exploring imaging polymers by nuclear magnetic resonance (NMR) and have demonstrated, for the first time, the two-dimensional (2D) imaging of a solid specimen.

Imaging in Liquids: Up to now, most NMR imaging has been restricted primarily to liquidlike specimens rather than the solids that are of direct interest to the Navy. The explosive development of magnetic resonance imaging in the medical field is altering, possibly revolutionizing, the way soft tissues and blood flow are visualized in the human body. Fortunately, the body is primarily water. The magnetic resonance images represent NMR signals of the hydrogen nuclei in this very mobile water.

Imaging in Solids: To appreciate why imaging a solid is more difficult, consider how the NMR imaging process works. As is well known, nuclei in a magnetic field absorb and emit radio frequency signals precisely at a frequency (resonance condition) determined by the strength of the magnetic field. In imaging, the strength of the magnetic field is made to vary across the sample, and so the resonance frequencies will also vary across the sample, with the resultant spectrum of frequencies creating an image of the specimen.

However, in a solid, the nuclei respond not only to the external magnetic field but also to the magnetic fields caused by neighboring nuclei, through their mutual magnetic dipolar couplings. Unless special steps are taken, this strong dipolar coupling creates local random fluctuations in the size of the total magnetic field. These variations can be three orders of magnitude larger than the variations conventionally used for imaging,

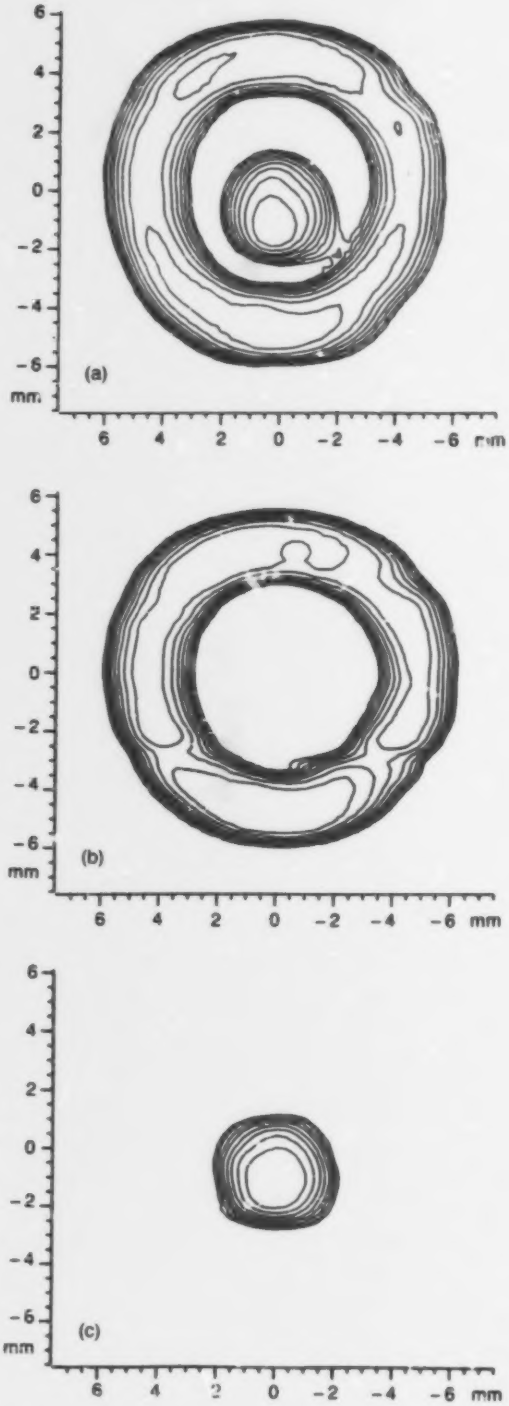

Fig. 6 – Hydrogen NMR images of a solid. The specimen is an inner cylinder of adamantane and outer annulus of neoprene rubber. The intensity plots in (a) represent essentially the hydrogen density while in (b) and (c) the pulse sequence has been altered to emphasize the mobile component (b) or the rigid component (c).

BEST COPY AVAILABLE

hopelessly blurring the NMR image. Of course, in liquids the corresponding dipolar interactions are already averaged to zero by rapid random molecular motions.

To overcome this broadening in the NMR signal, we have incorporated into the imaging procedure a special sequence of intense radio frequency pulses that reduces the hydrogen dipolar coupling by about two orders of magnitude. Over an individual 8-pulse cycle of 50-μs duration, the radio frequency pulses cause the dipolar coupling to switch from positive to negative values in such a way as to average to zero. Thousands of these cycles are used in practice.

By means of this technique, Fig.6 shows a 2D image of the hydrogen nuclei in a solid sample composed of an inner cylinder of the plastic crystal adamantane within an outer annulus of neoprene rubber. The key to useful imaging is to exploit a physical mechanism that produces image contrast. Molecular mobility is one such means of contrast for NMR. By a straightforward modification of the imaging process, one can produce an image weighted by the laboratory frame spin-lattice relaxation time T_1 (Fig. 6(b)) or the rotating frame relaxation time $T_{1\rho}$ (Fig. 6(c)). Because the neoprene rubber is more mobile than the adamantane (neoprene has shorter relaxation times T_1 and $T_{1\rho}$ than adamantane), the NMR image can emphasize more mobile or less mobile regions of the specimen, as in Figs. 6(b) and 6(c), respectively.

The imaging method as described uses hundreds of watts of radio frequency power to image a 15-mm specimen. Larger specimens require proportionately more power, representing a limitation of the present technique. Work is in progress on other methods not restricted to centimeter-sized samples.

[Sponsored by ONR]

Reference

1. G.C. Chingas, J.B. Miller, and A.N. Garroway, "NMR Images of Solids," *J. Magn. Resonance* **66**, 530-535 (1986). ■

Laser Studies of Flame Chemistry

J. W. Fleming, L. R. Pasternack,
and H.H. Nelson
Chemistry Division

Flame chemistry continues to receive attention from numerous research communities because of the emphasis on controlled burning and the direct correlation to fuel consumption. Diagnostic techniques including laser-induced fluorescence, multiphoton ionization, and coherent anti-Stokes Raman spectroscopy, continue to advance the data base for numerous flame environments. Our efforts have concentrated on two areas: examination of laser-assisted ignition studies and gas-phase kinetic measurements.

Ignition Studies: Understanding pathways to equilibrium is a key concern in combustion research. Results from other laboratories working on the perturbation of equilibrium flames (by weak focusing of near-ultraviolet laser sources) and monitoring key species as the flame reestablishes equilibrium have indicated that nonequilibrium conditions need further investigation. The area of ignition involves nonequilibrium flame conditions where the data base and theoretical models are at best qualitative. Ignition parameters are important in flammability studies, in flame propagation (since propagation is determined by the "ignition" of adjacent fuel/oxidizer regions), and stability requirements.

We have incorporated laser preignition techniques to reproducibly ignite fuel/oxidizer mixtures that cannot support sustained combustion. Flowing mixtures of methane and air have been irradiated with the 193-nm output of an ArF laser. Ignition resulted in those systems where the fuel/oxidizer ratio and flow rate were sufficient to sustain combustion. The presence of excited radicals was evidenced from the characteristic emission of C_2 and OH in these studies. In these

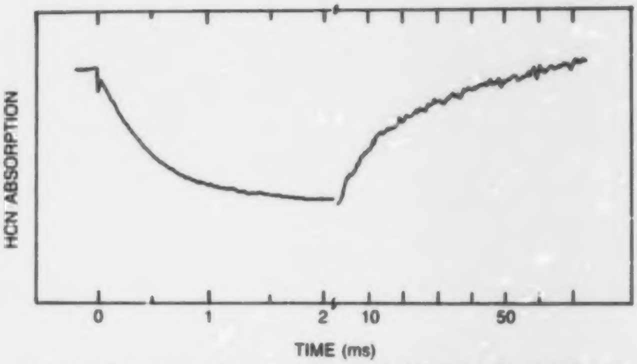

Fig. 7 — Plot of the growth and decay of HCN from the reaction of CN with H_2 at 298 K. $P_{C_2N_2}$ = 80 mTorr, P_{H_2} = 1.3 Torr, and P_{total} = 50 Torr (from Ref. 1).

experiments, ignition is probably by means of laser-induced breakdown, where a plasma is created and the system is not that sensitive to the choice of laser wavelength. However, total absorption of the incident laser radiation is important, and here the choice of laser wavelength will alter the ignition requirements. Note that these results are in contrast to thermal ignition schemes. These differences point out the importance of the buildup of certain critical radicals. Direct probing of these key radicals such as C_2 and CH during ignition will be performed to determine their roles.

Kinetics Studies: We have developed techniques to monitor reactions of radicals in systems where individual reaction can be isolated. We produce the radicals by laser photolysis. Absorption of ultraviolet radiation provides a clean source for many radicals such as C_2, CN, and C_2H. We can then monitor the disappearance of these radicals caused by reaction with various combustion species by using laser-induced fluorescence or infrared absorption with a diode laser. The latter method is also used to monitor the growth of reaction products. By using the infrared absorption techniques, reactions of CN with H_2, D_2, and CH_4 have been studied by monitoring the disappearance of CN and the rise of HCN (Fig. 7).

Conclusion: Information about the role of certain key radicals such as C_2, CH, CN, and C_2H will provide important information for many key areas in combustion including ignition thresholds, probabilities for ignition, and important reactive pathways. Our studies should provide critical data for modelling different flame conditions.

[Sponsored by ONR]

References

1. R.J. Balla and L. Pasternack, *J. Phys. Chem.* **91**, 73–78 (1987). ■

Advanced Fluorinated Polymers Meeting Navy Needs

R. L. Soulen, J. R. Griffith,
and R.F. Brady, Jr.
Chemistry Division

Fluorinated polymers have unique properties that can be used to advantage in the marine environment. Previous synthetic efforts at NRL produced fluorinated epoxy resins that can be converted into polyurethane resins. The resins have the low surface energy and *nonstick* features of poly(tetrafluoroethylene) combined with the easy handling and processability of conventional epoxy and polyol resins. These polymers are now being used successfully as coatings for tanks, bilges, and underwater hulls of surface combatant ships.

A new polyurethane coating for the radomes of Los Angeles-class submarines has now been produced from the fluorinated polyol resin. The

Fig. 8 – USS *Ohio* (SSN-726). The radome is the antenna structure.

radome, shown in Fig. 8, is the uppermost structure on the USS *Ohio* (SSN–726). A film of water on the antenna interferes with the strength and stability of communications, and a coating that facilitates fast draining of water reduces the time needed to achieve a stable signal. The NRL fluorinated coating offers low surface energy and resultant beading and fast runoff of water, resistance to weathering and seawater immersion, and a surface that resists abrasion from the bearings supporting the radome.

The NRL coating was first applied to one radome on the USS *Atlanta* (SSN–712) in December 1984. The coating received a highly favorable evaluation in November 1985 and was then applied to both radomes on the USS *Minneapolis–St. Paul* (SSN–708) and on the USS *Baltimore*. In June 1986, the coating was approved by the Naval Ship Systems Engineering Station for general use on Los Angeles–class fast–attack submarines and on Ohio–class ballistic missile submarines.

A new class of resins that also possess both low surface energy and easy processability has now been prepared. These resins are based on a fluoroaryl acrylate monomer containing four trifluoromethyl groups that can be synthesized in two steps in high yield. Previous NRL research has established that the trifluoromethyl group confers low surface energy and effective water barrier properties to many materials. The goal of this new work, therefore, was to create new acrylate polymer systems that maximized the number of trifluoromethyl groups in the monomer without compromising the mechanical, thermal, or optical properties of polymers made from it. The synthesis of the monomer relies on well–established laboratory and industrial procedures; Figure 9 shows the entire process through which the polymer is obtained.

Bulk polymerized castings of the fluoroaryl acrylate polymer have good optical clarity, improved nonwetting surface characteristics, and a thermal stability that is superior to industrial poly(methyl methacrylate). The thermogravimetric analysis curve in Fig. 10 shows the loss in weight with increasing temperature of a laboratory sample of the fluoroaryl acrylate and a commercial product based on poly(methyl methacrylate), and shows that the temperature at which rapid weight loss begins is higher for the fluoroaryl acrylate.

The fluoroaryl acrylate and methyl methacrylate monomers are miscible and may be copolymerized to achieve a range of surface

BEST COPY AVAILABLE

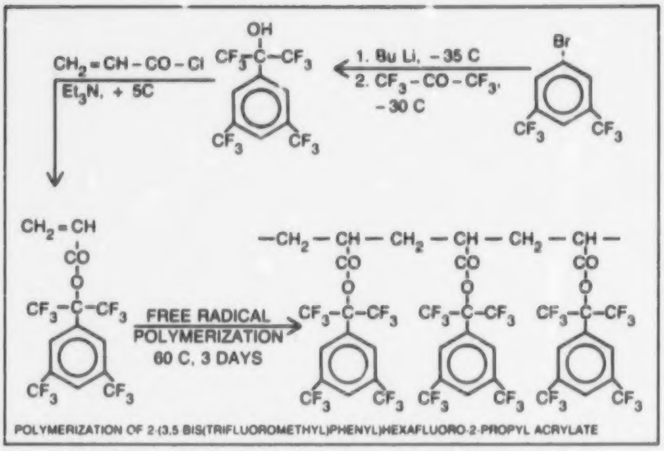
OH
CF_3-C-CF_3
$CH_2=CH-CO-Cl$
$Et_3N, + 5C$
1. Bu Li, −35 C
2. $CF_3-CO-CF_3$, −30 C
Br
CF_3
$CH_2=CH$
CO
O
FREE RADICAL POLYMERIZATION
60 C, 3 DAYS
$-CH_2-CH-CH_2-CH-CH_2-CH-$
POLYMERIZATION OF 2-(3,5 BIS(TRIFLUOROMETHYL)PHENYL)HEXAFLUORO-2-PROPYL ACRYLATE

Fig. 9 – Synthesis and polymerization of a fluoroaryl acrylate

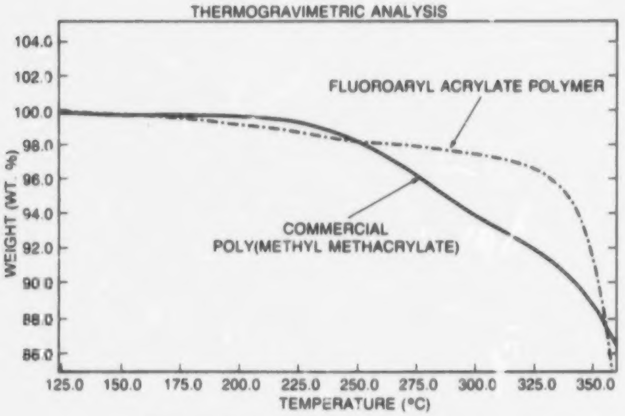

Fig.10 – Thermogravimetric analysis

chemical resistance, mechanical, optical, and thermal properties. Some of the copolymers may well provide the weather resistance and thermal and mechanical strength required for aircraft canopies. Many canopies in use today are made from polyacrylate or polymethacrylate materials that are chosen for their mechanical strength, processability, and optical clarity. However, these materials lack the resistance to chemicals and the nonwetting surface properties of the NRL fluoropolymers, and they develop surface crazing and a resultant loss of optical clarity during weathering.

[Sponsored by ONR and NAVSEA] ■

BEST COPY AVAILABLE

Metals, alloys, composites, and ceramics—the basic building blocks of the Navy—are at the heart of much of the research effort at NRL. The Material Science and Technology Division directs fundamental and applied research to materials behavior, properties, and processing, to materials composition and modification, and to materials performance and reliability in structures and devices. Fields of emphasis encompass mechanics and metallurgy, environmental effects, and the microstructure details that control successful materials use by the Navy.

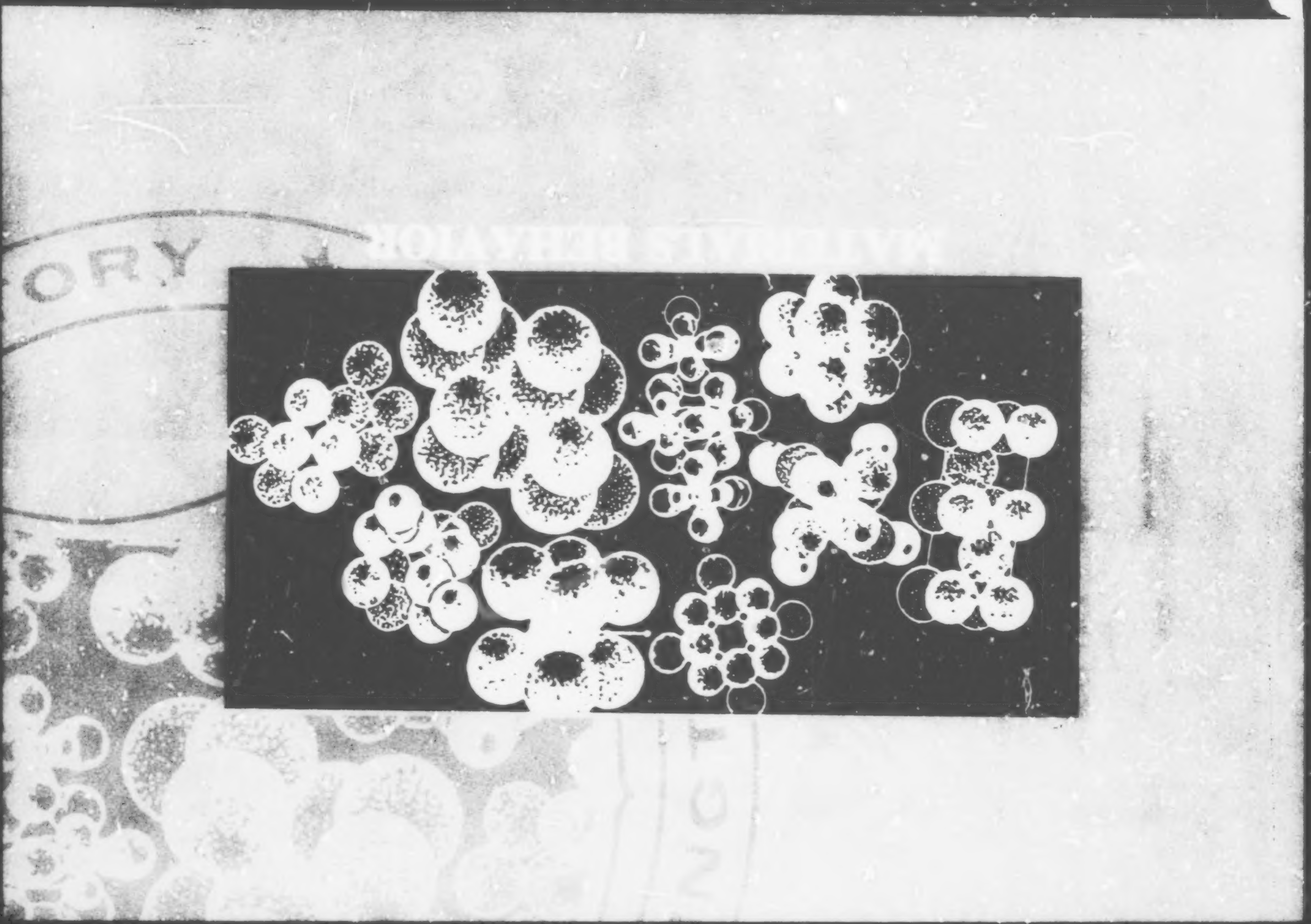
ORY

BEHAVIOR AND PROPERTIES OF MATERIALS

85 **Constrained-Layer Damping of Structure-Borne Sound**
Pieter S. Dubbelday

87 **Computer-Controlled Emissivity Measurement System**
John A. LaFemina and William E. Howell

89 **Measurement of Undercooling Effects in Gas-Atomized Metal Powders**
Iver E. Anderson, Jack D. Ayers, Michael P. Kamppainen, and Wayne P. Robey

92 **Surface Modification for Improved Corrosion Resistance**
Edward McCafferty, Paul M. Natishan, Peter G. Moore, and Graham K. Hubler

95 **Processing of High Critical Temperature Ceramic Superconductors**
David Lewis, III, Darla J. Schrodt, Jay S. Wallace, and Louis B. Toth

97 **Computer Modelling of Anisotropic Elasticity and Piezoelectric Effects in Ceramics**
Robert P. Ingel, David Lewis, III, and Manfred F. Kahn

102 **Mechanisms of Interdiffusion in Coated Superalloys**
Virgil Provenzano and James R. Reed

104 **Atomic Resolution Images**
John H. Konnert and Peter D'Antonio

Constrained-Layer Damping of Structure-Borne Sound

Pieter S. Dubbelday
Underwater Sound Reference Detachment

Constrained-Layer Concept: Figure 1 shows two definitions of the term "constrained layer." The present study concentrates on the second meaning. It is an everyday experience that most metal structures are able to sustain vibrations and sound for extended periods of time. This points out that sound is not well absorbed by metals. The eventual decay of such structure-borne sound is mostly due to radiation into the surrounding medium, generally air or water. To dampen such sounds for the sake of human comfort or to reduce detection by an inimical party, one turns to materials that strongly absorb sound. Again by daily experience one knows that rubberlike materials, collectively called elastomers, qualify for this purpose. They are said to possess the property of viscoelasticity: in addition to being elastic, they absorb mechanical or acoustical energy by internal friction (viscosity).

One would expect that attaching a layer of elastomer to a metal structure would improve the damping, and such "extensional damping" does give positive results. This damping is enhanced in turn, by attaching a thin layer of a stiff metal to the surface of the elastomer layer.

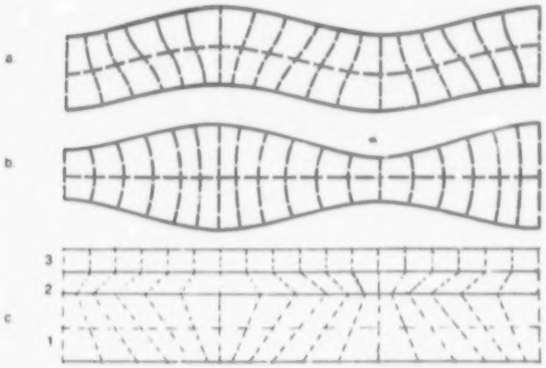

Fig. 2 – (a) Shape of flexural wave. (b) Shape of extensional wave. (c) Mechanism of constrained-layer damping of flexural waves. The elastomer layer (2) is forced into shear by the motion of the base plate (1) and near-quiescence of the constraining layer (3).

Figure 2 explains the mechanism of this constrained-layer damping (CLD). There are two types of waves that can propagate in an infinite plate distinguished by the appearance of the surface flexural (or bending) waves (Fig. 2(a)) and extensional waves (Fig. 2(b)). The sketches in Fig. 2 greatly exaggerate the displacements occurring in the plate. For both types of waves, the surface moves perpendicularly to the plate but also back and forth in the direction of the plate. The stiff overlying layer (3) in Fig. 2(c) is practically motionless; as a result the elastomer layer (2) is forced into shear. This increased shear enhances

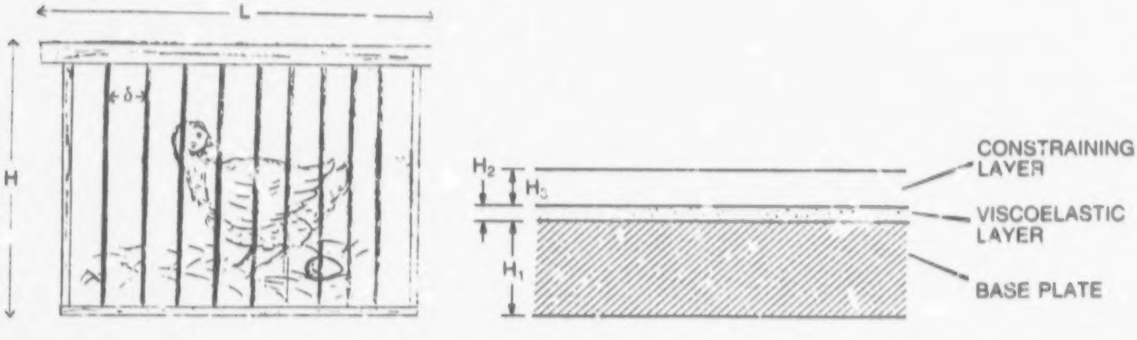

(a) (b)

Fig. 1 – Constrained-layer concept (a) Idea and artwork courtesy of Mr. T. A. Henriquez, Code 5971. (b) Schematic diagram of concept.

BEST COPY AVAILABLE

the damping because damping in elastomers is predominantly connected to shearing motion. Notice that in Fig. 2(c) the motion perpendicular to the plate is ignored.

As in most practical applications of ideas, one needs a model of the process to arrive at design criteria before scale-model or prototype testing. An early predictive model for CLD was given by E.M. Kerwin in 1959 [1]. By a careful choice of simplifying assumptions, Kerwin obtained an explicit expression for the damping effect as a function of the experimental quantities involved: frequency of the acoustic wave thickness of each of the three layers and elastic moduli of the materials, especially the shear modulus of the elastomer.

Extension and Comparison of CLD Models: Kerwin's model does not include extensional waves and is limited to plates that are thin compared with the wavelength of the sound. Therefore, a study was undertaken to extend this model and to verify its validity by comparison with models based on exact-elasticity theory.

First, Kerwin's model was extended to also cover the case of extensional waves. For comparison, a hybrid model was developed whereby the base plate is described by exact-elasticity theory, while the elastomer and constraining layers follow Kerwin's treatment [2].

Figure 3 shows the results for propagation of straight-crested waves in an infinite brass plate of 10-cm thickness, with a 1.2-mm-thick elastomer layer and a 2.5-mm-thick aluminum constraining layer. The attenuation is given in dimensionless form by the expression α/k, where α is the attenuation coefficient in the amplitude reduction factor $\exp(-\alpha/x)$ (x is the distance along the plate). The quantity k is 2π divided by the wavelength of the acoustic wave. The attenuation is presented as a function of the frequency in kilohertz.

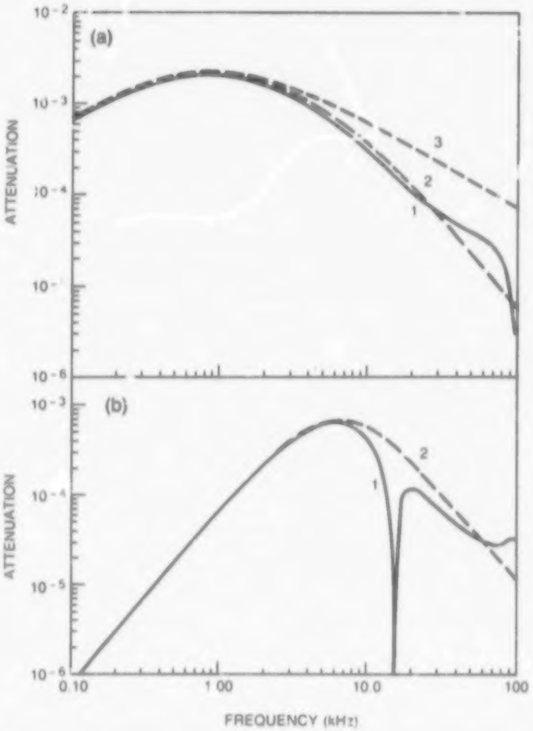

Fig. 3 – Comparison of constrained-layer models. (a) Flexural wave. Curve 1 – Hybrid model. Curve 2 – Extended Kerwin model with exact wave speed. Curve 3 – Extended Kerwin model with thin-plate wave speed. (b) Extensional wave.

Figure 3(a) gives the results for flexural waves. It compares the extended Kerwin model, curve 3, with the results of the hybrid model, curve 1. Apparently, up to about 1 kHz there is very good correspondence, but above this frequency the discrepancy increases. One might surmise that the discrepancy is due to the peculiarity of thin-plate theory to predict a propagation speed that differs from the value in exact-elasticity theory for increasing frequency. In confirmation of this suggestion, it was found that Kerwin's model with a wave speed derived from exact-elasticity theory results in a much better prediction of attenuation, as shown in Fig. 3(a), curve 1.

Figure 3(b) shows the results of extensional waves. Curve 2 gives the result of the extended Kerwin model, and curve 1 gives that of the hybrid model. One sees that there is a dip in the hybrid curve near 20 kHz. This dip is due to a specific wave motion in the plate. As a result, the surface does not move and there is a corresponding lack of damping used by shear that is not predicted by thin-plate theory. In the case of *extensional* waves,

there is no obvious advantage to using the correct wave speed instead of the wave speed from thin-plate theory, unlike the case of *flexural* waves.

The investigation is continuing by comparing results from the hybrid model with those from a model in which all three layers are described by exact-elasticity theory. Since the major purpose of constrained layer damping is to increase the viscoelastic damping over the energy radiated out into the medium, the relative contributions of these two effects to the total damping are being studied.

[Sponsored by ONR]

References

1. E.M. Kerwin, "Damping of Flexural Waves by a Constrained Viscoelastic Layer," *J. Acoust. Soc. Am.* **31**, 952-962 (1959).
2. P.S. Dubbelday "Constrained-Layer Model Investigation Based on Exact Elasticity Theory," *J. Acoust. Soc. Am.* **80**, 1097-1102 (1986). ■

Computer-Controlled Emissivity Measurement System

J. A. LaFemina and W. E. Howell
Tactical Electronic Warfare Division

The optical properties of materials at elevated temperatures have received greater interest in recent years because of technological advances in material fabrication and the search for alternate energy sources. Experimental data characterizing the high-temperature optical properties of materials is sparse, and hence a need exists for the measurement of the thermal radiative properties of such materials especially in the infrared region of the spectrum at both low and high temperatures. To meet this need, we designed, fabricated, and tested an automated apparatus for the measurement of the spectral emissivity of materials in the wavelength range 2 to 15 μm and in the temperature range 300°C to incandescence. This represents a rare measurement capability since only a few facilities in the country can cover this range on a wide class of materials. To determine the performance of the system, tungsten, an emissivity standard, was chosen to establish a calibration for the system. Results demonstrate that the present system functions properly. Recently, we have used the system to characterize the emissivity properties of candidate infrared decoy materials and have found that it provides us with a valuable tool for rapidly assessing the emissive properties of such materials.

Emissivity is defined as the ratio of the radiation from the surface of a material to the radiation from a blackbody at the same temperature. In the present setup, the integral blackbody method [1] was chosen whereby a metallic foil or ribbon is formed into a tube shape and is heated by the passage of direct current. This method involves the comparison of the radiant intensity from a sample tube surface to the radiant intensity from a blackbody hole in the tube wall. Since the blackbody and the sample tube are essentially at the same temperature one only needs to take the ratio of the radiation from the sample surface and the blackbody to determine the spectral emissivity of the sample.

System Description: The present system (Fig. 4) consists of the sample, sample chamber (Fig. 5), sample positioner, optical system, and the data processing system. The sample chamber is constructed from stainless steel vacuum components that allow the system to be evacuated to ultrahigh vacuum. This eliminates any surface contamination of the sample. The sample holder is water-cooled to prevent its deformation when the sample is heated to high temperatures. Solid-state infrared detectors are used to maximize the sensitivity of the system that allows emissivity to be measured as low as 300°C. A lock-in amplifier processes the chopped signals, and the Hewlett Packard 9836 computer records the blackbody hole and wall voltages. The computer automatically controls the wavelength counter as well as the sample wall and blackbody positions.

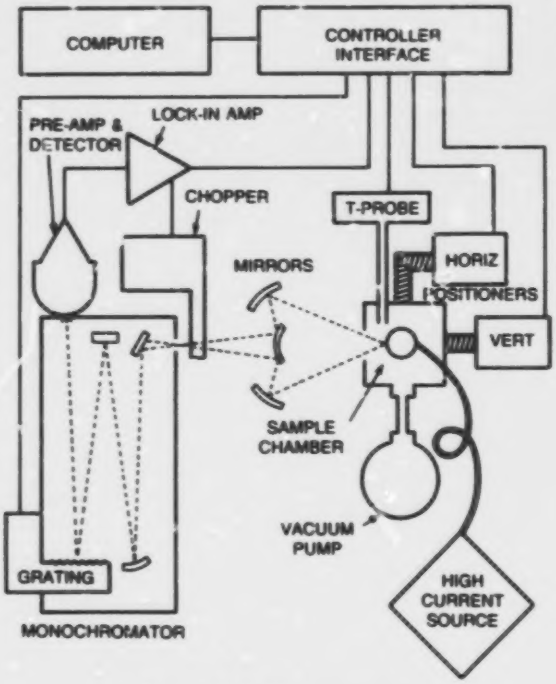
COMPUTER
CONTROLLER INTERFACE
PRE-AMP & DETECTOR
LOCK-IN AMP
CHOPPER
T-PROBE
MIRRORS
HORIZ
POSITIONERS
VERT
SAMPLE CHAMBER
VACUUM PUMP
HIGH CURRENT SOURCE
GRATING
MONOCHROMATOR

Fig. 4 – Emissivity apparatus

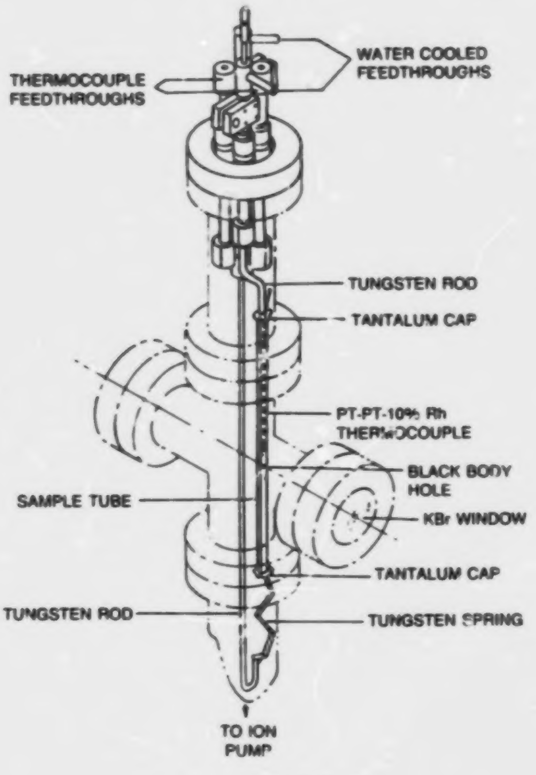
WATER COOLED FEEDTHROUGHS
THERMOCOUPLE FEEDTHROUGHS
TUNGSTEN ROD
TANTALUM CAP
PT-PT-10% Rh THERMOCOUPLE
BLACK BODY HOLE
SAMPLE TUBE
KBr WINDOW
TANTALUM CAP
TUNGSTEN ROD
TUNGSTEN SPRING
TO ION PUMP

Fig. 5 – Sample chamber

The temperature of the sample is determined by a thermocouple inserted inside the sample tube for temperatures below incandescence and by a precision microoptical pyrometer for temperatures above incandescence. In the region of incandescence, the two methods agree. Allowing for the sources of error (quality of the blackbody cavity, temperature gradients in the vicinity of the blackbody cavity, and effects of scattered flux), the overall accuracy of the emissivity system is estimated to be ±5%.

Results: A tungsten emissivity standard was fabricated from a 50-μm-thick unannealed tungsten foil supplied by the A.D. Mackay Company with a purity content of 99.95%. The cleaned tungsten ribbon was formed into a circular tube whose diameter was 0.635 cm with a 0.152-cm-diameter hole drilled in the center. Surface roughness measurements made at NRL [1] on the tungsten foil indicated an average roughness of one μm and waviness amplitude of 15 μm. Therefore, the "as is" tungsten surface was virtually contaminant-free but not optically smooth. Figure 6(a) shows the results from the measurement of the normal spectral emissivity of the tungsten sample from 2 to 15 μm at 1273 K. The present data compare well with literature values [2] on annealed tungsten samples, which demonstrates that the emissivity system functions properly.

Recently, we have used the emissivity system to characterize the spectral emissivity of activated and unactivated 1010 steel. Activation refers to a process that renders the 1010 steel surface extremely rough. The system was used to measure the resultant spectral emission from both surfaces at 1073 K. Figure 6(b) shows the increase in the spectral emissivity for the activated surface that demonstrated a uniform (0.8) graybody emission from 2 to 15 μm. These results show that modifications to the surface morphology can lead to drastic changes in the optical properties of materials.

BEST COPY AVAILABLE

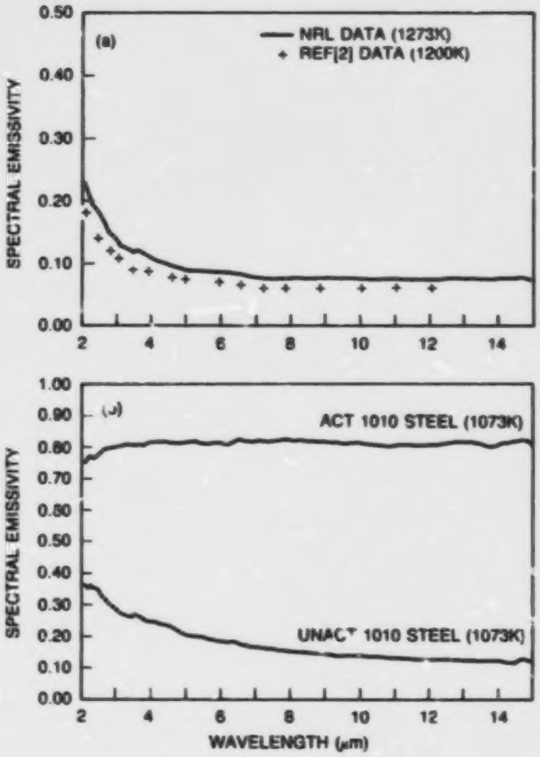

Fig. 6 – (a) Comparison of the spectral emissivity of NRL-measured tungsten standard with literature values and (b) activated vs unactivated 1010 steel measured at normal incidence to the samples

Future: Future use of the Computer Controlled Emissivity Measurement System will be in the basic research area supporting the evolution of next-generation infrared decoy technology. In that generation of technology, the requirement for high-heat output is expected to be accompanied with equal weight by a requirement for specific spectrum quality. Evident growth of sophistication in heat-seeking weapons is already leading decoy designers to search for a new class of heat source materials that emit infrared radiation only in selected wavelength intervals.

The common observation that good selective emitter materials tend to be poor heat sources, while good heat sources tend to have poor selective emitter properties has led us to pursue a dual-material approach for hot-surface type decoys. The composite includes a heat source substrate mated to and used to energize a film of a selective-emitter material. This approach allows us to choose any selective-emitter material independent of heat source constraints, but it introduces complexities that require an extension to the existing theory of emissivity. The extension, which is an accounting of the radiation ensuing from a back-heated selective-emitter film [3], must in turn be supported by emissivity measurements that test or validate new additions to the theory. These tests and validation experiments along with the acquisition of emissivity data on previously unreported new and unusual materials will continue to be the principal function of the Computer Controlled Emissivity Measurement System.

[Sponsored by ONT and ONR]

References

1. J.A. LaFemina and W.E. Howell, "Computer Controlled Apparatus for the Measurement of the Normal Spectral Emissivity of Materials," NRL Memorandum Report 4972, Nov. 1982.
2. W.K. Askwyth, R.J. Yahes, R.D. House, and G. Mikk, NASA-CR-56496, 56497, 56498, 1-277, 1962.
3. J.A. LaFemina and H.D. Ladouceur, "Radiative Heat Transfer and Selective Emission in Planar Slab Coatings on Hot Emissive Substrates," NRL Memorandum Report (in press). ■

Measurement of Undercooling Effects in Gas-Atomized Metal Powders

I. E. Anderson, J. D. Ayers, M. P. Kamppainen, and W. P. Robey
Material Science and Technology Division

Rapid solidification processing (RSP), especially by a powder metallurgy route, has emerged as an attractive approach to the generation of advanced alloys with unique crystalline or amorphous microstructures that can exhibit desirable properties. These properties can include

BEST COPY AVAILABLE

enhanced corrosion resistance, improved magnetic performance, and increased strength with significant ductility. The enhanced properties of such alloys arise from a number of microstructural effects of the process including a decrease in microsegregation spacing, an increase in the population density of dispersion strengthening agents, and the generation of metastable phases. The formation of these beneficial microstructures in gas-atomized alloy powders arises from the rapid solidification process that transforms the droplets in the atomized spray into powder particles.

A high particle-solidification rate is often attributed to the high convective cooling rate (10^5 to 10^6°C/s) of the gas atomization process that provides a high thermal gradient to drive the solidification front. The cooling rate should increase as particle size is reduced, an effect of an increasing particle surface area to volume ratio. Alternatively, the cooling rate should also increase as the quenching effect, i.e., heat capacity and thermal conductivity, of the atomization gas is increased.

Results of studies using other particulate production methods with slow cooling rates (10°C/min) have demonstrated that high liquid undercooling levels achieved before solidification starts also have a profound influence on the ability to obtain rapid solidification conditions. In fact, if a *hypercooled* level is achieved in a molten particle, the total heat evolved during solidification can be absorbed adiabatically without any external cooling of the particle. Such high undercooling levels are promoted by disintegrating a melt into fine droplets, preferably less than 10 μm in diameter. This isolates potent nucleation catalysts to a small fraction of the droplets and permits high undercooling in most of the nucleant-free droplet population.

In other words, rapid solidification would be promoted by producing finer particles with a gas atomizer because of both increased cooling rate and increased undercooling. Until this study was undertaken, the relative importance of the roles of cooling rate and undercooling in determining gas-atomized powder microstructures had not been characterized, especially over a range of powder sizes that includes ultrafine (< 10 μm) particles.

Procedures: Direct determination of atomized particle cooling rates would require a difficult procedure, probably involving high-resolution photoemission pyrometry. Heat transfer calculations are often used to estimate particle cooling rates based on specific models of the heat transfer mechanism. With a reasonable heat transfer model, calculations show that helium should have 10 times the cooling effect of argon in atomization. This quenching effect difference, which is independent of particle size, was used in two levels of particle cooling rate in our atomization experiments.

The measurement of the nucleation temperature of atomized droplets during flight is the only direct way to determine undercoolings for gas atomized powders, but this also remains an elusive measurement. However, a differential thermal analysis (DTA) technique was developed to provide a useful indirect measurement of the undercooling capability of gas-atomized powders as a function of particle size. The DTA measurements were performed on powder samples from the argon-atomized yield separated into size fractions of 15-20 μm, 5-10 μm, and <5 μm. Figure 7(a) shows each DTA sample dispersed in a ceramic medium, heated above its melting temperature, and slowly cooled (20°C/min) in a controlled atmosphere of purified argon. Powders of the same size from either the argon- or the helium-atomized batches should exhibit equivalent undercooling behavior in the DTA because the samples are remelted and cooled at a slow rate.

Results: Scanning electron microscopy and X-ray diffraction analysis revealed that the microstructure of the gas-atomized Cu-8.3 wt. % Al alloy powders appears to be independent of the choice of atomization gas and dependent on

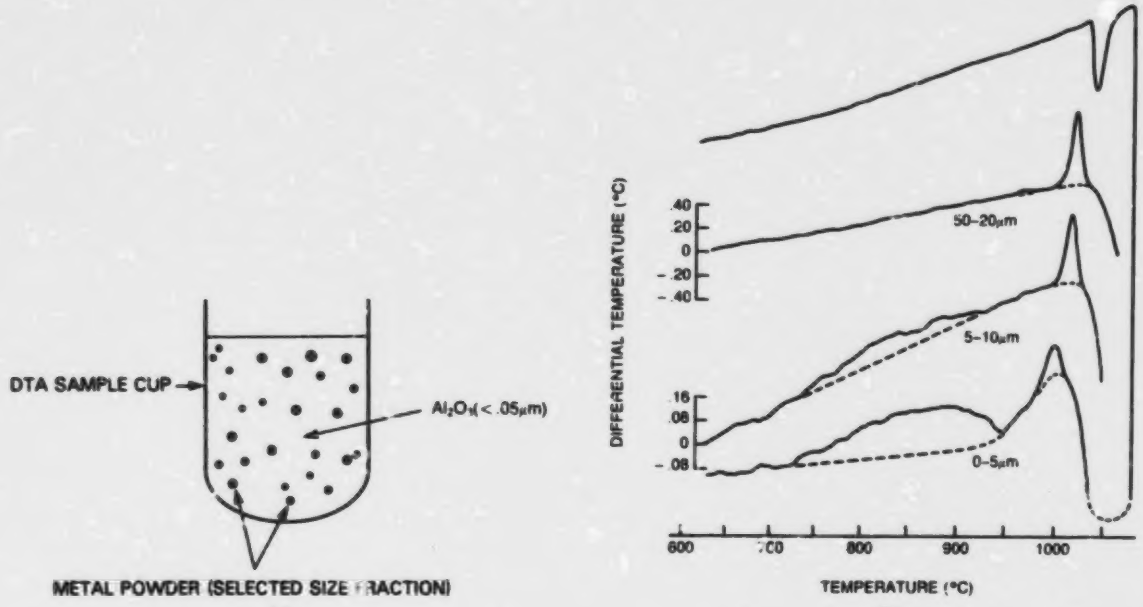

(a) (b)

Fig. 7 – (a) Powder sample preparation technique for DTA. (b) Summary of DTA results for size fractioned Cu–8.3wt. % Al powders. Solidification exotherms on cooling presented for each size fraction sample. Dashed lines indicate cooling baseline. One melting endotherm shown for direct comparison of undercooling.

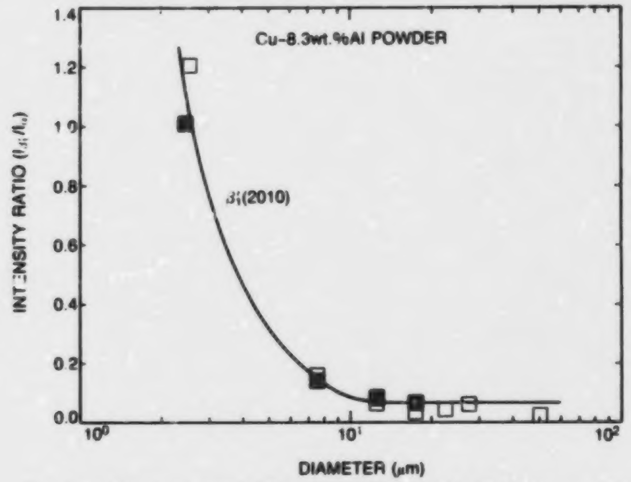

Fig. 8 — Measurements of Bragg peak ratio of β'_1 (2010) to α − CU (200) for various size fractions of Cu-8.3wt. % Al powders. Open squares are argon-atomized and solid squares are helium-atomized powder results. Each particle diameter value represents the midpoint of a size fraction.

particle size over a size range that includes ultrafine powders. Powder particles larger than about 20 μm generally exhibited a multiple cell-like morphology with a lamellar or platelike intracellular phase that occasionally appeared to extend from the cell boundary phase. X-ray diffraction measurements, summarized in Fig. 8, revealed the presence of a Cu(fcc) majority phase and a β'_1 martensite minority phase, as judged by a comparison of characteristic peak heights. A single-phase particle morphology, devoid of cells, appeared in a significant fraction of the particle

BEST COPY AVAILABLE

population smaller than about 10 μm. In these ultrafine powders the X-ray diffraction measurements of Fig. 8 also showed a marked increase in the martensite phase content of the powders relative to the Cu(fcc) phase. Both the argon- and helium-atomized powders exhibited equivalent morphologies and product phase contents in the same size classes. These results indicate that the difference in cooling rate between argon- and helium-atomized powders did not affect the particle microstructures.

The DTA results summarized in Fig. 7(b) indicate that ultrafine particles have an increased capability to sustain high levels of undercooling prior to solidification. The exothermic solidification of particles from the larger powder size class, 15 to 20 μm, began immediately after cooling below the eutectic temperature, essentially without any undercooling. In the 5–10 μm and the <5 μm particle samples, the DTA revealed that a large fraction of the total solidification exotherm is shifted to lower temperatures, i.e., greater undercooling. These results suggest that enhanced particle size refinement, i.e., increased melt subdivision, promotes the onset of high undercooling conditions.

Summary: The combined results indicate that the undercooling rather than the cooling rate appears to control the particle solidification morphology in gas-atomized powders, especially in the fine particle size range [1]. Thus further development of powder production techniques should concentrate less on increased cooling efficiency and more on particle size refinement. The high pressure gas atomization approach [2] using inexpensive gases such as argon or nitrogen rather than helium, appears to offer a technologically attractive solution to the production of high yields of premium, rapidly solidified powders. This work has broad implications for the general application of RSP solutions to the needs of the Navy for advanced alloys and structures, particularly for those fabricated by powder metallurgy processing.

[Sponsored by ONR]

References

1. I.E. Anderson and M.P. Kamppainen, "Undercooling Effects in Gas Atomized Powders," in *Proceedings of the Hume-Rothery Memorial Symposium on Undercooled Alloy Phases* (TMS-AIME, Warrendale, PA (1987), pp. 269–285.

2. J.D. Ayers and I.E. Anderson, U.S. Patent No. 4,619,845. ■

Surface Modification for Improved Corrosion Resistance

E. McCafferty, P. M. Natishan,
and P. G. Moore
Material Science and Technology Division

G. K. Hubler
*Condensed Matter and Radiation
Sciences Division*

In recent years there has been much interest in improving the corrosion behavior of metals and alloys by modification of their surfaces using directed energy beams [1-3]. Two active areas of research involve the processing of metal surfaces by ion beams or by high-energy lasers.

These surface modification techniques provide a method of conserving scarce, expensive, or critical materials by concentrating them in the surface where they are required for applications such as corrosion protection, wear resistance, or catalytic performance. Other advantages are alteration of the surface without sacrifice of bulk properties, production of novel surface alloys unattainable by conventional metallurgical techniques, and avoidance of coating adhesion problems.

Ion Implantation: Novel solid solution alloys have been prepared by ion implanting aluminum with selected chemical species (Si, Zr, Nb, Mo, Cr, Zn, or Al) at concentrations of 12 atomic percent (at.-%).

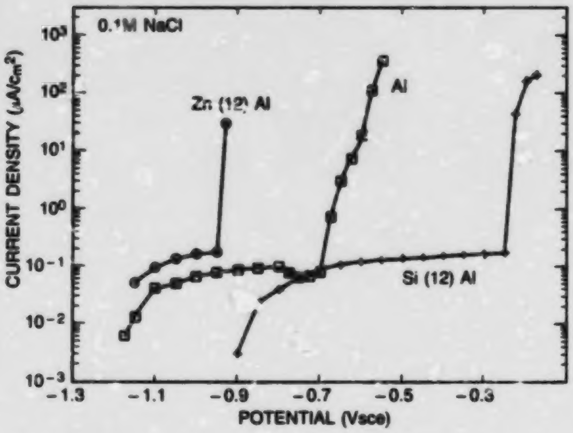

Fig. 9 - Anodic polarization curves for Zn (12at.-%) Al, Al, and Si (12at.-%) Al in 0.1 M NaCl

Figure 9 shows anodic polarization curves for Zn(12at.-%)Al, Si(12at.-%)Al, and unimplanted aluminum. The important characteristic of each curve is the pitting potential, i.e., the electrode potential at which there is a sudden increase in current density caused by the initiation of corrosion pits. At potentials below (less positive than) the pitting potential, pits do not initiate; above the pitting potential, pits initiate and grow. A higher (more positive) pitting potential represents an increased resistance to pitting corrosion. Thus ion implantation with Si increases the pitting potential of Al by 450 mV, whereas implantation with Zn decreases the pitting potential by 250 mV.

To cause pitting, a chloride ion must first adsorb at the oxide/solution interface. Ion implantation offers the possibility of inhibiting this first step by modifying the surface charge. An important parameter controlling the surface charge, and therefore the adsorption characteristics of an oxide-covered surface, is the pH of zero charge of the oxide. The pH of the point of zero charge of an oxide, pHpzc, is the pH at which the surface oxide has a net zero charge. At pHs lower than the pHpzc, the surface has a net positive character, and anions such as Cl- are electrostatically attracted to the surface and can adsorb. When the pH is higher than the pHpzc, the surface has a net negative charge, and anion adsorption is inhibited. Table 1 shows that implanted elements chosen because of the low pHpzc of their oxides (Si, Cr, Zr, Nb, and Mo) produced binary surface alloys that had higher (more positive) pitting potentials than aluminum. The implant chosen because of the high pHpzc of its oxide (Zn) produced a binary surface alloy with a pitting potential lower than that of aluminum. Additional work is in progress to determine the relationship between surface charge, adsorbability, and the breakdown of passive films on aluminum.

Table 1 — Effect of Various Implanted Ions on the Pitting Potential of Pure Aluminum

Implanted Ion	12 at.-%	pH_{pzc} Oxide
Mo	-0.545	1.95
Si	-0.340	2.10
Nb	-0.585	*2.80
Zr	-0.410	6.00
Cr	-0.565	6.2
Al	-0.700	** 9.10
Zn	-0.950	6.2

*The pH_{pzc} of niobium oxide is similar to that of tantalum oxide.

**Unimplanted Al: −0.700V (sce)

Laser Surface Alloying: Laser surface alloying consists of melting the surface of a metal, adding known amounts of other metals, mixing these components, and allowing them to rapidly resolidify. Molybdenum has been laser alloyed into a 304 stainless steel substrate at surface concentrations of 3% and 9% to produce Fe-Cr-Ni-Mo surface alloys. The 3% Mo-laser-surface-alloyed 304 stainless steel is within the specifications of the more corrosion resistant type 316 stainless steel. Figure 10 shows electron microprobe traces taken across the 3% Mo-surface alloy. It can be seen that Mo is

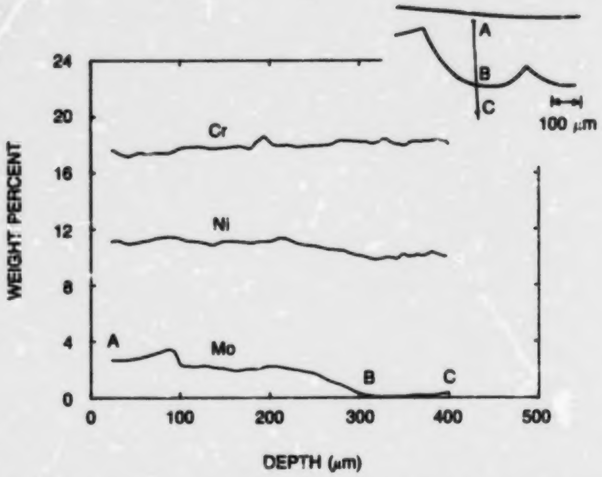

Fig. 10 – Microprobe traces across the 3% Mo surface alloy shown in Fig. 2. The inset to the right shows the outline of the melt.

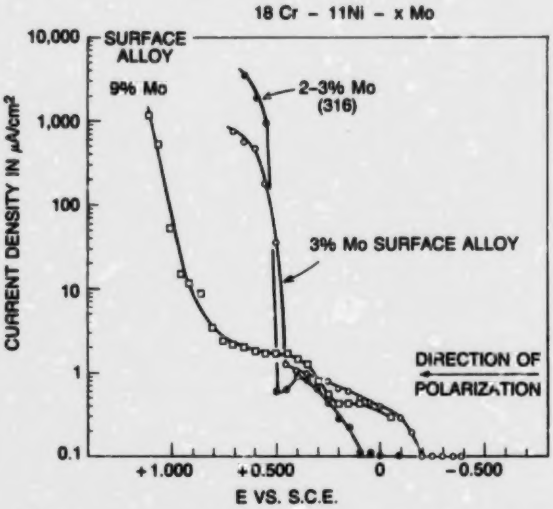

Fig. 11 – Anodic polarization curves for Fe–Cr–Ni–Mo alloys in 0.1 M NaCl

distributed evenly throughout the surface alloy, except at the bottom of the laser melted region. The 9% Mo-surface alloy was similar to the 3% Mo-surface alloy both in its microstructure and in the effectiveness of mixing and dispersion of the alloying additions.

The anodic behavior of the two Mo-surface alloys in 0.1 M NaCl is seen in Fig. 11, which shows that the pitting potential of a 3% Mo-surface alloy is similar to that of bulk 316 stainless steel. The 9% Mo-surface alloy did not undergo pitting up to potentials of oxygen evolution.

Thus the 3% Mo-surface alloy prepared by laser-surface alloying exhibits both a surface composition and a pitting resistance equivalent to type 316 stainless steel, but it conserves the amount of Mo required by restricting its presence to the near-surface region. The rapid solidification feature of the laser alloying process enables production of a 300-series type surface stainless steel containing 9% Mo, an amount in excess of that possible by conventional alloying techniques.

[Sponsored by ONR]

References

1. E. McCafferty and P.G. Moore, *J. Electrochem. Soc.* **133**, 1090 (1986).
2. P.M. Natishan, E. McCafferty, and G.K. Hubler, *J. Electrochem. Soc.* **133**, 1061 (1986).
3. E. McCafferty, G.K. Hubler, P.M. Natishan, P.G. Moore, R.A. Kant, and B.D. Sartwell. *Mater. Sci. Eng.* **86**, 1 (1987). ■

Processing of High Critical Temperature Ceramic Superconductors

D. Lewis, III, D. Schrodt, J. S. Wallace,
and L. Toth*
Materials Science and Technology Division

Recently a new family of superconducting materials has been discovered that is based on a mixed ceramic oxide. The initial discovery, first presented in November 1986, was a lanthanum barium copper oxide with the approximate molar composition of 1.9La:0.1Ba:1.0Cu. This oxide is superconducting at about 37 K (zero resistance at this temperature). This is a significant improvement over the best previous material that is superconducting at 23 K, discovered over a decade ago. Following the report on the mixed oxide superconductor and the critical confirmation of the full Meissner effect (expulsion of magnetic flux), intensive work was begun at NRL (and at many other research institutions). The work at NRL has been directed toward exploiting and extending the initial discovery and toward providing a strong basis for future work in this area. Naval Research Laboratory research has been devoted to two areas: processing the family of mixed oxide ceramic superconductors and determining the details of the crystal structure of the superconductor. The first effort involves working out the detailed parameters of the procedures necessary to produce useful components or test specimens of the superconductor and all the detailed interactions of the various processing steps with each other and with compositional changes in the material. The second research thrust, precisely determining the crystal structure of the various mixed oxide superconductors, relates directly to the need for fundamental understanding of the mechanism of superconductivity in this new class of materials. Some key experiments have been performed; these suggest that previous theoretical explanations for superconductivity in metallic materials may not be applicable to the ceramic materials.

Current research at NRL and elsewhere to optimize the material, e.g., by maximizing the temperature of superconductivity, has been largely empirical or semiempirical. This is because of the lack of theoretical understanding of the mechanism for superconductivity in the mixed ceramic oxides. One indication, from very recent results for the crystal structure, is a requirement for a crystal structure and copper valence states such that copper-oxygen chains are present in the structure and isolated from each other. Superconductivity appears also to require the presence of *excess* oxygen, equivalent to having approximately 50% of the copper in the 3+ valence, although the actual presence of Cu (3+) is still a matter of conjecture. Figure 12 shows the crystal structure obtained by using both X-ray diffraction and neutron diffraction techniques as developed by the National Bureau of Standards, in conjunction with NRL, and by other groups. The copper-oxygen chains thought to be responsible for the superconductivity are those at the top and bottom of the unit cell, with copper in a square planar coordination. This configuration would provide isolation of the copper-oxygen chains from each other as is thought to be required for superconductivity. The composition shown, yttrium barium copper oxide in the cation ratio, 1:2:3, is currently the best superconductor known and has a critical temperature in excess of 90 K. There are some indications that this material may be superconductive at approximately 100 to 110 K. The large amount of free space in the crystal

---

*National Science Foundation

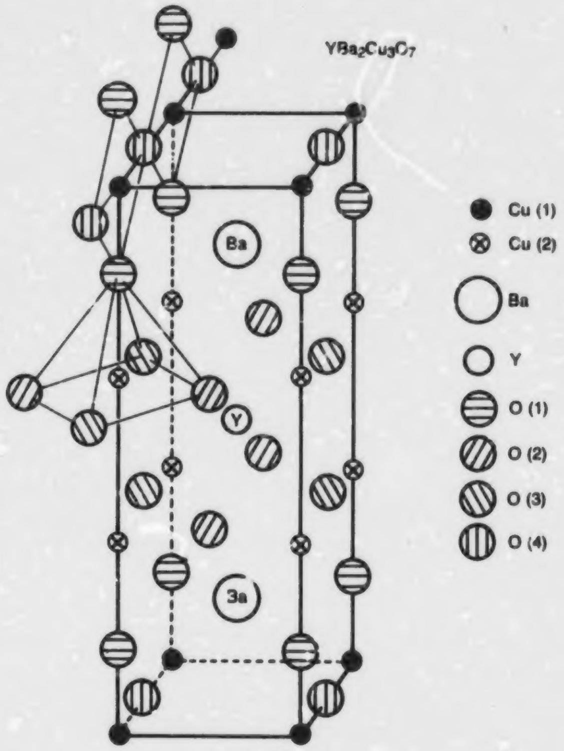

Fig. 12 – Crystal structure, unit cell, for yttrium barium copper oxide superconductor, as determined by X-ray diffraction (cation lattice) and neutron diffraction (anion lattice)

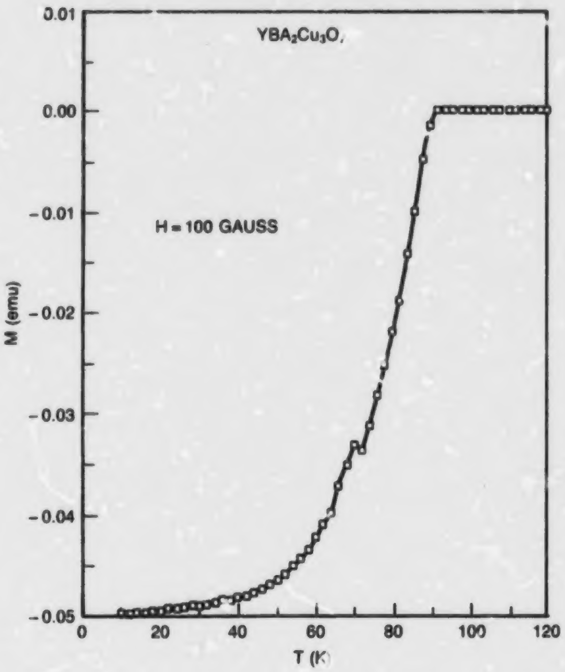

Fig. 13 – Magnetic susceptibility for the 1:2:3 compound, showing the Meissner effect expulsion of magnetic flux, complete at approximately 20 K.

structure, called a modified perovskite, permits substitution of a great variety of different cations in the structure, as well as large variations in the oxygen content (and thus the effective oxidation state of copper). However, no substitutions have been found that improve the results obtained with the 1:2:3 composition shown. Systematic studies at NRL, which substitute most of the lanthanides for the yttrium and the other alkaline earths for the barium and vary the oxidation state through various processing atmospheres, have been quite definite in this regard; most of the substitutions produce no increase in the critical temperature. The key ingredient appears to be the copper, which exhibits the Jahn–Teller effect, i.e., copper has an affinity for bonding atoms (e.g., oxygen) in a nonoctahedral fashion: square pyramidal for Cu (+2) and square planar for Cu (+1). Substituting other metals in the same column of the periodic table (silver and gold) that lack the nonoctahedral coordination produces materials that are not superconductors.

Work at NRL is now devoted primarily to improving the processing of the 1:2:3 compound through various advanced ceramic processing techniques to produce test materials of high density and to provide capabilities for production of useful components (e.g., films, conductors, and dense, smooth finish plates). The materials produced by earlier conventional ceramic powder processing techniques show the Meissner effect (see Fig. 13) and zero resistance at a temperature of about 93 K (see Fig. 14(a)), but these materials are far from fully dense and may not be homogeneous. The lack of dense materials prevents accurate determination of the critical current density, which controls the current-carrying capacity of superconductors and precludes certain uses. The lack of homogeneity is suggested by a feature that can be noted in Fig. 14(a), which indicates an onset of superconductivity at about 110 K. This suggests that the material has subtle variations from point to

BEST COPY AVAILABLE

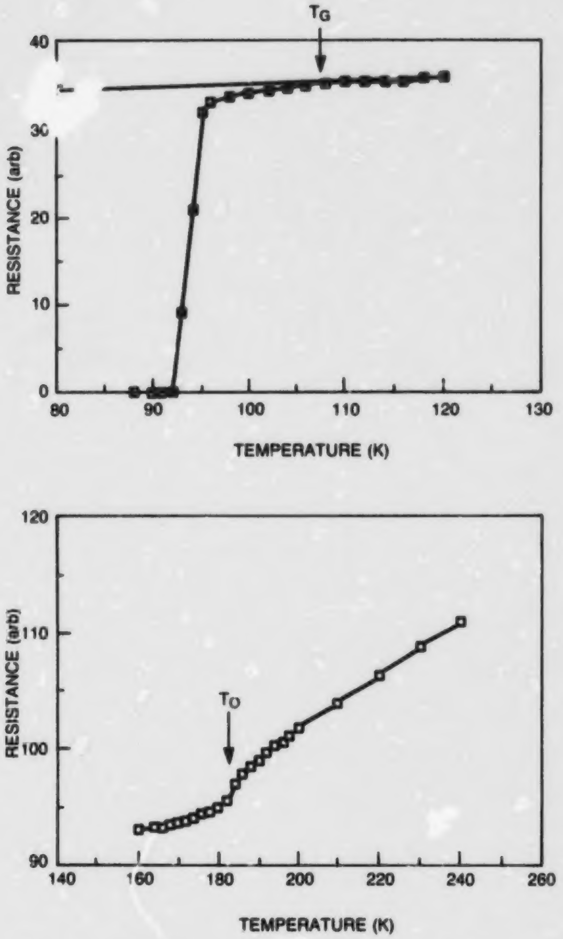

Fig. 14 – (a) Resistance vs absolute temperature for the 1:2:3 compound, showing onset of the superconducting transition at approximately 110 K, and zero resistance at approximately 93 K. (b) Upper temperature regime of resistance temperature curve, showing 'glitch' at approximately 190 K that may indicate a high-temperature phase transition or the presence of a higher critical temperature superconducting phase.

point that produce the range of transition temperatures, rather than a sharp transition at a particular critical temperature. The inhomogeneity must be a subtle effect, such as ordering of the oxygen vacancies in the lattice, since X-ray and neutron diffraction as well as microstructural analysis seem to indicate that the material has a single phase. Another possible indication of heterogeneity is seen in Fig. 14(b), where the resistance vs temperature curve shows a 'glitch' at approximately 190 K. This could be evidence of a superconducting transition in another phase present. These 'glitches' that occur at temperatures as high as 290 K have been the cause of several unfortunate news conferences and press releases, now recanted. The glitches could also be merely the result of some other phase transition in the base material and have no real consequence. A significant amount of processing improvement (to improve the homogeneity and refine the microstructure of the ceramic superconductor and to examine the details of the microstructure) is necessary to resolve these questions. Such research is currently under way at NRL and may lead to even higher critical temperature superconductors or to significant improvement in processing the current materials.

[Sponsored by DARPA] ■

Computer Modelling of Anisotropic Elasticity and Piezoelectric Effects in Ceramics

R. P. Ingel, D. Lewis, III, and M. Kahn

Material Science and Technology Division

Many of the complexities in the properties and utilization of ceramic materials arise from the anisotropic nature of the physical properties of these materials. Anisotropy implies a directionality of properties–a dependence of physical properties on orientation. Most of the common engineering materials are isotropic (or nearly so) on a macroscopic scale. These isotropic materials include most polymers, metals, glasses, and common ceramic materials. The lack of directionality in properties permits easy utilization of such materials. Anisotropy, on a macroscale as found in composites and single crystal materials, greatly complicates material development and utilization. The orientation dependence of properties must be characterized, and more complex and difficult analytical techniques must be employed for design calculations.

The anisotropy in materials such as composites and single crystal ceramics extends to a wide range of macroscopic material properties; however, even for macroscopically isotropic materials, there is a subtle dependence of the macroscopic properties on the microscopic anisotropy that is typically present. The optical losses in a polycrystalline ceramic (translucency or opacity) result in part from variations in refractive index from grain to grain, and between the grains and grain boundary phases. These variations result from the random orientation of individual grains, which are single crystals, and the orientation dependence of the refractive index. The elastic modulus (stiffness) of a polycrystalline material is an orientational average over the elastic moduli of the individual grains. The elastic constants in the individual single crystal grains can vary greatly with direction, especially for some ceramic materials. The macroscopic fracture toughness or fracture energy of a material also is determined ultimately by the microscopic properties and their anisotropy. The fracture process on a microscale involves the fracture energy of individual, randomly oriented, single crystal grains and grain boundaries. This process is also affected strongly by the microscopic residual stresses resulting from elastic and thermal expansion anisotropy.

Calculations related to determination of the effects of material anisotropy are most simple for those physical properties, electrical, thermal, optical, which are governed by second-rank tensors and second-order partial differential equations. Some of the more difficult problems lie with the mechanical properties and piezoelectric properties. Here the problems involve third-rank (piezoelectric) and fourth-rank (elastic moduli) tensors, and fourth-order partial differential equations. For these types of problems, there are few closed-form analytical solutions. The great majority of solutions to problems are obtained by various approximations or by numerical techniques of various types. At NRL, extensive analytical modelling has been performed that incorporates the anisotropic nature of the mechanical properties of ceramics. Computer analysis has also been used extensively to provide graphic two-dimensional (2-D) and three-dimensional (3-D) representations of the anisotropy of various mechanical and other properties in ceramics. Recently extensive computer analysis (3-D finite element and finite difference) has been devoted to predicting and optimizing the piezoelectric response and strength of novel ceramics developed at NRL. The novel materials incorporate ordered arrays of regular voids produced by a patented NRL process.

Piezoelectric Response Calculations: We show some examples of the calculations of piezoelectric response for a current sonar material, PZT5A, lead zirconate titanate, elastic modulus vs orientation for the same material, and elastic modulus vs orientation for a more anisotropic material-cubic yttria-stabilized zirconia. Figures 15 and 16 show the piezoelectric response that gives the electrical response produced by a uniaxial stress of arbitrary direction. Figure 15(a) is a 2-D plot of this response, and Fig. 15(b) is a 3-D plot; the response here is always measured in the Z-direction. The maximum response is for stress applied in the Z-direction (the conventional loading for these materials). The negative response in the *x*-*y* plane tends to limit the use of PZT5A in hydrostatic loading, with pressure applied in all directions. The effective response, cf. Fig. 15, is nearly zero. There is also a direction, about 55° from the Z axis, for which no electrical response will result from a stress applied in this direction. This particular result has been verified experimentally.

Figure 16 shows contours of effective Young's modulus vs orientation for the same PZT5A, derived from the elastic constant tensor for the material. Here this bulk ceramic, which is characterized as transversely isotropic when poled (one of the tetragonal crystal classes), shows only about a 50% difference in modulus between the most and least stiff directions. Note the lack of orientation dependence for planes normal to Z (cf. also Fig. 15(b)), resulting from the transverse isotropy of the material. Some other ceramic materials show both a greater degree of anisotropy and more variation with orientation. Figure 17 shows similar modulus plots for cubic zirconia

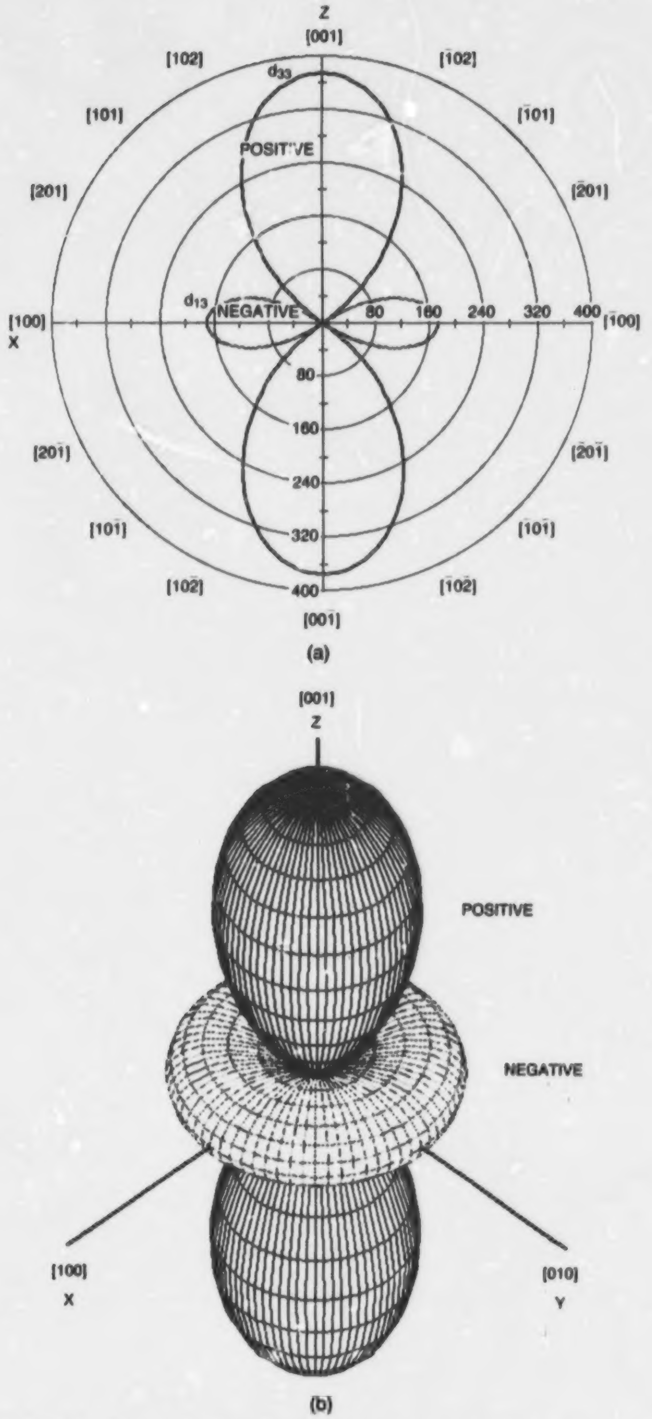

Fig. 15 – (a) Two-dimensional representation of the polarization in the z-direction produced by a unit stress at arbitrary directions in the x-z plane for poled PZT5A. (b) Three-dimensional representation for z polarization from a unit stress in arbitrary direction; note symmetry of polarization about z-axis.

BEST COPY AVAILABLE

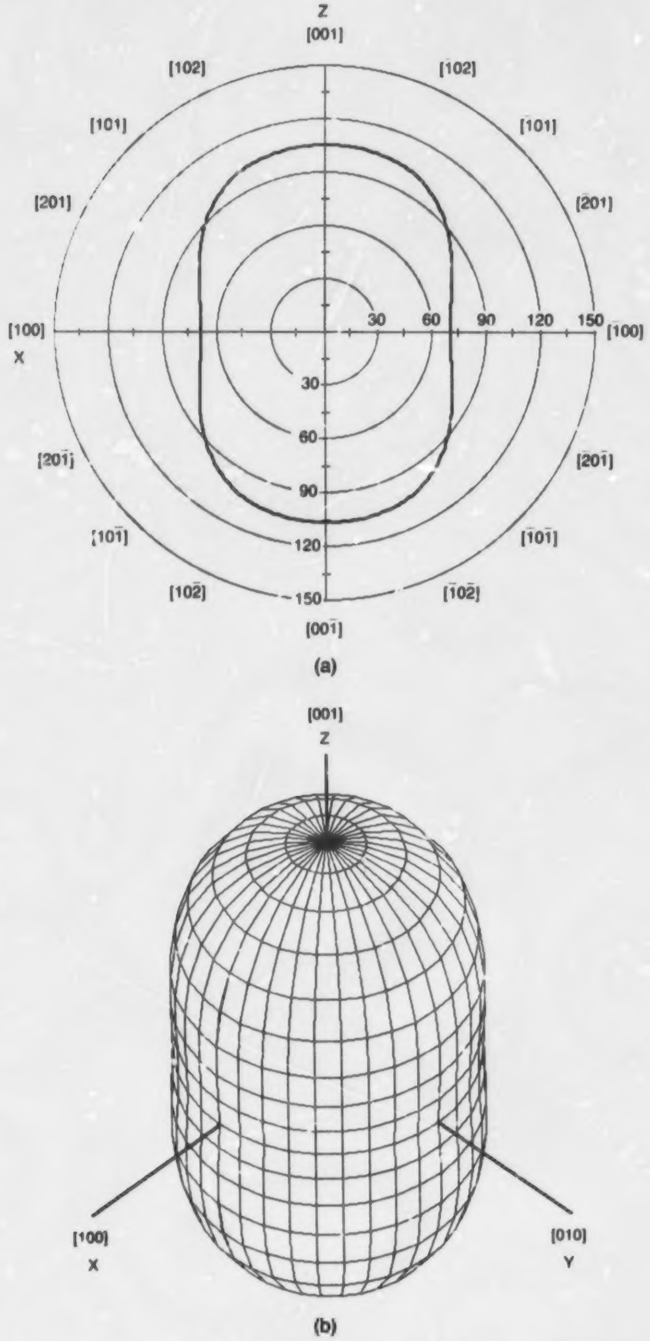

Fig. 18 – (a) Two-dimensional view of variation of Young's modulus (stiffness) of PZT5A, showing 50% variation in modulus with direction. (b) Three-dimensional representation of modulus showing symmetry about *z*-axis resulting from transverse isotropy (all directions in the *x*–*y* plane are equivalent).

BEST COPY AVAILABLE

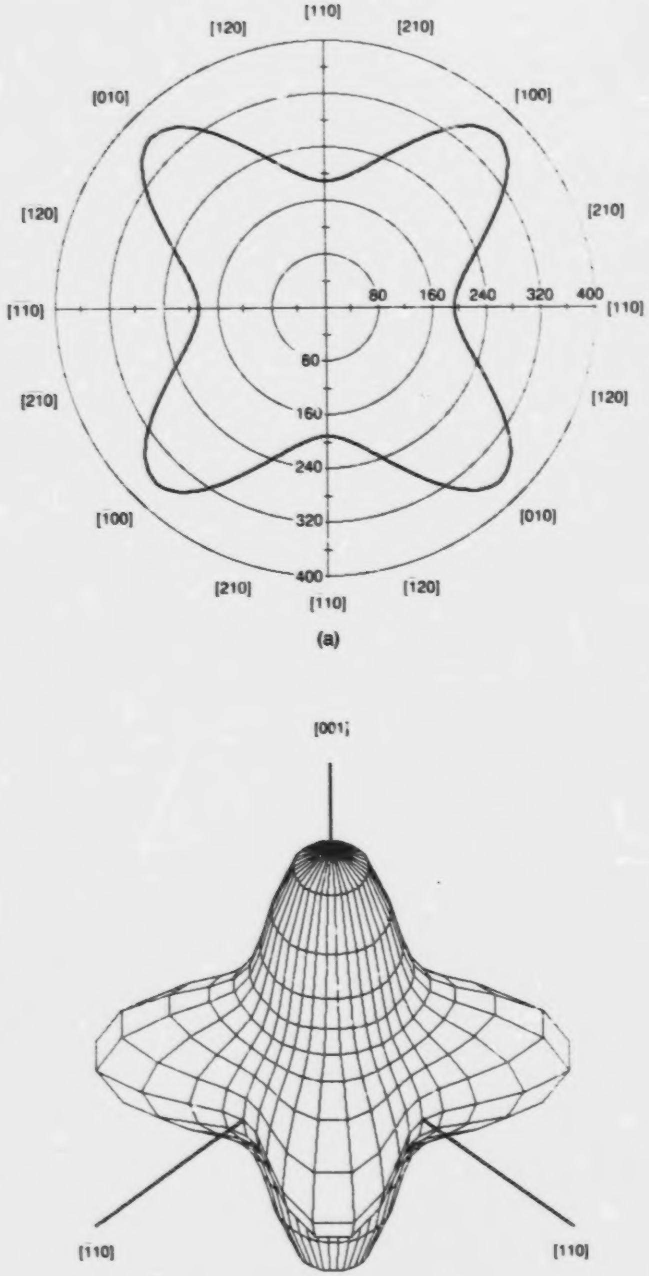

(a)

(b)

Fig. 17 – (a) Two-dimensional view of orientation dependence of Young's modulus for a cubic zirconia single crystal, showing much larger anisotropy (modulus variation) in this material. (b) Three-dimensional representation of Young's modulus variation with direction, illustrating cubic symmetry.

BEST COPY AVAILABLE

single crystals. Zirconia is currently seeing wide application in various types of heat engines, and the single crystals themselves have potential use as infrared window materials. For this single crystal material, the modulus variations are more pronounced, and there are now three extreme values for modulus vs two for PZT5A. In the zirconia crystal, the modulus reaches extreme values at the [100], [110], and [111] directions as seen in Fig. 17(b).

Results presented here are intended primarily as examples of applications of computer modelling and computer graphics, and the utility of such graphic presentation in visualizing material response. The human brain has been optimized as a visual image processor, and such graphic presentations, as shown here, are far more effective in providing descriptions of material behavior than purely analytical or numerical results.

[Sponsored by ONR] ■

Mechanisms of Interdiffusion in Coated Superalloys

V. Provenzano and J.R. Reed
Material Science and Technology Division

Blades and vanes (often referred to as hot-end components) used in high-performance gas turbine engines for Navy ships and aircraft are made of nickel-based alloys. Because of their elevated-temperature mechanical properties, these alloys are usually referred to as superalloys. These mechanical properties include high-temperature strength and resistance to high-temperature creep. Although alloy designs attempt to combine high-temperature properties with good resistance to environmental degradation, the alloys still require coatings to provide the necessary protection from high-temperature oxidation and from hot-corrosion attack. Hot corrosion attack is an oxidation-sulfation reaction caused primarily by sulfur present in the fuel as an impurity. The coatings normally used for environmental protection fall into two general categories: overlay MCrAlY (M stands for nickel, cobalt, or iron) coatings that are applied to the substrate alloy either by physical vapor deposition or by plasma spraying; and diffusion aluminides, for which aluminum is diffused into the surface of the substrate alloy to produce a layer of nickel aluminide at the surface.

The overlay MCrAlY coatings have the advantage over the aluminide coatings because their composition can be selected to provide maximum protection to the hot-end gas turbine components without regard to the composition of the underlying substrate alloy. However, as the engine operating temperature is raised for increased efficiency and for better performance, this advantage can be compromised severely by the phenomenon of interdiffusion between substrate and the coating. This interdiffusion, in extreme cases, degrades both the oxidation and hot-corrosion resistance of the coating and the high-temperature mechanical properties of the substrate. Because coating development has attempted to solve the interdiffusion problem along empirical lines, the basic mechanisms of interdiffusion on an atomic scale are poorly understood. The objective of the present study is to investigate the fundamental mechanisms of interdiffusion on simplified (model) coating/substrate combinations. The understanding obtained from the study of model systems will be used to gain deeper insight on the mechanisms of interdiffusion of more complex coating/substrate systems. This deeper insight will provide a rational framework for high-temperature coating/substrate alloy designs used in high-performance gas turbine engines.

Experimental: The binary nickel-aluminum alloys used for the interdiffusion experiments were prepared by arc melting. The resultant buttons were cold-rolled to about 2.5-mm-thick sections. The rolled sections were then annealed in vacuum for 1 hour at 900°C. Specimens were cut from the annealed sections to coupons approximately 2 ×

10 × 10 mm. Matching specimen coupons were sectioned from a commercially prepared nickel bar (99.99-wt. % pure). Two different binary alloys were prepared. These alloys were: Ni-5 wt. % Al and Ni-8 wt. % Al. The binary alloys were designed to simulate the coatings, while pure nickel was used to simulate the superalloy substrate. One surface of each specimen was metallographically polished with diamond powder to 0.5-μm finish. Diffusion couples with or without an intervening diffusion barrier layer were prepared by pressure welding two specimen coupons with the polished faces in contact; one specimen coupon was from the binary alloys, and the other was from the nickel coupons. Pressure welding was achieved by using specially built niobium clamps. Figure 18 is a schematic diagram of a diffusion couple and the niobium clamp. The diffusion couples were placed in alumina boats, sealed in tantalum foil, and then annealed in a vacuum furnace for 4 days at 1100°C. After the 4 days of vacuum annealing, the diffusion couples were removed from the niobium clamps and cut into approximately equal halves along a plane parallel to the diffusion direction. The cut sections were prepared by standard metallographic techniques. Concentration profiles of aluminum across the diffusion couples were measured with a JEOL model 35CF scanning electron microscope that is equipped with a Tracor Northern T2000 energy-dispersive X-ray analysis system. Two or more sets of X-ray measurements were made for each diffusion couple to ensure reproducibility.

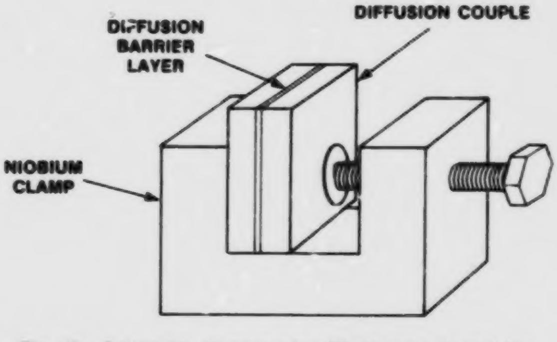

Fig. 18 - Schematic diagram of a diffusion couple and the niobium clamp used in the diffusion experiments

As previously mentioned, some diffusion couples contained an intervening diffusion barrier layer. Ion implantation was used to produce an intervening layer of either yttrium, tungsten, or tantalum, whereas a physical vapor deposition procedure was used to produce an intervening layer of platinum.

The diffusion coefficients of aluminum nickel with or without an intervening diffusion barrier layer were determined from the concentration profiles by using a modified form of the Boltzman-Matano method, first suggested by Sauer and Friese [1] and later elaborated by Wagner [2]. The relevant equation is:

$$D_{Al} = \frac{1}{2t}\left(\frac{dx}{dy}\right)_{x=x^*}(N_{Al}^{+} - N_{Al}^{-}) \quad (1)$$

$$\left\{(1 - Y^*)\int_{-\infty}^{x^*} Y\,dx + Y^*\int_{x^*}^{\infty}(1 - Y)dx\right\}$$

where D_{Al} is the diffusion coefficient, N_{Al}^{+} and N_{Al}^{-} are the atomic fractions of aluminum at the two ends of the diffusion couple, t is the annealing time, Y^* is the value of Y at position coordinate x^*; and the variable Y is defined by

$$Y = \frac{N_{Al} - N_{Al}^{-}}{N_{Al}^{+} - N_{Al}^{-}} .$$

where N_{Al} is the atomic fraction of aluminum at position coordinate x along the diffusion direction.

Results: The composition profile presented in Fig. 19 illustrates the type of interdiffusion data obtained from the interdiffusion experiments. Figure 19 shows a composition profile of aluminum obtained from an Ni5Al/pure nickel diffusion couple. Using the theoretical model previously outlined (Eq. (1)) for multicomponent diffusion, it was determined that contrary to previous experimental results, an intervening layer of platinum does not significantly reduce the

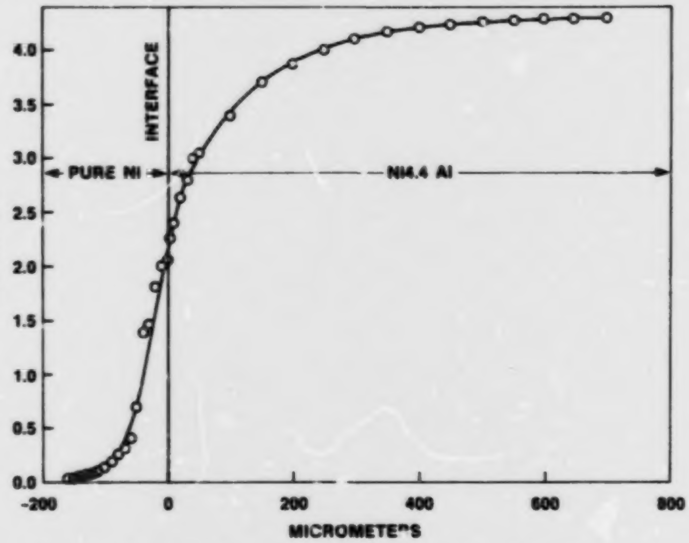

Fig. 19 – Concentration profile of aluminum along the diffusion direction in Ni5Al/pure nickel diffusion couple after 96 h annealing in vacuum at 1100°C

diffusion rate of aluminum in nickel at 1100°C, whereas an ion-implanted layer of yttrium reduced the diffusion rate of the same element by a factor of two in the same 1100°C. Also, it was found that neither an intervening layer of tungsten nor a layer of tantalum had any significant effect on the aluminum diffusion in nickel.

[Sponsored by NAVAIR]

References

1. F. Sauer and V. Friese, Z. *Elektrochem*. **66**, 353 (1962).
2. C. Wagner, *Acta Metall*. **17**, 1969. ■

Atomic Resolution Images

J. H. Konnert and P. D'Antonio
Laboratory for Structure of Matter

A scanning transmission electron microscope (STEM) scans or steps an electron beam of small diameter across the specimen to be studied. The electrons passing through the sample are scattered by the atoms in the irradiated volume. Conventionally, a portion of the resultant diffraction pattern is detected to provide a signal that is displayed as a function of beam position to form a magnified image of the object. The resolution of the image formed in this way is approximately the beam size, which can be as small as 3 Å in diameter with the use of a field emission electron source. However, each diffraction pattern contains extensive information that is not fully utilized by the conventional technique. Interatomic distance distribution information with a resolution of better than 1 Å is contained in these patterns. If this information could be extracted from the experimental data, it would be possible to determine the atomic structure within small volumes associated with defects in crystals, interfaces, and amorphous and catalytic materials. Interpretation, however, is complicated by the complexity of the incident electron wave function.

Microscope Simulation: As part of a theoretical effort to interpret such data, the Cray computer at NRL has been used to simulate microdiffraction patterns that may be obtained with a modern STEM. The Cray facilitates the rapid computations of patterns associated with known arrangements of atoms and specific instrumental conditions that determine the detailed

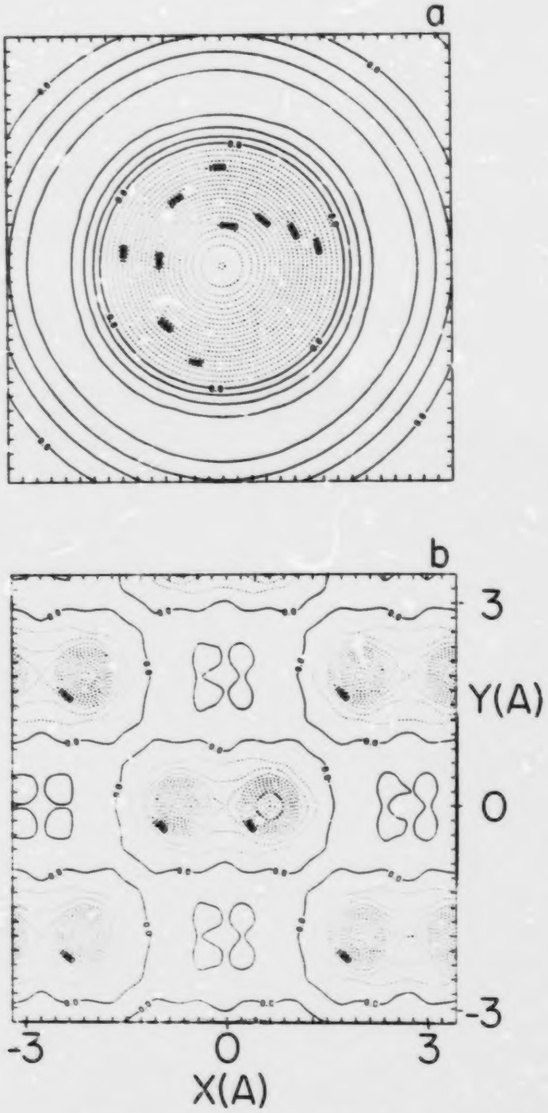

Fig. 20 — (a) Imaginary part of beam wave function for 3.8 Å-beam wave function. (b) Imaginary part of the scattering potential for silicon viewed along [1].

characteristics of the incident electron wave. This effort has led to the development at NRL of an atomic resolution image reconstruction technique [1] that uses microdiffraction patterns from overlapping regions of a specimen.

The diffraction patterns are calculated by interacting the electron wave function of the incident beam with the scattering potential of the atoms in the sample. Figure 20(a) shows the imaginary part of the complex function representing the beam for a set of microscope conditions. It illustrates the complex oscillatory character of a beam for which most of the intensity falls within a diameter of 3.8 Å. Figure 20(b) illustrates the imaginary part of the scattering potential for a 3.8 Å-thick slice of crystalline Si viewed in the [1] direction. The total effect of a sample on the incident wave is calculated by

BEST COPY AVAILABLE

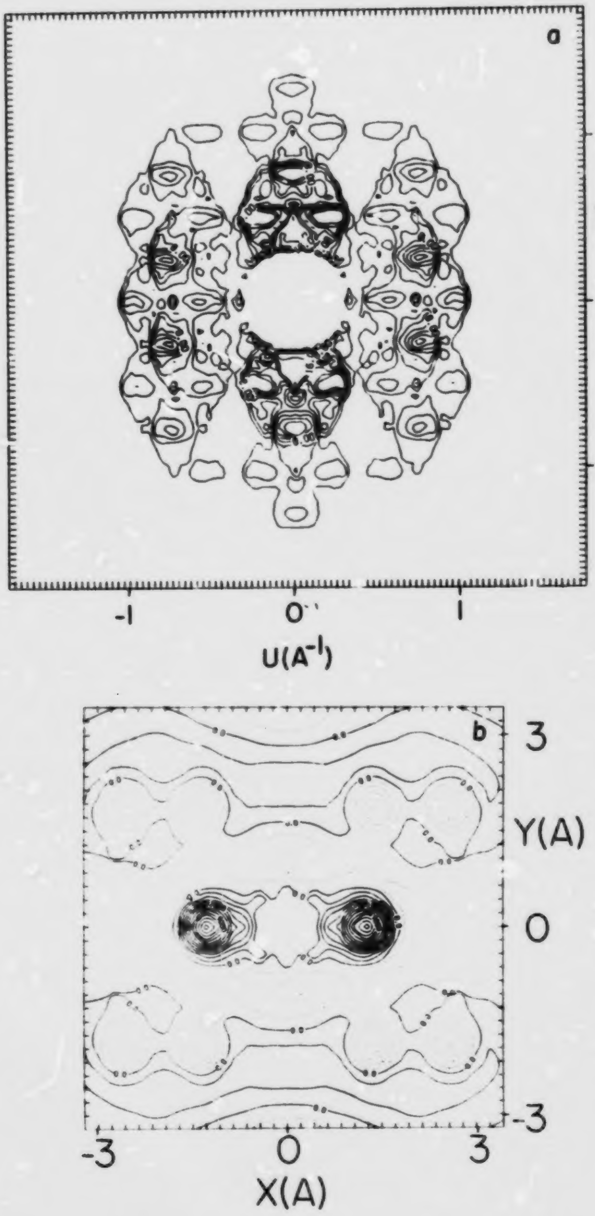

Fig. 21– (a) Diffraction pattern for beam in Fig. 20(a) centered on atoms in Fig. 20(b). (b) Real part of the autocorrelation function or Fourier transform of the pattern in Fig. 21(a).

dividing the sample into a series of thin slices [2]. The beam is interacted with the scattering potential of the first slice, propagated to the second slice, interacted with the scattering potential of the second slice, etc. The diffraction pattern corresponding to what can be obtained experimentally is the amplitude squared of the Fourier transform of the wave function at the exit surface of the sample.

Figure 21(a) displays the diffraction pattern obtained with the beam in Fig. 20(a) centered on the atoms in Fig. 20(b). The zeroed disc at the center represents the size of the main beam resulting from the beam convergence necessary to

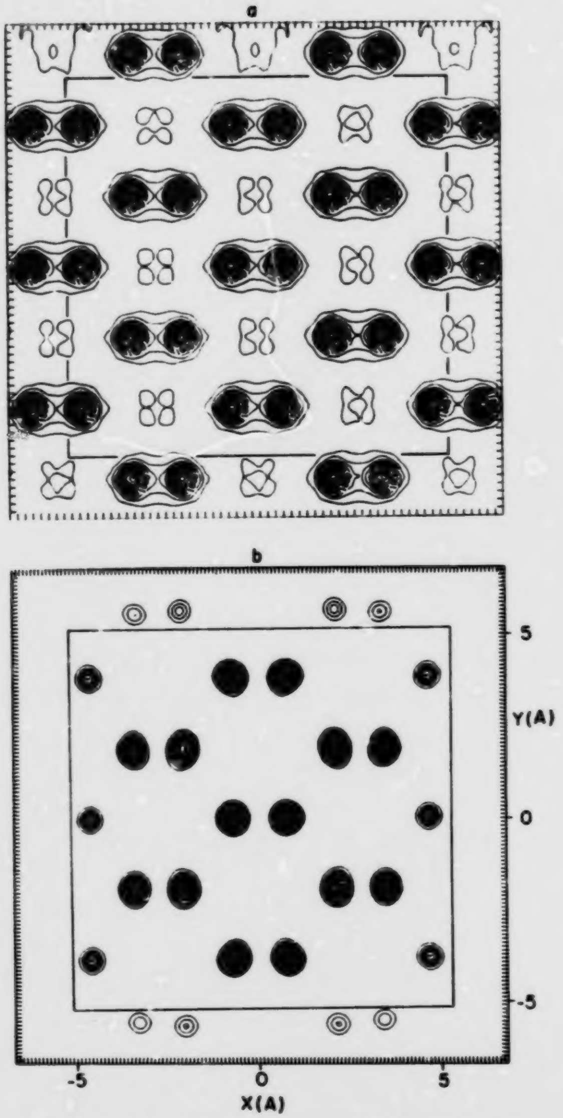

Fig. 22 — (a) Amplitude of scattering potential for Si viewed in [11] direction; inner box defines limits of beam centers for array of 225 beam positions separated by 0.75 Å for which microdiffraction patterns were calculated. (b) Image reconstructed from diffraction patterns.

obtain the small beam. It has been zeroed because it would probably not be usable in an experiment because of the intensity of the unscattered electrons. Such a pattern is characterized by discs centered at the Bragg peak positions. All discs are of the same diameter as the main beam, and, as a result, they interact coherently in their regions of overlap.

Image Reconstruction: Figure 21(b) is the real part of the Fourier transform of the diffraction pattern. It contains interatomic distance information modified by the electron beam. Positive peaks (solid contours) indicate interatomic vectors between atom pairs, both of which are in the central portion of the beam. Thus the vectors of +1.36 Å relating the two central atoms are positive. Atom pairs separated by crossovers in the beam (Fig. 20(a)) result in negative (dashed contours) peaks.

The image reconstruction technique takes advantage of the changes that occur in the diffraction patterns and their Fourier transforms (autocorrelation functions) as a function of beam position. The autocorrelation position is calculated for an array of beam positions surrounding the sample area of interest, and the beam positions that maximize the value for each vector are identified. Such maxima occur when the beam is centered between the related atoms. As a result, each resolved maximum serves to identify the positions of two atoms. Figure 22(a) displays the amplitude to the scattering potential for an extended region of Si. Microdiffraction patterns were calculated for a square array of 225 beam positions separated by 0.75 Å within the 10.5 × 10.5-Å region indicated. Figure 22(b) shows the atomic resolution reconstructed image.

Experiments are being carried out on a modified STEM at the National Microscope Facility at Arizona State University to determine if experimental patterns can be obtained with accuracy sufficient to form atomic resolution images.

[Sponsored by ONR]

References

1. J.H. Konnert and P. D'Antonio, "Image Reconstruction Using Electron Microdiffraction Patterns from Overlapping Regions." *Ultramicroscopy* **19**, 267–268, (1986).
2. J.M. Cowley, *Diffraction Physics* (North-Holland, Amsterdam, 1975). ■

NRL has been at the forefront of radar research and development since its discovery over six decades ago. Today, NRL carries out a broad program centered in the Tactical Electronic Warfare Division and in the Radar Division. Their projects emphasize electronic countermeasures, the simulation of signals, jamming, decoys, and the development of novel electronic warfare device and system technologies. Radar research focuses on advanced sensor concepts and technology and system feasibility, evaluation, and analysis that form a significant part of the Division's mission.

ELECTROMAGNETIC SYSTEMS AND SENSING

111 **Radar Target Detection in Non-Gaussian, Correlated Clutter**
Ben H. Cantrell

112 **Speckle in Space-Based Radar Images**
Jong-Sen Lee

114 **Open Ocean Shipboard Radar Sea Clutter Experiments**
Dennis B. Trizna

117 **Mark XV IFF Radar Mode**
Lawrence M. Leibowitz

Radar Target Detection in Non-Gaussian, Correlated Clutter

B. H. Cantrell
Radar Division

The optimum filter for detecting radar targets in Gaussian amplitude, distributed, correlated noise, referred to in the radar community as clutter, has been known for many years. This detector is the Wiener or matched filter followed by a threshold. It is obtained by using the Neyman–Pearson procedure that maximizes the probability of detection for a given probability of false alarm for a binary hypothesis. In applying this procedure to non-Gaussian, correlated noise, three problems are encountered. First, the required multivariate probability density of the noise is seldom known or cannot be easily measured; second, often there are unknown parameters that must be accounted for in some way; and third, the likelihood ratio obtained in the test sometimes is difficult to simplify. All three of these problems were addressed.

The most difficult problem encountered is obtaining the multivariate probability density of the noise. The new procedure constructs the desired multivariate density from one that can be analytically represented, such as a Gaussian one, by using a nonlinear transform to map the one into the other. The mapping is adjusted so that the marginal distributions and the first two moments of the constructed multivariate distributions are correct. Often these are the only properties of the clutter that can be measured easily. After the multivariate density is found, a Neyman–Pearson test can be obtained. In this test, the unknown parameters are the covariance matrix and the complex signal. The covariance matrix is usually estimated from reference cells. The unknown complex signal is eliminated by using an approximation to the test. This approximation also allowed the complicated test to be reduced to a simple form. Figure 1 shows the functional flow of the test. In essence, mapping is used to transform the random variable to a Gaussian distribution, and then a matched filter is applied to the signal after the nonlinear mapping and after the prewhitening process.

The mapping relationships required for the new detector were derived for both Weibull and log-normal clutter. The performance of these detectors was evaluated by using Monte-Carlo simulations for a number of cases. Figure 2 shows a typical result. The probability of detections is shown vs signal-to-clutter ratio for a square law detector λ_{sl}, matched filter λ_{mf}, and new detector λ_a for a probability of false alarm (pf_a) of 10^{-7} and a log-normal parameter $1 = 0.8$. Two pulses are used with a correlation coefficient on the clutter of 0.98 and a 90° phase rotation between the pulses that occur for the target. Figure 2 shows that the new detector outperforms both the matched filter and square-law detector. In general, it was found that the new detector performs better than the matched-filter detector as long as the clutter was spikey

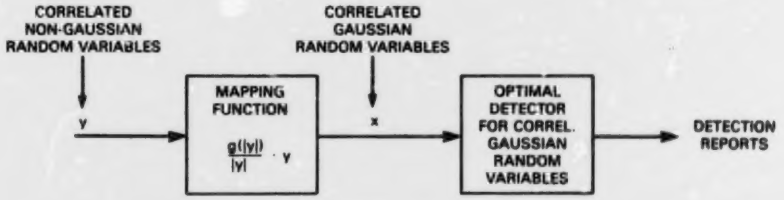
CORRELATED NON-GAUSSIAN RANDOM VARIABLES
y
MAPPING FUNCTION
$\frac{g(|y|)}{|y|} \cdot y$
CORRELATED GAUSSIAN RANDOM VARIABLES
x
OPTIMAL DETECTOR FOR CORREL. GAUSSIAN RANDOM VARIABLES
DETECTION REPORTS

g(|y|) nonlinear function
|y| magnitude of signal

Fig. 1 – Basic operation for non–Gaussian detector

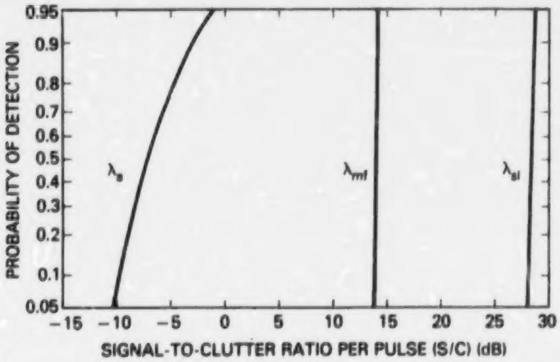

Fig. 2 – Detector operating characteristics for the example of log-normal clutter and $\sigma_l = 1.5$ and $Pf_a = 10^{-7}$

and non-Gaussian and approached the matched-filter performance as the clutter approached Gaussian clutter.

[Sponsored by ONR] ■

Speckle in Space-Based Radar Images

Jong-Sen Lee
Radar Division

A radar application of increasing importance is the high-resolution imaging of various natural and man-made targets. Some types of imaging radars, e.g. synthetic aperture radars (SAR), are capable of producing photographic-like images whose resolution rivals that of the images in the visual spectral region. This fact, coupled with an all-weather, day and night operation, large standoff distances, and great geographic coverage, provides an extremely powerful remote sensing instrument. Such instruments are suitable for both airborne and spaceborne applications [1]. Typical of the latter class are SEASAT SAR (1978), and Shuttle Imaging Radars A and B (SIR-A-1981, SIR-B-1984). High-resolution radars take on various forms depending on the intended mission. However, regardless of the application, all forms are coherent radars that generate images characterized by a "salt and pepper" appearance, the effect commonly referred to as "speckle." This effect, caused by the coherent interference between scatterers contained within a resolution cell, represents real-target signature as opposed to instrumental noise. Nevertheless, it acts like clutter, and therefore the effect presents a major difficulty to the image interpreter since it hampers such typical activities as segmentation and the associated target classification. Consequently, it is desirable to remove speckle's degrading effects without, at the same time, affecting the detectability of subtle detail such as bridges and coast lines. The subsequent discussion is concerned with the studies of speckle effect in spaceborne SAR images conducted at NRL's Digital Image Processing Laboratory in the past several years.

Statistical Model: Since the speckle pattern appears chaotic and random, the best way to describe it quantitatively is by the methods of probability and statistics. It is assumed that the reflectances of the elementary scatterers and their phases are statistically independent and the phases are uniformly distributed. Furthermore, one can assume with reasonable confidence that the in-phase (real) and quadrature (imaginary) components are random variables having a Gaussian distribution. The intensity of a SAR image is the sum of squares of these components. Consequently, the probability density function of pixel intensities will have the form of a negative exponential distribution while their amplitudes, which are the square root of the intensities, are Rayleigh distributed. The ratio of the standard deviation to the mean for both the intensity and the amplitude are constant. This indicates that speckle acts like multiplicative noise in the sense that the higher the average intensity, the noisier the area appears. A multiplicative noise model has been developed during the studies [2]. The ratio that represents the strength of the multiplicative noise turns out to be the standard deviation in the noise model. One way to reduce the speckle effect in a SAR image is through multilook azimuth processing in which one divides the synthetic array length into N sections (each section is processed independently), then the corresponding images are averaged incoherently. The noise model developed in our work applies to images generated in this manner. The statistical model was verified experimentally with both SEASAT and SIR-B images. As shown in Fig. 3, the multiplicative nature of the effect is evident from the linear dependence of the standard deviation on the mean. Furthermore, their ratio agrees with the values predicted by theoretical model.

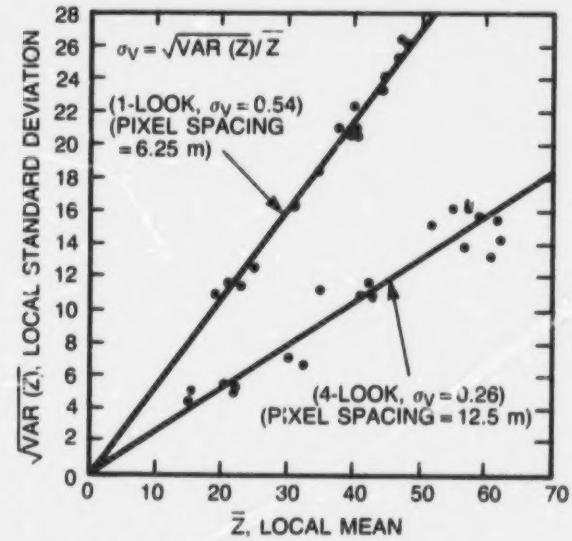

Fig. 3 - SIR-B speckle noise characteristics (NRL SAR processing)

Speckle Smoothing: Based on the previous noise model, two algorithms have been developed to suppress the speckling effect in SAR images in the postprocessing phase. The attractive feature of these algorithms is that they preserve sharp edges and distinctive subtle features. The common approach to noise filtering is the application of low-pass filters. This procedure, however, fails to preserve the image sharpness. The images will become blurred because the spatial high-frequency components of sharp features become attenuated. The more sophisticated Wiener and Kalman filters also fail because of the spatially variant characteristics of most SAR images. Two algorithms developed in our studies adaptively smooth the speckle by using different smoothing actions for slowly varying areas and the edge areas. The local statistics algorithm regulates the local averaging process according to the local mean and local variance of a small 5 pixel × 5 pixel or 7 pixel × 7 pixel window. The other algorithm, based on the sigma probability of Gaussian distribution, also operating in a small window, selectively averages only those pixels within the two-sigma range while excluding significantly different pixels. Consequently, edges and linear features are preserved.

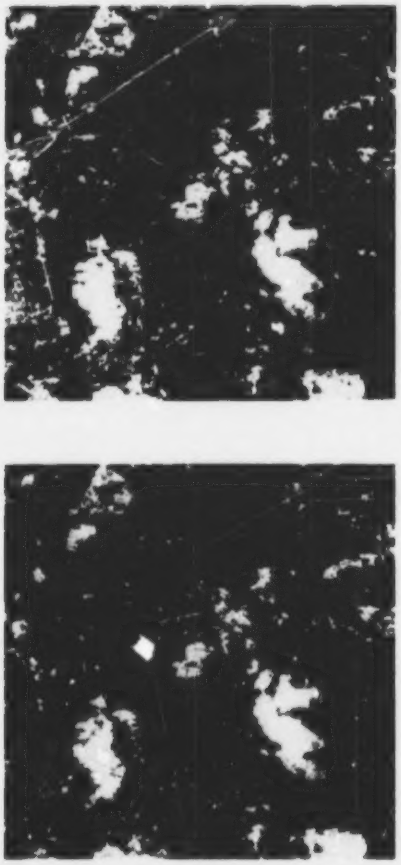
(b)

Fig. 4 - Speckle smoothing of SEASAT SAR image. Image has 256 × 256 picture elements; (a) SEASAT SAR original (Baltimore Harbor) and (b) Sigma filter (7 × 7 twice 5 × 5 twice)

Experimental Results: The two algorithms were treated with SEASAT SAR and SIR-B images. Figure 4 shows the SEASAT SAR image of the Baltimore Harbor and the corresponding

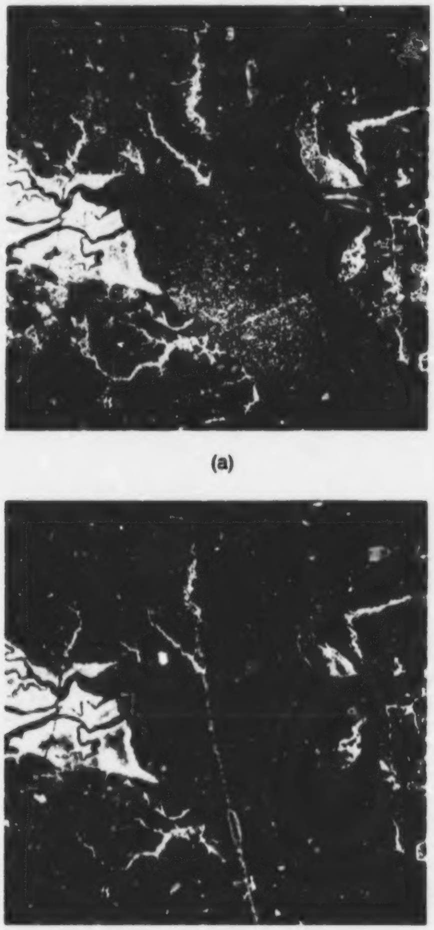

(a)

(b)

Fig. 5 – Speckle smoothing of SIR–B image. Image has 512 × 512 picture elements; (a) SIR–B original (Albermarle Sound, North Carolina) and (b) Sigma filtered twice with 5 × 5 window

filtered image. The quality of the image has been improved significantly by suppressing speckle while preserving the sharpness of the bridge and shorelines. Figure 5 shows another example of applying the sigma filter. Figure 5(a) shows the four–look processed SIR–B image of Albermarle sound, North Carolina while Fig. 5(b) shows the sigma filtered image. The sigma filtering significantly suppresses the speckle without blurring sharp edges and linear features such as the highway over the Roanoke River.

[Sponsored by ONR]

References

1. C.S. Weller et al., "Space Based Imaging Radar," *1986 NRL Review*, pp. 214–217.
2. J.S. Lee, "Speckle Suppression and Analysis for Synthetic Aperture Radar Images," *Opt. Eng*. 25 (5), May 1986. ■

Open Ocean Shipboard Radar Sea Clutter Experiments

D. B. Trizna
Radar Division

Radar sea scatter experiments have been conducted aboard ships at sea to acquire data for use in development of models for low–grazing–angle sea scatter statistics. Such models are necessary for the prediction of probability of detection of targets in sea clutter. Locations of experiments include the North Atlantic, the Pacific, and the Sargasso Sea during the ONR–sponsored FASINEX experiment.

The low–grazing–angle surface illumination geometry imposed by a shipboard radar presents several difficulties not encountered for airborne or satellite radars, as is indicated in Fig. 6. First, most shipboard radars designed for marine surveillance or navigation use horizontal polarization. Large–amplitude horizontally polarized radar returns from crest regions, known as radar "sea spikes," are more prevalent than vertical polarization. Because pulse lengths of the order of 10 m are much less than the dominant wavelengths on the sea surface, individual surface features can be imaged with such radars. Sea spike scattering models include wedge scattering and double scatter from spilling breaker features seen in the bottom example near the left end. Second, applying the two–scale Bragg scatter model to the low–grazing–angle case predicts a wider range of radar echo amplitudes from surface tilt modulation than for intermediate angles used by airborne radars. Finally, as seen in Fig. 6, shadowing of portions of the sea surface occurs because of the high crests of the large waves, so that a large

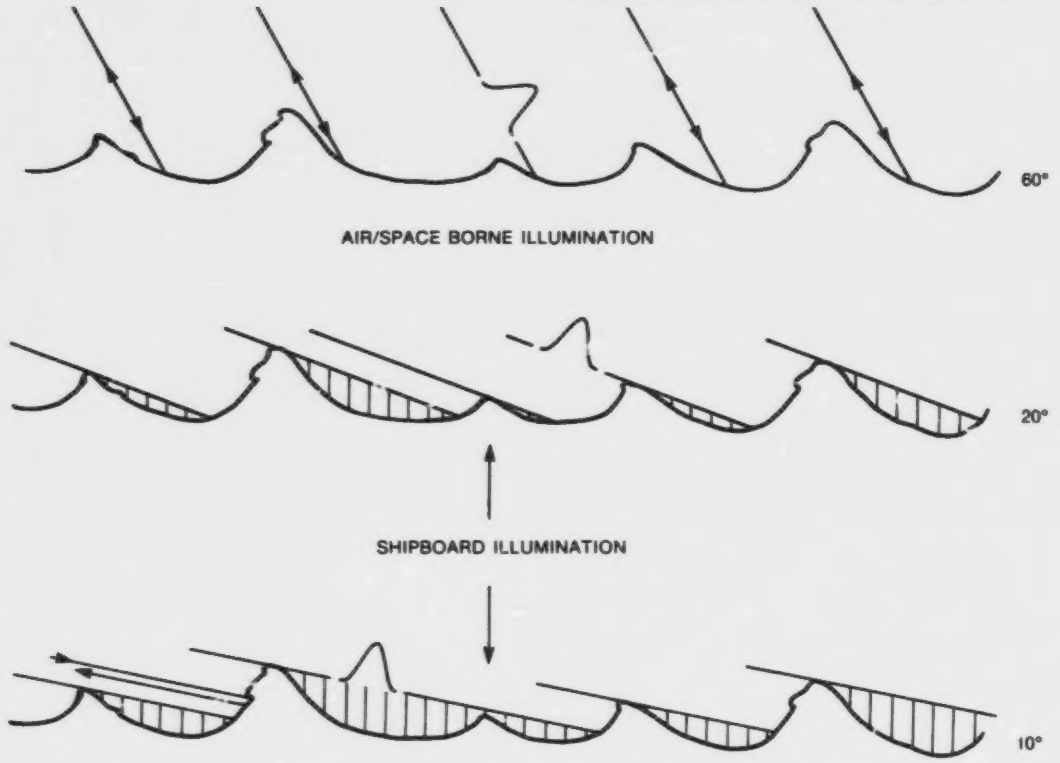

Fig. 6 – The geometry of illumination of the surface for a space or airborne radar is shown in the top figure, with no shadowing occurring and returns from wave crests of no major significance. The lower two figures show the effects of surface shadowing by wave crests, and indicate that scatter from regions near the wave crest become important, contributing the so-called 'sea spike' radar return.

fraction of the sea surface is not illuminated. For these shadowed regions, receiver noise is sampled, presenting the lowest level amplitudes of the receiver radar echo distribution. Thus the problem can be summarized as one of determining the characteristics of the trimodal echo amplitude distribution (sea spikes, Bragg scatter, and receiver noise) over an 80 dB dynamic range, as a function of environmental conditions such as wind speed and the ocean wave-height variance spectrum.

Figure 7 shows an image of normalized radar cross section (NRCS) as a function of range and azimuth extending to roughly 1 km from the ship. The maximum brightness in azimuth corresponds to the wind direction, which was very light on this occasion. Under stronger winds, wave patterns emerge in the image. The ship's wake is very apparent as a region of suppressed radar scatter, except for the upwind edge that appears quite bright. The problem of target detection in sea clutter displayed in such an image using automatic detection algorithms requires knowledge of the NRCS amplitude statistics within a given range-azimuth portion of such an image. These statistics can be expected to vary with angle to wind, depression angle or range, and environmental conditions.

To analyze the NRCS behavior, ten range bins were chosen, each within a 60° sector azimuthally centered about the NRCS-maximum azimuth. With several rotations of the antenna, a sufficient number of NRCS values in an azimuthal sector were obtained to allow cumulative distribution functions to be calculated and displayed as in Fig. 8. Data for three different wind speeds are shown here.

For the mildest wind conditions, the cumulative distribution is nearly a straight line on the Rayleigh coordinate system. With increasing

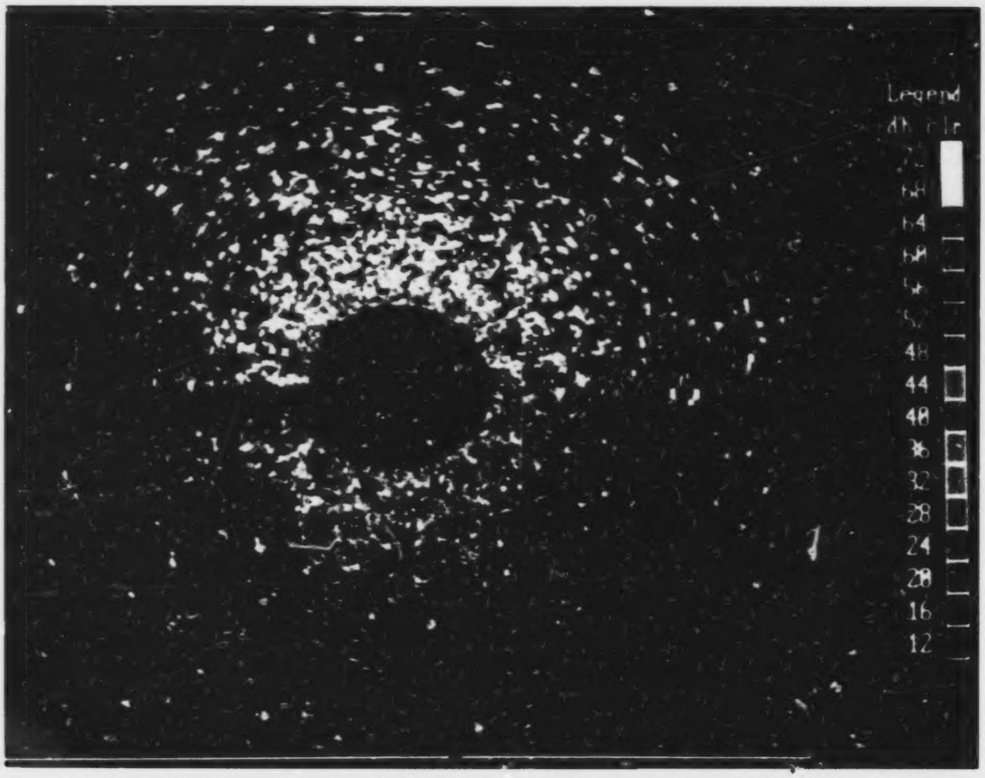

Fig. 7 – An image of receiver video signal is shown for one rotation of a marine navigation radar, showing the azimuthal asymmetry of the sea scatter. Winds were a few knots, so no ocean waves are imaged. Note the weak return from the center of the ship's wake

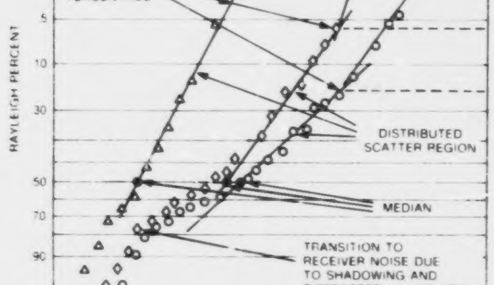

Fig. 8 – The cumulative distribution of three sets of high-resolution sea clutter samples are shown plotted on Rayleigh probability paper for increasingly strong winds. The pair of straight line fits indicate double Weibull distributions corresponding to sea spikes and a distributed scatter mechanism. The intersection of these pairs, the percent occurrence of sea spikes, varies with wind speed in a similar manner to white-cap coverage.

wind and sea state, the distribution is resolved into two Weibull distributions plus a rounded region corresponding to low-level noise samples. The two Weibull distributions have been shown [1] to be associated with a distributed scatter mechanism, such as Bragg scatter, from the noise level through the midlevel NRCS regions. The Weibull distribution covering the highest NRCS region is due to sea spikes, previously identified [2] with crest regions of the surface. The percent-value of the intercept of the two Weibull lines has been shown to scale with wind speed to the 3.75 power [1] in a manner similar to white-cap coverage as shown by Wu [3]. Since white-capping can be associated with sharp-edged wave crests, it is not surprising that sea spikes and whitecap coverage both scale in a similar manner with wind speed. Further experiments are planned to quantify this relationship.

The median backscatter level, generally the 50% intercept of the distributed scatter Weibull fit, has been further correlated with wind speed. This measure can be considered as the analogue to scatterometers operating at higher grazing angles from aircraft and spacecraft. The median NRCS variation with wind speed, U, and depression angle, θ_{dep}, can be characterized as follows:

$$\log (\mathrm{NRCS}_{med}/\mathrm{NRCS}_{10m/s}) = m(\theta) * \log \ (U/10\,\mathrm{m/s}),$$

where

$$10 \log \mathrm{NRCS}_{10m/s}\ (\theta) = 31.8 \text{ dB} + .467 \log (\theta_{dep}\ (\text{deg})),$$

and

$$m(0) = 2.5 + 5 \log (\theta_{dep}(\text{deg})) \text{ for } 1.0 < \theta < 4.5 = 5.75 \text{ for } 4.5 < \theta < 8.0.$$

The slopes of the Weibull fits increase with increasing wind speed, as seen in Fig. 8, and this variation is interpreted as being due to tilt modulation by long-wave slope. The higher the wind, the steeper the front face of waves, and the wider range in dB over which the NRCS can be expected to vary. Details of this behavior can be found in Ref 1. Further experiments are planned to determine the effects of the long-wave slope by conducting experiments using directional buoys to measure wave spectra as a surface truth comparison.

[Sponsored by ONR]

References

1. D.B., Trizna, "Measurement and Interpretation of North Atlantic Ocean Marine Radar Sea Scatter," NRL Report (in press).
2. J.P. Hansen and V.F. Cavaleri, "High Resolution Radar Sea Scatter: Experimental Observations and Discriminants," NRL Report 8557, March 1982.
3. Jin Wu, "Oceanic Whitecaps and Sea State," J. of Phys. Oceanogr., 9, 1064-1068 (1979).

■

Mark XV IFF Radar Mode

L. M. Leibowitz
Radar Division

Identification Friend or Foe (IFF) systems have been used since World War II to distinguish friends among platforms detected by radar or other means. In response to an encoded radio-frequency (RF) interrogation signal, friendly platforms respond with an appropriate RF signal reply. The current Mark XII IFF, used on platforms of all three military services, transmits on-off keyed signal pulses at fixed L-band interrogation and reply frequencies.

The United States and its NATO allies are currently involved in the development of the improved Mark XV IFF system as defined in Standard NATO Agreement (STANAG) 4162. The U.S. Tri-Service Development Program is directed by the Combat Identification Systems Program Office, Wright Patterson AFB, Ohio. NRL, under Naval Air Systems Command sponsorship, is a leader in the technical analysis, management, development, and evaluation of the Mark XV IFF system.

The Mark XV uses modern communications technology at L-band to provide improved interrogation/reply performance over the present Mark XII systems. Also included in the new system is a radar mode (RM), providing interrogations at radar frequencies using available platform weapons system radar resources. IFF RM provides increased angular resolution, reduced interference with other systems, and other advantages.

The RM interrogation incorporates self-synchronization, error detection and correction (EDAC) coding, and communications security (COMSEC) coding. Replies to RM interrogations will be transmitted by available Mark XV L-band transponders. Although the United States plans to include RM reply in its Mark XV IFF transponders, there are no present plans

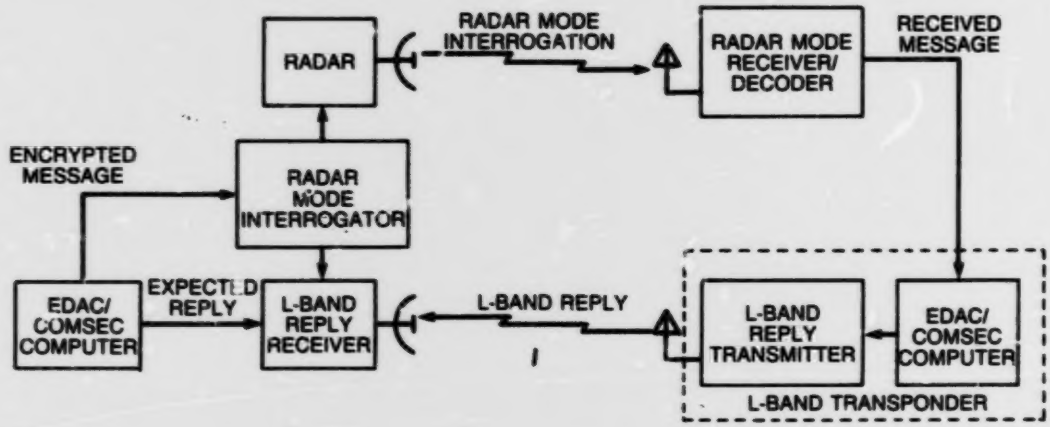

Fig. 9 – IFF radar mode system

for U.S. RM interrogation. However, the use of RM interrogation in some U.S. weapons system radars is being studied as it is particularly attractive for platforms without a current interrogation capability.

IFF Radar Mode Concept: Figure 9 shows the generalized Mark XV IFF system. The RM interrogation message with EDAC and COMSEC coding is provided by the interrogator EDAC/COMSEC computer. The message is properly formed and modulated by the RM interrogator and transmitted at radar frequencies through an available radar and associated antenna.

The RM interrogation is received at the transponder platform by a combined RM/L-band omnidirectional antenna and demodulated by the RM receiver. The demodulated message is presented to the transponder EDAC/COMSEC computer for error correction and decryption processing. Verified interrogations initiate L-band replies. These replies are received by the L-band reply receiver and compared to acceptable replies provided by the COMSEC computer for authentication.

A number of approaches are used to integrate RM into available radar systems. The appropriateness of each is dependent on the radar system. These approaches vary from maximum sharing of radar resources to the sharing of only the radar antenna. A separate RM interrogator without a radar, such as proposed for the man portable air defense system (MANPADS), is also feasible.

Several techniques for receiving and processing the RM interrogations have been developed. These techniques involve both synchronous and asynchronous techniques. As in the present Mark XII IFF, the RM transponder uses a top- and bottom-diversity antenna system to prevent blocking of the RM interrogation signal by aircraft structures. A multiband omnidirectional antenna is required to receive L-band as well as RM interrogations.

History and Status: RM was first used in the earliest IFF systems of World War II by transmission of reply pulses in the radar band in response to friendly radar signals. Frequency proliferation with rapid radar developments led to the use of dedicated uplink/downlink frequencies. RM was proposed by the Federal Republic of Germany in 1977, and it was subsequently accepted as part of the NATO Mark XV IFF. At that time, the UK began developing an IFF RM approach that led to a STANAG RM waveform and specification for RM interrogators and transponders.

In the late 1970s, NRL began looking into the feasibility of an IFF RM for shipboard radar. Several studies and analyses showed that despite problems relative to signal design and integration with available radars, such a mode was feasible.

The NRL efforts led to the successful development and testing of an experimental IFF RM for the L-band Senrad developmental shipboard radar located at the NRL Chesapeake Bay Detachment test facility.

Late in 1983, NRL began to investigate the suitability of the STANAG-proposed IFF RM and the feasibility of associated hardware. This investigation led to the development of RM transponder hardware using the basic synchronous approach proposed by the United Kingdom. NRL performed extensive performance and jamming tests and developed several transponder design improvements. This included an alternative asynchronous approach that uses multiphase processing with increased use of digital circuitry. This approach has been implemented and has undergone successful laboratory testing at NRL.

Under an amendment to the Defense Appropriations Act of 1986, the Navy has established a cooperative IFF RM effort with the United Kingdom. In this effort, under NRL technical direction, UK IFF RM equipment is being acquired by the Navy for laboratory and field testing. The equipment will be laboratory tested at NRL by using a radar mode test system (RMTS) specified by NRL. The UK RM equipment will then be integrated with U.S. equipment and field-tested at the Naval Air Test Center, Patuxent River, MD.

[Sponsored by NAVAIRSYSCOM] ■

Basic electronic properties of semiconductors and other solids are coupled to the development and fabrication of devices and the systems that use them. The research program centers around microstructure electronics and components and circuits, and it may involve the diverse fields of surface physics, microwave and millimeter wave technology, superconductors, molecular beam epitaxy, optical sensors, and organometallic chemical vapor deposition. Projects in all of these areas are emphasized in the Electronics Technology Division.

ELECTRONICS RESEARCH

ELECTRONICS RESEARCH

123 Designing Systems with VHSIC Components
Michael F. Walder

126 Surface Chemistry in Semiconductor Processing Using Laser Ionization
Ming C. Lin and David W. Squire

128 Ga Interstitials in AlGaAs Epitaxial Layers
Thomas A. Kennedy and Michael G. Spencer

130 Phase-Controlled Gyrotron Oscillators
Carter M. Armstrong and Robert K. Parker

133 β-SiC Transistor Development
Galina Kelner, Paul E.R. Nordquist, Jr., and William J. Moore

136 Kinetic Inductance Microstrip Lines
Jeffrey M. Pond and William L. Carter

Designing Systems with VHSIC Components

Michael F. Walder
Radar Division

As integrated circuit (IC) technology has advanced over the past several decades, there has been an ever-increasing delay in fielding military systems that use modern IC technology. Part of the reason is that commercial parts must be militarized, that is, certified to operate under the extreme environmental conditions that military systems are likely to encounter once deployed. A second reason is that commercial needs differ from military needs and therefore few parts are manufactured that can be directly inserted into military systems (Table 1). The Very High-Speed Integrated Circuits (VHSIC) program was conceived by the Department of Defense to influence commercial manufacturers to produce components with the most up-to-date technology that meet the processing needs and operational requirements of military systems.

Over the past several years, the Radar Division has been a participant in the VHSIC program. One effort has been to test several of the VHSIC devices and to confirm their functionality. An ongoing task involves designing a prototype signal processing system based on VHSIC technology. Many of the lessons learned in the testing of the devices have been applied to the design of the system.

Device Testing: The involvement in the testing has required the assembling of a custom test-bed to meet the unique requirements of these chips. At the time the testing was initiated, no reasonably priced commercial tester was available that could accommodate the high (100+) pin counts of these chips. To fill the testing requirements, a test-bed was constructed that consisted of a device fixture that was custom wired for each chip, a programmable read only memory (PROM) emulator/logic analyzer (emulyzer), and a controlling computer. The emulyzer is configured to send control signals and data inputs (stimulus) to the chip from its program memory and to store the outputs from the chip (response) in its trace memory. The controlling computer communicates with the emulyzer by the IEEE 488 General Purpose Interface Bus (GPIB). Software was written to control the operation of the emulyzer as well as to generate the stimulus signals for each VHSIC device. These stimulus signals are loaded into the emulyzer's program memory at the start of the test routine. After the emulyzer has captured the response from the device under test, the response signals are uploaded to the computer for comparison to the expected results. Any differences between the device outputs and the expected outputs are reported to the computer screen.

Three devices have been tested and confirmed as functional. The first device to be tested was the IBM complex multiplier/accumulator (CMAC). This chip performs the mathematical operations that are necessary to implement digital signal processing algorithms requiring complex arithmetic operations. The second device tested was the TRW matrix switch. This device is, as its

Table 1 — Integrated Circuit Market Drivers

Commercial	Military
Data processing	High-speed signal processing
Microprocessors	Military qualification
Memory	Radiation tolerant
	Built-in-test

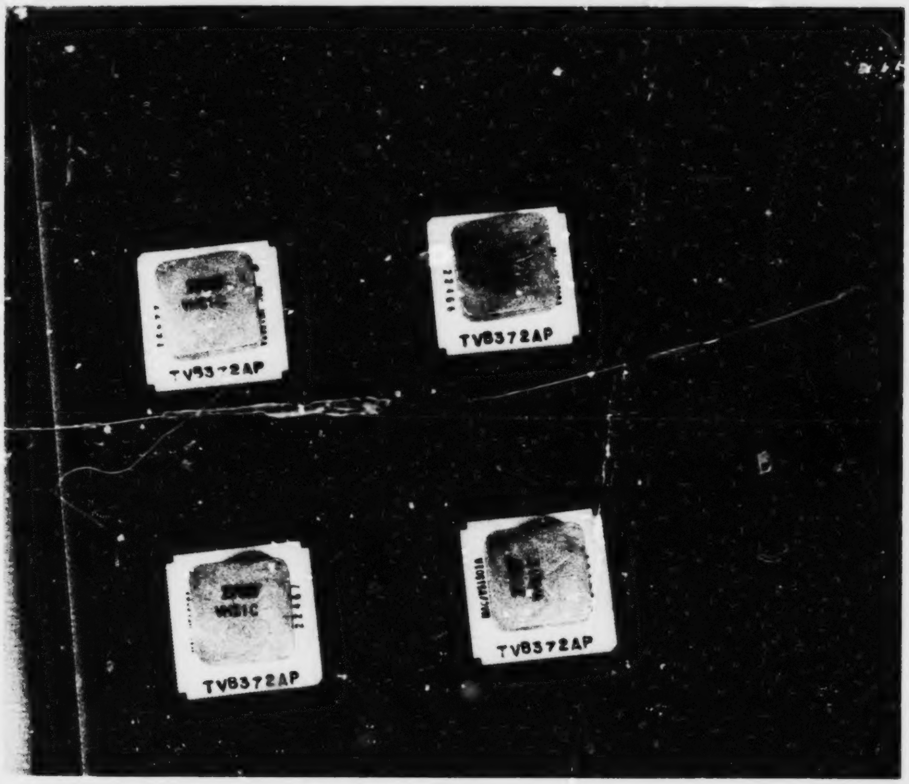
TV8372AP
TV8372AP
TV8372AP
TV8372AP

Fig. 1 – TRW multiplier/accumulator (MAC) device

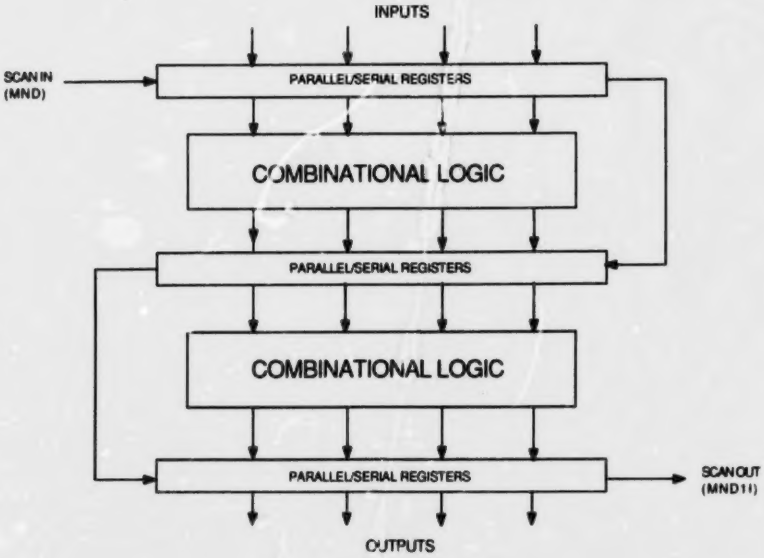
INPUTS
SCAN IN
(MND)
PARALLEL/SERIAL REGISTERS
COMBINATIONAL LOGIC
PARALLEL/SERIAL REGISTERS
COMBINATIONAL LOGIC
PARALLEL/SERIAL REGISTERS
SCAN OUT
(MND11)
OUTPUTS

Fig. 2 – Maintenance node scan path

BEST COPY AVAILABLE

name implies, little more than a switch. But it is a switch with eight input ports and eight output ports that can be configured to relay data from any of the input ports to any of the output ports. The most recently tested device was the TRW multiplier/accumulator (MAC) (Fig. 1). This device is similar to the CMAC in function, but it performs real arithmetic operations and has random access memory (RAM) on chip.

Prototype Design: To demonstrate the advantages of VHSIC technology, the Radar Division is developing a signal processor with VHSIC components. The design incorporates off-the-shelf VHSIC devices (MACs) and involves the customization of two Motorola VHSIC gate-arrays.

Because of the complexity of these devices, traditional design procedures (generate schematic, breadboard, and debug) would be stressed to their limit. Therefore, the VHSIC program has encouraged the concurrent development of design aids for these devices and also has encouraged the application of existing design tools to VHSIC. Chief among these tools is the computer-aided engineering (CAE) workstation.

The system was designed on CAE workstations. These computers are specifically made to accelerate the design and simulation of electronic circuits and systems and allow the system function to be confirmed before a commitment is made to hardware. The gate-array designs required the development of software models for the components of the gate-array. These models allow the designer to do complete simulation and verification of the design to be implemented on the gate-array by using the workstations. Since gate-arrays cannot be modified after they are manufactured, these models must accurately simulate the device performance under various operating conditions to ensure a functional device.

Not only were the CAE workstations used for the gate-array design, but they were also used to simulate the system design. To do so required the development of a hardware model for the MAC. The hardware model allows the chip itself to be used in the simulation of the system. Combining the software models of the gate-array with the hardware model of the MAC allowed for the simulation of the processor design. To allow the MAC to be used with the hardware modeler required a software *shell* to be written to associate the channels available from the workstation with pin numbers on the chip. This shell also contains timing information on the MAC for the workstation to use for the simulation.

All VHSIC devices are required to have self-test capability. This includes the VHSIC gate-arrays; therefore, included in the design for the gate-arrays was the maintenance node. The maintenance node is an implementation of the set/scan test methodology that allows a normally parallel design incorporating several levels of pipelining to be converted to a sequential circuit. This is done by connecting all registers in the design into a serial string. When the maintenance node is enabled, these registers, normally in the parallel mode, are changed to the serial mode and the scan path is now available to load data (Fig. 2). After the data are loaded into these registers, one parallel clock is sent to the registers to capture the output from the combinational logic, and the data now residing in the scan path are shifted out for comparison to known good values.

Results: Because of the involvement in the VHSIC program, the Radar Division has gained much experience in designing VHSIC systems and has developed many necessary tools to permit efficient design work. The developed tools include the software model library that was developed for the MAC. Experience was gained in the implementation of the self-test features required of the VHSIC devices and in the proper design of gate-arrays. Through this effort, NRL has developed the tools and expertise to aid future users of this technology.

[Sponsored by ONT] ■

Surface Chemistry in Semiconductor Processing Using Laser Ionization

M. C Lin and D. W. Squire*
Chemistry Division

Understanding the complex chemistry involved in the synthesis and etching of advanced semiconductors is essential to the improvement of both the quality and quantity of new microelectronic components. Under practical, high-pressure conditions, direct gas/surface reactions occurring in these processes are totally obscured by flow dynamics (such as boundary layers). No information on the mechanisms of gas/surface reactions could be obtained under practical operational conditions. We have recently employed the technique of multiphoton ionization/mass spectrometry (MPI/MS) to elucidate the mechanisms of gas/surface reactions during the thermal etching of silicon and the decomposition of group III metal alkyls on heated substrates under single collision conditions. The combined selectivity and sensitivity of both laser and mass spectrometry allow us to unambiguously identify atomic and free radical species desorbing from solid surfaces, as well as their formation, as a function of reactant pressure, substrate temperature, and additives.

In our recent investigation of the thermal etching of Si(110) by F_2, NF_3, and XeF_2 [1,2] an exhaustive search was made to detect free radical products, SiF_x ($X = 1-3$). The only radical product detected was SiF_2, which was probed by three-photon laser ionization with two-photon resonant enhancement by the $\tilde{B}\,{}^1B_2$ state at 160.6 nm. The apparent activation energies for SiF_2 and SiF_4 production were measured over the temperature range of 300 to 1200 K[1,2]

Table 1 — Apparent Activation Energies E_a for Total Etch Rate SiF_2 and SiF_4 Production in the Etching of Silicon

Product/Method	F atom	F_2	NF_3	XeF_2	T(K)
Electron Depth	2.10±0.1(a)				220-400
				-3.6(b)	270-360
		8.7±1.8(c)			337-473
				5.7(b)	450-630
		8(d)			330-470
SiF_4/Electron Ionization	---		20.0±1.2	5.6±0.8(e)	300-1200
		10(d)			300-470
SiF_2/Chemiluminescence	2.2±0.3(a)				220-400
		8.0±0.1(c)			337-460
SiF_2/Laser Ionization	---	8.9±0.3	22.1±1.7	6.7±0.5(e)	300-1200

(a) Ref. 3
(b) Ref. 5
(c) Ref. 4
(d) These values are only approximate because of the presence of breaks that limit the number of data points available for the least-squares analysis.
(e) Ref. 2

---

*NRC/NRL Postdoctoral Resident Associate (1984–1986): present address GEO-CENTERS, INC., Suitland, MD 20746 by using MPI/MS and electron impact (EI) IMS, respectively. These results are summarized in Table 1 for comparison with other related data obtained by Donnelly, Flamm, and coworkers [3-5]. The production of both SiF and SiF_3 radicals is believed to be thermochemically not favored [1,2].

Earlier we applied the MPI/MS technique to study the mechanism of $(CH_3)_3M$ (M = Al and Ga) decomposition on heated substrates (Cu, Al, GaAs, and SiO_2) [6-9]. In these deposition reactions, CH_3 radicals, which can be detected by 2-photon-enhanced resonance ionization at 333.4 nm, were detected to be generated with apparent activation energies several times lower than the first and strongest $M-CH_3$ bond dissociation energies. This finding was attributed to the surface enhanced decomposition [6-8]:

$$(CH_3)_3M + (s) \rightarrow (CH_3)_3M\ M(s) \rightarrow$$
$$(CH_3)_{3-x}M - M(s) + XCH_3(g).$$

The apparent activation energies for methyl radical production were determined to be 13+ 2 [6,7] and 26 ± 3 [8] kcal/mole for the decomposition of $(CH_3)_3Al$ and $(CH_3)_3$ Ga, respectively. Additionally, for $(CH_3)_3$ Ga, Ga atoms were also detected by MPI/MS to desorb from the hot substrates above 900 K, with an apparent desorption energy of 34 ± 3 kcal/mole (see Fig. 3) [9].

Our ability to detect these key reactive intermediates allows us to study for the first time the effect of group V hydrides [9] (such as N_2H_4, which we have employed recently as an efficient N-source in the preparation of GaN) on their formation under varying experimental conditions (see Fig. 4).

It was found that N_2H_4 did not affect the production of methyl radicals, but inhibited the production of gas-phase Ga. This result suggests that the N_2H_4 is not involved in the initial decomposition of $(CH_3)_3$ Ga, but serves to bind the Ga atom into the lattice.

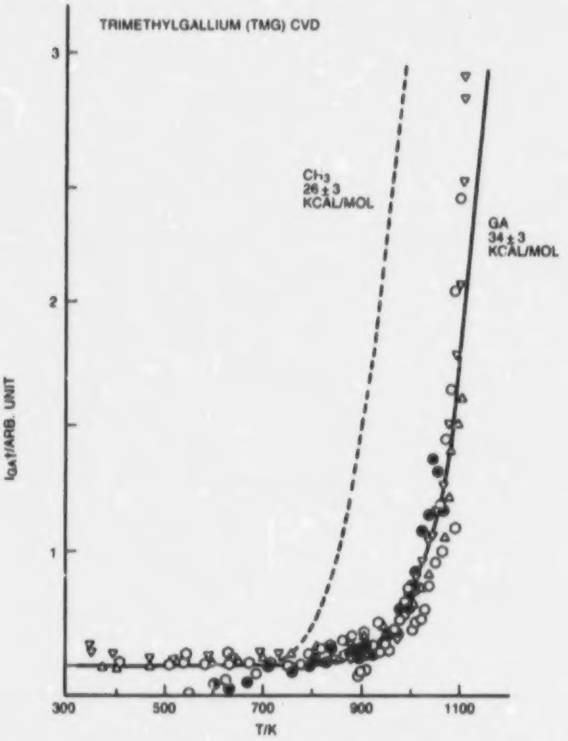

Fig. 3 – Ga ion signal as a function of substrate temperature for $(CH_3)_3$ Ga striking a copper surface. A least squares fit to an Arrhenium form gives an activation energy of 34 kal/mole (solid line). The dashed line is the similar line found for methy radical from $(CH_3)_3$ Ga

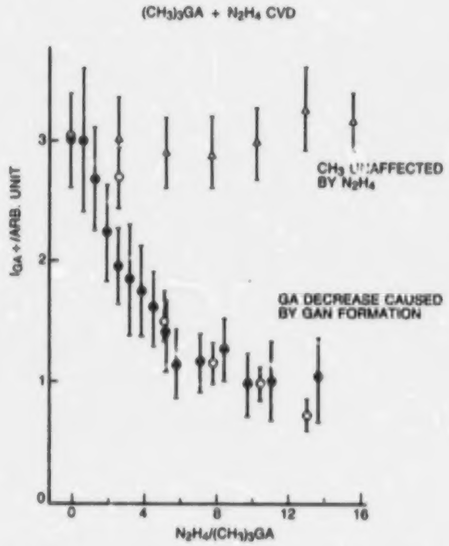

Fig. 4 – The effect of added N_2H_4 on methyl radical signal (Δ) and on Ga atom signal (o)

If these results hold true for GaAs and other III–V compounds, it should establish the first consistent surface mechanism for chemical vapor deposition processes, explaining the known surface catalytic effect of deposition enhanced by the presence of the surface itself. The knowledge of the surface chemistry of deposition and etching is essential for controlling the rates of these processes through realistic theoretical modelling.

[Sponsored by ONR]

References

1. D.W. Squire, J.A. Dagata, D.S.Y. Hsu, C.S. Dulcey, and M.C. Lin, *J. Chem. Phys.*, (in press).
2. J.A. Dagata, D.W. Squire, C.S. Dulcey, D.S.Y. Hsu, and M.C. Lin, *J. Vac. Sci. Technol.*, in press.
3. D.L. Flamm, V.M. Donnelly, and J.A. Mucha, *J. Appl. Phys.* **52**, 3633 (1981).
4. J.A. Mucha, V.M. Donnelly, D.L. Flamm, and L.M. Webb, *J. Phys. Chem.* **85**, 3529 (1981).
5. D.E. Ibbotson, D.L. Flamm, J.A. Mucha, and V.M. Donnelly, *Appl. Phys. Lett.* **44**, 1129 (1984).
6. D.W. Squire, C.S. Dulcey, and M.C. Lin, *Chem. Phys. Lett.* **116**, 525 (1985).
7. D.W. Squire, C.S. Dulcey, and M.C. Lin. *J. Vac. Sci. Tech.* **B3**, 1513 (1985).
8. D.W. Squire, C.S. Dulcey, and M.C. Lin, *Mater. Res. Soc. Proc.* **54**, 709 (1986).
9. D.W. Squire, C.S. Dulcey, and M.C. Lin, *Chem. Phys. Lett.* **131**, 112 (1986). ■

Ga Interstitials in AlGaAs Epitaxial Layers

T. A. Kennedy and M. G. Spencer
Electronics Technology Division

Semiconductor microstructures, such as multiquantum wells or superlattices consisting of alternating layers of epitaxially grown GaAs and AlGaAs, are forming the basis for a new generation of microelectronic and optoelectronic devices. A critical issue in the successful development of novel or high-performance microstructural devices is the identification and control of deleterious defects in the epitaxial AlGaAs layers. Traditional techniques for defect identification, such as electron paramagnetic resonance, require relatively large sample volumes and are not readily applicable to these thin film materials. However, we have shown that optically-detected magnetic resonance, in which small changes in luminescence intensity are caused by the electron paramagnetic resonance of defects, can be applied successfully to the study of epitaxial layers. Optically detected magnetic resonance spectra of AlGaAs layers grown by molecular beam epitaxy have revealed Ga interstitials through the signature of the ^{69}Ga and ^{71}Ga nuclear magnetic moments.

Defects and Optically Detected Magnetic Resonance: Any imperfection in the crystalline lattice of AlGaAs causes changes in the optical and magnetic properties. When pure material is excited by laser light, it emits light at a characteristic wavelength. This effect is called *photoluminescence* and is similar to the electroluminescence of light-emitting diodes and lasers. Defects destroy this emission and either convert it to heat or produce emission at longer (typically infrared) wavelengths. Because they do not match the lattice bonding well, defects often have unpaired spins and magnetic moments. The spins can reveal the symmetry and chemical identity of the defects; however, direct absorption by the spins is difficult to detect in the AlGaAs layers that are typically only 1-μm thick. There is an interaction between the spin and optical properties of a defect—the intensity of the deep luminescence depends weakly on the magnetic spin state. Thus an induced spin flip at the defect (electron paramagnetic resonance) produces a small change in the intensity of the photoluminescence (optically detected magnetic resonance). Since the entire luminescence process takes place within 1 μm of the surface, optically detected magnetic resonance is ideally suited to the study of thin epitaxial layers.

The experiment is performed by placing a 2 × 5 mm sample of AlGaAs grown on a GaAs substrate into a microwave cavity in an optical liquid helium dewar (see Fig. 5). The sample is excited by blue light from a Kr ion laser, and the deep luminescence is detected by a cooled Ge photovoltaic detector. Changes in emission that are coherent with the chopped microwave power are detected as a function of magnetic field. The magnet can either be an external electromagnet or a superconducting magnet that is an integral part of the optical cryostat.

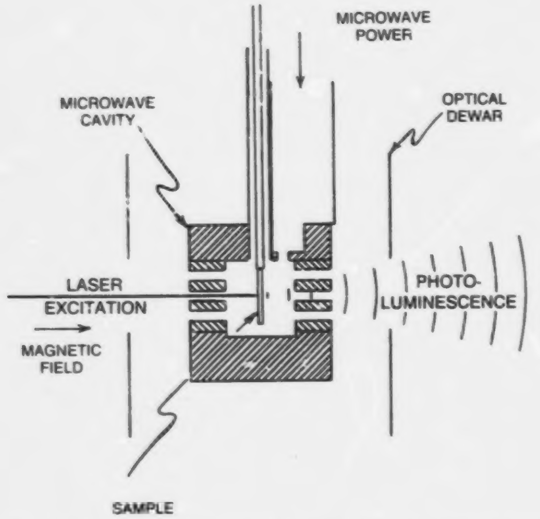

Fig. 5 - Experimental setup. The sample is placed in a microwave cavity immersed in liquid He in an optical dewar. Luminescence (shown red) is excited by blue laser light and detected by a Ge detector (not shown). Changes in the luminescence coherent with the chopped microwave power are measured as a function of magnetic field.

Ga Interstitial Identification: To grow AlGaAs of high quality by using molecular beam epitaxy, substrate temperatures of at least 670°C are required; however, at these higher temperatures, dopants, such as Si tend to diffuse and thus sharp doping profiles cannot be obtained. We have applied the optically detected magnetic resonance technique to AlGaAs grown at lower substrate temperatures and identified one of the residual defects that limit the material's quality.

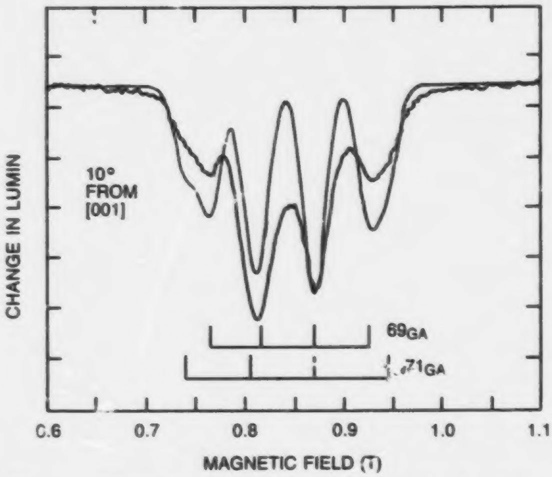

Fig. 6 - ODMR data and simulation for molecular beam epitaxy-grown AlGaAs. The resonances are decreases in emitted light. The four-line spectrum can be attributed uniquely to a gallium-centered defect through simulation with the known isotopes and their abundances.

The response (see Fig. 6) is negative, indicating that the defects responsible are decreasing the photoluminescence in the spectral range detected. The spectrum is split into four partially resolved lines. Little angular dependence is observed, indicating that the splitting is caused by magnetic hyperfine interaction, that is interaction between the electron-spin magnetic moment and the magnetic moment of the nucleus at the center of the defect. Since there are four lines, the nuclear spin is 3/2. On closer inspection, the outer lines reveal a further broadening, which indicates the element at the center of the defect has two spin 3/2 isotopes with slightly different nuclear moments. Of the elements that have two spin 3/2 nuclei, only gallium fits the spectrum. Figure 6 also shows a simulation using the proper ratio of nuclear moments and natural abundances. Although there are discrepancies in the amplitudes, the lineshape of each component is well fit. Thus gallium, a major constituent of AlGaAs, is the core of the defect that reduces the luminescence efficiency.

The exact position of this gallium defect can be deduced by comparison with current theory. Only an interstitial, that is a gallium atom not on a regular lattice site, would produce such a large hyperfine interaction. Thus the atomic structure of the defect consists of an extra Ga atom probably surrounded by regular As atoms (see Fig. 7).

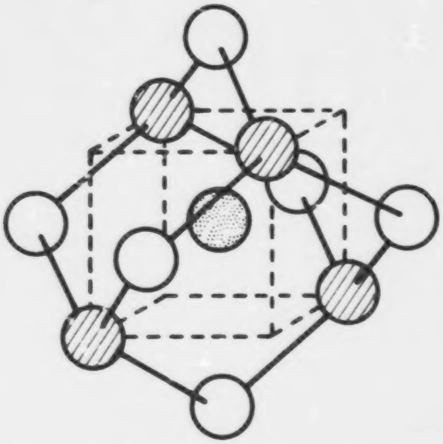

Fig. 7 – The Ga interstitial in AlGaAs. The central Ga atom has four (shaded) As nearest neighbors. The six (open) second nearest neighbors are Al and Ga atoms.

Summary: The identification of Ga interstitials in AlGaAs by optically detected magnetic resonance is very exciting for several reasons. This work is the first identification of an intrinsic defect in AlGaAs and provides information that should lead to the improved growth of AlGaAs by molecular beam epitaxy. It also demonstrates the importance of the technique as a tool for defect investigations in thin films and opens up the possibility of defect studies in microstructures and at interfaces.

[Sponsored by ONR] ■

Phase-Controlled Gyrotron Oscillators

C. M. Armstrong and R. K. Parker
Electronics Technology Division

A continuing need exists for efficient, high-power sources of electromagnetic radiation in the microwave and millimeter wavelength range for such applications as plasma fusion heating and as sources for advanced radio-frequency (RF) accelerators and radar. Gyrotron devices using the electron cyclotron resonance maser (ECRM) instability are particularly attractive as sources in these frequency ranges because they have the potential of providing high average power density and good electronic efficiency. Gyrotron oscillators are the most advanced of the ECRM devices, having demonstrated efficiencies in excess of 35% with peak output powers of 175 kW at 140 GHz [1]. For narrow-band applications requiring phase coherence such as for radar and RF accelerators, phase-synchronized gyrotron oscillators are attractive since they could combine the high-efficiency characteristic of oscillators with the phase control provided by amplifiers.

Gyrotron Phase Locking: The gyrotron interaction mechanism involves a natural resonance between a relativistic gyrating electron beam and an electromagnetic cavity mode. Electrons originating from a thermionic source are injected along a strong magnetic guide field into a resonant RF structure. The electrons spiral around the local magnetic field lines at the relativistic cyclotron frequency. Coupling of the electron beam to a transverse electric cavity mode occurs as a result of the cyclotron resonance maser instability. The cyclotron resonance instability uses the energy dependence of the relativistic electron cyclotron frequency to phase-bunch the electrons in their cyclotron orbits. The resultant coherent interaction then results in a net transfer of beam energy to electromagnetic field energy.

One method for controlling the phase of a free-running oscillator is phase locking. Injection phase locking is the synchronization of the phase and hence the frequency of a free oscillation to a stable external drive signal. It occurs when a nonlinear oscillator is driven strongly enough near its natural resonant frequency. The frequency band over which an oscillation can be locked for a given drive power can be expressed in a straightforward way. This relationship, first derived by *R.* Adler, is applicable to a broad class of oscillators including microwave cavity oscillators and lasers. In a microwave system, Adler's equation is written as

$$\frac{Q_e \left[f_d - f_o\right] \left[P_o / P_d\right]^{1/2}}{f_o} < 1,$$

where the subscripts d and o refer to the drive signal and oscillator, respectively, f is the frequency, P is the power, and Q_e is the external quality factor of the oscillating cavity.

There are two straightforward methods for phase locking a gyrotron oscillator. One is to directly inject the RF radiation drive signal into the cavity oscillator and the other is by premodulating the electron beam at the drive frequency before it reaches the cavity. With the three-cavity gyroklystron device at NRL [2], a thorough experimental study has been performed comparing these two phase-locking methods [3]. This work has been performed in collaboration with Mr. Alan McCurdy of Omega P Inc. and the Applied Physics Section at Yale University, New Haven, CT. It represents the first experimental demonstration of gyrotron phase locking using electron-beam modulation.

Experiment: Figure 8 shows the three-cavity gyroklystron used in this study. Figure 9 shows the device schematically. A magnetron injection gun is used to produce a thick annular-rotating electron beam. The electron beam parameters are 6.2 A at 28 keV with a perpendicular-to-axial velocity ratio of about 1.0. The experiment is pulsed with a pulse duration of 4 μs and a repetition rate of 60 Hz. The RF circuit consists of three mechanically tunable rectangular cavities operating in the fundamental transverse electric 101 electromagnetic mode at a frequency of around 4.5 GHz.

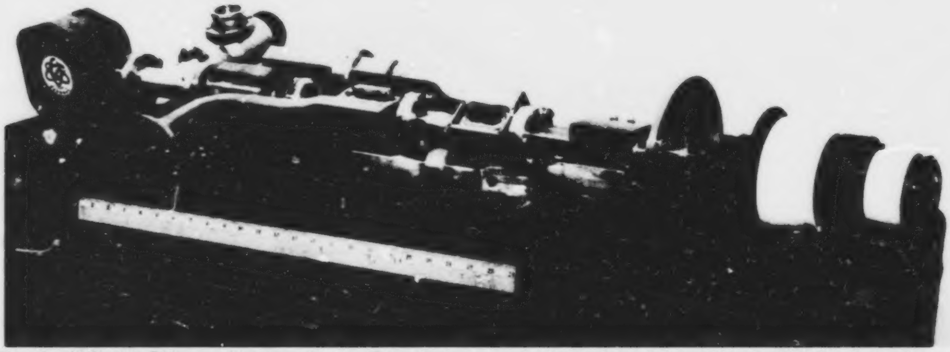

Fig. 8 – NRL 4.5 GHz gyroklystron device. The electron gun is at the right, followed by the RF circuit, the beam collector, and a vacuum pump for evacuating the device. During operation, the tube is immersed in a strong magnetic field produced by nine water-cooled solenoidal magnet coils.

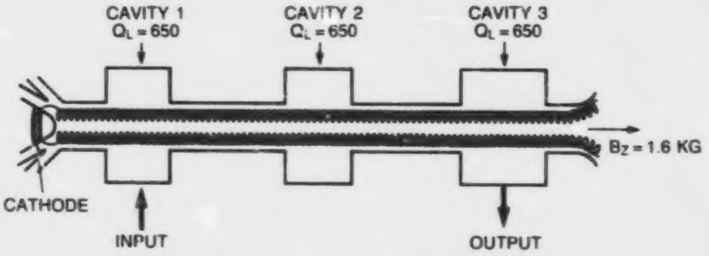

Fig. 9 – Three-cavity gyroklystron configuration

BEST COPY AVAILABLE

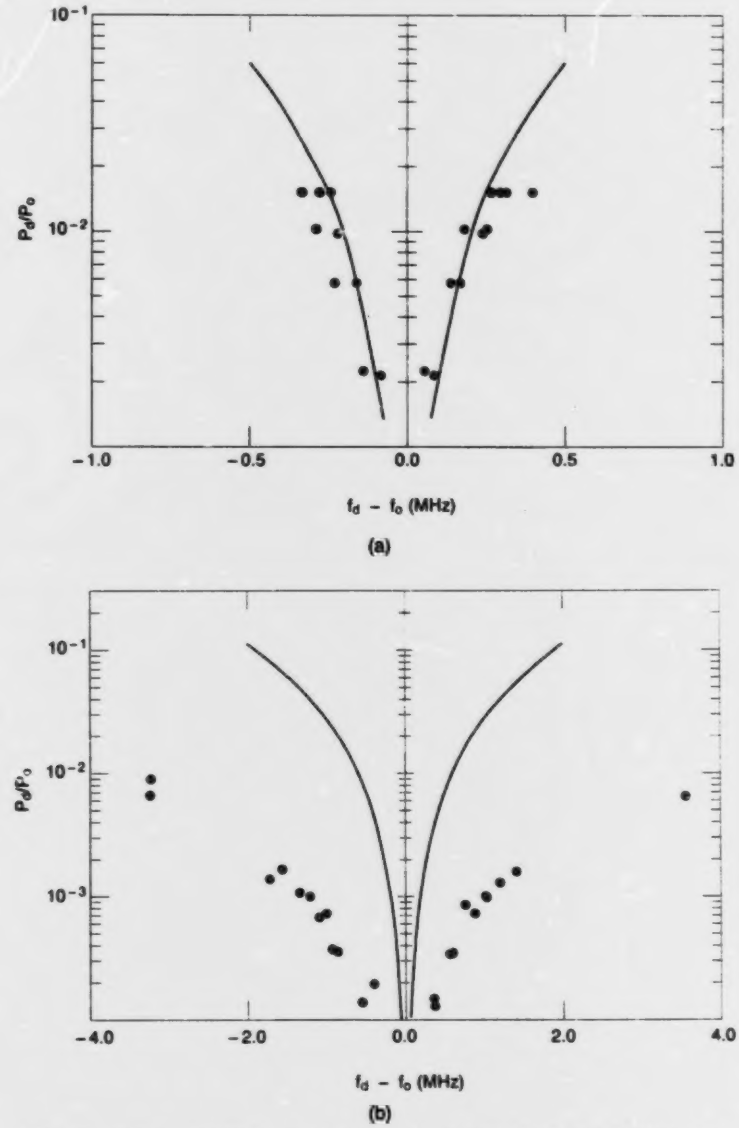

(a)

(b)

Fig. 10 – Gyrotron oscillator phase-locking bandwidths for (a) direct RF injection (cavity No. 1) and (b) beam modulation using two prebunching cavities (cavity No. 3). Note that the experimental locking bandwidth (solid dots) exceeds the theoretical prediction (solid curves) in the premodulation case.

The cavities are separated by cylindrical drift sections that are cut off to the generated RF radiation. The RF drive signal is applied to cavity No. 1 to begin electron beam modulation by electron cyclotron resonance absorption. The beam is then further modulated by ballistic bunching in the drift regions and interaction in cavity No. 2. The modulated beam phases the oscillation in the last cavity. The last cavity is made unstable by tuning the natural cavity resonance very close to the beam relativistic cyclotron resonance. Output power is extracted by means of a waveguide coupled through the side wall of the cavity.

Results: It is found, by use of the three-cavity gyroklystron configuration, that phase locking can be obtained at drive power levels more than an order of magnitude below that predicted by Adler's equation. Figure 10(a) shows the phase-locking bandwidth as a function of drive power as calculated from Adler's equation and as measured experimentally for a single-cavity gyrotron oscillator (cavity No. 1). The phase-locking bandwidth for direct RF injection into the cavity oscillator agrees closely with Adler's equation as long as $P_d / P_o << 1$. The exciting new result, shown in Fig. 10(b), is that phase locking of an oscillation in cavity No. 3 by electron beam modulation with the gyroklystron requires, that the drive power needed to lock the gyrotron be reduced by more than an order of magnitude over Adler's prediction. This reduction in the drive power can be explained in part as caused by the natural amplification of the beam modulation occurring between the input and output cavities of the gyroklystron.

Phase locking by means of electron beam premodulation has many advantages over the direct-injection method. By using the gain of the extended gyroklystron configuration, the drive power required for locking is significantly reduced. The configuration also provides a natural separation between the driving section and the high-power cavity oscillator. The input section can then be tuned for efficient absorption without degrading the oscillator performance. Furthermore, the high degree of isolation between the cavities in the configuration results in little oscillator power feeding back into the drive circuit. Another advantage of phase locking is that it results in a reduction in the fluctuations in the gyrotron oscillator amplitude and frequency. The noise reduction caused by phase locking is important to applications requiring extremely stable sources such as radar and RF accelerators. Finally, although the possibility has not yet been investigated, premodulation may also prove useful as a method for exerting mode control in an overmoded gyrotron oscillator and as a means for accessing the high-efficiency regimes of gyrotron operation desirable for plasma fusion heating.

[Sponsored by ONR and ONT]

References

1. K.E. Kreischer, J.B. Schutkeker, B.G. Danly, W.J. Mulligan, and R.J. Temkin, *Int. J. Electron.* **57**, 835 (1984).
2. W.M. Bolien, A.H. McCurdy, B. Arfin, R.K. Parker, and V.L. Granatstein, *IEEE Trans. Plasma Sci.* **13**, 417 (1985).
3. A.H. McCurdy, C.M. Armstrong, W.M. Bollen, R.K. Parker, and V.L. Granatstein, *Phys. Rev. Lett.* **57**, 2379 (1986). ■

β-SiC Transistor Development

G. Kelner, P. E. R. Nordquist, Jr.,
and W. J. Moore
Electronics Technology Division

Cubic or beta-silicon carbide (β-SiC) is emerging as an important electronic device material to be used in applications requiring high-power microwave devices, high-temperature electronic devices, and harsh-environment-tolerant devices. With a variety of useful physical properties such as large bandgap, chemical inertness, and high theoretical saturated drift velocity, for many years β-SiC has been thought as capable of surpassing the power, microwave frequency, and radiation tolerance limitations of the current silicon and gallium arsenide electronic device technologies. NRL has taken a substantial step toward realizing this thought through the fabrication of the first β-SiC metal-semiconductor field-effect transistor (MESFET) in the United States. The MESFET effort is part of a larger SiC project supported by ONR. It includes epitaxial growth of thin SiC films, characterization of these films, and development of the process technology required to fabricate the MESFET.

Materials' growth and characterization studies have supported the device development. Both *n*- and *p*-type SiC layers are grown on (100) *p*-type (boron doped) silicon substrates at 1623 K with silane and propane as reactants.

The *n*-type dopant is believed to be nitrogen, while aluminum doping produces *p*-type layers. During growth, silane and propane, as 1% mixtures in hydrogen, pass over the inductively heated susceptor in a carrier gas of palladium-diffused hydrogen (Figure 1). Epitaxial layers up to 20 μm thick have been grown. Layer characterization is by infrared reflection spectroscopy (for thickness and estimation of carrier density) [1], photoluminescence (Fig. 2), Raman spectroscopy, and Hall effect measurement. Typical unintentionally doped SiC layers are specular, *n*-type, have Hall mobilities of 250 cm^2/V-s with carrier concentrations between 3 and 5 × 10^{17} cm^{-3}, and their quality is sufficient for device studies. *P*-type layers have typical doping densities in the 1 × 10^{17} to 5 × 10^{17} cm^{-3} range.

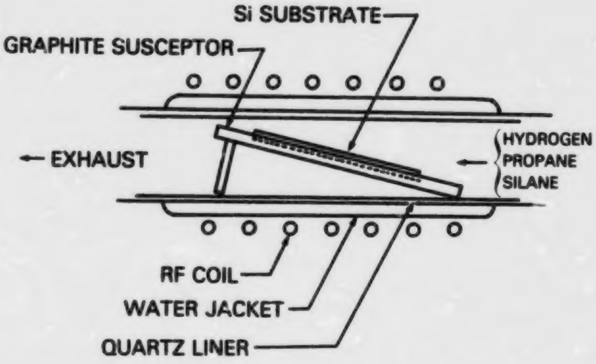

Fig. 11 – Reactor for vapor phase epitaxial growth of β- silicon carbide

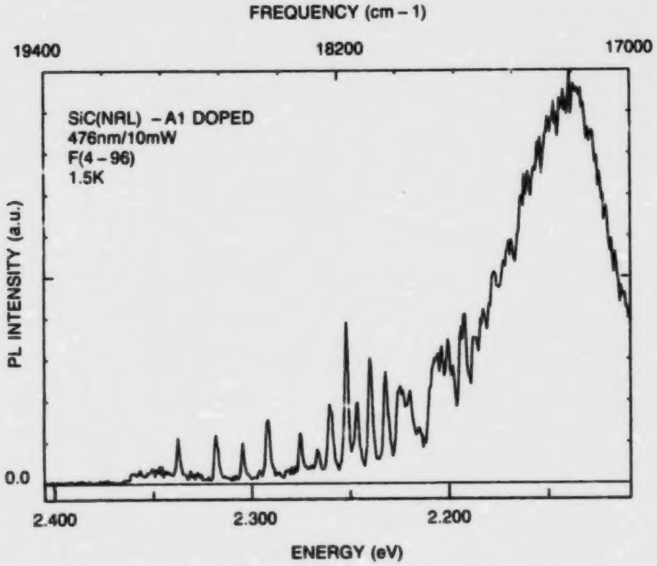

Fig. 12 – Photoluminescence (arbitrary units) spectrum of A1–doped β–SiC showing fine structure arising from donor acceptor pair recombination involving the A1 acceptor and a donor with a binding energy of 53 meV identified as nitrogen. The observation of donor acceptor pair structure demonstrates the very high quality of this NRL-grown β–SiC film.

BEST COPY AVAILABLE

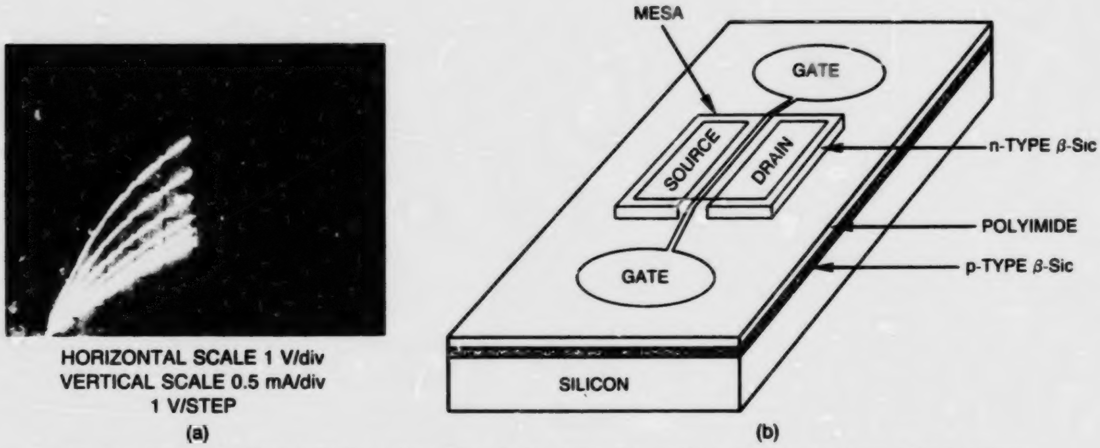

Fig. 13 – (a) FET I–V characteristics. The voltage on the gate controls the current flowing from drain to source. (b) Schematic view of fabricated device.

Using characterized epitaxial layers of SiC, NRL has developed a MESFET technology. Both ohmic (nonrectifying) and Schottky (rectifying) metal contacts, necessary for the MESFET, have been developed for SiC epitaxial layers. WSi_2, $MoSi^2$, $TaSi_2$, and Cr/Ni have been used for ohmic contacts while Au, PtW, and TiW have been deposited for Schottky barrier contacts. The best Schottky diodes are obtained by using resistive evaporation of Au on chemically prepared or on oxidized and stripped surfaces. This type of Au Schottky barrier remains rectifying to at least 500°C while its sputtered Au counterpart is ohmic up to 700°C. $TaSi_2$ and Cr/Ni provide the most satisfactory room-temperature ohmic contacts with specific contact resistances between 5×10^{-5} and 4×10^{-4} ohm-cm^2, respectively. The first β-SiC MESFETs used a large area buried p layer as illustrated in Fig. 13(b) [2]. This design is one of the three being investigated. They all require some form of SiC isolation to insulate the gate from the substrate. Inherently insulating or semi-insulating substrates for epitaxial SiC do not yet exist. Such substrates may be critical to MESFET microwave performance; therefore they need to be developed.

The fabrication process starts with an epitaxial SiC structure 3000-Å thick n-type SiC layer on a p-type SiC layer grown by chemical vapor deposition on a 7-μm thick p-type SiC layer grown by chemical vapor deposition on a p-type Si(100) substrate. Electrical isolation of the topside n-type channel is accomplished by using SF_6 plasma etching. The source and drain contacts to the n-type material were thermally evaporated Cr/Ni/Au; alloying was not required to produce ohmic contacts. Gold was used as the Schottky barrier gate metallization with an 8-μm spacing between the source and drain and a gate length of 5 μm. The gate bonding pads rest on a polyimide layer to avoid contacting the buried p-layer. MESFET I-V characteristics of a fabricated device are shown in Fig. 13(a). The transconductance or change in drain current with applied gate voltage is about 2 to 2.5 mS/mm of drain width. Work is under way to fully explain these I-V characteristics and to improve them by using innovative MESFET designs and improved epitaxial growth procedures.

[Sponsored by ONR]

References

1. R.T. Holm, P.H. Klein, and P.E.R. Nordquist, Jr., *J. Appl. Phys.* **60**(4), 1479-85 (1986).
2. G. Kelner, S. Binari, K. Sleger, and H. Kong, submitted for publication to *IEEE Electron Device Lett.* (1987). ■

Kinetic Inductance Microstrip Lines

J. M. Pond and W. L. Carter
Electronics Technology Division

Requirements for the processing of radar and communications signals are expected to place increasing demands on devices and circuits as frequencies become higher and algorithms become more sophisticated. In addition, the size of these systems must be kept small. The approach we are pursuing uses a superconducting microstrip transmission line in the kinetic inductance regime as the building block. Kinetic inductance is due to the inertial mass of the current carriers in a conductor. It is possible to fabricate microstrip where the inductance is primarily kinetic rather than magnetic (caused by the energy of the magnetic field in the dielectric). The solution to the electromagnetic boundary value problem of a layer of dielectric sandwiched between two superconducting films is well known [1]. The microstrip lines that we have fabricated have low loss, low dispersion, and phase velocities of less than one hundredth the speed of light. This is about five times slower than has been reported previously. This slow velocity can be exploited to fabricate small filters.

We have shown that, if thin identical superconducting films are used, the phase velocity is accurately predicted by

$$v_p = (v_d/\lambda)\,(dt/2)^{1/2}$$

where d and t are the dielectric and superconductor thicknesses, respectively, λ is the magnetic penetration depth in the superconductor, and v_d is the speed of light in the dielectric. Since λ is a function of the superconducting electron pair density, the phase velocity can be varied, changing the electrical length of the microstrip. This makes tunable filters, phase shifters, and delay lines possible.

Device Fabrication: A 150-Å niobium nitride (NbN) ground plane was deposited on a quartz substrate, followed by 250 Å of hydrogenated silicon (Si:H). After processing, 150 Å of Si:H was deposited followed by a second NbN layer of 140 Å. A 25-μm wide 20.1-cm long microstrip line, with contact pads at each end, was then patterned in the second NbN film. The contact pads were covered by 100 Å of Cr, 1000 Å of Au, and indium solder dots to have repeatable contacts.

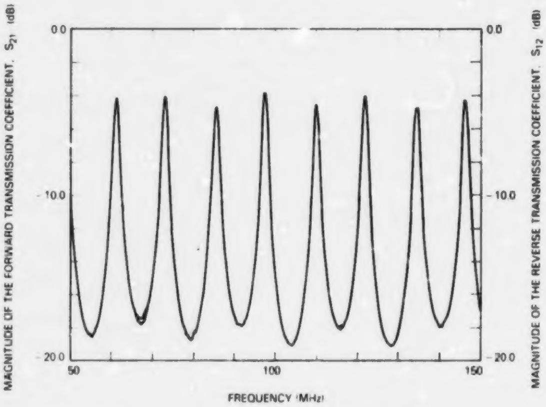

Fig. 14 – The magnitude of the transmission response of the microstrip at 4.2 K from 50 to 150 MHz

Experimental Results: Frequency responses were measured with Hewlett Packard automatic network analyzers. Figure 14 shows the magnitude of the forward transmission coefficient for the microstrip at 4.2 K. The microstrip has a repeatable resonance signature indicating relatively low loss within the microstrip. The peaks of the curve in Fig. 14 correspond to frequencies where the microstrip is an integral number of half-wavelengths long. This is due to the large impedance mismatch and discontinuity that causes the microstrip to appear as a weakly coupled cavity with an input and output port. The spacing between the peaks corresponds to a phase velocity of 0.016 c, where c is the speed of light in vacuum. Similar measurements were obtained at other frequencies and temperatures, and the resonant peaks remained well defined through the highest frequency, 2.0 GHz, that measurements were made.

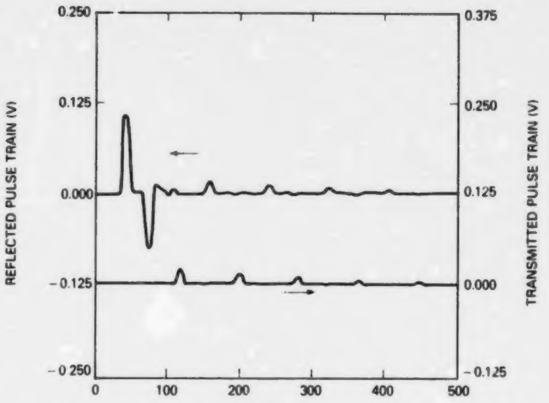

Fig. 15 – The reflected and transmitted transient response of the microstrip, due to an incident 10 ns pulse

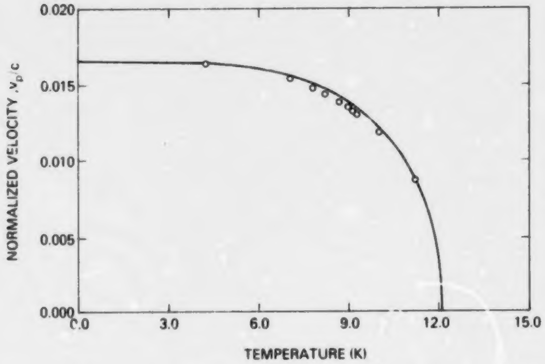

Fig. 16 – The normalized measured phase velocity, *vp/c* as a function of temperature (dots) is compared to the expected behavior (solid line)

Figure 15 shows the time domain response with a 10-ns input pulse. The first pulse is the input pulse, and the second pulse, with negative polarity, is the pulse reflected from the input to the microstrip. The transmitted pulse is reflected many times within the microstrip, yielding pulse trains at the input port and output port. The pulses were undistorted with a spacing that corresponds to the double transit time of the line.

Discussion: These measurements were used to accurately determine the phase velocity of the microstrip. Figure 16 shows the normalized measured phase velocity vs temperature. The measured values are compared to the expected behavior, given the temperature dependence of λ. The transition temperature, 12.15 K, was determined by observing the temperature at which no signal was transmitted. Additional work has been conducted to model these microstrip lines, including the loss mechanisms [2].

Conclusions: The particular advantages of this technique are the possibility of obtaining very short wavelengths in a very small area due to the reduced velocity and small coupling between lines and the flexibility of tuning the phase velocity. The processing is compatible with Josephson junction technology, allowing sophisticated signal processing functions as well as combined analog and digital functions.

The primary area for improvement of this device is the reduction of the loss in the dielectric film. The loss mechanisms of the film have been measured and identified. Much lower losses should be obtainable with high-quality dielectric films. Other areas of emphasis for future work will be in the implementation of specific devices such as phase shifters, tunable filters, taps, and coupled lines with this microstrip.

[Sponsored by ONR]

References

1. J.C. Swihart, "Field Solution for a Thin-Film Superconducting Strip Transmission Line," *J. Appl. Phys.* **32,** 461-469 (1961).

2. J.M. Pond, J.H. Claassen, and W.L. Carter, "Measurements and Modelling of Kinetic Inductance Microstrip Delay Lines," submitted to *IEEE Trans. Microwave Theory and Tech.* ■

The energy of the universe comprises the world of the Plasma Physics Division. Here, research fields of plasma, atomic, and laser physics; pulsed power sources; and electron and ion beams are directed to high atmospheric and plasma dynamics, including nuclear weapon and charged beam effects on the atmosphere. Much emphasis is placed on numerical simulation on a large scale in these research areas, but there is, as well, a practical interest in the formation of intense ion beams and the interaction of laser energy with matter.

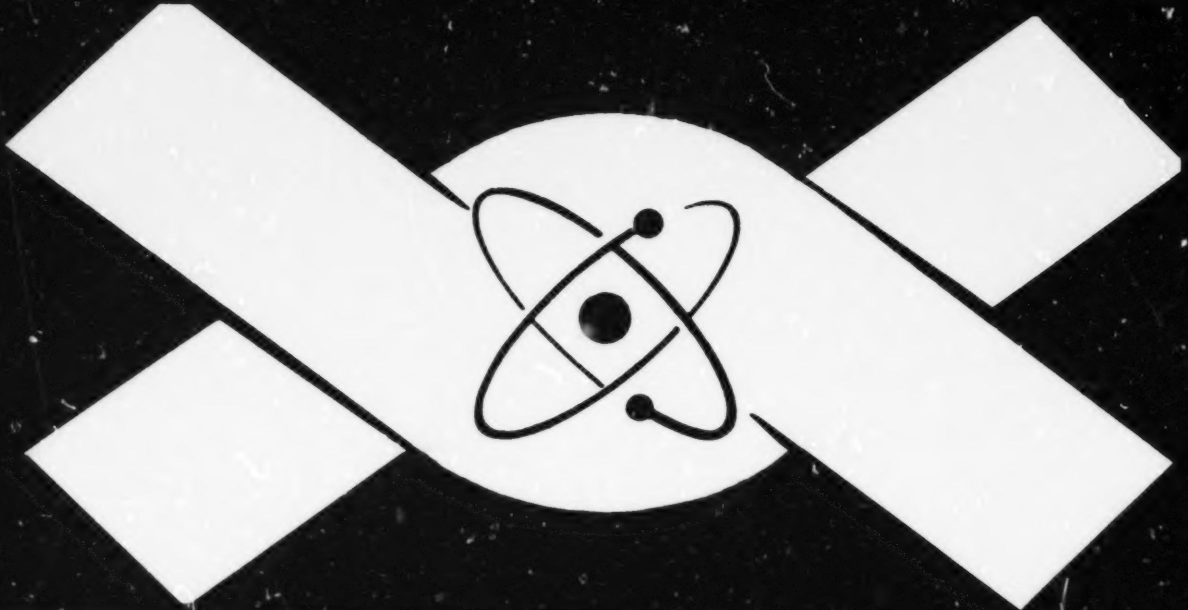

ENERGETIC PARTICLES & BEAMS

139

ENERGETIC PARTICLES AND BEAMS

141 **Soft X-ray Laser Generation**
Tong N. Lee, Edgar A. McLean, and Raymond C. Elton

143 **Modulated Intense Relativistic Electron Beams**
Moshe Friedman and Victor Serlin

145 **Charged-Particle Beam Propagation**
Martin Lampe, Glenn Joyce, Richard F. Hubbard, Steven P. Slinker, Richard F. Fernsler, and A. Wahab Ali

147 **Advanced Concepts in Radiation Sources and Particle Acceleration**
Phillip Sprangle and Cha-Mei Tang

Soft X-Ray Laser Generation

T. N. Lee, E. A. McLean, and R. C. Elton
Plasma Physics Division

The idea of creating a laser generating a wavelength in the soft X-ray regime ($\lambda < 300$ Å) has attracted the imagination of many scientists since the laser was invented over 25 years ago. Such an X-ray laser has many potential applications. These include

- interferometry of very small volumes,
- X-ray lithography used in the fabrication of microcircuits,
- flash radiography of dense plasmas,
- high-resolution imaging of life biographical materials,
- plasma temperature and density diagnostics, and
- numerous other applications.

Host of important additional applications would no doubt arise when such lasers are readily available to researchers in diverse disciplines of science and engineering. Naturally, the Department of Defense could find many uses for such short wavelength lasers. We have created a soft X-ray laser at NRL, and it is described here.

Requirements: Many difficulties occur when creating an X-ray laser. Since the lasing wavelength is much shorter than visible wavelengths, the lasing transitions must come from highly charged ions instead of atoms. Thus an enormous concentration of pumping power is required to invert the populations of the energy levels of these highly charged ions to create the conditions needed for lasing. If an inverted population is achieved, the lasing lines are amplified as they pass through the length of the hot ionized plasma, a process called *amplified stimulated emission*. This amplification is nonlinear so that the lasing intensity grows exponentially with the length of the hot plasma.

Typical conditions of the plasma required for X-ray lasing are: the plasma must be several centimeters long, have a diameter less than a few millimeters, be very uniform, have a high temperature (about 10^7 K), and have a density of 10^{19} to 5×10^{20} electrons/cm^3. One way to create such high-energy plasmas is to make use of high-power ($\sim 10^{12}$ W) lasers. These lasers have been highly developed in recent years, primarily for inertial confinement fusion research. The elongated plasma can be produced by focusing such a laser beam (with a cylindrical/spherical lens) in a thin line onto a desired target. We have used such an approach to successfully produce soft X-ray lasings in neonlike (ten electron) copper ions.

NRL Result: In the NRL experiment [1], the Pharos III Nd-laser operating at the wavelength of 1.05 μm, 350 to 500 J, and 2-ns pulse width is focused in a 200-μm-wide line onto a copper target as shown in Fig. 1. The power concentration at the line focus is in the mid-10^{12} W/cm^2, which produces a suitable plasma. We mainly used an ultrathin target composed of 1000-Å-thick coating of copper over a 1200-Å-thick Formvar substrate. The extreme ultraviolet spectra (170 to 550 Å) observed axially show three neonlike Cu^{19+} 3p $\rightarrow$ 3s lines whose intensities increase exponentially with the length of the target, indicating an axial gain. The power output of each of these lasing lines is estimated to be ≈ 1 kW. These results are similar to those found earlier by Matthews et al [2] with selenium targets. Two of these lines are identified as $J = 2$ to 1 transitions at 279.31 and 284.67 Å, and a the third as $J = 0$ to 1 transition at 221.11 Å. The gain coefficients, which are derived from the measured exponential curves (see Fig. 2) for the $J = 2 \rightarrow 1$ and $J = 0 \rightarrow 1$ lasing lines, are $\alpha = 1.7 \pm 0.2$ cm^{-1} and $\alpha^1 = 2.0 \pm 0.2$ cm^{-1}, respectively. The ratio of these coefficients $\alpha^1/\alpha \approx 1.2$ obtained in the experiment agrees with the recently calculated value [3] of $\alpha^1/\alpha = 1$ to 2 and far exceeds the experimental value of $\alpha^1/\alpha < 0.2$ as reported in Ref. 2. This ratio

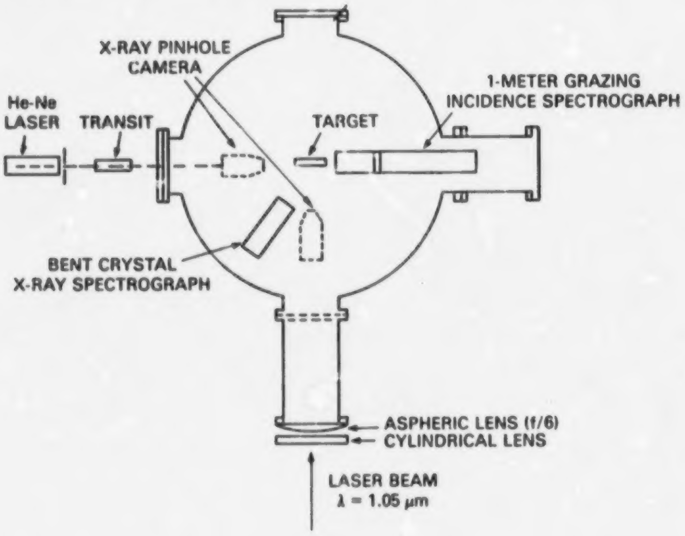
X-RAY PINHOLE CAMERA
He-Ne LASER
TRANSIT
TARGET
1-METER GRAZING INCIDENCE SPECTROGRAPH
BENT CRYSTAL X-RAY SPECTROGRAPH
ASPHERIC LENS (f/6)
CYLINDRICAL LENS
LASER BEAM
λ = 1.05 μm

Fig. 1 - The experiment

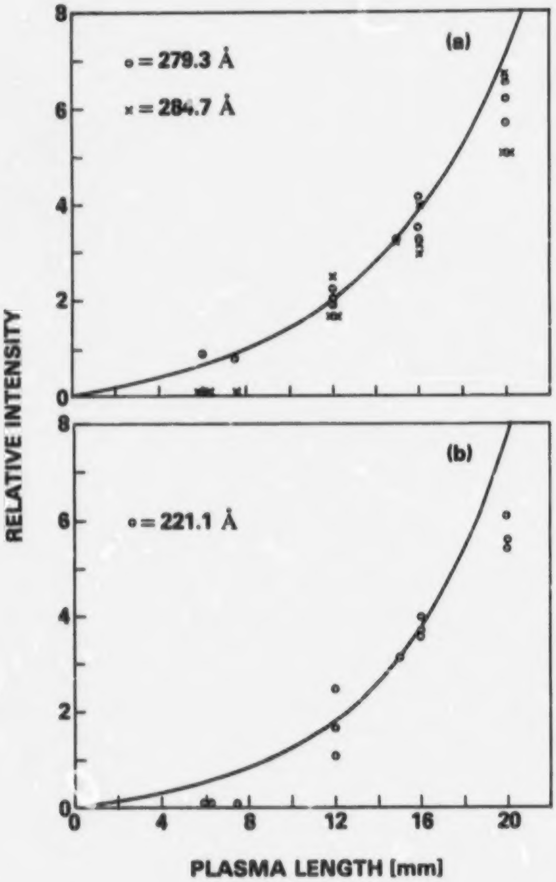

Fig. 2 — Relative intensities vs plasma length for: (a) the 279.31 and 284.67 Å (J = 2 to 1), and (b) the 221.11 Å (J = 0 to 1) lasing lines, along with calculated gain curves for gain coefficients of 1.7 and 2 cm^{-1}, respectively.

BEST COPY AVAILABLE

(α^1/α) is a strong indication that electron collisional excitation is the primary pumping mechanism in this experiment.

Future: Having demonstrated soft X-ray lasing in Cu^{19+} ions, we are now in a position to improve the efficiency of these lasers by modification in the geometry, making them useful laboratory devices. Also, it would be valuable to investigate other materials to achieve lasing at shorter wavelengths that could penetrate thicker and denser materials.

[Sponsored by ONR and SDIO]

References

1. T.N. Lee, E.A. McLean, and R.C. Elton, submitted to *Phys. Rev. Lett.* (1987).

2. D.L. Matthews et al., *Phys. Ref. Lett*, **54**, 110, 106 (1985).

3. D.L. Matthews et al., *J. de Physique* **47** C6-1 and U. Feldman, J.F. Seely and G.A. Doschek, *J. de Phys.* **47**, C6-187 (1986). ■

Modulated Intense Relativistic Electron Beams

M. Friedman and V. Serlin
Plasma Physics Division

The physics of intense relativistic electron beams (IREBs) is governed by the beam electric and magnetic self fields. There are many applications of IREBs that exploit these self fields. Examples can be found in research areas on high-power microwave generation, collective acceleration of charged particles, and plasma heating to thermonuclear temperature. NRL has an interest in these areas of research, and for the last 6 years investigations were undertaken to understand the role of self-fields in the various applications. A new mechanism emerged from this research that makes it possible to efficiently modulate IREBs at power levels exceeding 10^9 to 10^{10} W. With the knowledge accumulated during this period, we can project radio frequency (RF) sources, using modulated IREBs, capable of generating gigawatts to terawatts of RF power with pulse energies in the 100-kJ range. This kind of power and energy makes such devices interesting, not only for military applications, but also for heating plasmas to thermonuclear temperatures and for powering large RF accelerators.

Phenomenology [1]: During the experimental investigation of IREB transport through drift space, we found that high levels of coherent oscillation appeared on the IREB current. The drift space consists of a smooth metallic tube in which two or more wall perturbations are inserted. Figure 3 shows an example of such a behavior of an IREB propagating through a smooth drift tube with various numbers of perturbations that, for this example, have taken the form of coaxial cavities. For the preceding example, the following important characteristics are observed:

- The frequency of oscillation depended strongly on the geometry and weakly on IREB current and voltage.
- The frequency of modulation was monochromatic and could be tuned between 60 MHz and 3 GHz.
- Electron beams at various accelerating potentials and currents were fully modulated with an efficiency of nearly 100%.

Theory [1]: A simple theoretical model based on space-charged waves on IREB gave excellent agreement with the experimental observation. Numerical simulations agreed with the theory and extended it into the nonlinear region. Both theory and simulation showed that the electric and magnetic self-fields of the IREB and the induced electric field cause by IREB propagation through cavities generate virtual cathodes in the drift region. Electrons were reflected from the virtual cathodes producing an oscillating current in the drift region. The interaction of this current with the cavities caused redistribution of energy within the IREB in such a way that coherent bunches of electrons were formed.

Generation: It is well known that RF power can be extracted from modulated electron beams (e.g. klystron). Thus a device was built that converted the kinetic energy of the modulated IREBs into either trains of high-voltage pulses or an RF pulse. Nearly 50% efficiency was achieved.

Amplifier [1]: During the investigation of self-modulation of IREBs described earlier, we were able to show theoretically that a mechanism exists that can be used to construct an RF amplifier of power over 10^9 W. This theoretical prediction was verified experimentally, and an RF amplifier using an IREB was built at NRL. Figure 4 shows the schematic of the high-power RF amplifier.

The most significant results from the amplifier work are:

- A low-power RF source completely modulates an IREB that has 10^4 to 10^5 times higher power.
- Unlike a conventional klystron, a long drift length for beam bunching is not necessary.

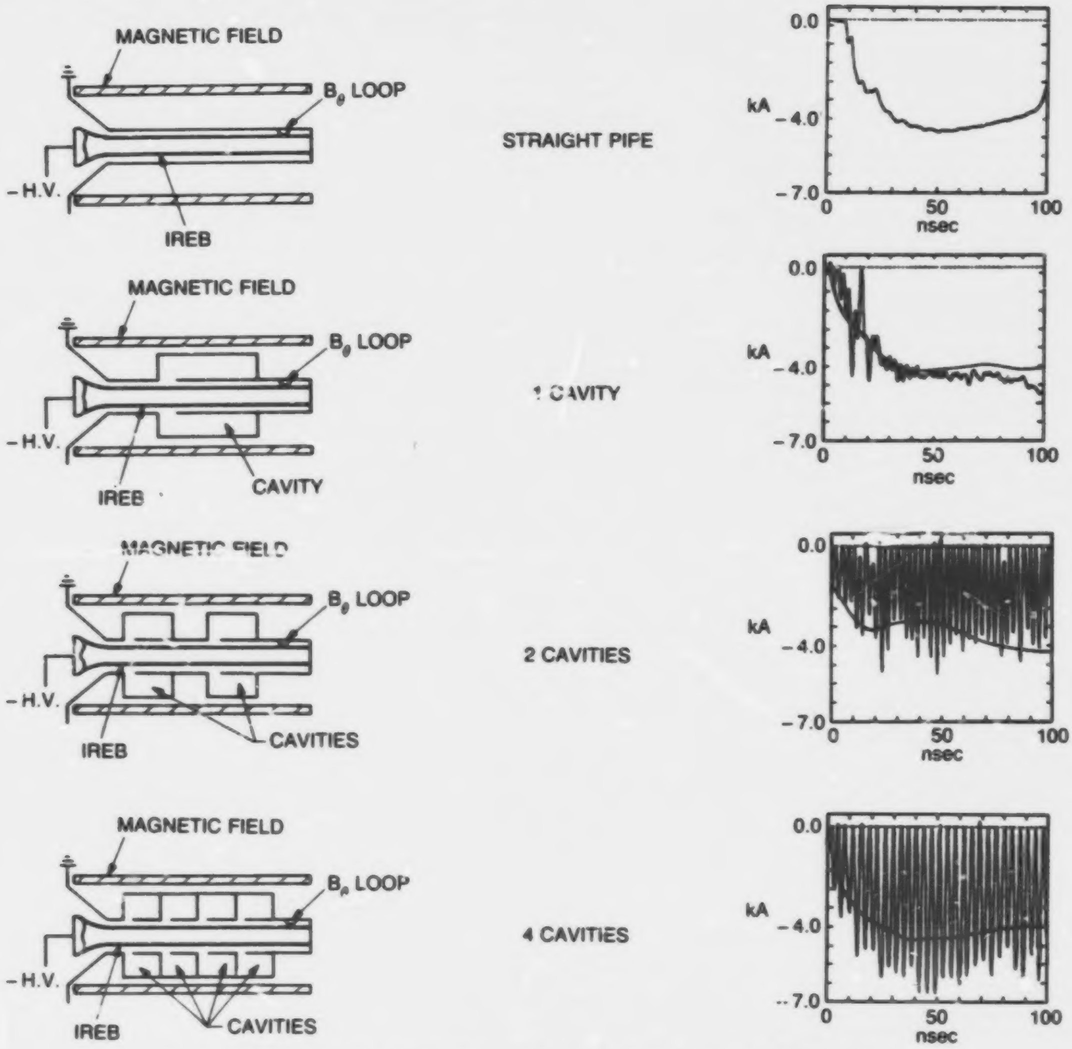

Fig. 3 - IREB propagation inside different structures (left). Current profiles emerging from the structures (right)

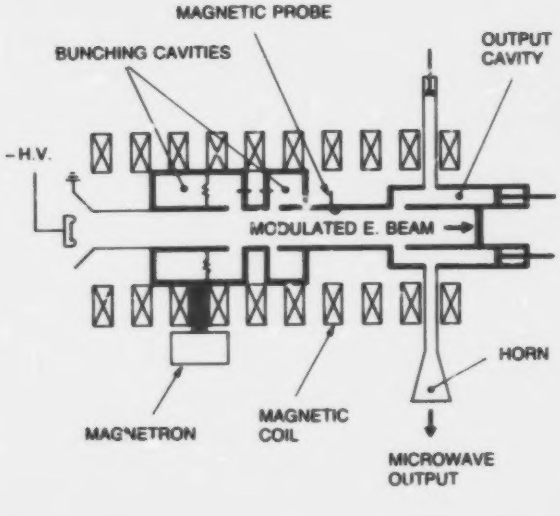
MAGNETIC PROBE
BUNCHING CAVITIES
OUTPUT CAVITY
-H.V.
MODULATED E. BEAM
HORN
MAGNETRON
MAGNETIC COIL
MICROWAVE OUTPUT

Fig. 4 - Experimental arrangement of the GW high-power RF amplifier operating at 1.3 GHz (L-band)

BEST COPY AVAILABLE

- The frequency of modulation is 1.3 GHz, and phase variation is less than 4°.
- RF power extraction with an efficiency of 50% has been achieved.
- Theoretical analysis predicts that beam modulation and RF power extraction at higher frequencies (probably as high as 10 GHz) is possible with similar gain and power level.

Other Applications: As previously mentioned, applications of modulated IREBs can be found in many other areas. Two of the more interesting examples are:

- A modulated IREB offers a promising plasma heating technique. With this technique a resonant-heating process can be frequency-tuned to deliver energy on a controlled surface within the plasma. Moreover, greater RF penetration into the plasma seems possible since the RF is carried inside the plasma by the modulated IREB.
- The modulated IREB can be used to power particle accelerators. The new mechanism for acceleration [2] employs two beams of charged particles that interact by means of a metallic structure. The first beam, the modulated IREB, generates an electromagnetic field, which in turn accelerates a second beam of particles. Voltage gradients in excess of 100 MV/m can be established by the new mechanism, accelerating electrons, or ions to GeV energies. This mechanism is now under investigation at NRL.

[Sponsored by ONR]

References

1. M. Friedman and V. Serlin, "Modulation of Intense Relativistic Electron Beams by an External Microwave Source," *Phys. Rev. Lett.* **55**, 2860 (1985).
2. M. Friedman and V. Serlin, "Particle Accelerators Powered by Modulated Intense Relativistic Electron Beams," *Appl. Phys. Lett.* **49**, 596 (1986). ■

Charged-Particle Beam Propagation

M. Lampe, G. Joyce, R. F. Hubbard,
S. P. Slinker, R. F. Fernsler, and A. W. Ali
Plasma Physics Division

Charged-particle beam propagation has been studied at NRL and other laboratories for a number of years. Propagation of intense relativistic electron beams in dense gases, or *endoatmospheric* propagation, is of interest to the Navy because of the potential for intercepting antiship missiles at long ranges. NRL's Plasma Theory Branch has engaged in computational and theoretical studies of the complex phenomena of propagation that include air chemistry, plasma instabilities, energy-loss mechanisms, and hydrodynamics. The branch also studies propagation in the ion-focused regime. Propagation in this low-pressure regime is of interest for accelerator transport of high-current beams and for some strategic defense missions.

Endoatmospheric Stability: Beam propagation can be disrupted by a variety of plasma instabilities that arise from the interaction between the electron beam and the plasma that it generates as it propagates. The resistive hose instability is the most serious of these. NRL's SARLAC particle simulation code was the first computer model to treat this instability in its large amplitude (nonlinear) limit for a wide range of realistic beam parameters. Figure 5, taken from a SARLAC simulation of the 4.5 MeV, 7 kA Experimental Test Accelerator (ETA) experiment at the Lawrence Livermore National Laboratory, illustrates the extent to which this instability can disrupt propagation [1]. NRL has been a leader in developing techniques for controlling this instability and has assisted with planning and analysis of stability experiments at several laboratories.

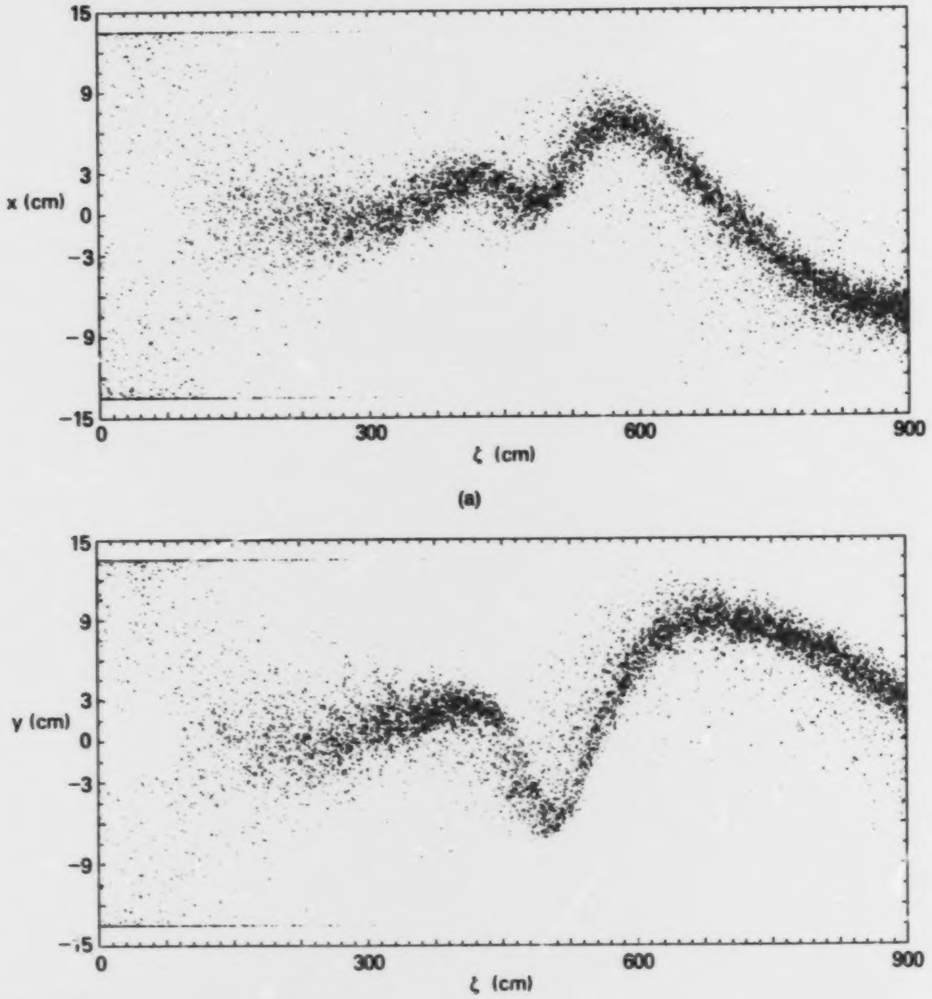

BEST COPY AVAILABLE

(b)

Fig. 5 – (a) The *x* position of simulation particles vs the distance from the beam head. The large contortions are due to the hose instability. (b) The *y* positions for this SARLAC simulation [1].

Current Multiplication: Electron beams normally generate plasma currents that flow in the opposite direction to the beam. However, some experiments have detected large forward-going plasma currents. This mysterious current multiplication phenomenon was eventually explained by NRL as being due to large-amplitude hose instability motion by the beam. As the beam approaches the conducting wall of the propagation chamber, the axial electric field $E(r,8)$ reverses sign in certain regions. Figure 6 plots $E(r,8)$ in a cross section of the propagation tube taken as the SARLAC simulation beam in Fig. 5 nears the edge of the chamber [1]. Forward-going currents flow in the green, blue, and violet contour regions, leading to a 70% enhancement of the net current.

Multiple-Pulse Phenomena: Endoatmospheric propagation to long ranges requires that several pulses be used to "drill" a reduced density path through the atmosphere. Many techniques have been proposed to ensure that the later beam pulses will remain in this low-density channel. Several such techniques have been invented or

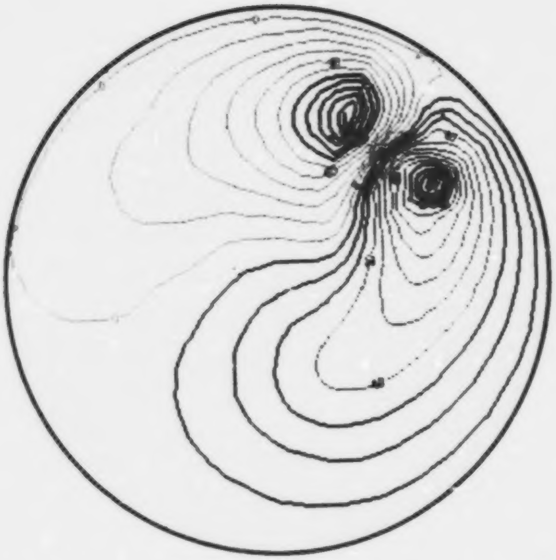

Fig. 6– Contours of the axial electric field $E(r,\theta)$ for the same simulation used in Fig. 5. The beam has propagated 2.7 m, and the fields are measured at 6.3 m from the beam head. The red and yellow contours define regions where the plasma current is negative (the usual case), while the green, blue, and violet contours are where E drives a forward plasma current [1].

explored theoretically at NRL. Simulations such as SARLAC have been a major theoretical tool for studying multiple-pulse propagation modes. Experiments to simulate multiple-pulse propagation are planned for the new beam propagation facility at NRL.

Ion-Focused Regime Propagation: This is a relatively new technique in which the plasma electrons are expelled by strong beam-generated radial electric fields. Left behind is a positive ion column that can electrostatically pinch the relativistic electron beam. The secondary plasma can be generated by beam impact ionization or by preionization with a suitable laser. NRL has developed axisymmetric propagation codes to study both cases. Phenomena of interest include erosion or beam loss caused by inductive fields and degradation of the pulse resulting from motion of the ion column. Ion-focused regime transport in the accelerator was crucial to the success of the advanced test accelerator, and the technique appears to have many applications.

If the beam propagates in a large volume of dilute plasma, the secondary electrons are not completely expelled and can be drawn back into the ion column. This induces an oscillating axial electric field that can autoaccelerate some portions of the beam and degrade other portions. This is in fact the basis of the *wake field accelerator* that has been proposed previously by workers in accelerator physics.

[Sponsored by DARPA and SDIO]

Reference

1. R.F. Fernsler, R.F. Hubbard, B. Hui, G. Joyce, M. Lampe, and Y.Y. Lau, *Phys. Fluids* 29, 3056 (1986). ■

Advanced Concepts in Radiation Sources and Particle Acceleration

P. Sprangle and C. M. Tang
Plasma Physics Division

In recent years, interest has renewed in the development of concepts and devices for the production of efficient, tunable, high-power coherent electrometic radiation and high-energy, high-quality electron beams. The advanced concepts presently under study at NRL are the free electron laser (FEL), the induced resonance electron cyclotron maser (IREC), the inverse free electron laser accelerator (IFEL), and the plasma beat wave accelerator (PBWA). These radiation and acceleration sources not only are important basic research subjects, but are also of potential importance to national defense. The FEL, for example, has been chosen to be the prime laser source for SDI applications.

Free Electron Laser: These lasers are tunable and efficient devices for converting electron-beam energy to coherent electromagnetic radiation. In the FEL, a high-energy electron beam is sent through a transverse periodic magnetic field (wiggler). The wiggling of the electrons by the magnetic field can generate coherent radiation at a wavelength that is related to the energy of the

BEST COPY AVAILABLE

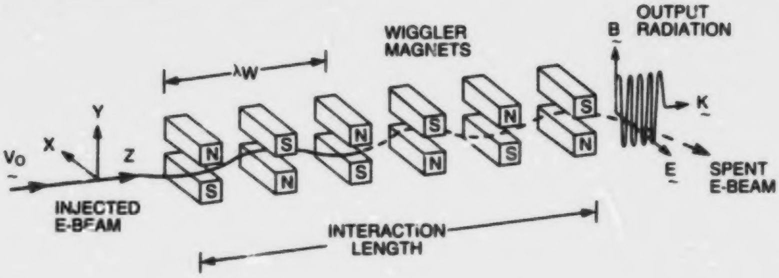

Fig. 7 – A free electron laser

electron beam (Fig. 7). In the FEL, the radiation field, wiggler field, and electron beam resonantly couple to modify the refractive index in the vicinity of the electron beam. The resultant complex refractive index can lead to radiation focusing [1]. This phenomenon allows the radiation to grow around the electron beam for extended distances. Without this focusing effect, FELs could not achieve the high efficiency needed for SDI applications. NRL investigators have developed a source-dependent expansion method to study optical focusing, guiding, and steering in FELs [2]. Figure 8 is a computer simulation showing the narrowing of the width (focusing) of the radiation beam as the electron beam propagates through the FEL for a distance of four Rayleigh lengths.

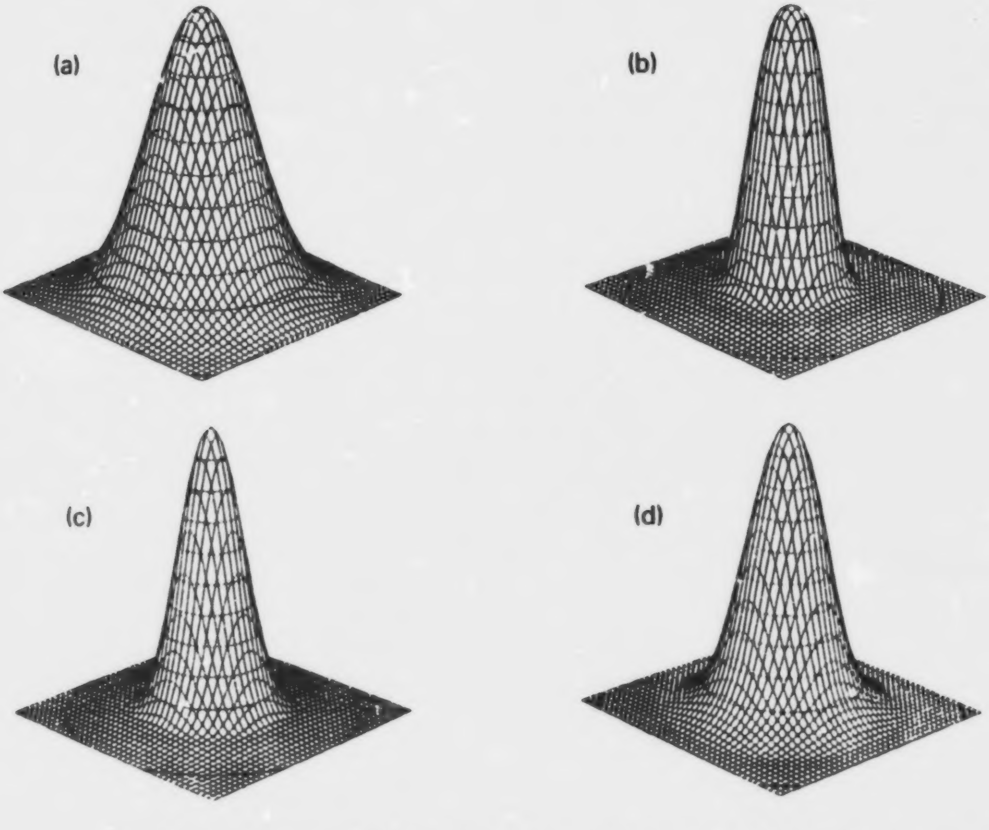

Fig. 8 — The transverse intensity profile of the free electron laser radiation at four equally separate distances: (a) $z = 0$, (b) $z = z_o$, (c) $z = 2\ z_o$, and (d) $z = 3z_o$, where z_o is the Rayleigh length of the input radiation. The radiation focusing associated with the FEL overcomes the free space diffraction.

BEST COPY AVAILABLE

NRL is collaborating with the National Bureau of Standards on an FEL driven by a CW racetrack microtron for material science and biomedical research [3]. Some of the exceptional characteristics of this accelerator that are needed for the FEL are continuous-beam operation, high- and small-energy spread, good beam quality, excellent energy stability, and high average power. The racetrack microtron FEL is expected to generate radiation from 10 μm down to 0.2 μm.

Induced Resonance Electron Cyclotron Maser: The IREC quasioptical maser [4] is a promising advanced concept for generating coherent radiation in the millimeter to the infrared wavelength regime. It is highly efficient and relatively insensitive to the electron beam's energy spread. It has been shown that by appropriately tapering the applied magnetic field, the interaction efficiency can be greatly enhanced. It is anticipated that efficient, high-power millimeter submillimeter, and infrared radiation sources can be realized with the IREC maser configuration.

Acceleration of High-Power Electron Beams: High-quality, intense electron beams could have exciting applications in a wide variety of areas, ranging from FELs and national defense to X-ray radiography. A number of programs in this area are under way at NRL, ranging from modified betatrons to laser-driven accelerators. The availability of high-power laser beams ($> 10^{14}$ W) suggests the possibility of accelerating electrons to TeV and beyond. A summary of two types of laser-driven electron accelerating schemes follows.

- *Inverse Free Electron Laser Accelerator*

In the IFEL acceleration concept, coherent radiation is used to accelerate electrons to high energy by using a mechanism similar to that of the FEL. Incoherent synchrotron radiation is emitted by the wiggling electrons in the magnetic wiggler field of the IFEL. This radiation emission can effectively cool the electrons and improve the beam quality. We have studied the dynamics of the electrons in an IFEL accelerator with a fully relativistic formulation and find that the beam quality improves exponentially. However, because of the recoil of the electrons as quanta of synchrotron radiation are emitted, statistical fluctuations called quantum excitations eventually limit further enhancement of the beam quality. In high-energy IFEL accelerators, we found that strong transverse focusing forces on the electrons are required to reduce the effects of the quantum excitations.

- *Plasma Beat Wave Accelerator*

The PBWA is a collective acceleration scheme that uses the enormous self-fields of an excited plasma wave. The plasma wave is excited by the parametric coupling of two laser beams with a frequency difference equal to the characteristic plasma frequency. Electrons can be trapped and accelerated by the plasma wave. NRL is studying the self-focusing of the laser beams and the possibility of tuning the phase velocity of the plasma wave to obtain ultrahigh energies.

The various novel radiation and acceleration concepts outlined here have been the subject of intense national and international research. The results of this research have indicated that these sources may represent important additions to the arsenal of radiation and acceleration devices.

[Sponsored by U.S. Army Strategic Defense Command, ONR, and DOE]

References

1. P. Sprangle and C.M. Tang, *Appl. Phys. Lett.* **39**, 677 (1981).
2. P. Sprangle, A. Ting, and C.M. Tang, accepted for publication in *Phys. Rev. A* (1987) and *Phys. Rev. Lett.* (1987).
3. C.M. Tang, P. Sprangle, S. Penner, B.M. Kincaid, and R.R. Freeman, *Nucl. Instrum. Methods Phys. Res.* **A250**, 278 (1986).
4. P. Sprangle, C.M. Tang, and P. Serafim, *Appl. Phys. Lett.* **49**, 1154 (1986). ■

The near ultraviolet to the far infrared makes up the realm of the Optical Sciences Division. Theory and experiment are aimed at principles and mechanisms in optical phenomena, devices, and materials. Research, both basic and applied, is directed to the diverse areas of laser physics, holography, quantum optics, IR surveillance, optical warfare, atmospheric propagation, and a range of optical data processing studies. The development of special optical materials, such as those used in recording, and the generation of missile seeker technology are of concern.

OPTICAL SYSTEMS

153 **Optical Studies of Aerosols**
Anthony J. Campillo, Horn-Bond Lin, Thomas J. Manuccia, Jr., and Mark Seaver

155 **Photoemitter Membrane Light Modulator Device for Optical Processing**
John N. Lee and Arthur D. Fisher

158 **Parametric Raman Gain Suppression**
John F. Reintjes and Michael D. Duncan

162 **Fiber-Optic Magnetic Sensors**
Frank Bucholtz, Aileen M. Yurek, and Anthony Dandridge

165 **Development of Infrared Focal Plane Arrays for Advanced Navy Sensors**
Melvin R. Kruer, Dean A. Scribner, and Cecil J. Gridley

Optical Studies of Aerosols

A. J. Campillo, H.-B. Lin, T. J. Manuccia, Jr.
and M. Seaver
Optical Sciences Division

Droplets in Gas Flows: Instances of two-phase fluid flow abound in both the natural environment and in engineering applications. Unfortunately, many important properties of these flows remain without a firm theoretical or experimental base. For example, considering only flows of liquid drops in a gaseous environment, items such as evaporation rates, heat and momentum transfer, collisions between drops, the effects of bulk additives, surfactants, and surface films are not well understood. Thus engineering design predictions of great economic importance can be in error. This impacts fields as diverse as combustor design, antimisting aircraft fuels, fire-fighting chemicals and their dispersal methods, smoke, other obscurants and CBW agents, and acid rain.

We have developed an experimental program to provide data and methodology for these fields. Central to this effort is the technique of levitating liquid drops with a strong (150 dB), high-frequency acoustic field, and then flowing gas past the drops. The required sound pressure levels are produced in a cylindrical resonator that is made part of a free jet wind tunnel through openings in the curved wall of the resonator. In this configuration we have performed the first experiments on evaporation of levitated drops with airspeed independent of drop size. We have successfully suspended millimeter-sized drops in airflows up to 300 cm/s.

Cloud physicists today are addressing the question of water-drop evaporation after the drop has been coated by a nonvolatile hydrocarbon film. Figure 1 shows the first experimental result on evaporation of such oil-coated drops in an airflow. There we see that evaporation is suppressed.

A second effect that has never been quantitatively measured is the "proximity effect" caused by flow perturbations expected at drop separations below 10 diameters. Figure 2 shows a photograph from the first experiment in which drop spacing and air flow are accurately controlled. With drop spacing of ~4 diameters, evaporation results for the central drop with zero, one or two neighbors show that a drop evaporates faster when it has close neighbors.

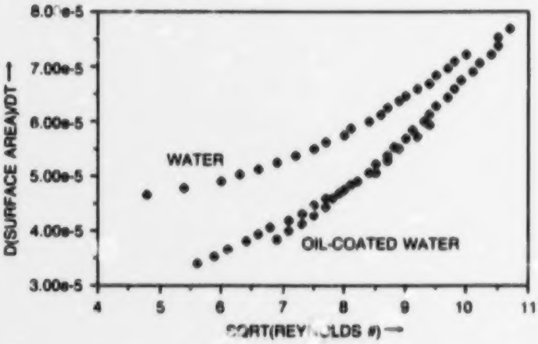

Fig. 1 – Evaporation rate of an uncoated water drop and oil-coated water drops

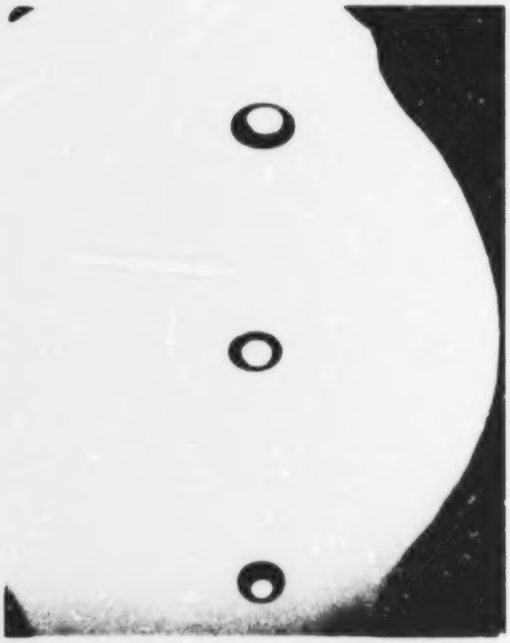

Fig. 2 – Three levitated water drops. Air speed is 135 cm/s with flow from right to left. Drop diameters are, ~1.4 mm horizontal and ~1.0 mm vertical. Measurements are performed on the central drop.

Future work using laser techniques will address questions such as drop rotation, drop temperature, and internal circulation. Laser diagnostic and imaging techniques will also be applied to the flow field around the drops to ascertain concentration profiles and stream functions.

Ultrafine Particle Optics: Ultrafine particles only a few micrometers in diameter have dimensions comparable to the wavelength of light and exhibit resonant optical behavior that is being exploited in defense-related applications.

Smokes have long been used as effective cover in warfare. Obscurants are now designed to improve behavior over a wide wavelength range (microwave to visible). Prior to this work, little experimental data were available for single particles and data from clouds were difficult to interpret because of the complexity of deconvolving the averaging effects of orientation and size and shape distributions. Consequently we have been studying the complex light-scattering profiles from single oriented particles. The charged particles are suspended in an electric quadrupole levitator that fixes their position and orientation in space. Subsequent laser illumination and angular resolution of the scattered light provide data that are compared to theory and the ultimate consequences of variation of parameters such as size, shape, and complex index of refraction.

Another important problem involves understanding the chemistry and growth of volatile aerosols. Defense-related applications include fuel chemistry, toxic aerosol cleanup, and growth of marine aerosols. Several novel particle specific photothermal spectroscopies have been developed that allow broadband infrared (IR) spectra to be obtained on single levitated droplets and subsequent chemical analysis to be deduced. A photothermal spectroscopy is one in which the effects of heating following light absorption are measured. For example, in "Photothermal Modulation of Mie Scattering," an IR source is used to heat the particle thereby inducing a size change in proportion to its absorption coefficient and the resultant change is subsequently monitored by observing variations in the scattered light. Other photothermal schemes employed are based on photophoresis and interferometric probing of the heated gas envelope surrounding the particle.

Fine particles also show interesting nonlinear optical properties. Applications include particle diagnostics, phase conjugate mirrors, bistable devices for optical memories, and space-based lasers. The spherical droplet shape provides a

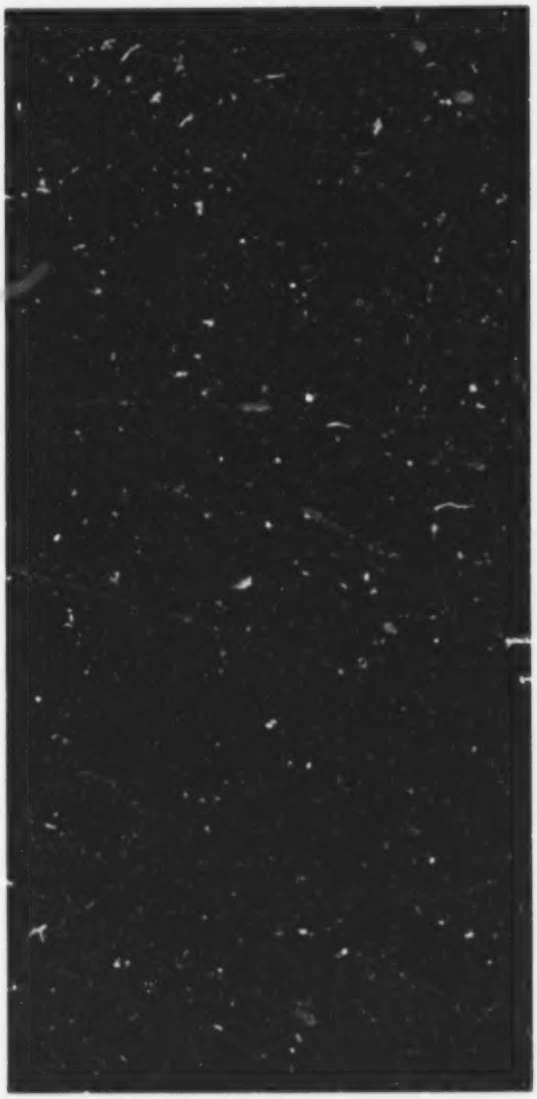

Fig. 3 – A linear stream of falling lasing droplets

BEST COPY AVAILABLE

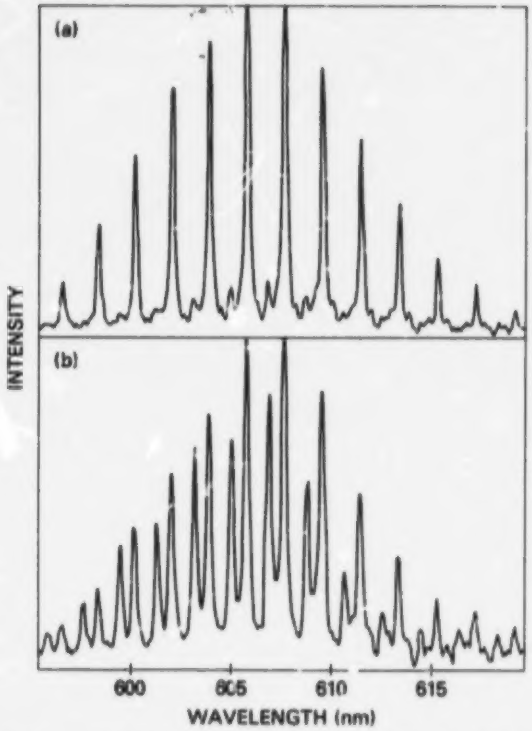

Fig. 4 – Typical spectral mode patterns from lasing droplets. In (a) the pump polarization has been adjusted to force lasing in predominantly transverse electric character. In (b) both transverse electric and transverse magnetic modes are present.

natural resonant cavity for stimulated processes (lasing, Raman processes, etc.). Figure 3 shows several lasing Rhodamine 590/water solution droplets pumped by a green laser. The falling particles are generated with a vibrating orifice (size is kept constant to 1 part in 10,000). The observed spectral output as shown in Fig. 4 remains constant for hours and may be tuned by varying the orifice frequency.

[Sponsored by ONR] ■

Photoemitter Membrane Light Modulator Device for Optical Processing

J. N. Lee and A. D. Fisher
Optical Sciences Division

Optical information processing systems can potentially exploit the inherent speed, parallel-processing, and three-dimensional interconnection capabilities of optics to offer considerable performance advantages in solving problems in signal, data, and image processing. To date, only a minimum of this potential has been realized, due in large part to the performance limitations in currently available spatial light modulator (SLM) technologies in framing speed, resolution, and sensitivity. A two-dimensional (2-D) SLM is a key component in an optical processor; it can be thought of as an optical transducer that spatially modulates the intensity, phase, or polarization of a readout laser beam in response to optical or electronic input information. Figure 5 illustrates how one might envision the functioning of an

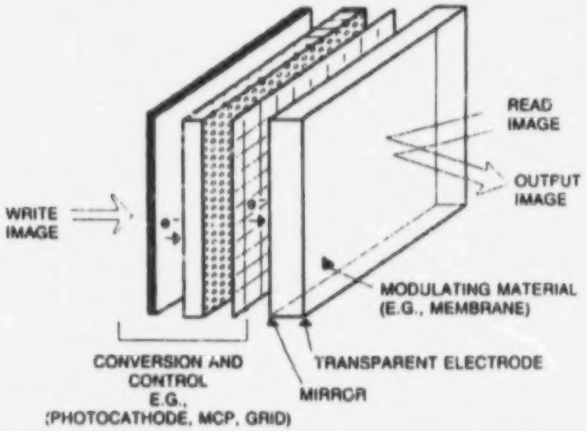
READ IMAGE
OUTPUT IMAGE
WRITE IMAGE
MODULATING MATERIAL (E.G., MEMBRANE)
TRANSPARENT ELECTRODE
MIRROR
CONVERSION AND CONTROL E.G., (PHOTOCATHODE, MCP, GRID)

Fig. 5 – General construction for an optically addressed spatial light modulator. Specifics for the PEMLM in parentheses.

BEST COPY AVAILABLE

optically addressed SLM as layers in a *sandwich* structure. Such a device allows control of one optical beam by another beam. This device can be used as an incoherent-to-coherent converter at the input stage of an optical processor or it can be used as a *reusable*, real-time replacement for photographic film (e.g., in real-time holography, Fourier-plane convolution/correlation filters, and in synthetic aperture radar), and in advanced applications such as feature extraction from images, high-resolution adaptive optics, optical matrix-algebra computing, and optical interconnects.

Device Advantages: The photoemitter membrane light modulator (PEMLM) device offers the potential of overcoming many of the previously mentioned limitations of existing SLMs (such as liquid crystal light valves). For example, most current SLM devices are limited by fundamental physics to a resolution-speed tradeoff that equates to throughputs of <100 million pixels/s. Experiments and analyses show the physics of the PEMLM should be capable of >10 billion pixels/s, with $>10\times$ advantages in both resolution and speed. In addition, the PEMLM offers quantum-noise-limited sensitivities nJ/cm^2 to pJ/cm^2, whereas most existing SLMs are more than three orders of magnitude less sensitive. Finally, the PEMLM possesses a number of desirable features for an SLM:

- information storage times of hours to days;
- either parallel or serial addressing; and
- capability to perform in real-time image-processing operations such as contrast enhancement/reversal, edge enhancement, image addition/ subtraction, and synchronous detection.

Device Description: The PEMLM, the conversion and control structure consists of a photocathode, a microchannel plate (MCP), and a grid structure (see Fig. 5). The modulating material consists of a thin deformable membrane mirror (100-nm-thick nitrocellulose coated with indium) stretched over the array of MCP pores. A transparent electrode is needed for membrane deflection and for read beam access. A 2-D write image incident on the photocathode creates an electron image that is subsequently amplified by the MCP and deposited onto the membrane array. The charges on the membrane are electrically attracted to the transparent electrode, causing the membrane to deform. A coherent readout beam reflected off the deformed membrane array is thus phase-modulated by the information encoded on the membrane array. The grid structure between the MCP and the membrane is needed for high-speed framing capability; it allows rapid removal of electrons from the membrane by controlling the energy of the incident primary electrons to induce excess secondary emission. The PEMLM concept was first described by Somers [1]; initial fabrication and imaging were demonstrated, but the devices had no framing capability, and no special processing capabilities were demonstrated.

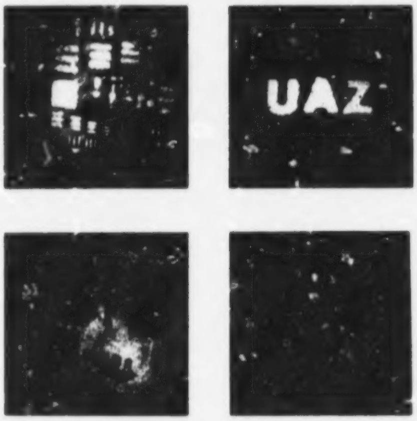

Fig. 6 – Images obtained with the PEMLM. Contrast reversal operation is shown in the lower pictures.

Experimental: Figure 6 shows the imagery obtained with the PEMLM. The actual resolution of the device is beyond that of Fig. 6. Figure 7 shows phase-contrast photomicrographs of a device with stored information. Full contrast

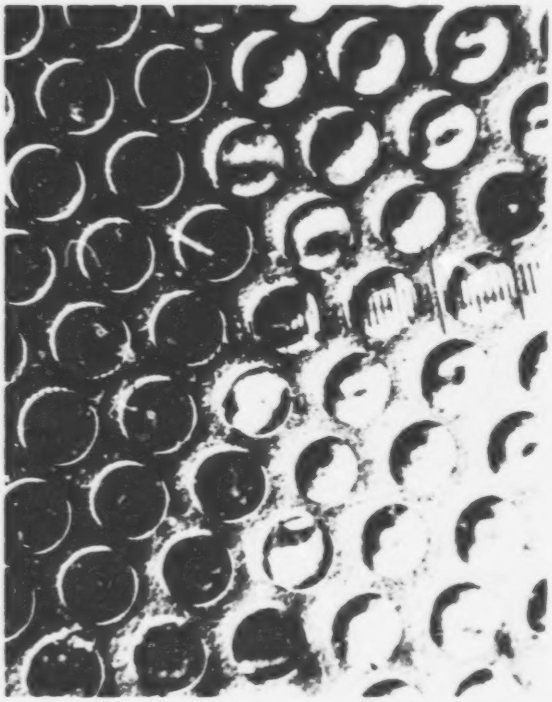

Fig. 7 – Phase–contrast microscope image of the membrane array. Note full contrast difference between some adjacent pixels due to storage of step–function image.

difference is obtainable between two neighboring pixels separated by 30 μm. Pixel separations much smaller than this distance should therefore be possible. Figure 6 also shows the contrast reversal operation by the PEMLM. Also demonstrated were thresholding, edge detection, image addition/subtraction, and synchronous detection whereby the PEMLM acts as a pixel array of lock–in detectors to detect in an image only those features oscillating at a prespecified frequency.

A grid electrode is needed for high–speed framing capability, but a screenlike grid structure is not feasible; mounting the membrane, physically supporting the screen, preventing its collapse under applied voltage, and preserving high resolution would be major challenges. A *monolithic* grid concept was conceived, whereby a metallization layer is placed between a sandwich of SiO_2 layers, all deposited directly onto the microchannel plate; voltages may then be applied to the metallization layer. Especially critical in fabricating the monolithic grid are layer thickness and avoidance of electrical shorting of the metallization to the microchannel plate while still maintaining control of electron energy. The effectiveness of this novel grid structure has been theoretically analyzed and experimentally demonstrated [2] by successful write–erase cycling of the device.

The ultimate speed of the PEMLM is determined by the mechanical response of the membrane. Membrane response is optically monitored; the observed submicrosecond response time, oscillation period, and damping are well described by the theory for drumhead resonance vibrations. The actual speed limit is probably caused by factors other than the mechanical membrane response, e.g., MCP current, photocathode efficiency.

Lifetime and aging characteristics of the membrane are deduced from the optically measured membrane resonance frequency. No observable changes in resonance frequency are observed after the first few write-erase cycles. Further, no changes in frequency are observed because of flexing of the membrane (induced with an alternating voltage) over more than a million cycles.

Plans: Experiments are under way to demonstrate the actual limits on PEMLM speed by incorporating a high-quantum-efficiency photocathode and to demonstrate several of the applications, such as rapid extraction of peaks from a 2-D data array produced by a high-speed optical processor.

[Sponsored by ONR]

References

1. L.E. Somers, "The Photoemitter Membrane Light Modulator Image Transducer," *Advances in Electronics and Electron Physics* (Academic Press, New York, 1972, Vol. 33A.

2. A.D. Fisher, L.C. Ling, J.N. Lee, and R.C. Fukuda, "Photoemitter Membrane Light Modulator," *Opt. Eng.* **25**(2), 261-268 (1986). ■

Parametric Raman Gain Suppression

J. Reintjes and M. D. Duncan
Optical Sciences Division

When a high-power laser beam propagates through a material, it can be affected by any of several nonlinear optical effects. One of these, stimulated Raman scattering, causes the power in a laser beam at one frequency to be transferred to a beam at a lower frequency. If the laser beam is powerful enough, it can create its own secondary beam (effectively a lower sideband) in the material and then transfer its power to it. This behavior can be detrimental in many applications of high-power lasers, especially those that require the power in the original beam to be transported from one place to another. Under certain circumstances, however, the lower sideband, termed the Stokes wave, can couple to an upper sideband, termed the anti-Stokes wave, with the result that the growth of both sidebands beyond a certain point is suppressed. The optical power then remains in the original beam.

A condition that is necessary for this gain suppression to take place is that the anti-Stokes wave, which is created by the interference of the laser and Stokes waves, is phase matched, that is, it stays in phase with the nonlinear polarization that is responsible for its creation. Under usual conditions, the phase-matching requirement is not met because of the dispersion in the refractive index that occurs naturally in all materials. When the waves propagate at special angles with respect to one another, however, the necessary phase matching can occur and the gain suppression takes place. In most materials the angles are of the order of several to tens of milliradians. In certain situations, for example, rotational Raman scattering in nitrogen molecules in the atmosphere, the required angles are very small and the gain for the sidebands that propagate in the forward direction can be suppressed. This can be an important consideration for the propagation of high-power laser beams in the atmosphere when stimulated Raman scattering is important, because the forward propagating sideband usually has the longest interaction length and therefore would be expected to have the largest Raman gain.

At NRL we have studied the parametric coupling between the Stokes and anti-Stokes waves that results in the suppression of Raman amplification. This work has provided the first quantitative measurements of the amount of gain suppression that can be achieved as well as the first reported observations of the suppression of the anti-Stokes growth. Figure 8 shows the experimental arrangement used to study the suppression of Raman amplification. The pump radiation for the process is obtained by frequency doubling the light from a pulsed Nd:YAG laser, operating at an infrared wavelength of 1.064 μm. The resultant radiation, which has a green wavelength of 532 nm, is divided into two parts.

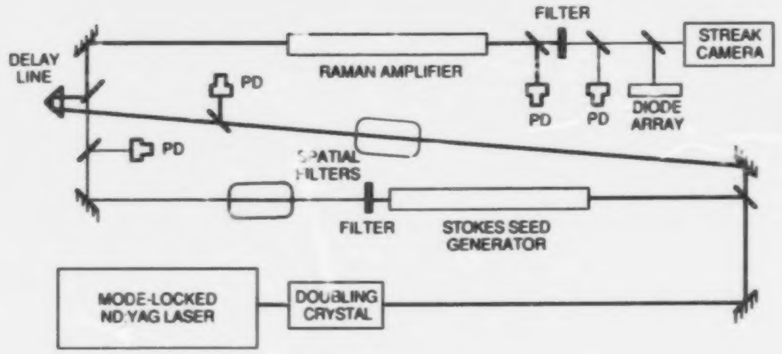

Fig. 8– The apparatus used for measuring parametric Raman gain suppression. The pump radiation for the interaction is obtained by frequency doubling infrared radiation from a Nd:YAG laser. The Raman amplification is measured by using a weak Stokes probe wave generated with part of the pump radiation.

The major amount of the pump light is used to drive the main Raman interaction, while the smaller amount is used to create a weak Raman Stokes beam to probe the main interaction.

The main Raman interaction takes place in a cell containing either hydrogen or deuterium gas at a pressure of several atmospheres. The details of the gain suppression mechanism are studied by measuring the amplification of the Stokes probe wave, as the crossing angle between the Stokes probe and the main pump beam is varied about the phase-matching direction.

If the pump radiation is strong enough, it will create the Stokes and anti-Stokes sidebands without an input Stokes probe wave. Figure 9 shows the far-field pattern of anti-Stokes radiation produced in this manner from vibrational scattering in hydrogen gas. The center spot corresponds to non-phase-matched radiation generated in the forward direction. The main part of the anti-Stokes radiation is produced near the phase-matched angle of 7.5 mrad and forms a blue ring about the original direction of the pump radiation. No anti-Stokes radiation is produced in the gain-suppressed region at the exact phase-matching angle. This causes a dark band to appear in the anti-Stokes emission ring, giving rise to the apparent double-ring structure in the figure.

Fig. 9 – Anti-Stokes radiation generated in hydrogen gas. Most of the anti-Stokes radiation is emitted near the phase-matching angle of about 7.5 mrad, forming a ring about the forward direction of the original laser. The blue color of the anti-Stokes is a result of the combination of the Raman shift in hydrogen and the green light used for the original laser. The growth of the anti-Stokes radiation at the exact phase matching angle is suppressed, producing a dark band in the center of the emission ring and giving the impression of a double ring pattern. The small blue spot in the center originates from non-phase-matched anti-Stokes radiation generated in the forward direction.

BEST COPY AVAILABLE

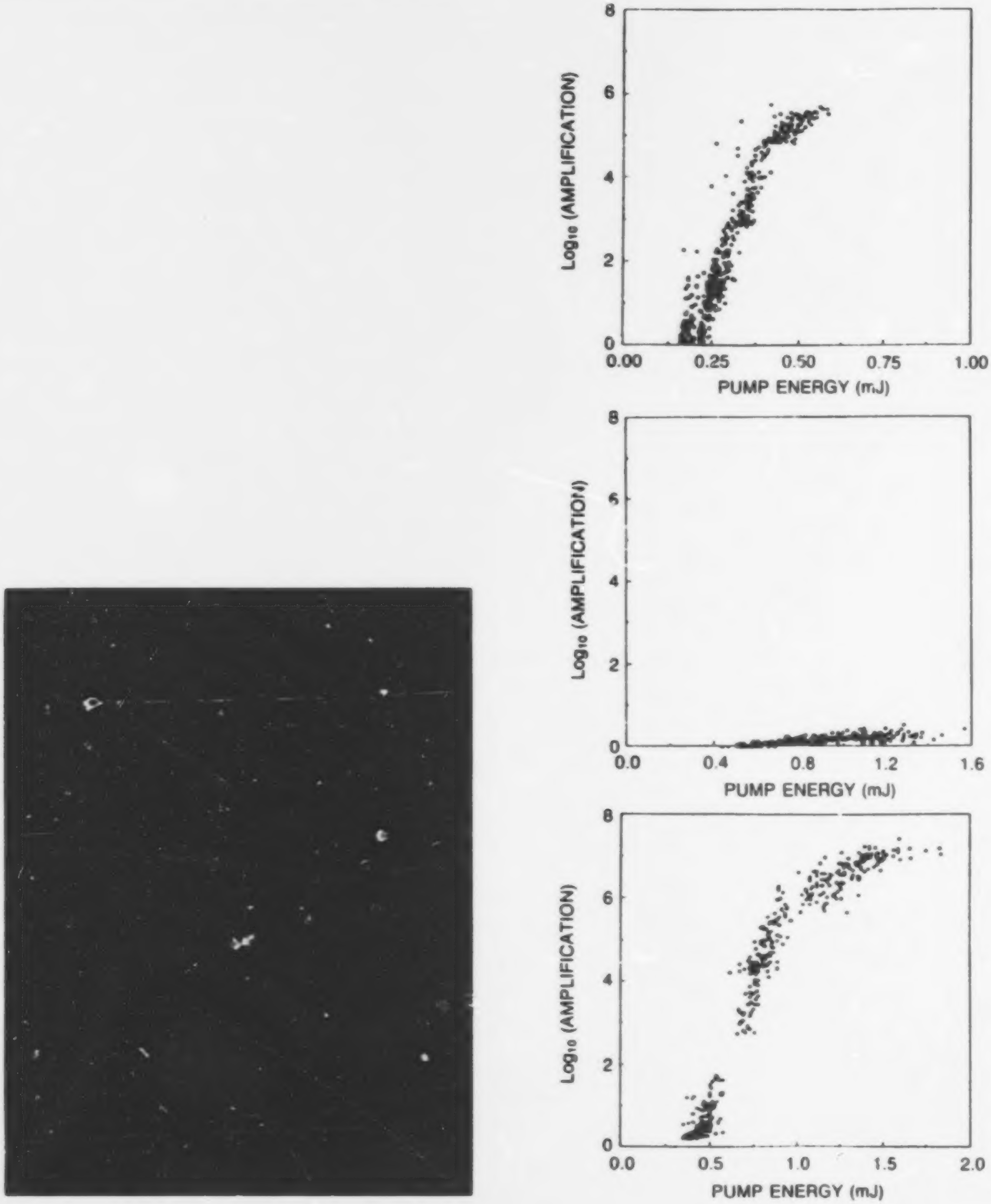

(a) (b)

Fig. 10 – (a) A typical emission pattern for Stokes amplification in deuterium gas. The process is characterized by large gain in the forward direction that falls off as the angle increases. At the phase–matching angle, there is a dark band where the Stokes gain is suppressed. The red spot in the dark band is due to the weak probe Stokes beam used to measure the amplification. (b) Measurements of Stokes amplification just inside (top), at (middle), and just outside (bottom) of the phase–matching direction. The amplification reaches as high at 10’ on either side of the phase–matching angle, but is only a factor of 2 at the phase–matching direction.

BEST COPY AVAILABLE

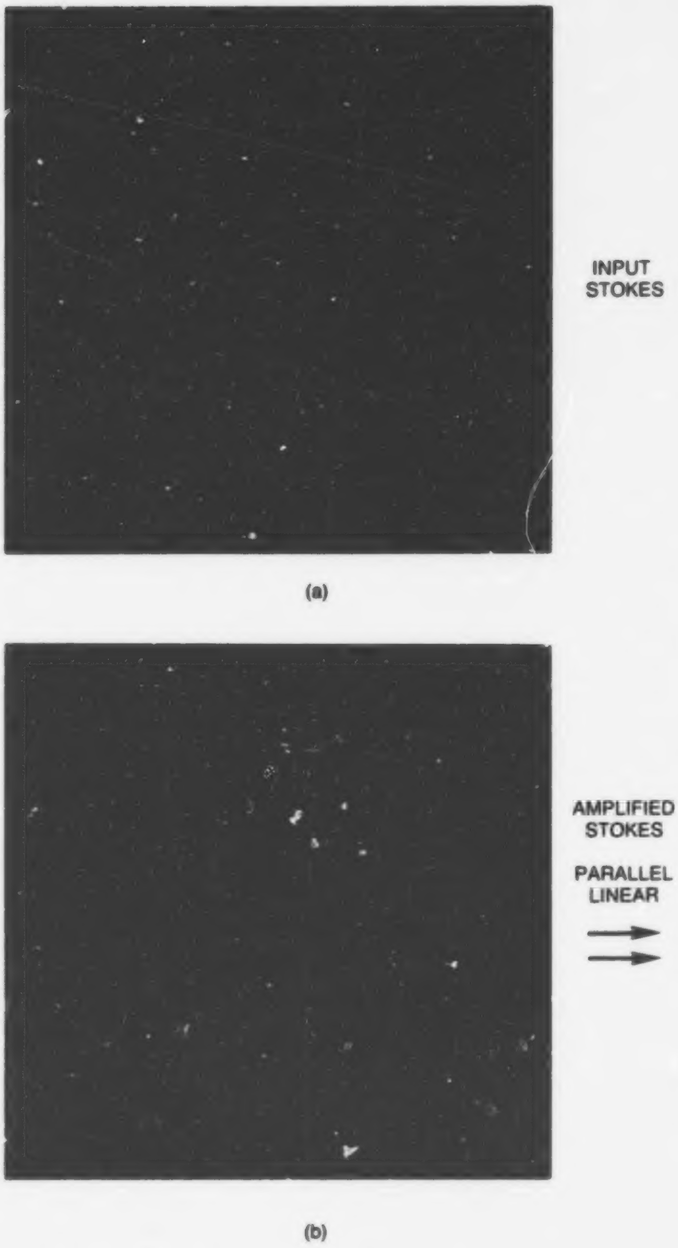

Fig. 11 — The Stokes emission for rotational Raman scattering in hydrogen. Because of the much smaller frequency shift in the rotational process (587 cm^{-1} vs 4155 cm^{-1} for the vibrational scattering), the Stokes light is green instead of red. In addition, the gain is suppressed near the forward direction, instead of at a larger angle, as shown by the low intensity of the Stokes light in the center of the pattern. This behavior can lead to an increase in the stimulated Raman threshold and a subsequent reduction in the loss of the original laser power.

Gain suppression is also evident in the Stokes emission pattern from deuterium shown in Fig. 10(a). Here the Stokes emission is emitted primarily in the forward direction but is suppressed in a ring with an angular diameter of about 7 mrad. The probe wave used to measure the amplification near the suppressed region is evident as the small bright spot in the dark band. The amount of gain suppression was determined by measuring the amplification of the Stokes probe wave near the phase-matching direction. Figure 10(b) shows these measurements for crossing angles that are smaller than, equal to, and larger than the phase-matching angle. The amplification on either

BEST COPY AVAILABLE

side of the phase-matching direction reached as high as about 10^7, while the maximum amplification observed at the phase-matching angle was of the order of 2. The amplification was thus reduced by a factor of the order of 10^7 through the gain suppression mechanism.

If the dispersion in the medium is small, the gain suppression can extend to the forward direction. Figure 11 shows an example of this behavior in which the Stokes pattern is shown for rotational scattering in hydrogen. Here the phase-matching angle is smaller because of the smaller shift associated with the rotational mode of the molecule. As a result, the gain suppression causes a reduction of the Stokes intensity in the forward direction. For the rotational scattering, the amplification was typically reduced by factors of the order of 10^3 to 10^4, and the threshold for stimulated Raman scattering was increased by a factor of the order of 3.5.

These results have contributed to our understanding of various aspects of a fundamental interaction between light and matter that is also of one of the important limitations on the transmission of high-power laser radiation through the atmosphere.

The authors appreciate the assistance of Dr. R. Mahon, of Jaycor, Inc., and Prof. L. L. Tankersley, of the U.S. Naval Academy, in carrying out the research described here.

[Sponsored by SDIO and ONR] ■

Fiber-Optic Magnetic Sensors

F. Bucholtz, A. M. Yurek, and A. Dandridge
Optical Sciences Division

The capability to measure very low-level magnetic fields ($< 10^{-5}$ G) at low frequencies (<10 Hz) is extremely important in military, medical, and commercial applications. The most sensitive magnetometers currently available employ superconducting technology where the requirement for maintenance of low temperatures can be a drawback. Fiber-optic magnetometers operate entirely at room temperature and are theoretically capable of performance levels approaching those of superconducting devices. NRL produced the first interferometric fiber-optic magnetometer in 1980 [1] and has recently demonstrated record performance for this type of device, less than 6×10^{-7} G per root Hz at 1 Hz [2]. Areas of research over the past 6 years have included materials processing and characterization, signal processing techniques, transducer engineering, and studies of noise mechanisms in laser sources, fiber interferometers, and magnetic materials.

Method: All interferometric sensors work on the basis of a phase shift induced by an external measurand, e.g., magnetic field, pressure, or temperature. Typically, the measurand produces a strain in a transducing material that, in turn, produces a strain in an optical fiber coupled to the transducer. Changing the optical path length of the fiber in this way affects the phase of light propagating through the fiber by an amount proportional to the strength of the measurand. This phase shift is measured by using all fiber-interferometric configurations that are capable of resolving 10^{-6} rad per root Hz (6×10^{-5} deg per root Hz) above 100 Hz. The corresponding resolvable length change is approximately 10^{-13} m (meters) for a system driven by a laser diode at 830-nm wavelength.

Figure 12 shows a basic fiber interferometer configured as a magnetometer. The optical source is a single-mode laser. Light in the fiber is split into two paths by a fused fiber coupler and recombined in a second coupler where interference occurs between light from the two fiber paths. This sensor uses metallic glass bonded to multiple passes of fiber to form the transducing element. Metallic glass is chosen because of its excellent magnetomechanical properties. In particular, this material exhibits extremely high magnetostriction—the change in length of a material in the presence of a magnetic field.

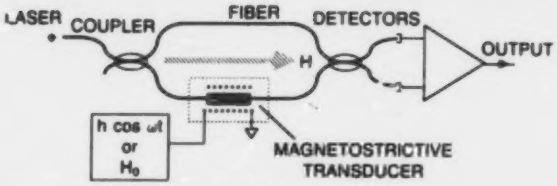

Fig. 12 - An all-fiber interferometer configured as a magnetic sensor. Strain induced by a magnetic field at the transducer is connected to a phase shift and measured at the detectors.

A crucial magnetomechanical property of metallic glass is the nonlinear relationship between strain e and magnetic field H

$$e = CH^2 \tag{1}$$

where the magnetostrictive parameter C depends on material and preparation. By applying an oscillating, or dither, magnetic field to the metallic glass, the nonlinear magnetostriction can be used advantageously to mix the dither field with static or low-frequency (<10 Hz) measurand fields. Hence, by measuring the response at the dither frequency—typically in the range 0.5 to 100 kHz—information on fields at low frequencies can be obtained. This is extremely valuable since, although a direct measurement of fields at low frequencies is possible, noise caused by thermal and mechanical sources often totally obscures the signal to be measured.

The transducing element is the most critical element of the sensor system. Figure 13 shows our most successful transducer design. It consists of a coil of fiber bonded to a cylindrical metallic glass element that has been heat treated to improve its performance. Earlier transducer designs incorporated a simple flat strip of metallic glass bonded to one or more passes of fiber.

Results: By applying a dither field at 27 kHz to the transducer shown in Fig. 13, low-frequency fields can be measured by monitoring the output with a phase-sensitive detector. Figure 14 shows the minimum detectable field that is conveniently specified by recording the low-frequency power spectrum of the detector. Three spectra are shown: dc to 100 Hz, with a calibrating signal at 10 Hz; dc to 10 Hz; and dc to 1 Hz. The noise level, specified as a field level normalized to a 1 Hz bandwidth varies in power inversely with the frequency from 20 milligamma per root Hz at 10 Hz to 200 milligamma per root Hz at 0.1 Hz. (1 milligamma $= 10^{-8}$ G.)

Current and Future Work: Current efforts are aimed at increasing the sensitivity of the transducers and understanding the noise mechanisms in all parts of the system. In addition, the present performance levels are sufficient to

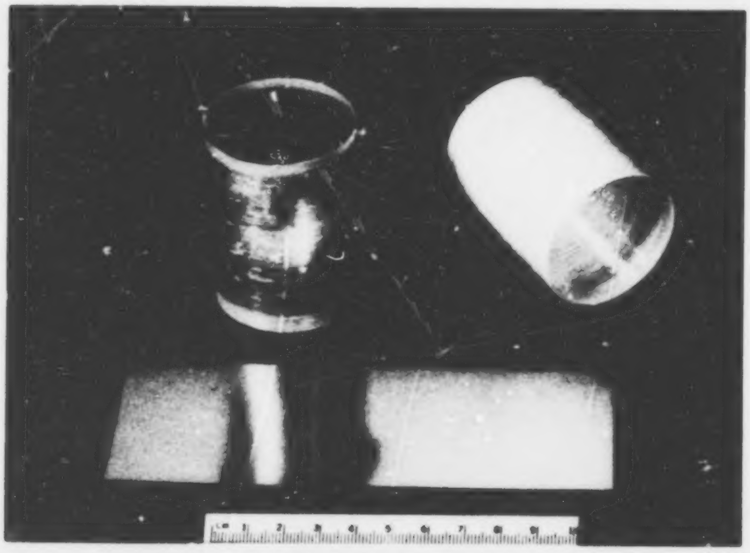

Fig. 13 - Magnetostrictive transducing element consisting of an optical fiber coil and metallic glass cylinder

BEST COPY AVAILABLE

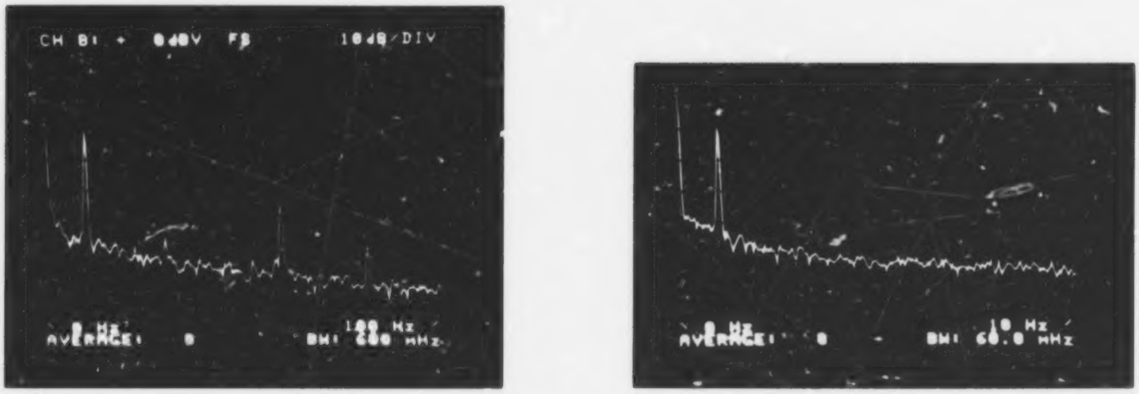

10 Hz

20 mγ/√Hz

1 Hz

60 mγ/√Hz

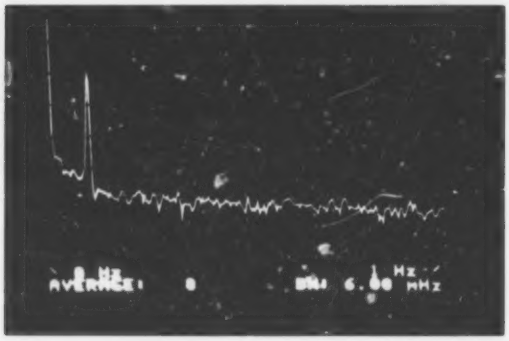

0.1 Hz

200 mγ/√Hz

Fig. 14 — Demonstrated noise levels (a) dc to 100 Hz with a 0 Hz calibration signal (b) dc to 10 Hz, and (c) dc to 1 Hz; noise levels given in milligamma per root Hz. 1 milligamma = 10^{-8} G = 10^{-12} T = 10^{-12} V · s/m^2.

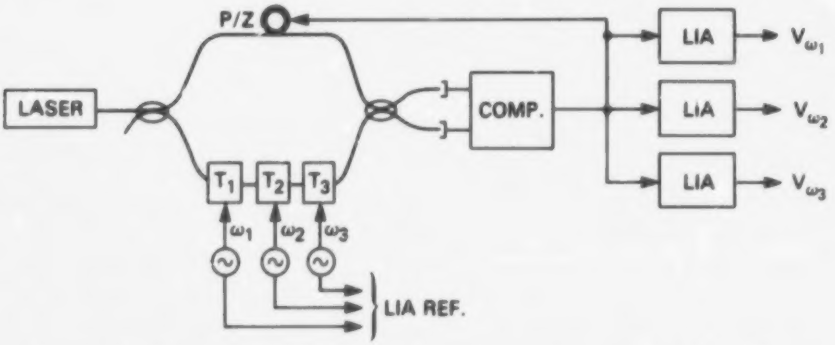
P/Z
LASER
COMP.
LIA
LIA
LIA
V_{ω_1}
V_{ω_2}
V_{ω_3}
T_1
T_2
T_3
ω_1
ω_2
ω_3
LIA REF.

Fig. 15 - A multiple-sensor configuration employing three orthogonal magnetic transducers (T_1, T_2, T_3) dithered at frequencies (ω_1, ω_2, ω_3) on a single interferometer driven by a single laser source.

BEST COPY AVAILABLE

warrant application in a host of areas. One such application requires sensing of magnetic fields along three orthogonal axes. Once again, the nonlinear magnetostriction of the metallic glass can be exploited by dithering each of three transducing elements at a different frequency, as shown in Fig. 15. A parallel array of phase-sensitive detectors is used to demultiplex the output. The entire multisensor configuration, which is easily expandable, uses a single interferometer driven by a single laser source.

[Sponsored by ONT and ONR]

References

1. A. Dandridge, A.B. Tveten, G.H. Sigel, Jr., E.G. West, and T.G. Giallorenzi, *Electron. Lett.* **16**, 408 (1980).
2. F. Bucholtz, A.M. Yurek, K.P. Koo, and A. Dandridge, *OFC/100C '87 Technical Digest* **T414** (1987). ■

Development of Infrared Focal Plane Arrays for Advanced Navy Sensors

M. R. Kruer, D. A. Scribner, and C. J. Gridley
Optical Sciences Division

The detector technology in present-generation Navy infrared (IR) sensors is analogous to electronic systems that existed before the invention of the integrated circuit. Current IR detection systems consist of either a single detector or a linear array of semiconductor detectors in a low-temperature cryogenic assembly. These detectors convert the incident IR radiation to an electronic charge that is then conducted to a matching array of preamplifiers. Each detector/preamplifier pair is connected by a wire that must pass through the wall of the cryogenic dewar. Another set of wires then transmits the signal from each preamplifier to a signal processor that performs a variety of electronic functions to provide signals either for a visual display or for automatic data processing and system control.

For many tactical applications, however there is a need for increased resolution and sensitivity. This requires detector arrays containing from several hundred detectors for smart ordnance to tens of thousands of detectors for imaging missile seekers and for search sets having time delay and integration. For space applications, both scientific and strategic, even larger numbers of detectors are desirable. The detectors' requirements for such systems can be met only by an improved approach that is capable of multiplexing all the detector signals on the focal plane.

Focal Plane Array Concept: The objective of focal plane array (FPA) technology is to satisfy the requirement for much larger detector arrays by using the integrated circuit approach. The goal of this approach is to perform all necessary functions, prior to signal processing, on the focal plane. The signals from all detectors can then be read out to the signal processor by as little as one wire per chip having thousands of detectors. The FPA technologies include both hybrid and monolithic arrays (charge-coupled devices, charge-injection devices, and charge-imaging matrices).

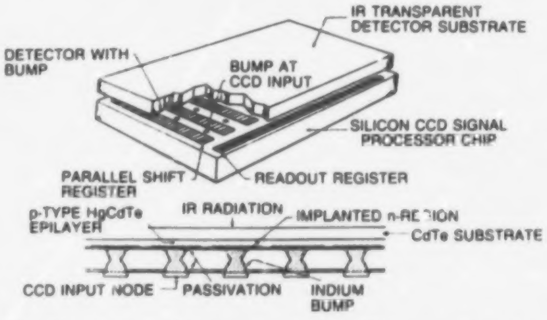

Fig. 16 – A second-generation hybrid FPA consisting of a two-dimensional array of HgCdTe photodiodes that is connected with indium bumps to a two-dimensional signal multiplexer fabricated in silicon

Figure 16 shows a specific approach to FPA technology. This hybrid approach consists of a two-dimensional array of mercury cadmium telluride (HgCdTe) photovoltaic detectors coupled with indium bumps directly to an array of silicon charge transfer devices. The IR radiation incident on a detector is converted to an electrical charge that is immediately transferred into the silicon device directly beneath. The charge is integrated in a storage array fabricated adjacent to the parallel shift register. A series of electrical pulses applied to this shift register transfers each charge packet in series to the readout register. Another set of pulses applied to the readout register transfers this charge from one row of the array to the preamplifier. These steps are repeated until all rows of the shift register have been read to the signal processor, providing one frame of the IR scene.

FPA Development Problems: The demonstration of adequate FPA performance is often hampered by several technical problems. Specific problems that are encountered by all FPA approaches include, among others, saturation, nonuniformity, charge transfer efficiency, noise, and crosstalk.

Saturation: Sensitivity is increased by collecting all available photons, but saturation becomes a problem in FPAs because charge is integrated and stored on the focal plane in an area that is often less than one square mile. The problem is minimized by instituting some form of gain control or subframe addition. Gain control requires that extra circuitry be added to dump the dc contribution from the ambient optical background, further complicating the microelectronics. Subframe addition is achieved by reading out the FPA several times faster than the desired frame rate and summing the signals off the focal plane.

Nonuniformity: The response of individual detectors in the array can differ because of nonuniformities in the semiconductor, the photolithographically defined device areas, and/or the device processing.

Charge transfer efficiency, noise, and crosstalk: Charge transfer efficiency describes the overall efficiency of the FPA's readout mechanism to transfer signal carriers generated in the detector off the focal plane. Reducing device noise to the level where it is less than the noise caused by the random generation of photons by the scene is difficult because of the high-density packing of the individual circuits in the multiplexer. Often the signal being read out from one detector is picked up (crosstalk) by a nearby circuit in a poorly designed FPA.

FPA Evaluation: The electrical and optical performance of developmental IR FPAs must be monitored to assess the state of development of the technology and to provide guidance to further development. The evaluations of diverse types of FPA technologies require extensive equipment to provide clocking, video signal processing, high-speed/high-resolution (> 12 bits) digitization, and reduction of large volumes of digital video data. Although conventional optical sources are needed for calibration, more sophisticated optical probes such as modulated lasers are needed for measurements of lag, saturation, and temporal response variances.

Examples of measurements pioneered at NRL include lag, ramped operation of linear charge-injection devices (CIDs) for high-flux operation, characterization of failure in thermally cycled hybrid arrays, laser overload, calibration techniques for performance efficiency, and measurements of array temporal and spatial noise to determine their effects on sensor signal-processing algorithms for target detection. The current-voltage curves shown in Fig. 17 illustrate the degradation measured in a hybridized HgCdTe photovoltaic array following thermal cycling of the device. The figure illustrates that some pixels indicated by triangles degraded from failure of the indium bump contact and the subsequent appearance of a large impedance in series with the detector. Other pixels indicated by crosses lose sensitivity as the result of excessive leakage currents.

Lag affects the response of a detector to changing flux levels. An ideal detector irradiated by a pulse of light should yield an electrical signal at the first read sequence following illumination and then yield zero signal for subsequent readings. However an InSb CID exhibits lag and yields an

BEST COPY AVAILABLE

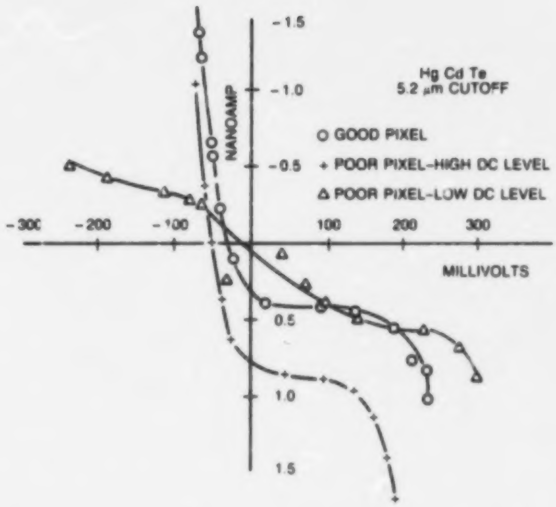

Fig. 17 – Current-voltage curves of selected pixels of a hybrid HgCdTe FPA exhibiting characteristics of a good pixel, a pixel degraded by a high impedance in series with the detector, and a pixel degraded by excessive leakage current

electrical signal for several readings following termination of a light pulse. Figure 18 shows the response of an InSb CID exhibiting lag. If the same detector is operated with more favorable operating voltages, the electrical amplitude rises and falls more quickly.

FPA Status: Midwave (3 to 5 μm) FPAs having InSb, silicon Schottky, extrinsic silicon, or midwave HgCdTe detectors are much more mature compared to longwave HgCdTe detectors. These detectors in the form of linear FPAs or staring arrays of moderate size (128 × 128) are considered sufficiently mature for producibility demonstrations. These arrays have sufficient numbers of detectors and performance to be considered for advanced sensor systems. Longwave HgCdTe FPAs are limited to a cutoff wavelength of about 11 μm because of material limitations associated with purity, carrier lifetime, and surface passivation.

[Sponsored by ONT] ■

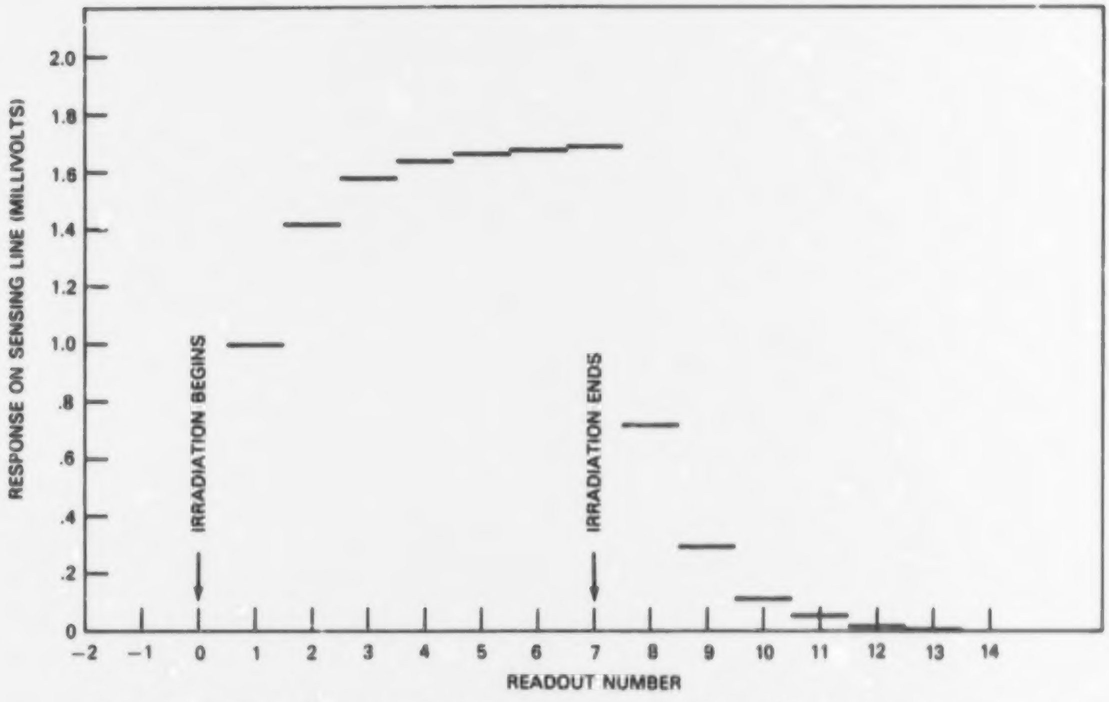

Fig. 18 – Response of an detector of an InSb linear CID to pulsed radiation lasting seven integration periods showing the effect of lag on signal amplitude during and following the irradiation. Measurements were performed with a reference bias of –7 V, an internal injection voltage of 1.2 V, and ambient optical background.

Numerical modeling is used in all areas of fundamental and applied research. The range of computer facilities encompasses the Cray X/MP and the desktop personal computers available to all professionals, as well as a variety of intermediate devices for special purposes. The Cray is used by every NRL research division. The Laboratory for Computational Physics and Fluid Dynamics develops and applies advanced numerical simulation techniques not only to Navy problems, but to other programs of national interest; research centers on the field of fluid dynamics.

110
101
10
100
100
010

NUMERICAL SIMULATION

171 **Renormalized Inverse-Scattering Theory for Dielectric Profiles**
Arthur K. Jordan and Harold D. Ladouceur

173 **Direct Numerical Simulation of Turbulent Channel Flow**
Robert A. Handler and Richard I. Leighton

175 **Synthetic Line-of-Sight Simulations**
William M. Morris

177 **Vortex Motions in Stratified Wakes**
Yee T. Fung and Simon W. Cheng

179 **Analytic Representations of Viscoelastic Moduli**
Anthony J. Rudgers

Renormalized Inverse-Scattering Theory for Dielectric Profiles

A. K. Jordan
Space Science Division

H. D. Ladouceur
Chemistry Division

The fabrication of materials that are composed of different dielectrics has opened up new applications for electromagnetics and optics. Many applications require materials that are designed to have specified reflectances to incident radiation. Two examples are low-reflectance coatings for lenses and high-reflectance mirrors for astronomy. In the past, layers of constant refractive index have been applied to obtain high or low reflectances. This method produced unwanted reflections at the interfaces and had narrow-band reflectances. The availability of broadband sources and detectors for electromagnetic radiation and the need for broadband information channels stimulated the effort to formulate more accurate design methods for broadband reflectors and coatings.

It is possible to produce materials whose refractive indexes vary continuously as a function of depth—these are the "dielectric profiles." This means that the reflectances of the dielectrics at different electromagnetic wavelengths will be different. By accurately choosing the gradients of refractive index, the reflectances can be made to vary in a prescribed manner over a broad band of wavelengths.

General mathematical and computational methods were used to design dielectric profiles with specified reflection properties instead of starting with a known dielectric profile—these methods are known as "inverse-scattering theories." In the past, several inverse-scattering theories have been developed, but they have generally been characterized as being abstract, exact mathematical theories that are difficult to apply or specialize, approximate theories that can only be applied to limited cases. We have developed an accurate design method by starting with an exact inverse theory and solving it by successive approximations, i.e., by perturbation methods [1,2]. There will be terms in the perturbation series that will diverge. The series can be effectively summed by the method of "renormalization," which enforces energy conservation for the electromagnetic field in the dielectric so that the divergent terms are eliminated.

Previous approximate theories have relied on the assumptions of weak-scattering approximations (smoothly varying profiles with small reflectances) or short-wavelength approximations (high-frequency or physical optics). The renormalized theory begins with the weak-scattering approximation as a zero-order solution to the exact theory. We found that continuing the analysis to the second order provided more accurate designs that have larger useful bandwidths than designs obtained by using the weak-scattering approximation.

To test the inverse theory, we ran computer experiments that used one program to generate complex reflectance data from a variety of different profiles. These reflectance data are solutions to the "direct-scattering" problem. A separate program applied the inverse method to these data to reconstruct the profile. When the correlation between the reconstructed profile and the "true" profile was close to one, we had a successful reconstruction.

If the profile has steep gradients and sharp corners, then the weak-scattering theories cannot yield an accurate reconstruction. The renormalized theory successfully reconstructs these discontinuities since it uses high-frequency reflectance data to reconstruct the profile in the neighborhood of the discontinuity and low-frequency data to reconstruct the profile in the interior of the dielectric region.

Figure 1 illustrates this inverse-scattering theory. The reflection data shown were generated by solving the direct scattering problem for the

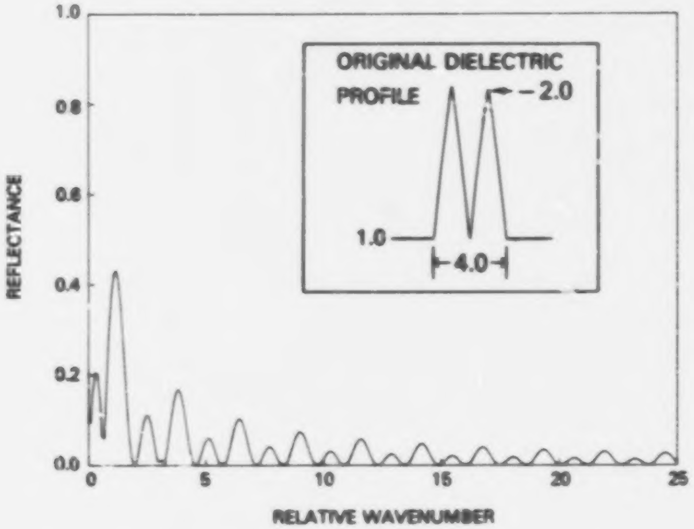

Fig. 1 – Simulated reflection data for electromagnetic wave scattering from the double triangular dielectric profile shown in the insert

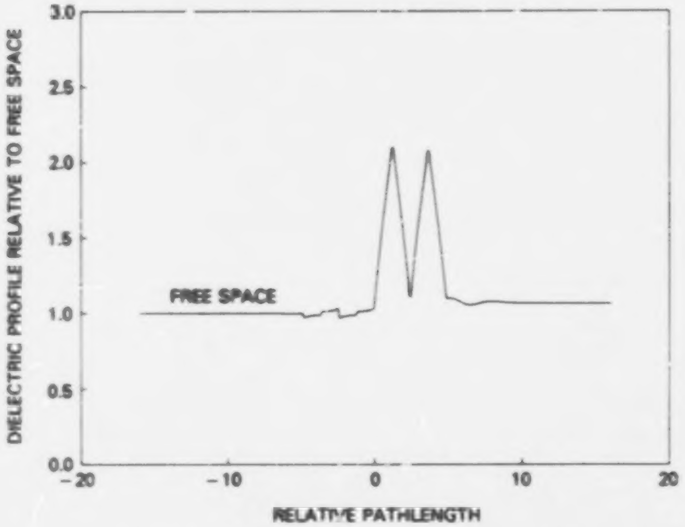

Fig. 2 – Dielectric profile reconstructed from the reflection data of Fig. 1 shown as a function of electromagnetic pathlength

dielectric profile in the inset. The inversion method was applied to these data. Phase information (not shown) as well as the amplitude information of Fig. 1 was used. This profile exhibits several characteristics that cannot be accurately treated by previous theories. There are several discontinuities as well as smooth regions, the profile is multivalued (there are peaks and a valley), the reflection data can be very strong as well as very weak, and the data extend over a large bandwidth (on this scale the weak-scattering approximation is valid only for $0 < k < 0.6$).

Figure 2 shows the reconstructed dielectric profile; the profile was calculated as a function of the electromagnetic pathlength—roughly the geometric distance scaled by the wavelength in the dielectric. This inverse theory can also rescale the pathlength back to the geometric distance so that the width, the height, and the shape of the profile will be accurately reconstructed. Since the transformation to geometric space reconstructed the original profile shown in the inset of Fig. 1, with an error less than 5.0%, it is not repeated here.

[Sponsored by ONR]

References

1. A.K. Jordan and H. Douglas Ladouceur, "Renormalization of an Inverse Scattering Theory for Inhomogeneous Dielectrics," *J. Opt. Am.* **A2**, 1916–1921 (1985).
2. H.D. Ladouceur and A.K. Jordan, "Renormalization Techniques for Inverse Scattering," *SPIE Proc.*, **558**, 47–52 (1985).

■

Direct Numerical Simulation of Turbulent Channel Flow

R. A. Handler and R. I. Leighton
Laboratory for Computational Physics and Fluid Dynamics

Turbulent flows are among the most complex of all flows found in nature. An adequate understanding of these flows is essential to the development of technologies of interest to the Navy. For example, an understanding of turbulence-induced wall pressure forces may lead to the eventual control of flow noise, radiated sound, and unwanted structural vibrations. One approach that may lead to a deeper understanding of turbulence is to simulate these flows from the governing equations of fluid dynamics. The results of such simulations provide very detailed information that can be studied in depth in much the same manner as one would study experimental results. This is the approach that has been taken at NRL.

Computational Requirements for Turbulence Calculations: In undertaking these calculations, several problems must be considered by the computational fluid dynamicist. The first problem stems from the observation that turbulence in nature is composed of structures having a size range covering many orders of magnitude. When we observe the turbulent convection of air in a heated room, for example, we find that the largest flow structures are about the size of the room and the smallest may be only a few millimeters. Any direct calculation of turbulence must therefore contain sufficient degrees of freedom to represent the largest flow structures simultaneously with the smallest. This is of critical importance since most of the energy is contained in the large-scale structures and is dissipated at the smallest scales. In addition, the governing equations indicate that vortex stretching, which accounts for the production of turbulence, is solely a three-dimensional phenomenon. Scaling arguments based on these requirements suggest that we need R^3 words of computer memory to accurately represent such a flow, where R is the Reynolds number (ratio of inertial to viscous forces). For a typical flow, R (as defined here) can range from 100 to 1000, so that even a low Reynolds number simulation requires 10^6 words of memory. If we include the requirement of high computational speed, we conclude that today's supercomputers are capable of simulating only low Reynolds number turbulent flows.

Computational Methods: The details of the computational methods are described in Ref. 1. Briefly, the velocity is represented by a Fourier series in both the flow and cross-stream directions. Chebyshev polynomials are used in the direction normal to the wall. The incompressible form of the governing equations of fluid dynamics is then solved by standard time-splitting methods in which the computation of the nonlinear terms is separated from the calculation of the effects of pressure and viscous forces.

Computational Parameters and Results: In the most recent calculation performed at NRL, turbulent flow was computed in a channel whose dimensions in the streamwise, spanwise, and wall

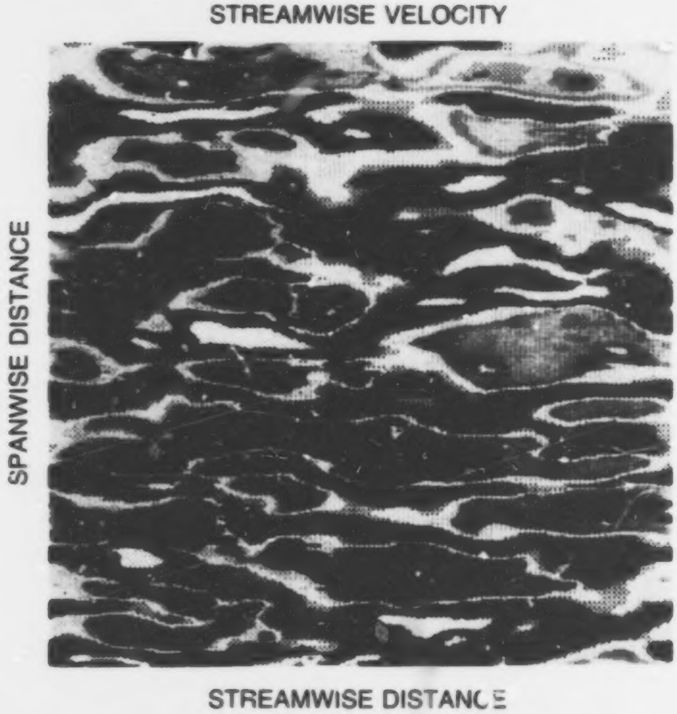

Fig. 3 – Enhanced color plot of the streamwise velocity in a turbulent channel flow. The data are taken on a plane 0.142 half widths from the wall of the channel, and the flow is from left to right. The axes are scaled in units of the channel half-width.

normal directions were, respectively, 5, 5, and 2 in units of the channel halfwidth *h*. The velocity and pressure were computed at 532,480 grid points. The flow was driven to a statistically steady state by imposing a constant driving force in the flow direction. The Reynolds number of the flow based on the average velocity and *h* was about 3350.

We have plotted in Fig. 3 the streamwise velocity field at one instant in time on a horizontal plane a distance 0.142 half widths from the wall of the channel. The colors range from purple (fast-moving fluid) to white (slow fluid). Highly elongated regions of slow and fast fluid are clearly evident in the figure. This elongated structure is typical of so-called "streaky" structures found in experiments. This streaky structure has been identified in the last 10 to 15 years with a well-organized or coherent flow structure composed of elongated vortices whose axes are aligned in the flow direction. Such plots of the raw velocity data are, however, not easily interpreted.

One can obtain a clearer representation of the coherent events in the flow by using a technique called *conditional sampling*. In this method the flow field is sampled only when certain predetermined criteria are met. These samples of the flow are then added together to form an ensemble. Figure 4 presents the flow patterns that were obtained by using three methods—negative slope VITA (variable interval time averaging) detection, second quadrant Reynolds stress detection, and positive slope VITA detection. These methods are described in Ref. 2. Each plot represents a horizontal view of the velocity field in which the spatial coordinate is measured in units of the viscous length l^* where l^* is a length based on the viscosity of the fluid and the shear stress at the wall of the channel. These figures portray different

BEST COPY AVAILABLE

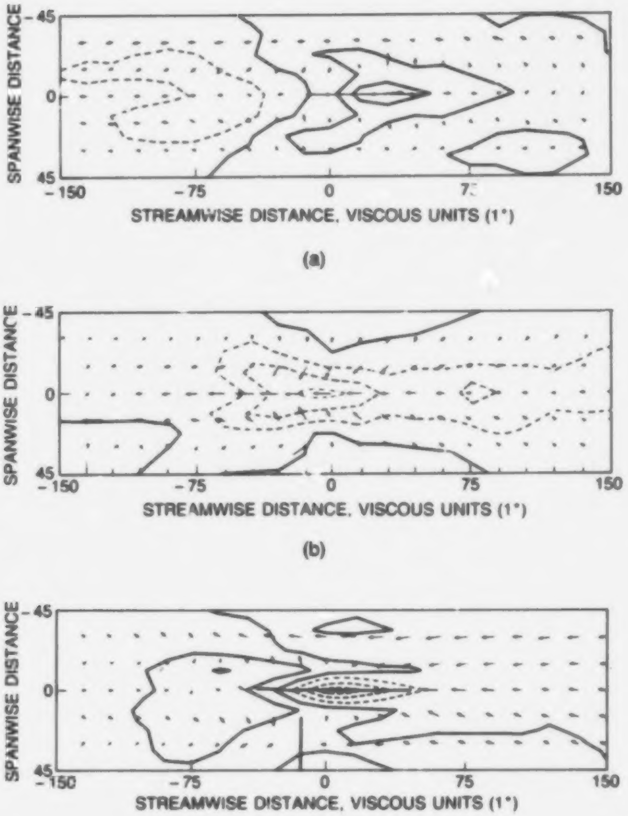

(a)

(b)

(c)

Fig. 4 – Velocity and wall-pressure field during a coherent event. Results from three methods are shown.

aspects of a cycle of events termed the burst–sweep cycle in which low momentum fluid is ejected from the wall in a "burst" followed by an impinging jet of high-momentum fluid. Note also that in regions where fluid has been ejected, the pressure at the wall is strongly negative, and in regions where fluid is impinging on the wall, it is positive.

Future work in analyzing the data generated from these computations may lead to a better understanding of shear flow turbulence and an understanding of the relationship between coherent turbulent processes and the pressure field.

[Sponsored by ONR]

References

1. S.A. Orszag and L.C. Kells, "Transition to Turbulence in Plane Poiseuille and Plane Couette Flow," *J. Fluid Mech.* 96, 159–205 (1980).
2. R.I. Leighton, "Investigation of Burst Structures in a Turbulent Channel Flow Simulation Using Conditional Sampling Techniques," Ph.D. Thesis, University of Michigan, 1986. ■

Synthetic Line-of-Sight Simulations

W. M. Morris
Tactical Electronic Warfare Division

The Central Target Simulator (CTS) facility in the Tactical Electronic Warfare Division was developed to evaluate electronic warfare (EW) systems and techniques for countering radar-guided missile threats to the Navy. Missile attacks on Navy ships and aircraft are simulated in the CTS facility by simulating the electromagnetic environment the missile would experience in a real-world tactical engagement. The simulation is provided by an 8 to 18 GHz radio frequency environment simulator (RFES), a three-axis flight motion simulator (TAFS), and a digital computer system. The simulations provide the U.S. Navy and allied fleets with detailed information concerning countermeasures effects against known or projected threats. The unique value of the information provided is a result of the test article missile hardware interacting with the aircraft and ships' onboard and/or offboard EW assets. While at-sea testing is very important, it is performed under difficult conditions and only for a limited number of cases. In the laboratory, the number of test variants of interest grows exponentially with the number of scenarios considered. In the laboratory, simulated engagements are modeled and controlled by use of the facility's digital computers. For scenario flexibility, true and synthetic line-of-sight (SLOS) simulation methods are used to model the inertial and rotational frames of reference of the engagement. Both schemes have been incorporated into the CTS facility with each designed to maximize simulation capability.

Line-of-Sight Methods: The true line-of-sight method simulates the relative geometry of a missile and its intended targets in inertial coordinates. The angular motion provided by the TAFS is the true angular motion of the missile with respect to inertial space. The apparent position of the target, as seen by the missile, is affected by target features, relative geometry, and environment. The RFES accommodates the apparent target motion by transmitting simulated radar reflections from a large spherical antenna array. These antennas are distributed at fixed locations within a 20° elevation by 30° azimuth field of view. For the true line-of-sight method, the RFES simulates only the targets' apparent motion effects.

The SLOS method simulates apparent motion effects by using the TAFS and allows a tactical engagement to be simulated by using a single element from the RFES antenna array. All simulated geometry for SLOS must be the same as for true line-of-sight. This is accomplished by allowing the angular orientation of simulated north, east, and down coordinates with respect to CTS facility coordinates to change with time. If the missile seeker could not perceive its own rotation rate, then its simulated illusion of reality would be unspoiled. However, some seekers do measure line-of-sight rates. Thus the TAFS, RFES, and missile seeker all require compensating terms during SLOS simulation.

SLOS Implementation: The SLOS method is controlled by the rotational transformation from fixed coordinates to CTS-facility coordinates. Fixed coordinates do not rotate with respect to inertial space and may coincide with north, east, and down coordinates. CTS-facility coordinates are used to describe the orientation of TAFS gimbals and RFES antenna positions in the facility. The direction of the target and electronic countermeasures return to the missile defines which two components of the SLOS rotation rate are required to stabilize the antenna position in the facility. The third component is calculated to stabilize roll. Each coordinate rotation is represented by a quaternion that is factored into tilt and roll components. The coordinate rotation for each component is calculated from a single complex variable.

Missile-body angular rates and positions are required for TAFS control. When these are transformed to facility coordinates the TAFS angular rates must be reduced by the SLOS rotation rates. While the target and electronic countermeasures return are stabilized to radiate from a single RFES antenna, the reflections from nearby ships and decoys are simulated on the full array. Since the RFES is controlled with the speed of electronic devices, the ships' and decoys' apparent dynamics may be controlled by updating their positions in CTS-facility coordinates.

During simulation design, the missile test article is examined and its functions are partitioned into TAFS mounted hardware, stationary hardware, and computer models. Missile-seeker SLOS compensation must be performed if gyroscopes are included in the TAFS-mounted hardware. The SLOS rotation rates may be injected into the TAFS-mounted seeker hardware or the computer model. A shaping filter for each seeker type may be required to force the seeker output signal to be the same for both true and SLOS simulation methods. Some scenarios may be run by using either true or SLOS simulation methods. SLOS is judged to be valid when repeated simulations of both methods produce functionally identical results for the scenarios of interest.

Conclusions: The CTS facility is designed with sufficient simulation flexibility to permit its adaptation to a variety of missile electronic warfare engagement situations. Each new entry in the CTS missile-model library is a candidate for SLOS simulation. The advantages of the SLOS method, which include the flexibility of more targets and a larger field of view, make the more difficult implementation worth the extra effort required.

[Sponsored by ONT] ■

Vortex Motions in Stratified Wakes

Y. T. Fung
Laboratory for Computational Physics and Fluid Dynamics

S.W. Chang
Space Science Division

When an axisymmetric body is towed through a stably stratified fluid, i.e., a fluid heavier at the bottom and lighter on top, vortices are first shed without any preference in direction. The region immediately behind the towed body is in a turbulent state. This state of turbulence is eventually inhibited by the density stratification in the gravitational direction. The flow tends to meander horizontally and gradually rolls up into horizontal "pancake" vortices. The resultant pattern formed in the late wake, even though inherently three-dimensional, is confined within a relatively thin horizontal layer. The visualized pattern is often reminiscent of the two-dimensional Kármán vortex street if observed from the gravitational direction [1]. Such vortex patterns do not exist if the fluid in which the axisymmetric body is towed through is homogeneous.

We have developed a three-dimensional, time-dependent computer code [2] to simulate those internal vortex patterns and the corresponding free-surface signature generated by the motion of the vortices.

Physical Model: The flow is assumed to be incompressible and hydrostatic, i.e., the buoyancy effect dominates the vertical motion of the flow. It is bounded by a free surface on top and a rigid bottom that lies in the x-y plane of an x, y, z Cartesian coordinate system. The density of the fluid is originally stratified in the gravitational direction along the z axis.

A rectangular, staggered grid system is chosen with the towing direction of the sphere along the positive x-direction. To carry out the simulation of flow patterns within a limited computational domain, the grid spacings in both the upstream and downstream regions can be stretched to allow us to observe the slowly evolving vortex patterns at a region of interest while keeping the sphere moving downstream.

Mode Splitting: A central-difference technique is used to solve the Navier-Stoke equations, the continuity equation, and the incompressible condition. The hydrostatic assumption allows us to integrate the equation of vertical motion directly. The presence of the free surface, however, introduces a phase velocity that moves a lot faster than the towing velocity. To efficiently handle these two different velocities, a split-explicit method is used to separately integrate the two corresponding sets of equations in time. A

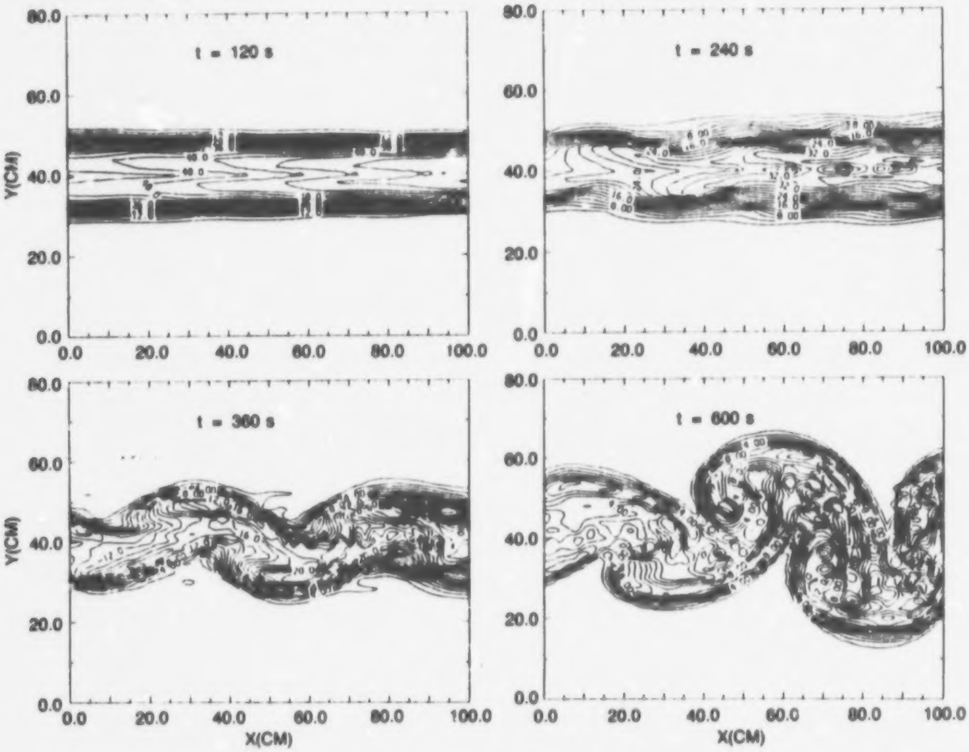

Fig. 5 – Horizontal flow patterns revealed by tracer

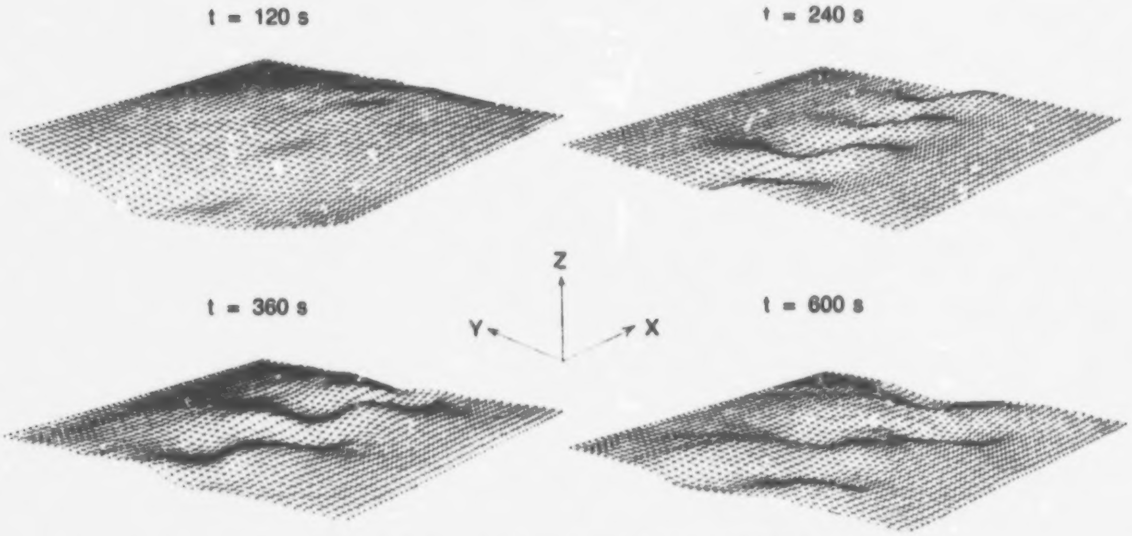
t = 120 s
t = 240 s
t = 360 s
t = 600 s
Z
Y
X

Fig. 6 – Surface signatures (magnified 1.5 × 10^3 times)

BEST COPY AVAILABLE

much smaller time step is applied to the equations corresponding to the fast-moving velocity to avoid numerical instability. This method enables us to economically observe the time history of the slowly evolving vortex patterns while including the free surface effect.

Numerical Results: The illustrations presented here were extracted from the results generated by a 125 × 41 × 15 grid with the horizontal grid sizes equal to 2 cm. At $t = 0$, we started towing the sphere in the middle layer of the fluid. The tracer contours in Fig.5 demonstrate the evolution of the vortex pattern in the middle layer at $t = 120, 240, 360$, and 600 s. After being released from the sphere, the tracer spread, meandered, and slowly rolled into organized patterns. Figure 6 shows the corresponding surface signatures. At $t =$ 120 s, the surface signature was only caused by the early turbulent wake caused by the passage of the sphere. There is no indication that organized structures exist within the flow field at this time as also demonstrated in the tracer contour in Fig. 5. The vortex pattern, however, evolved with time and eventually appeared as peaks and troughs in the surface signatures. A trough represents a pressure drop owing to the rotation of an organized structure within the flow field.

[Sponsored by ONR]

References

1. H.P. Pao and T.W. Kao, "Vortex Structure in the Wake of a Sphere," *Phys. Fluids* **20** (1977).

2. Y.T. Fung and S.W. Chang, "Simulation of Internal Vortex Motions in Stratified Wakes," Third International Symposium on Stratified Flows, California Institute of Technology, Pasadena, Feb. 1987. ■

Analytic Representations of Viscoelastic Moduli

A. J. Rudgers
Underwater Sound Reference Detachment

Elastomeric materials are widely used to control vibration and sound radiation in military as well as in commercial devices and systems. In theoretical analysis and in numerical modeling of such devices and systems, mathematical formulas are required that describe the viscoelastic behavior of such materials. Any mathematical representation of viscoelasticity, if it is to be useful in the investigation of acoustical and vibration problems of interest to the Navy, must be sufficiently general to encompass elastomeric materials of many different kinds. Only through use of such general representations can the effect of material properties on system performance be properly evaluated.

Mathematical Model: Recently we developed a method of finding mathematical expressions that represent the dynamic (i.e., frequency-dependent) viscoelastic moduli of elastomeric materials having a variety of mechanical properties. For example, an analytic expression can be found to describe an elastomer with particular stiffness properties at low and at high frequencies, with its rubber-to-glass transition located in the vicinity of a specific frequency, and with a specified broadness in the peak of its damping factor [1]. The method is based on representation of a viscoelastic material by a statistical ensemble of microscopic springs and dashpots.

Microscopic springs, with spring constants described by the random variable r, and dashpots, with dashpot constants described by the random variable l, are considered to be interconnected (in a network sense) in the series-parallel scheme illustrated in Fig. 7. (Figure 7 shows a finite number of finite springs

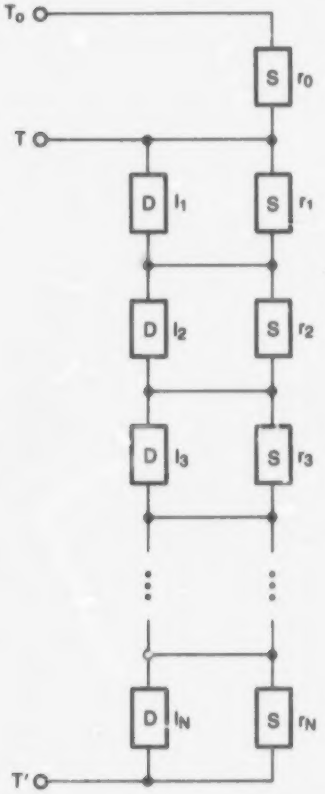

Fig. 7 — A finite network analog of the viscoelastic modulus of an elastomeric material comprising N springs with spring constants r_i and N dashpots with constants l_i. The additional spring with constant r_0 represents the static stiffness of the material. The dynamic modulus of the material is represented by the total impedance connected between the terminals TT'.

r_i and dashpots l_i, since an infinite number of infinitesimal impedance elements cannot be depicted.) If $P_{RL}(r, l)$ is the joint probability density function for r and l, a dynamic viscoelastic modulus $M(\omega)$ is calculated as the expected (i.e., average) value of the impedance that is connected between terminals TT' in the infinite analog of the network shown in Fig. 7. This impedance is expressed by the two-dimensional integral

$$M(\omega) = \int_0^\infty \int_0^\infty \frac{j\omega rl}{r + j\omega l} P_{RL}(r, l) dr dl, \quad (1)$$

where j is the imaginary unit. The modulus M is a complex function of the angular frequency ω. Usually one assumes r and l are independent random variables so that the relation $P_{RL}(r, l) = P_R(r) P_L(l)$ holds, in which P_R and P_L are, respectively, the probability densities of r and l.

Deriving Expressions for Viscoelastic Moduli: To derive expressions for the complex function $M(\omega)$ that can be used to characterize elastomeric materials with different kinds of viscoelastic behavior, the integral in Eq. (1) was analytically evaluated by using different functional forms for the probability density P_{RL}. Typical functional forms for probability density functions that might be used in this evaluation are shown in Fig. 8. The graph in Fig. 8 pertains to the case of independent random variables r and l with density functions of the same form. In this situation, either of these random variables may be described by the generic variable x, with $\bar{X}$ as its expected value and with P_X as its probability density. The quantity β_x in Fig. 8 is the nondimensional random variable $\beta_x = x / \bar{X}$.

Each of the four functional forms for P_{RL} shown in Fig. 8, or any other such form, gives rise to a particular form for $M(\omega)$ when the integral in Eq. (1) is evaluated. One tailors the functional form of M to the viscoelastic properties of a particular elastomeric material by the choice of the functional form taken for P_{RL}. As an example, consider the Maxwell probability density,

$$P_X(\beta_x) = (8 / \pi^2 \bar{X}) (2\beta_x)^2 \exp[-(2\beta_x^2) / \pi], \quad (2)$$

which results in the peaked solid curve in Fig. 8. When Eq. (1) incorporating this probability density is evaluated, one obtains a formula (not reproduced here) that leads to the complex viscoelastic modulus depicted by the solid curves in Fig. 9. The variable ζ in Fig. 9 is a nondimensional form of the frequency expressed by the equation

$$\zeta = \omega \tau_0, \quad (3)$$

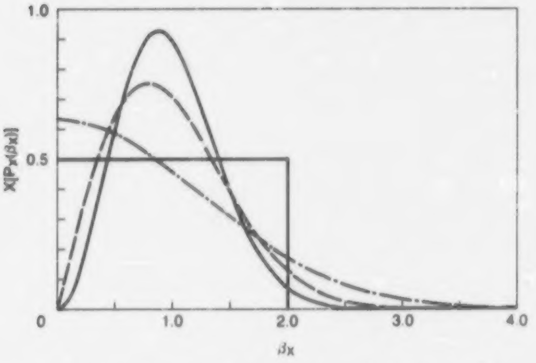

Fig. 8 — Various nondimensional probability density functions that can be used to describe ensembles of microscopic springs and dashpots. The upper solid curve illustrates a Maxwell probability density function (see Eq. (2)). The dashed curve illustrates a Rayleigh probability density function. The chain-dashed curve illustrates a semi-Gaussian probability density function. The lower solid curve illustrates a low-pass uniform probability density function. The average value $\bar{X}$ is the same for all the probability density functions shown.

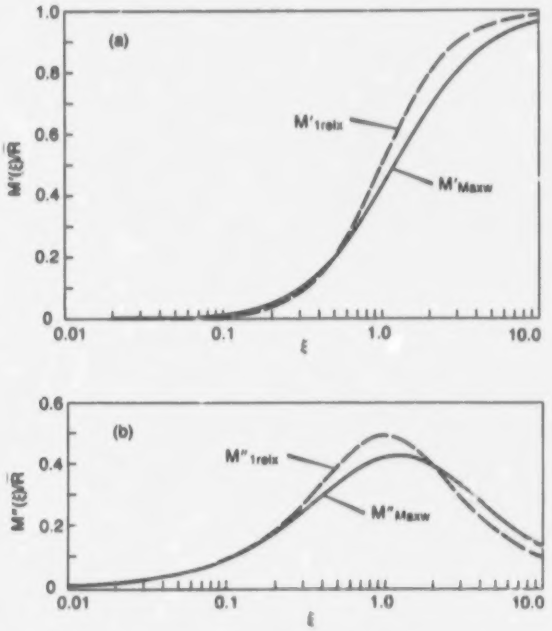

Fig. 9 — The complex viscoelastic modulus $M_{Maxw}(\zeta)$ of a material characterized by a joint Maxwell probability density function describing spring and dashpot constants compared with the complex modulus $M_{1relx}(\zeta)$ of a material characterized by a single relaxation time. Solid curves depict the real and imaginary parts of M_{Maxw} normalized by $\bar{R}$, and dashed curved depict the real and imaginary parts of M_{1relx} normalized by $\bar{R}$, where $\bar{R}$ is the average value of the spring constant. (a) Single primes denote the real parts of the moduli. (b) Double primes denote the imaginary parts of the moduli.

where

$$\tau_0 = \bar{L} / \bar{R} \tag{4}$$

is a relaxation time calculated from the average value $\bar{R}$ of the random spring constants and the average value $\bar{L}$ of the dashpot constants that characterize the viscoelastic material being modeled. Since any dynamic modulus of an elastomeric material is a complex function of ω, the variation with frequency (i.e., with ζ here) of both its real part M'_{Maxw} (Fig. 9(a)) and its imaginary part M''_{Maxw} (Fig. 9(b)) must be considered.

Behavior of Elastomeric Materials: In Fig. 9, the real and imaginary parts of the modulus M_{Maxw} (solid lines) are compared with the respective real and imaginary parts of the modulus M_{1relx} (dashed lines). The quantity M_{1relx} is the dynamic modulus of a rudimentary viscoelastic material characterized by a single relaxation time τ, which, for the comparison shown, is taken equal to τ_0 in Eq. (4). For most actual elastomeric materials displaying simple viscoelastic behavior, it is known that the viscoelastic modulus one observes differs from the modulus of a material characterized by a single relaxation time in just the way that the solid curves differ from the dashed curves in Fig. 9. That is, the step-like transition in the real part of a viscoelastic modulus of an actual material is less abrupt than that in a material having a single relaxation time (upper curves in Fig. 9); and the peak in the imaginary part of that modulus is lower and broader than the corresponding peak in the imaginary part of the modulus of the material with a single relaxation. Thus the procedure described is capable of producing analytic representations for dynamic moduli that mimic the viscoelastic behavior exhibited by actual elastomeric materials.

[Sponsored by ONR]

Reference

1. J.C. Snowdon, *Vibration and Shock in Damped Mechanical Systems* (Wiley, New York, 1968), pp. 7- 17. ■

BEST COPY AVAILABLE

Telecommunication and information processing technologies are under development to support battle management. NRL is active in the development of network designs for secure transmission of information and decision support systems that are needed in managing complex combat situations. Artificial intelligence, parallel computing, information security, and human - computer interface technology supplement communication sciences in the Information Technology Division.

INFORMATION TECHNOLOGY

185 **Integrated Battle Group Communications Networks**
Donald G. Kallgren and Dennis N. McGregor

188 **Single-Board Digital Signal Processor for Voice and Data Applications**
David L. Tate and Raymond Cole, Jr.

190 **SDI Mid-Course Battle Management**
Leslie J. Pierre and Kurt Askin

Integrated Battle Group Communications Networks

D. G. Kallgren and D. N. McGregor
Information Technology Division

Naval telecommunication currently uses a number of networks and links, each optimized for a specific service and operating independently. Automated network operation and internetwork information transfer is a means of supporting evolving Fleet command and control requirements, for which expansion of the battle area, reduced reaction times, and high volumes of data are predicted. To address this problem, a Unified Network Technology (UNT) Program [1] has been designed to demonstrate the benefits of new networking and internetworking technologies that can be applied to naval telecommunications.

The System Concept: Figure 1 shows the system concept embodied by the UNT project. As in the current Naval Telecommunication System, a variety of transmission media will provide connectivity between Battle-Group Command and Control (C^2) elements and Shore-Based elements. Transmission assets will be provided by current development efforts in robust radio communication, such as the High-Frequency Anti-Jam (HFAJ) Program, the Joint Tactical Information Distribution System (JTIDS), and the Navy extremely high frequency (EHF) Satellite Communications Program (NESP, in conjunction with the MILSTAR EHF satellite communication system).

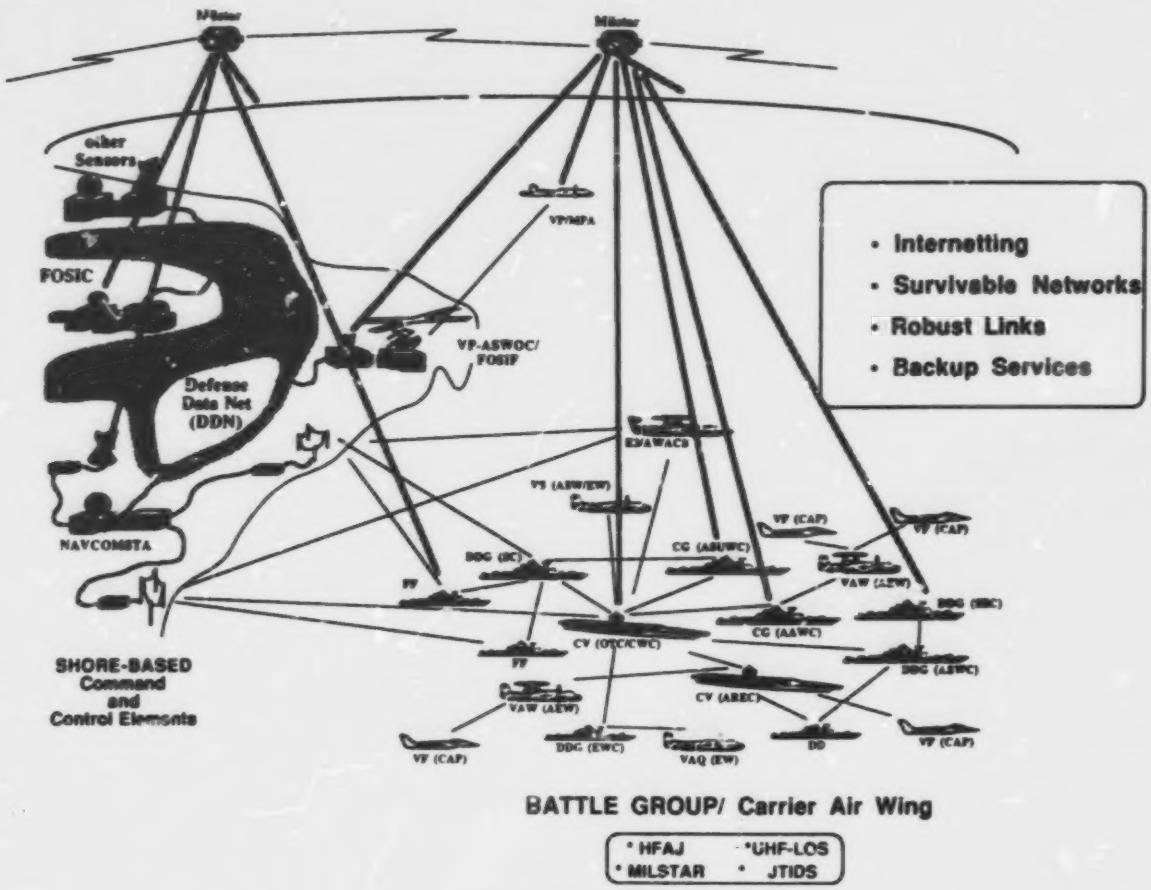
Milstar
Milstar
other Sensors
FOSIC
VP/MPA
VP-ASWOC/ FOSIF
Defense Data Net (DDN)
E3/AWACS
VS (ASW/EW)
NAVCOMSTA
VF (CAP)
VF (CAP)
CG (ASUWC)
DDG (SC)
VAW (AEW)
FF
DDG (SSC)
CV (OTC/CWC)
CG (AAWC)
FF
DDG (ASWC)
SHORE-BASED Command and Control Elements
VAW (AEW)
CV (AREC)
VF (CAP)
DDG (EWC)
VAQ (EW)
DD
VF (CAP)
• Internetting
• Survivable Networks
• Robust Links
• Backup Services
BATTLE GROUP/ Carrier Air Wing
• HFAJ
• UHF-LOS
• MILSTAR
• JTIDS

Fig. 1 – UNT system concept

BEST COPY AVAILABLE

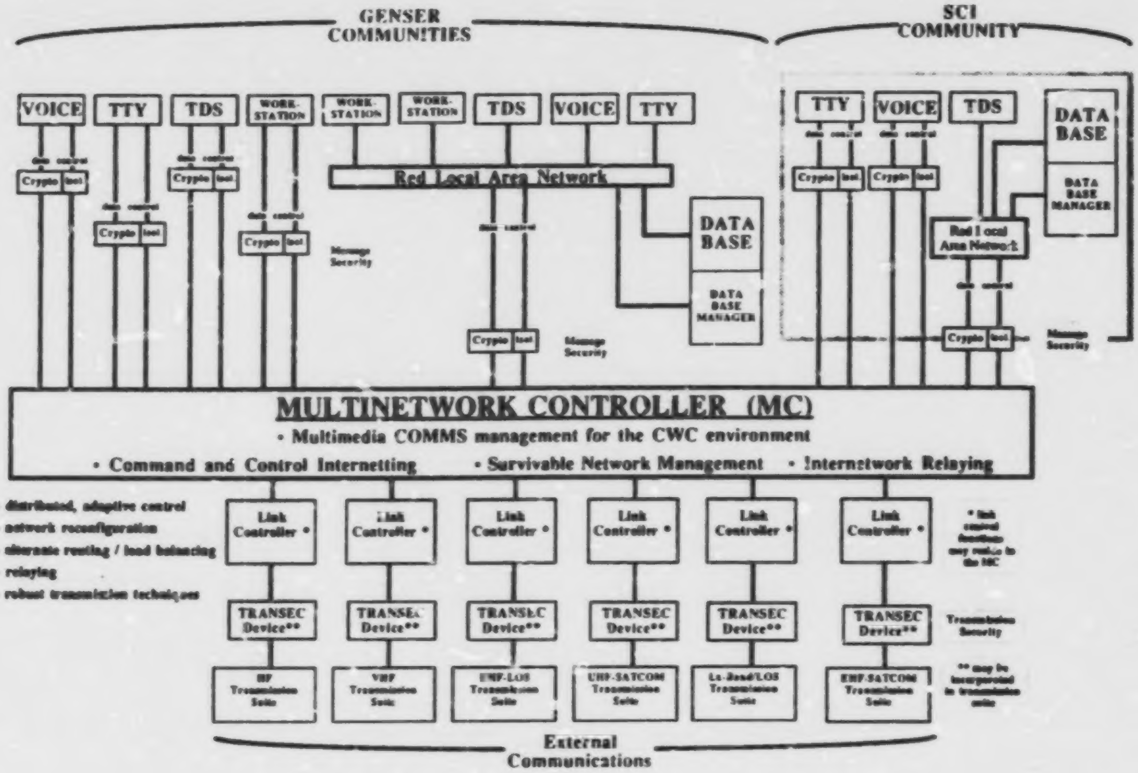
GENSER COMMUNITIES
SCI COMMUNITY
VOICE
TTY
TDS
WORK-STATION
WORK-STATION
WORK-STATION
TDS
VOICE
TTY
TTY
VOICE
TDS
DATA BASE
DATA BASE MANAGER
data control
Crypto
Red Local Area Network
Red Local Area Network
DATA BASE
DATA BASE MANAGER
Message Security
Message Security
Message Security
MULTINETWORK CONTROLLER (MC)
• Multimedia COMMS management for the CWC environment
• Command and Control Internetting
• Survivable Network Management
• Internetwork Relaying
- distributed, adaptive control
- network reconfiguration
- alternate routing / load balancing
- relaying
- robust transmission techniques
Link Controller *
TRANSEC Device**
HF Transmission Suite
VHF Transmission Suite
EHF-LOS Transmission Suite
UHF-SATCOM Transmission Suite
Lx-Band/LOS Transmission Suite
EHF-SATCOM Transmission Suite
* link control functions may reside in the MC
Transmission Security
** may be incorporated in transmission suite
External Communications

Fig. 2 – Unified multinetwork architecture

A multinetwork controller (MC) at each communication node is the central component of the UNT system concept (Fig. 2). In the context of the reference model for open systems interconnection (OSI) [2], the MC performs functions in the network and transport layers of the seven-layer model. It must be compatible with and augment protocols for internetwork communication currently defined for these layers, such as the transmission control protocol (TCP) and internetwork protocol (IP). These protocols are required for use in Department of Defense packet-switching networks and are used in the networks to which Naval C^2 centers and communication stations ashore are connected; they are unsuited for use in the naval tactical environment without some augmentation or modifications.

Multiple Network Control and the Tactical Internetwork Environment: Research on the MC architecture is focused on protocols for the tactical-internetworking environment and a new model of internetwork operation for integrated battle-group communication networks. The MC manages requests for communication services by C^2 elements, manages the connections between C^2 resources throughout the Battle Group, and supports internetwork relaying.

Unlike the so-called catenet model on which the current internetworking protocol suite [3] is based, the model of the tactical-internetwork environment used in defining the MC architecture, shown in Fig. 3, places all networks in parallel. This model permits load balancing and alternate routing of traffic throughout the mixed-media transmission system.

The current internetwork protocol suite is inadequate for this model since it uses only the number of networks traversed by a path as the distance metric for computing routes between

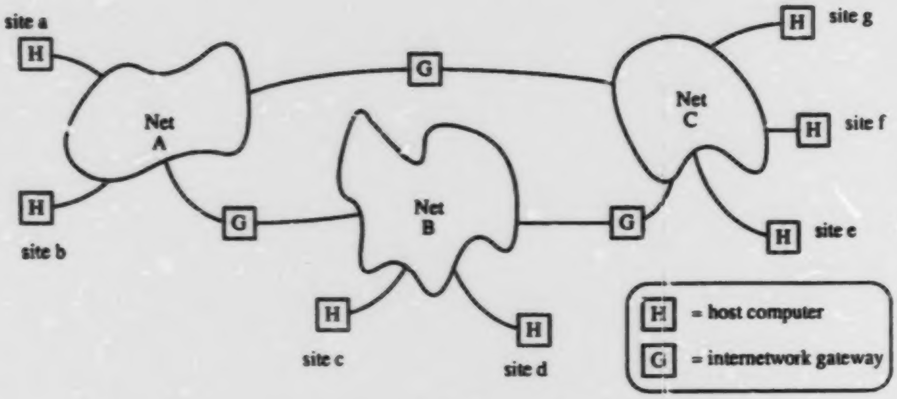
site a
H
Net A
H
site b
G
G
Net B
H
site c
H
site d
G
Net C
H
site g
H
site f
H
site e
H = host computer
G = internetwork gateway

Fig. 3(a) – The catenet (concatenated network) architecture on which current internetworking protocols are based (typical)

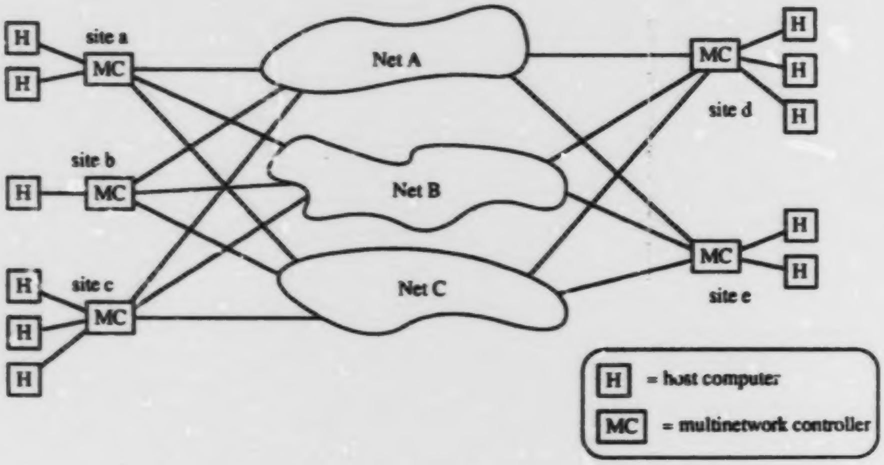
H
H
site a
MC
site b
H
MC
H
H
H
site c
MC
Net A
Net B
Net C
MC
site d
H
H
H
MC
site e
H
H
H = host computer
MC = multinetwork controller

Fig. 3(b) – The parallel architecture on which internetworking protocols in the UNT system are based

nodes. If this metric were used in the parallel-network model, routes traversing multiple networks would not be created or used, because the internetwork "distance" between nodes would be one in all cases.

Protocols for the tactical-internetwork environment and the parallel-network model must use other distance metrics for traffic routing, and will require tight coupling between the link control elements and data bases. Thus, the resultant system concept resembles a single network comprised of links using different transmission media, rather than a more loosely coupled concatenation of networks.

While the MC is the key element that supports integrated battle-group communications, other issues are currently under investigation by the UNT program. These include methods of providing message and transmission security in the system, protocols and algorithms for providing robust, jam-resistant transmission techniques. Though the use of system layering concepts such as the OSI model provides some measure of isolation for MC functions, all of these issues affect to some degree the functions performed by MC, and the degree to which battle-group communications can be fully integrated.

Future Plans: In conjunction with other Navy laboratories, NRL will perform advanced technology demonstrations in the future to meet the objectives of the UNT Program:

- Demonstration of new technologies to support C^2 internetting,
- Demonstration of survivable network structures for intrabattle-group communication,
- Incorporation of robust transmission techniques, and
- Transition of new internetworking and networking technologies to communication systems currently under development.

[Sponsored by ONT and NOSC]

References

1. "Program Plan for Unified Network Technology (UNT)," Communication Systems Engineering Branch, Information Technology Division, NRL, 12 Nov. 1986.
2. Draft International Standard ISO/DIS 7498: Information Processing Systems-Open Systems Interconnection-Basic Reference Model (Apr. 1982).
3. "Internet Protocol Transition Workbook," Network Information Center, SRI International, Mar. 1982. ■

Single-Board Digital Signal Processor for Voice and Data Applications

D. L. Tate and R. Cole, Jr.
Information Technology Division

Signal processing techniques have been used for many years to improve the capabilities of many telecommunication products. With the recent advances in computer technology, digital signal processing (DSP) is used to further enhance performance. To provide this increase in performance to small portable equipment, it is necessary to have a compact, low-power device that is capable of high-speed signal processing. NRL has developed a real-time digital signal processing board with these capabilities that meets the requirements of a variety of voice bandwidth applications such as speech processing, audio spectrum analysis, and high-speed modems.

Signal Processor Board: The digital signal processor board (see Fig. 4) measures 2.75 × 4.375 × 0.5 in. A 40-pin connector provides power, control signals, analog input and output (I/O), and eight bits of digital I/O. The board requires only 100 mA at 45 V and 10 mA at -5 V during normal operation giving a total power consumption of approximately 0.5 W. The design has been specifically aimed at a small size and low power consumption and requires only 10 integrated circuits (ICs) for a fully functional system.

The central processing unit (CPU) used is the Texas Instruments TMS320C25 digital signal processor, especially designed to support real-time digital signal processing and computation-intensive applications such as digital filtering and speech processing. The TMS320C25 can use a clock frequency of up to 40 MHz to give an instruction time of 100 ns, or ten million instructions per second (10 MIPs). The CPU provides 32-bit fixed-point logical and arithmetic instructions including a single-cycle 16-bit multiply. The 16-bit data/address bus allows up to 65,536 (64K) words of 16-bit data memory and 64K words of program memory.

Application program storage is provided in nonvolatile erasable programmable read-only memories (EPROMs). This allows the board to function as a stand-alone system that begins

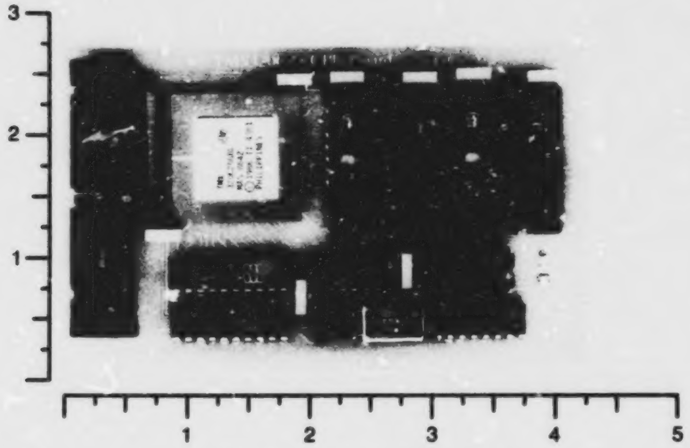

Fig. 4 – Single board digital signal processor

the circuit. The use of high-speed memories allows the processor to run without memory wait states. One pair of 2048 (2K) bits × 8 bits EPROMs provides 2K of 16-bit program memory. If additional program memory is required, then one pair of 8192 (8K) bits by 8 bits EPROMs can be used in place of the 2K EPROMs to provide 8K of program memory. Storage for program variables and data is provided in a pair of 2K by 8-bit random access memories (RAMs). Nonvolatile data tables and initial variable values are stored along with the program memory in the EPROMs.

Companion connectors are provided to permit the EPROMs to be reprogrammed without removing them from the board. This feature is useful in areas where the board may be subject to vibrations that would cause the EPROMs to be jarred from their sockets. With on-board programming, the EPROMs can be soldered onto the board and programmed through the companion sockets.

Analog and Digital Interfaces: Audio signals are interfaced to the single-board DSP through a single integrated circuit that performs both the digital to analog (D/A) and analog to digital (A/D) conversion. This chip digitizes the incoming analog signal and encodes the sampled value using a mu-law compression/expansion algorithm to convert a 12-bit sample value to an 8-bit serial data byte that is transmitted to the CPU serial interface. The CODEC (coder/decoder) contains the D/A and A/D converters, the serial data interface to the CPU, and an integral filter in a single IC. The CODEC can drive a 300-Ω load, reducing the amount of external drive circuitry required.

The digital interface provides 8 bits of input and 8 bits of output data. The input signals are read with a nonlatching interface that requires no external clocking signals. Input data can be either status information such as switch positions or alarm indicators, or serial data information such as an operator's terminal or a personal computer serial interface. Data that contain inherent timing can be read reliably through the use of either the internal timer in the CPU or software timing loops. Eight bits of separately controllable output bits are buffered and latched to provide either control functions such as relay control, or serial output to devices such as data loggers. Timing for the output signals can also be performed under software control in the CPU.

Design Approach: A unique design approach has been used to derive the necessary timing and control signals with a minimum number of interface ICs. By carefully selecting the CPU clock frequency and deriving other timing signals from the CPU signals, all the necessary signals for the serial interface and memory circuits are provided with only two standard ICs. Additional design strategies provide for compatibility with the TMS32020 processor or lower processor speeds for reduced power consumption.

Applications: The single-board digital signal processor is useful for any application that uses audio frequency analog signals. The CODEC described in this article is designed for analog signals in the 0 to 4000 Hz range, but other devices can be used to provide additional capabilities.

One of the current applications for the single-board digital signal processor is a modem for high-frequency radio applications. This device uses advanced DSP techniques to allow digital data communication over a difficult communication medium. Another application that uses the DSP processor board is an audio frequency spectrum display. This device digitizes the incoming analog signal, performs a fast Fourier transform on the data, and displays the resultant spectrum through the analog output signal. Other application areas under development include advanced digital speech compression techniques and new areas of speech synthesis.

Summary: The use of state-of-the-art complimentary metal-oxide silicon (CMOS) technology has allowed NRL to design a 3 × 5 in. single-board signal processor that uses only one-half W of power and is capable of operating at instruction rates of 10 million operations per second. The combination of low power, small size, and high-speed operation opens up a number of new application areas for advanced digital signal processing techniques. ■

SDI Midcourse Battle Management

L. J. Pierre and K. Askin
Information Technology Division

NRL is engaged in the development of algorithms that are necessary to perform midcourse battle management functions for the Strategic Defense Initiative (SDI). The functions include correlation and tracking of ballistic objects, and discrimination between reentry vehicles and decoys. These functions are supported by the subsystems shown in Fig. 5. The algorithms are being designed, coded, and tested on an algorithm development facility at NRL. This test-bed will allow the various parts of the midcourse battle manager to operate interactively in response to synthesized sensor data. The development facility comprises a network of SUN workstations, VAX computers, and a BBN Butterfly Machine Parallel Computer. Two of the major battle management functions are addressed in more detail below.

Tracker/Correlator (T/C): The T/C algorithm is based on a Bayesian approach for assigning sensor reports to tracks and scoring feasible (candidate) scenes. The sensor reports may contain either bearing only or bearing and range data, as well as nonkinematic attributes. Because of the ambiguity that arises caused by the large number of targets, target proximity, and sensor resolution, a key element of the algorithm is that multiple views (scenes) that represent our current knowledge of the state (number, position, type, etc.) of the targets are generated and processed.

Figure 6 shows that the major processing steps in the algorithm may include generating a maximum likelihood score for associating sensor reports to tracks, using a heuristic search technique for generating candidate scenes, and updating the kinematic and attribute states of the targets. The

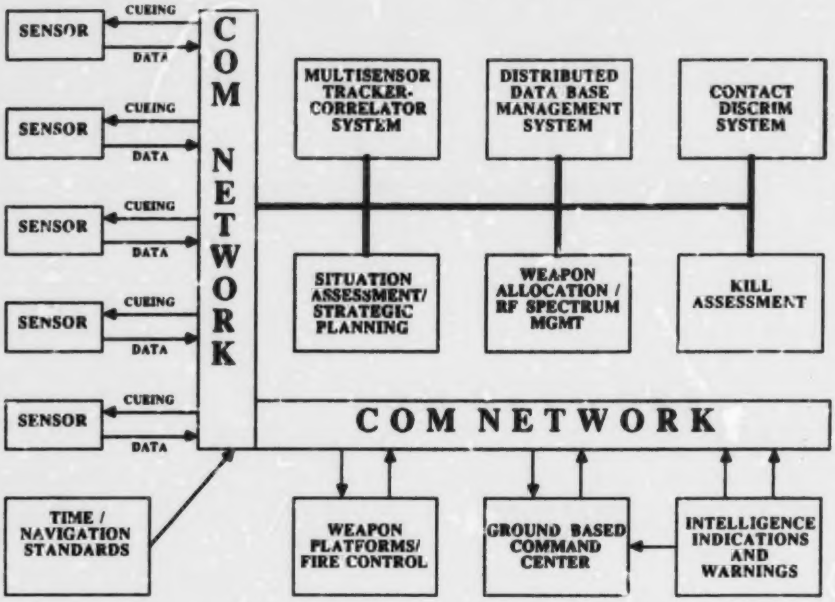
SENSOR
CUEING
DATA
SENSOR
CUEING
DATA
SENSOR
CUEING
DATA
SENSOR
CUEING
DATA
SENSOR
CUEING
DATA
COM NETWORK
MULTISENSOR TRACKER-CORRELATOR SYSTEM
DISTRIBUTED DATA BASE MANAGEMENT SYSTEM
CONTACT DISCRIM SYSTEM
SITUATION ASSESSMENT/ STRATEGIC PLANNING
WEAPON ALLOCATION / RF SPECTRUM MGMT
KILL ASSESSMENT
COM NETWORK
TIME / NAVIGATION STANDARDS
WEAPON PLATFORMS/ FIRE CONTROL
GROUND BASED COMMAND CENTER
INTELLIGENCE INDICATIONS AND WARNINGS

Fig. 5 – SDI battle management

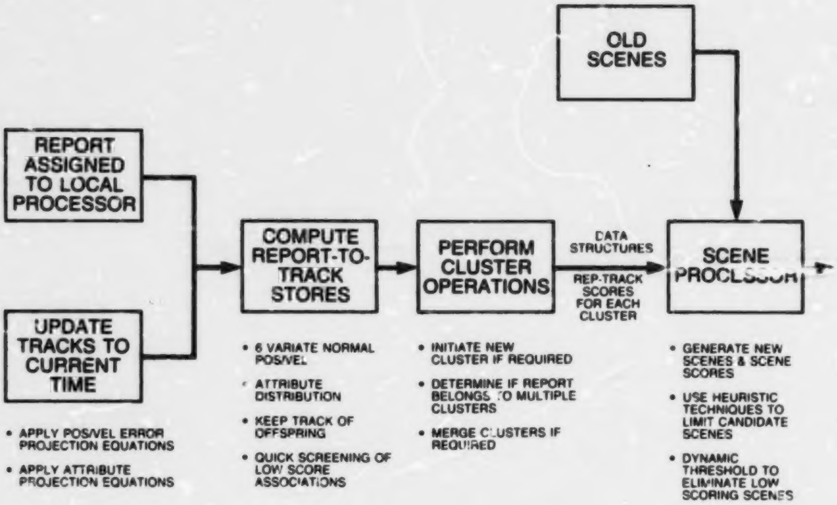
OLD SCENES
REPORT ASSIGNED TO LOCAL PROCESSOR
UPDATE TRACKS TO CURRENT TIME
COMPUTE REPORT-TO-TRACK STORES
PERFORM CLUSTER OPERATIONS
DATA STRUCTURES
REP-TRACK SCORES FOR EACH CLUSTER
SCENE PROCESSOR
• APPLY POS/VEL ERROR PROJECTION EQUATIONS
• APPLY ATTRIBUTE PROJECTION EQUATIONS
• 6 VARIATE NORMAL POS/VEL
• ATTRIBUTE DISTRIBUTION
• KEEP TRACK OF OFFSPRING
• QUICK SCREENING OF LOW SCORE ASSOCIATIONS
• INITIATE NEW CLUSTER IF REQUIRED
• DETERMINE IF REPORT BELONGS TO MULTIPLE CLUSTERS
• MERGE CLUSTERS IF REQUIRED
• GENERATE NEW SCENES & SCENE SCORES
• USE HEURISTIC TECHNIQUES TO LIMIT CANDIDATE SCENES
• DYNAMIC THRESHOLD TO ELIMINATE LOW SCORING SCENES

Fig. 6 – Tracker/correlator data flow

number of report-to-track scores that must be computed is limited by use of a clustering concept, in which targets with similar attributes are grouped into clusters that are treated as a single object for processing purposes.

Report-to-track scores are computed only for targets in certain feasible clusters, and then a "best" cluster is selected for each report. Only targets in their best cluster are candidates for updating within the given report. The clustering concept also provides a natural parallelism to the process. This can be exploited with parallel processing hardware.

Report-to-track correlation scores are based on both kinematic (motion related) and nonkinematic attributes of the targets and represent

BEST COPY AVAILABLE

the likelihood of observing the target. Since the observations in position/velocity space are assumed to be independent of the observations in attribute space, the association scores may be expressed as the product of the position/velocity score and the attribute score.

The scene processor portion of the algorithm generates and updates the scenes within each cluster from a set of new report-to-track associations. Since each cluster can be handled independently, the scene processor offers another opportunity for exploiting parallel processing techniques. Under the assumption that a scan of reports consists of a set of unique objects, the scene processor examines a preferred subset of possible track extensions. A track is extended by assigning a report to a track, and various heuristics are employed to restrict the number of possible scenes. An extended scene will consist of three types of tracks: report extended tracks, propagated tracks, and offspring tracks. Report extended tracks are those tracks extended by the assignment of a new report. Propagated tracks are updated in position and attributes but are not assigned a new report. Offspring tracks result when two previously unresolvable objects become resolved and appear as distinct targets. Scene pruning is performed based on scene scores to reduce the possible number of feasible scenes. The scene score is a product of the old scene score, the report-to-track scores, and a score for all unassociated reports.

Future extensions to the algorithm will provide track file updates based on information from the contact discrimination module. Sensor tasking requests will be generated and sent to the sensor allocation module to provide additional information on selected targets.

Contact Discrimination: After the battle manager decides on the allocation of reports to associated tracks, it is necessary to classify the object being tracked to determine if it is a potential nuclear warhead or not. If it is not a warhead, it could either be a bit of junk associated with the warhead (such as nuts and bolts or parts of the casing), or a deliberately placed decoy. Usually, space junk can be characterized as such by using a bulk filter. It is the decoys that can cause problems for the battle management discriminator.

As part of the SDIO effort, NRL is developing algorithms for the discrimination of tracked objects. The assumptions in this project are that the SDI system has little if any a priori knowledge of what sort of warheads and decoys threaten the United States. Based on the scientific and engineering constraints placed on the designers of decoys and warheads, it is possible to derive rules that will enable the battle manager to discriminate between threatening warheads and nonthreatening decoys, and therefore permit optimal allocation of weapons to defend against the lethal warhead.

A prototype algorithm has been developed to perform contact discrimination of objects in ballistic trajectory. This algorithm is based on an expert knowledge base, using warhead and decoy engineering design paradigms. The knowledge base can be divided as shown in Fig. 7: (a) rules that enable the contact discriminator to characterize the object, (b) rules that can be developed as a result of the decoy design engineer attempting to create a decoy that best matches the warhead, and (c) rules that depend on the deployment strategy (or payload partitioning) of a specific booster. The prototype algorithm currently includes over 200 rules in the three sections of the expert system.

As a system of sensors reports on an object, values for physical parameters are available that will enable the expert system to characterize the object. Radar, for example, might provide by Doppler imaging the spin of the object and precession of the nose cone. The expert system could then characterize the object as being long and slender or short and broad on laws of physics relating to the moments of inertia. Rules like this are part of the first of the knowledge base sections.

Design of decoys depends on the need to simulate the warhead. A decoy cannot be an exact replica of a warhead, for if it were, it would be counterproductive to build the decoy rather than

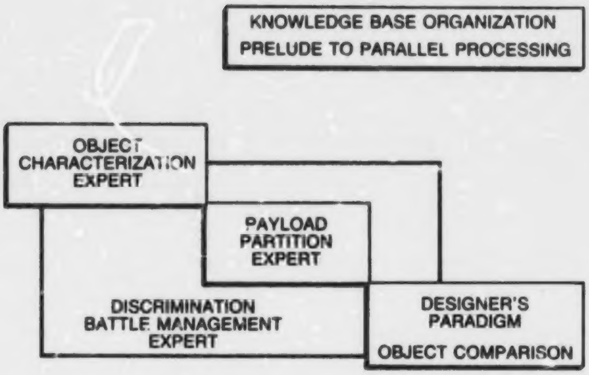
KNOWLEDGE BASE ORGANIZATION
PRELUDE TO PARALLEL PROCESSING
OBJECT CHARACTERIZATION EXPERT
PAYLOAD PARTITION EXPERT
DISCRIMINATION BATTLE MANAGEMENT EXPERT
DESIGNER'S PARADIGM
OBJECT COMPARISON

Fig. 7 – Knowledge base organization

the weapon. If, for example, a decoy is to be developed that will imitate a warhead as seen by an infrared sensor, thermal mass might be duplicated. Unless the decoy has the actual mass of the warhead (which would require a one-to-one substitution of a decoy for a warhead—an unnecessary loss of payload), the designer must change shape or size of the decoy, causing changes in the radar cross section of the decoy. Rules quantifying these changes are part of the second section of the expert system.

Finally, the number and type of objects that can fit on an individual rocket booster are fixed by throwweight and volume limitations. If, for example, ten warheads can be packaged in the payload of a single booster, then introduction of decoys requires that they be exchanged for weapons. If the sensor identifies seven of one type object and three of another type closely matched in size and shape to the first, it is most likely that the group of three objects are decoys and the group of seven are weapons. Rules based on configuration of the booster payload comprise the third section of the expert knowledge base.

The power of this contact discrimination computer code depends on the fact that it is based on laws of physics, engineering, and strategy, rather than on knowledge of the sensor characteristics of actual warheads and decoys.

[Sponsored by SDIO] ■

The Naval Research Laboratory is proud of its many scientists and engineers. A few of these have been recognized for their exceptional commitment to continued productivity, intellectual integrity, and outstanding research at the cutting edge of science and technology. In this chapter, they are identified and recognized as recipients of numerous scientific and publication awards presented by NRL and the Department of Defense.

EXCELLENCE IN RESEARCH FOR TOMORROW'S NAVY

197 Special Awards and Recognition

205 Individual Honors

215 Alan Berman Research Publication Awards

SPECIAL AWARDS AND RECOGNITION

NRL continues to acknowledge Dr. Jerome Karle for the awards and praise he has received in recognition of the honor he has brought to his country and the Laboratory by winning the Nobel Prize in Chemistry in 1985.

To Jerome Karle
With best wishes, Ronald Reagan

President Ronald Reagan presents the promotion to the Presidential Rank of Distinguished Executive in the Senior Executive Service to Dr. Jerome Karle, Chief Scientist at NRL's Laboratory for Structure of Matter.

Dr. J. Karle also received, among numerous other awards,

> The President's Award for Distinguished Federal Civilian Service:
>
> "...using structural analysis diffraction methodology, (Dr. Karle) introduced new fundamental, revolutionary concepts and developed their implications in such a way that analytical skills have been greatly enhanced and practical implementation has flourished throughout the world. His achievements have contributed significantly to the strength and preservation of our Nation."

as well as the Navy Award for Distinguished Achievement in Science and the Rear Admiral William S. Parsons Award of the Navy League.

Harold L. Hughes
Electronics Technology Division

NAVAL RESEARCH LABORATORY 1985 E. O. HULBURT ANNUAL SCIENCE AND ENGINEERING AWARD

"...For his outstanding contributions in identifying mechanisms of radiation induced defects and the means to overcome them by the development of processes to increase microelectronic survivability, especially in the area of metal-oxide-semiconductor radiation-hardening..."

Dr. Thomas G. Giallorenzi
Optical Sciences Division

1986 HARRY DIAMOND MEMORIAL AWARD

"For contributions to the development of naval electro-optics and optical fiber technology."

and

DEPARTMENT OF DEFENSE DISTINGUISHED CIVILIAN SERVICE AWARD

"...For his exceptional and significant contributions to the defense of the United States. His innovations and initiatives have increased the capabilities of the Navy in all aspects of electro-optics and have contributed to the solution of several significant technological problems of the Department of Defense. Dr. Giallorenzi's many contributions clearly warrant the Distinguished Civilian Service Award."

Dr. David W. Kerr
Radar Division

THE AMERICAN DEFENSE PREPAREDNESS ASSOCIATION CROZIER PRIZE

"...For his pioneering work in developing Inverse Synthetic Aperture Radar for the imaging and classification of ship targets through Project Profile. This unique technology permits the imaging of moving targets in real time by radar at long range in all weather, day or night. This combination of long range and classifiable quality imagery is a potent addition to military capability..."

Dr. David Kerr's solid achievement and sustained effort in advancing radar technology reflect great credit upon himself, the United States Navy, and the Nation.

Howard Lessoff
Electronics Technology Division

FEDERAL LABORATORY CONSORTIUM SPECIAL AWARD FOR EXCELLENCE IN TECHNOLOGY TRANSFER (1986)

"... For his leadership in developing both the Liquid Encapsulated Czoohralski (LEC) growth method of semi-insulating updoped gallium arsenide (GaAs) and the processing for wafers production and then transferring the technology to industry. Mr. Lessoff's new production method will result in significant savings to the Department of Defense..."

Dr. Norman C. Koon
Condensed Matter &
Radiation Sciences Division

THE AMERICAN PHYSICAL SOCIETY INTERNATIONAL PRIZE FOR NEW MATERIALS

"For his pioneering research on the preparation and characterization of rare earth-iron-boron materials which led to the discovery of a new class of permanent magnets of unusual scientific interest and technological promise."

Dr. David L. Venezky
Chemistry Division

DEPARTMENT OF THE NAVY SUPERIOR CIVILIAN SERVICE AWARD

"For his outstanding contributions in scientific research, and research management. As a Branch Head and researcher, Dr. Venezky has an enviable record. His polymer matrix system for removal of rust not only has had a marked impact in the Navy but found other quite interesting uses, such as in the current renovations of the Statue of Liberty and at Three-Mile Island. His solution of the high pressure boiler scaling problem increased the overhaul times of the high pressure 1200 psi Navy boilers markedly, thus allowing ships to stay on line longer... Dr. Venezky has distinguished himself as a leader in professional societies bringing honor and recognition to the Naval Research Laboratory. His work has increased the well-being of the nation and society. Dr. Venezky is a most worthy recipient of the Navy Superior Civilian Service Award."

George P. Nelson
Radar Division

DEPARTMENT OF THE NAVY SUPERIOR CIVILIAN SERVICE AWARD

"For his dedication, remarkable fundamental and detailed understanding of the Identification of Friend and Foe (IFF) system design, operation and performance which have been instrumental in guiding Navy policies and actions in regard to the Mark XII Technical Improvement Program and the new Tri-Service Mark XV IFF system..."

Dr. Isabella L. Karle
Laboratory for Structure of Matter

THE INTERAGENCY COMMITTEE FOR WOMEN IN SCIENCE AND ENGINEERING (WISE) 1986 WISE LIFETIME ACHIEVEMENT AWARD

"...As being the most outstanding woman scientist in the Federal Government who, throughout her long and successful federal career, has made significant contributions to science."

Dr. Robert L. Jones
Chemistry Division

NRL-SIGMA XI APPLIED SCIENCE AWARD FOR 1986

"For his pioneering work in low temperature hot corrosion which determined the role of NaCl vapor, leading to the elucidation of the mechanisms of hot corrosion in turbines and guiding the development of Navy turbine materials."

Dr. Kia L. Ngai
Electronics Technology Division

NRL-SIGMA XI PURE SCIENCE AWARD FOR 1986

"For his contributions to the field of relaxation phenomena in complex systems through postulation of a generalized concept which describes phenomena as diverse as polarization, stress and electric fields in systems such as glasses, amorphous polymers and semiconductors, ionic conductors and viscous liquids. He has changed the study of relaxation phenomena in complex systems by his penetrating analysis and development of new predictions."

Dr. Herbert Friedman
Space Science Division

MARTIN MARIETTA CHAIR

Dr. Herbert Friedman has been selected to occupy the Martin Marietta Chair of Space History at the Smithsonian's National Air and Space Museum, 1986.

Dr. Warren E. Pickett
Condensed Matter & Radiation
Sciences Division

THE WASHINGTON ACADEMY OF SCIENCES
WASHINGTON, D.C.
1985 AWARD FOR SCIENTIFIC ACHIEVEMENT IN PHYSICAL SCIENCES

"The physical sciences award for pioneering researches into the theory of the basic properties of solids."

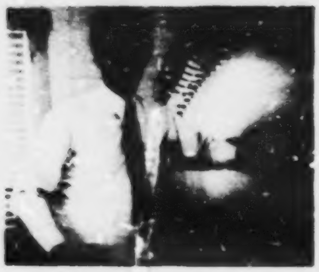

Dr. Karl Gerlach
Radar Division

AEROSPACE AND ELECTRONICS SYSTEMS SOCIETY 1986 RADAR SYSTEMS PANEL AWARD

"For the development of ECCM and signal processing for Navy Radar Systems."

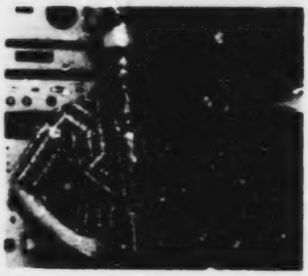

Dr. Stuart Wolf
Plasma Physics Division

DEPARTMENT OF THE NAVY MERITORIOUS CIVILIAN SERVICE AWARD

"...For his outstanding leadership and significant contributions in the field of inhomogeneous superconductivity both in enhancing our basic understanding of this new class of materials and in recognizing and vigoriously pursuing development of those aspects of superconductvity which have important Navy and technological impact..."

Dr. John A. Montgomery
Tactical Electronic Warfare Division

DEPARTMENT OF THE NAVY MERITORIOUS CIVILIAN SERVICE AWARD

"...In recognition and appreciation of Meritorious Service which has been of high value and benefit to the Navy."

Dr. William A. Hoppel
Space Science Division

DEPARTMENT OF THE NAVY MERITORIOUS CIVILIAN SERVICE AWARD

"In recognition of his major achievements in development of ion mobility instrumentation and theoretical modeling to delineate electrical characteristics of the troposphere and the planetary boundary layer near the sea surface."

Dr. Richard D. Gilardi
Material Science & Component
Technology Directorate
Laboratory for Structure
of Matter

DEPARTMENT OF THE NAVY MERITORIOUS CIVILIAN SERVICE AWARD

"For structural investigations of a number of very important substances whose results have shed important light on their structural characteristics, their function and, when appropriate, their potential for large-scale synthesis... Dr. Gilardi's active research in medicinal and biochemistry has resulted in his collaborating in a Walter Reed Army Medical Research Institute program which aims to develop new drugs to combat drug-resistant malaria..."

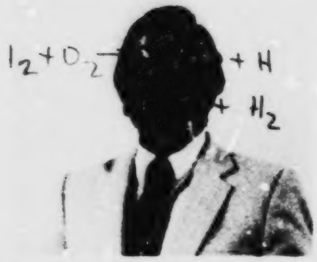

Dr. Jimmie R. McDonald
Chemistry Division

1986 THE SOUTHWESTERN UNIVERSITY ALUMNI ASSOCIATION CITATION OF MERIT AWARD

"...In recognition of outstanding service and accomplishments in the field of Lasers in Chemical Diagnostics..."

A Team Effort

Researchers from NRL's Space Science Division received the Navy Award of Merit for Group Achievement in a special ceremony held at the Lab. These people were awarded for their work with Spacelab 2 and the HRTS and SUSIM experiments or with the SPARTAN project. Pictured from left to right bottom row: Brian Dohne (HRTS), Benjamin Au (SUSIM), Nancy Linder (SUSIM), Dr. Dianne Prinz (Spacelab 2), Donald Lilley (HRTS), Dennis Socker (HRTS), Kenneth Dere (HRTS), Robert Tait (SPARTAN), Dr. Raymond Cruddace (SPARTAN). Top row: Allen Oliver (Spacelab 2), James Smith (HRTS), Dr. Guenter Brueckner (Spacelab 2), Michael VanHoosier (SUSIM), Donald Woods (SPARTAN), Gilbert Fritz (SPARTAN), Dr. John-David Bartoe (Spacelab 2).

INDIVIDUAL HONORS

Laboratory employees received numerous scientific medals, military service awards, academic honors, and other forms of recognition, including election and appointment to offices in technical societies. The following is an alphabetical list of persons who received such recognition in 1986.

Aberg, R.L., *Chairperson, Radio Frequency Countermeasures (RF–CM) Committee, Joint Directors of Laboratories Technology Panel for Electronic Warfare (JDL– TPEW).*

Ali, A.W., *Fellow, American Physical Society; Chairperson, Source Antenna and Propagation Sub-Panel, High Power Microwave Executive Steering Group, Office of Under Secretary of Defense Research and Engineering, Military Systems Technology (MST).*

Anderson, W.T., *Chairman, Technical Program, 1986 GaAs Reliability Workshop; Member, Combined Radiation Effects Working Group; Member, JEDEC Committee JC– 50 on GaAs; Panel Member, 1986 GaAs IC Symposium.*

Apruzese, J., *Member, Program Committee. American Physical Society Conference on Atomic Processes in Plasmas.*

Baer, R.N., *Member, Underwater Acoustics Technical Committee Acoustical Society of America.*

Batra, N.K., *Associate Technical Editor—Materials Evaluation, Journal of American Society for Nondestructive Testing; Chairperson, NDE of Composite Session, IEEE Ultrasonic Symposium, 1986; Member , IEEE UFFCS Advisory Committee; Member, IEEE 1986, 1987 and 1989 Ultrasonics Symposium Committee.*

Beal, R.T., *Member, American Institute of Aeronautics and Astronautics (AIAA), Space Transportation Technical Communication.*

Berkson, J. M., *Coeditor, Ocean Seismo–Acoustics: Low– Frequency Underwater Acoustics.*

Bishop, S.G., *Coeditor, Materials Research Society Proceedings, Microscopic Identification of Electronics Defects in Semiconductors; Member, Program Committee, Gordon Research Conference on Point Defects, Line Defects, and Interfaces in Semiconductors; Member, Technical Review Committee, Joint Services Electronics Program; Member. Review Panel, ONR University Research Initiative; Adjunct Professor, State University of New York and University of Utah.*

Boyer, L.L., *Chairperson, Phase Transitions Session, American Physical Society (APS).*

Brady, R.F., *Contributing Editor, Journal of Protective Coatings and Linings; Chairperson, Admissions Committee. American Chemical Society (ACS); Member, Membership Affairs Committee, American Chemical Society (ACS); Editorial Board Member, Journal of Coatings Technology.*

Bucaro, J.A., *Chairperson, Assessment Committee, Echo Ranging Test Facility.*

Bultman, J. D., *Associate Editor, Journal of Biotropica.*

Buot, F.A., *Member, National Group in Supercomputing and Simulation of Solid Devices, National Center for Supercomputing Applications (NCSA), University of Urbana, Illinois.*

Campbell, F. J., *Fellow, Institute of Electrical and Electronics Engineers (IEEE); Fellow, American Institute of Chemists (AIC); Chairperson, Awards Committee, Dielectrics and Electrical Insulation Society; Chairperson, Task Force on Wire Insulation Tracking, American Society for Testing and Materials (ASTM).*

Carhart, H.W., *Chairperson, National Academy of Sciences International Symposium, Explosion Hazard Classification of Vapors, Gases and Dusts; Chairperson, National Academy of Sciences Committee, Studies on Hazardous Substances.*

Carpentier, G.S., *Secretary, Local Arrangements Committee, American Physical Society Division of Plasma Physics Convention.*

Carruthers, G.R., *1985 Commanding Officer's Award for Achievements in the Field of Equal Employment Opportunity (FEO); Editor, Journal of the National Technical Association; Chairperson, NTA Editorial Review Committee.*

Carter, W.H., *Coeditor, Journal of the Optical Society of America, Nos. 7 & 8 (1986), "Applications of Coherence and Statistical Optics"; Chairperson, Fellows Committee, Society of Photo-Optical Instrumentation Engineers (SPIE).*

Chang, C.I., *Editor, Journal of Theoretical and Applied Mechanics; Chairperson, Structural Materials Panel, SDI Materials & Structures Planning Panel; Cochairperson, Tri-Service Laser Hardened Structures Group; Member, Metal Matrix Composite (MMC) Steering Committee.*

Cherkis, N.Z., *Member, U.S. Board on Geographic Names, Advisory Committee, Undersea Features.*

Christou, A., *Member, Technical Program Committee, International Reliability Physics Symposium; Member, Technical Program Committee, 13th International Symposium on Gallium Arsenide and Related Compounds; Panel Member, 1986 GaAs IC Symposium.*

Cooper, J. C., *Electromagnetic Compatibility Society of IEEE Special Citation; Presented, IEEE meeting, Boston, MA.*

Crooker, T.W., *Member, Standing Committee, Publications of the American Society for Testing and Materials.*

Crowe, C.R., *Member, Executive Committee Washington Chapter, American Society for Metals (ASM).*

Cruddace, R.G., *NASA Medal for Exceptional Scientific Achievement; Fellow, British Interplanetary Society; Member, American Institute of Aeronautics and Astronautics (AIAA); Member, High Energy Astrophysical Observatory.*

Davis, J., *Fellow, American Physical Society Editorial Board.*

DeMarco, R.A., *Chairperson, 8th Winter Fluorine Conference, Fluorine Division of the American Chemical Society; Treasurer, Chemical Society of Washington.*

Diachok, O.I., *Fellow, Acoustical Society of America.*

Dubbelday, P.S., *Fellow, Acoustical Society of America.*

Feldman, B.J., *Chairperson, R. W. Wood Prize Committee, Optical Society of America.*

Fliflet, A.W., *Editor, International Journal of Electronics.*

Flippen-Anderson, J.L., *Member, Standing Program Committee, American Crystallographic Association.*

Ford, R.T., *Treasurer, IEEE EMC Society.*

Fox, R.B., *Regional Director and Ex-Officio Councilor, American Chemical Society (ACS); Chairperson, ACS Board Committee on Public Affairs and Public Relations; Member, ACS Committee on Publications; Member, ACS Committee on Professional Member Relations; Member, ACS Committee on Planning; Member, ACS Committee on Nomenclature; Chairperson, Task Forces to evaluate the journal "Macromolecules" and to recommend an ACS position on pension policy, International Union of Pure and Applied Chemistry; Secretary, Interdivisional Committee on Nomenclature and Symbols.*

Garroway, A.N., *Member, Executive Committee of Experimental NMR Conference.*

Secretary of Defense Caspar Weinberger presents the Distinguished Civilian Service Award to Dr. Thomas G. Giallorenzi, Superintendent of the Optical Sciences Division at NRL. Dr. Giallorenzi won the award for his outstanding leadership and research in the electro-optical field.

NRL's Commanding Officer, CAPT William C. Miller, presents the Navy Meritorious Civilian Service Award to Dr. Richard D. Gilardi for his research at NRL's Laboratory for Structure of Matter. Mrs. Gilardi takes part in the ceremony.

Giallorenzi, T.G., *1986 Harry Diamond Memorial Award; DoD Distinguished Civilian Service Award; Editor-in-Chief, IEEE Optical Society of America (OSA), Journal of Lightwave Technology; Editor, Editorial Board IEEE Circuits and Devices; Chairperson, Award Committee, IEEE/OSA Tyndall Award; Chairperson, IEEE/OSA Conference on Lasers and Applications (CLEO); Chairperson, Navy's Fiber Optical Committee; Cochairperson, Triservice Fiber Optics Committee; Member, John Fritz Board of Awards, Professional Society/Committees, Ultrasonics Conference; Member, Infrared Information Sysposium (IRIS); Member, IEEE Lasers and Electro-optics Long Range Planning Committee; Member, International Optical Communications Steering Committee: Member International Fiber Optical Sensor Conference Steering Committee; Member, Industrial Advisory Boards for Engineering at University of New Mexico and University of Virginia; Member, National Research Council Panel on Photonics 1986–88; Member, US National Committee for International Commission for Optics (National Research Council).*

Gilardi, R.D., *1986 Navy Meritorious Civilian Service Award; Member, American Crystallographic Association Continuing Education Committee.*

Gilfrich, J.V., *Fellow, American Institute of Chemists; Editor-in-Chief, Journal "X-Ray Spectrometry"; Cochairperson, Annual Conference on Applications of X-Ray Analysis, Denver, CO; Certified Professional Chemist, Credentialed by the National Certification Commission in Chemistry and Chemical Engineering.*

Gold, S.H., *Editor, Second Special Issue of the IEEE, Transactions on Plasma Science on High Power Microwave Generation; Member, Proposal Evaluation Panel and Site Visit Committee, Office of Naval Research (ONR) and Defense Advanced Research Projects Agency (DARPA) University Research Initiative (URI) Program, Free Electron Laser Opportunities.*

Grabowski, K.S., *Cochairperson, Electrochemical Society Symposia, Bohmische Physical Society.*

Griffin, O.M., *Associate Editor, Ocean Engineering, Ocean Physics and Engineering; Member, Editorial Board, Journal of Fluids and Structures; Member, Organizing Committee, International Conference on Flow Induced Vibrations, Bowness-on-Windermere, England.*

Gubser, D.U., *Cochairperson, 1986 Applied Superconducting Conference, Baltimore, MD.; Member, Executive Committee American Physical Society.*

Dr. William A. Hoppel is "pinned" by his wife Shirley as he receives the Navy Meritorious Civilian Service Award. Hoppel was cited for his contributions in developing ion mobility and aerosol size spectrometry instrumentation and for theoretical modeling.

Hahn, T.A., *President, Thermal Expansion Symposium.*

Hubler, G.K., *Cochairperson, 1987 Materials Research Society Meeting.*

Hurdle, G., *Cochairperson, Session Z, Signal Processing and Beamforming 12th Annual International Congress on Acoustics–Associated Symposium on Underwater Acoustics, Halifax, N.S., Canada.*

Jacobs, V.L., *Fellow, American Physical Society (APS).*

Jajodia, S., *Chairperson, IEEE Computer Society, Technical Committee on Database Engineering; Member, IEEE 2nd International Data Engineering Conference, Los Angeles, CA.*

Jeck, R.K., *Member, Working Group for Aircraft Icing, National Aircraft Icing Program Council; Member, Atmospheric Environment Technical Committee, American Institute of Aeronautics and Astronautics (AIAA).*

Johnston, K.J., *Member, Committee on Space Astronomy and Astrophysics, National Research Council; Member, Visitor's Advisory Committee, National Radio Astronomy Observatory.*

Jones, H.N., *Chairperson, LTH-4 (SDI) Non–Energetic Materials Panel.*

Kabler, M. N., *Fellow, American Physical Society (APS).*

Kahn, M., *Fellow, American Ceramics Society.*

Kapetanakos, C.A., *Fellow, American Physical Society (APS); Fellow, Washington Academy of Science; Member, Accelerator Committee for the Net Technical Assessment of Charged Particle Beam Weapons; Member, Organizing Committee for the 1987 Particle Accelerator Conference.*

Karle, I.L., *Congressional Testimony, May 21, 1986, session with 1985 USA Nobel Laureates; Lifetime Achievement Award, 1986 WISE, Interagency Committee for Women in Science and Engineering; Honorary Doctor of Science degree, University of Maryland, May 24, 1986; Member, Advisory Board of Chemical and Engineering News; Lecturer, First International Meeting on Molecular Structure, Beijing, China, Sept. 1986, Subject of "Profiles in Chemistry" by Maureen Julian, Journal of Chemical Education* 63, 66–67 (Jan. 1986).

Karle, J., *National Library of Medicine Medal; Albert A. Michelson Award of the Chicago Museum of Science and Industry; Townsend Harris Medal of the Alumni Association of the City College of New York; Golden Plate Award of the Academy of Achievement; Several special lectureships and honorary doctorates; Membership on committees of the International Council of Scientific Unions, the International Union of Crystallography, and the National Academy of Sciences.*

Kaufman, B., *Editor, Advances in the Astronautical Sciences; Astrodynamics 1985; Vice–chairperson, American Astronautical Society, Technical Committee on Space Flight Mechanics; Technical Cochairperson, 1988 Astrodynamics Conference, American Institute of Aeronautics and Astronautics and American Astronautical Society.*

Keramidas, G.A., *Coeditor, Proceedings (CADMO86) and Proceedings, (CMEM86); Organizer and Cochairperson, International Conference, Computational Methods and Experimental Measurements, Sept., 1986, Greece (CMEM86); Organizer and Cochairperson, International Conference, Computer*

Aided Design, Manufacture and Operations in the Marine and Offshore Industries, CADMO86 Washington D.C., Sept. 1986; Sessions Chairperson, International Conference, Hydraulic Engineering Software, HYDROSOFT86, Southampton, England, Sept. 1986.

Killiany, J.M., *Chairman, 1986 IRIS Detector Conference; Member, Paper Selection Committee IRIS Detector Conference; Member, NAVAIR IRST Red Stripe Team; Deputy Navy, Member IR FPA Producibility Initiative Team.*

Klein, B.M., *Chairperson, International Workshop on Electronic Structure of Defects in Metals and Alloys, Argonne, Illinois, 1-13 June 1986.*

Klein, P.H., *Cochairperson, Second Workshop on Purification of Materials for Crystal Growth and Glass Processing, American Association for Crystal Growth.*

Kline, E.L., *Member, Industrial Advisory Committee, Department of Electrical Engineering, College of Engineering, West Virginia University, Morgantown, W. VA.*

Koon, W. C., *1986 American Physical Society International Prize for New Materials; Editor, 1986 Conference on Magnetism and Magnetic Materials, Baltimore, MD, Nov. 17-20, 1986; Member, Steering, Advisory and Program Committees, 1986 Conference on Magnetism and Magnetic Materials; Cochairperson, 1987 Spring Symposium on Permanent Magnet Materials, Materials Research Society, Anaheim, CA April 21-25, 1987.*

Krowne, C.M., *Member, 1986 MTT Panel for Millimeter Wave Integrated Circuit Sources.*

Kuperman, W.A., *Associate Editor, Underwater Acoustics of the Journal of the Acoustical Society of America.*

Kurfess, J.D., *Member, Committee on Space Astronomy and Astrophysics of the National Academy of Sciences; Member, NASA Headquarters Advisory panel Gamma-ray Program Working Group.*

Lampe, M., *Fellow, American Physical Society.*

Landwehr, C., *Vice-chairperson, IEEE Technical Committee on Security and Privacy; U.S. National Leader and Chairperson, Technical Panel 1 (Trustworthy Computing Technologies), Subgroup X (Computing Technology), Technical Cooperation Program; Chairperson, Database Security of Technical Committee 11, Computer Security, International Federation of Information Processing (IFIP); Member, Program Committee, IEEE Symposium on Security and Privacy; Member, Program Committee, Aerospace Computer Science Conference; Chairperson, National Computer Security Center Invitational Workshop on Database Management Security Guidelines; Best Paper Award, IEEE Symposium on Security and Privacy; Speaker, Navy/Marine Corps ADP Security Workshops.*

Lau, Y.Y., *Fellow, American Physical Society.*

Lessoff, H., *Federal Laboratory Consortium Special Award for Excellence in Technology Transfer; Member, Electronic Materials Committee, Metallurgical Society of AIME; Member, International Awards Committee, American Association of Crystal Growth; Liaision Member, Committee on Process Challenges in Compound Semiconductors, National Research Council of the National Academy of Sciences; Representative, Coordinating Committee, Multi Lateral Export Controls (COCOM); Member, Technical Working Group 5 and Technology Transfer Group F; Secretary of Organizing Committee, 3rd International Conference on Metalorganic Vapor Phase Epitaxy.*

Lindberg, R.E., *Associate Editor, Journal of the Astronautical Sciences; Member, Astrodynamics Technical Committee, American Institute of Aeronautics and Astronautics (AIAA); Council Member, National Capital Section (AIAA).*

Mack, I., *Member, Technical Program Committee, International Solid State Circuits Conference (ISSCC).*

McCafferty, E., *Chairperson, Corrosion Division, The Electrochemical Society; Member, Ways and Means Committee, The Electrochemical Society.*

Manheimer, W.M., *Senior Member, Institute of Electrical and Electronic Engineers (IEEE); Member, Office of Secretary of Defense High Power Microwave Effects Panel.*

Mariska, J.T., *Secretary, Solar Physics Division, American Astronomical Society.*

Michel, D.J., *Member, Technical Program Committee, 13th ASTM International Symposium on the Effects of Radiation on Materials; Member, Task Force on Crack Propagation Technology, Metals Properties Council and American Society of Mechanical Engineers, Boiler and Pressure Vessel Code Subcommittee on Properties of Metals; Professorial Lecturer, The George Washington University.*

Mied, R.P., *Member, University Research Initiative (URI) Review Panel for the Office of Naval Research (May–June); Chairperson, American Geophysical Union (AGU) Spring Meeting Session, "Internal Waves and Fine Structure."*

Dr. John A. Montgomery of the Tactical Electronic Warfare Division receives the Navy Meritorious Civilian Service Award. The Director of Naval Warfare, VADM James Hogg, USN, presents the award.

Moniz, W.B., *U.S. Navy Representative, Technical Panel 3, Organic Materials, Subgroup P of the Technical Cooperation Program.*

Mowery, R.L., *Chairperson, Lubricant Subcommittee, DoD Instrument Bearing Working Group; Member, Organizing Committee, Ball Bearing Symposium, 1987.*

Mueller, G.P., *Chairperson, 6th DoD Conference, Vulnerability, Survivability and Effects; Member, Organizing Committee, 6th DoD Conference, Vulnerability, Survivability and Effects.*

Murday, J. S., *Chairperson, American Vacuum Society Board of Directors, Local Arrangements Committee, 10th International Vacuum Congress; Member, Governing Board, American Institute of Physics; Member, Organizing Committee, 2nd International Conference on Scanning Tunnelling Microscopy.*

Nisenoff, M., *Treasurer, 1986 Applied Superconductivity Conference.*

Oran, E.S., *Director, Board of Directors, Progress in Energy and Combustion Science, American Geophysical Union Committee on Statutes and Bylaws; Editor, Fluid Dynamics, Physics News; Member, Publication Committee, American Institute of Aeronautics and Astronautics; Member, Organizing Committee, Symposia of the Combustion Institute; Member, Executive Committee, Fluid Dynamics Division, American Physical Society; Invited Guest, USSR Academy of Sciences, Moscow and Novosibirsk, 1986.*

Ossakow, S.L., *Member, Nominating Committee for Officers, American Physical Society (APS) Plasma Physics Division; Member, Office of Naval Research (ONR) University Research Initiative (URI) Evaluation Panel; Advisor, ONR, Ionospheric Research; Advisor, ONR URI, Stimulated Auroral Ionosphere Research; Convenor, Special Session, Plasma Instability Processes, XXIInd International Union of Radio Science (URSI) General Assembly, Tel Aviv, Israel, 1987.*

Pechacek, R.E., *Chairperson, 1986 American Physical Society, Division of Plasma Physics Convention, Baltimore, MD.*

Pierre, L. J., *Member, Command Control Communication and Intelligence (CI) Technical Committee, American Institute of Aeronautics and Astronautics (AIAA).*

Plant, W. J., *Associate Editor, Journal of Geophysical Research.*

Porter, M.B., *Chairperson, 111th Meeting, Acoustical Society of America.*

Prinz, G.A., *Chairperson, Waterfall Glenn Conference, Magnetic Materials Research Using Synchrotron Radiation, Argonne National Laboratory, October 1986; Chairperson, Metals, Magnetism and More, 4th International Conference, Molecular Beam Epitaxy, University of York, England, Sept. 1986; Chairper-*

Dr. Reintjes, representing the NRL Chapter of Sigma Xi, The Scientific Research Society, presents the 1986 Pure Science Award to Dr. Kia L. Ngai and the 1986 Applied Science Award to Dr. Robert L. Jones.

son, Monolayers and Overlayers, 31st Annual Conference, Magnetism and Magnetic Materials, Baltimore, MD, Nov. 1986.

Ramaker, D.E., *Member, Local Arrangements Committee, 10th International Vacuum Congress, Baltimore, MD.*

Rath, B.B., *Member, of the Board of Directors, and Director of Publications, Metallurgical Society of AIME; Co-Chairperson, Scholarly Activities Committee, Washington Academy of Sciences; Chairperson, Surfaces and Interfaces Committee of ASM-MSD; Member, Board of Directors, Maryland Institute of Metals; Member, Organizing Committee of the Metals Congress 1988; Member, Editorial Board of the International Metallurgical Review of ASM; Member, Honors and Awards Committee of the Washington Chapter of ASM; Member, National Materials Advisory Board, National Academy of Sciences; Navy representative for panel on Metals and Materials in Structures for the Technical Cooperation Program (TTCP) countries; Participant of the Indo-US Joint Commission on Science and Technology; Member, Advisory Board, Department of Metallurgical Engineering, Colorado School of Mines; Member, Steering Committee of the Light Metal Center, University of Virginia; Member, Advisory Board of the Materials Science Department, Carnegie-Mellon University; Panel Member, ONR University Research Initiative (URI) Program.*

Reinecke, T.L., *Secretary, Steering Committee, Greater Washington Solid State Physics Colloquium.*

Reintjes, J., *Fellow, Optical Society of America.*

Resing, H.A., *Member, Editorial Board "Langmuir"*, American Chemical Society Journal; Member, Advisory Committee, 4th International Symposium on Magnetic Resonance in Colloid and Surface Science, Munster, West Germany.*

Richmond, E.D., *Member, Technical Committee, 1986 SOS/SOI Technology Workshop; Member, Local Arrangements Committee, 33rd Nation Vacuum Symposium, 10th International Vacuum Congress, 6th International Conference on Solid Surfaces.*

Ripin, B.H., *Fellow, American Physical Society (APS); Associate Editor, Physical Review Letters and Transactions on Plasma Science; Chairperson, APS, Division of Plasma Physics (APS/DPP) Publication Committee; Senior Member, IEEE; Member, APS, Plasma Phys-*

ics Executive Committee; Member, APS/DPP Executive Committee.

Ritter, J.C., *Session Chairperson, Hardness and Survivability Session, 1986 Space Electronics Conference, Albuquerque, NM; Member, Technical Program Committee, 1986 Space Electronics Conference, Albuquerque, NM; Member, Editorial Board, Special Issue on System Generated EMP for the Journal of Defense Research.*

Rosenblum, L.J., *Chairperson, IEEE Computer Society Technical Committee, Computer Graphics.*

Dr. and Mrs. George Nelson are ready to cut the cake to celebrate his receiving the Navy Superior Civilian Service Award.

Rudgers, A.J., *Fellow, Acoustical Society of America; Chairperson, Technical Committee, Physical Acoustics, Acoustical Society of America.*

Sadananda, A.K., *Coeditor and Chairperson, Symposium on Creep and Creep-Fatigue Crack Growth, Orlando 1986; Chairperson, Symposium on the Effect of Minor Elements on Mechanical Properties; Member, ASM, Flow and Fracture Committee; Member, AIME Physical Metallurgy Committee, Structural Materials Committee; Speaker, International Conference on Creep, Tokyo, 1986.*

Saenz, A.W., *Coeditor Local and Global Methods of Nonlinear Dynamics, Proceedings of Workshop, 23–26 July, 1984, Naval Surface Weapons Center, Silver Spring, MD; Coeditor, Perspectives in Nonlinear Dynamics, Proceedings of Workshops, 28–30 May, 1985, Naval Surface Weapons Center, Silver Spring, MD; Organizer, Workshop, Methods and Applications of Nonlinear Dynamics, 1–5 Sept. 1986, Medellin, Colombia.*

Saks, N.S., *Coorganizer and lecturer, IEEE Short Course entitled "Radiation effects in Semiconductor Devices," 1986 IEEE Nuclear Science Symposium.*

Sartwell, B.D., *Editor, Journal Surface and Coatings Technology; Program Chairperson, 14th International Conference on Metallurgical Coatings; Member, Executive Committee, Vacuum Metallurgy Division, American Vacuum Society.*

Schneider, I., *Fellow, American Physical Society; Fellow, Sigma XI.*

Schultz, A.C., *President, Student Chapter, Association for Computing Machinery (ACM), George Mason University.*

Schwartz, P.R., *Chairperson, NRAO Millimeter Array Science Working Group Sub-Group; Cochairperson, NRL Incentive Awards Board; Member NSF Millimeter-Wave Observatory Site; Member, ATLAS and Subsequent Investigator's Working Group (ATLAS-IWG).*

Senasack, H.E., *Member, AIAA Space Systems Technical Committee.*

Sheeley, N.R., *Member, Scientific Committee on Solar-Terrestrial Physics (SCOSTEP) Planning Committee, Solar Interplanetary Variability; Member, SCOSTEP Steering Committee, Solar Interplanetary Variability.*

Sheinson, R.S., *Treasurer, Combustion Institute, Eastern States.*

Silberberg, R., *Member, National Nuclear Data Center; Lecturer, National Academy of Sciences Symposium, Lunar Bases and Space Activities of the 21st Century; Lecturer, International School of Cosmic Ray Astrophysics; Contributed paper, Manned Mars Missions Workgroup.*

Skelton, E.F., *Fellow, American Physical Society; Spokesperson, High Pressure Insertion Device Team, National Synchrotron Light Source, Brookhaven National Laboratory; Writer, Extended Article, "High Pressure Research," for the Encyclopedia of Physical Science and Technology..*

Skolnik, M.I., *Editor, National Academy of Engineering (IEEE) Proceedings.*

Sleger, K.J., *Publicity Chairperson, IEEE GaAs IC Symposium.*

Smidt, F. A., *Fellow, American Society for Materials (ASM).*

Smith, H.A., *Cochairperson, Strategic Defense Initiative Office (SDIO) Working Group, Solid State Photo Multiplier (SSPM) Devices.*

Spencer, J.H., *Consortium Member, US Very Long Baseline Interferometry (VLBI); Board Member, Interagency Washington Correlation Management.*

Spielman, B.E., *Vice President, Administrative Committee, IEEE Microwave Theory & Techniques Society; Chairperson, IEEE–MTTS National Technical Committees; Member, IEEE Microwave Theory & Techniques AdCom; Member, Technical Program Committee, 1986 International Microwave Symposium; Member, Technical Program IEEE Microwave and Millimeter–wave Monolithic Circuits Symposium; Member, Steering Committee, 1986 IEEE MW & MMW Monolithic Circuits Symposium; Member, Awards Committee, IEEE Cledo Brunetti Award.*

Sprangle, P., *Fellow, American Physical Society (APS); Chairperson, 9th International Free Electron Laser Conference; Member, Program Committee, 1987 Particle Accelerator Conference.*

Stamper, J.A., *Fellow, American Physical Society (APS)*

Steiger, D., *Chairperson, IEEE Computer Society Technical Committee, Oceanic Engineering and Technology; Chairperson, 4th Working Symposium, Oceanographic Data Systems.*

Strom, U., *Member, Advisory Committee, 12th International Conference, Infrared and Millimeter Waves, Orlando, Florida.*

Szu, H.H., *Editor, SPIE Advanced Institute Series, State of the Art Review on Optical and Hybrid Computing; Chairperson, Optical Society of America, Notational Standardization Committee.*

Treado, P.A., *Editor, National Nuclear Physics Summer School, Lecture Notes and Seminar Notes; Member, Southeastern University Research Association Board of Trustees; Member, NAS/NRC Ford Minority Fellowship Panel; Member, Organizing Committee, Research and Applications with Accelerators Conference; Director, National Nuclear Physics Summer School.*

Trzaskoma , P.P., *Cochairperson, National Capital Section of Electrochemical Society; Member, Publications Committee, Electrochemical Society; Member, Future Meetings Committee, Electrochemical Society.*

Tolstoy, A.I., *Chairperson, 111th Meeting of Acoustical Society of America.*

Tsao, C., *President, Sigma Xi/NRL Chapter.*

Turner, N.H., *President, American Chemical Society (ACS) Chemical Society of Washington; Member, Local Arrangement Committee, 10th International Vacuum Congress, 6th International Conference on Solid Surfaces, 33rd National Symposium of the American Vacuum Society; Secretary, Division of Colloid and Surface Chemistry, American Chemical Society.*

Valenzuela, G.R., *Chairperson, Membership Committee of Commission F, International Union of Radio Science; Representative, Scientific Committee on Oceanic Research, International Union of Radio Science.*

Van Buren, A.L., *Fellow, Acoustical Society of America; Chairperson, ANSI Working Group, Standards for Transducer Calibration; Member, Technical Program Committee, Fall Meeting, Acoustical Society of America.*

Vermillion, G.M., *Navy Commendation Medal.*

Vitkovitsky, I.M., *Chairperson, Pulse Power Panel of the Interagency Advanced Power Group.*

Vogt, P.R., *Coeditor, Vol. M., Decade North American Geology (DNAG), "Western Atlan-*

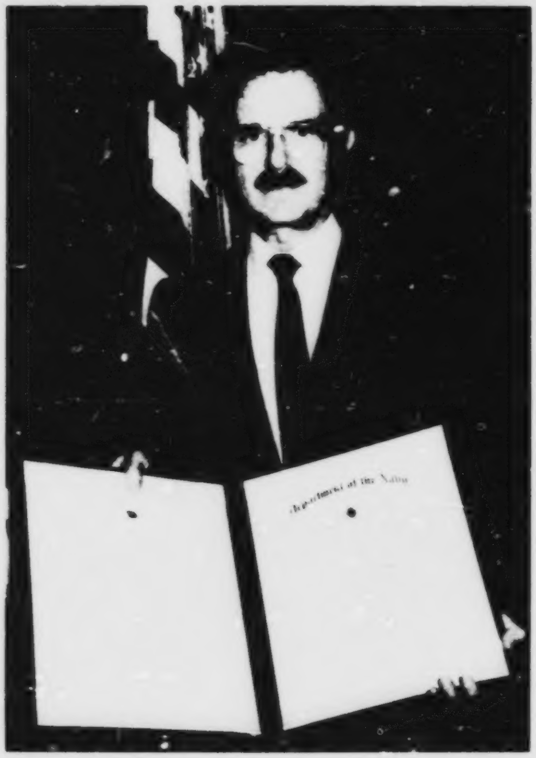

Dr. David L. Venezky, presently assigned as Scientific Director for the Office of Naval Research, London, and former Associate Superintendent and Branch Head in Chemistry Division at NRL, displays the Department of Navy Superior Civilian Service Award he received for his outstanding research accomplishments during his tenure at the Laboratory

tic Region;" Member, National Academy of Sciences Panel.

Wagner, R.J., *Member, Program Committee, 1986 US Workshop on the Physics and Chemistry of Mercury Cadmium Telluride; Member, Program Committee, IRIS Specialty Group on IR Materials.*

Wang, H.T., *Chairperson, 1986 Symposium, Offshore Mechanics and Arctic Engineering.*

Webb, A.W., *Writer, Extended Article, "High Pressure Research," Encyclopedia of Physical Science and Technology.*

Webb, D.C., *Member, Technical Program Committee, 1986 Ultrasonics Symposium IEEE; Member, Technical Program Committee, 1986 International IEEE Microwave Theory and Techniques Symposium.*

White, C.T., *Director, Condensed Matter Theory Program, Division of Materials Research, NSF.*

White, J.D., *Chairperson, 1981 Precise Time and Time Interval (PTTI) Planning Meeting.*

Willett, J. C., *Member, Committee on Atmospheric and Space Electricity, American Geophysical Union (AGU).*

Williams, C.M., *Member, National Science Foundation's Materials Research Advisory Committee.*

Williams, F.W., *Chairperson, Combustion Institute, Eastern States.*

Wolf, S.A., *Meritorious Civilian Service Award; Fellow, Acoustical Society of America; Chairperson, APS Symposium on 2D Superconductivity, March APS Meeting, Las Vegas, NV; Cochairperson, 1986 Applied Superconductivity Conference.*

Zedd, M.F., *Senior Member, Guidance Navigation, Control Technical Committee, American Institute of Aeronautics and Astronautics (AIAA).*

ALAN BERMAN RESEARCH PUBLICATION AWARDS

The Annual Research Publication Awards Program was established in 1968 to recognize the authors of the best NRL publications each year. These awards not only honor individuals for superior scientific accomplishments in the field of naval research, but also seek to promote continued excellence in research and in its documentation. In 1982, the name of this award was changed to the Alan Berman Research Publication Awards in honor of its founder.

There were 216 separate publications published in 1986 that were considered for recognition. Of those considered, 30 were selected. These selected publications represent 83 authors each of whom received a publication awards certificate, a bronze paperweight, and a booklet of the publications receiving special recognition. In addition, NRL authors share in their respective division's monetary award.

The unclassified winning papers with their respective authors are listed below by their research units. Non-Laboratory coauthors are indicated by an asterisk.

Engineering Services Division

Family of Curves for the Rough Surface Reflection Coefficient
Allen R. Miller and Emanuel Vegh[1]

An Incomplete Lipschitz-Hankel Integral of K_0, *Part I*
Allen R. Miller

Space Science Division

The Origin of the 28- to 29-Day Recurrent Patterns
of the Solar Magnetic Field
Neil R. Sheeley Jr. and C. Richard DeVore[2]

The Decay of the Mean Solar Magnetic Field
Neil R. Sheeley Jr. and C. Richard DeVore[2]

Laboratory for Computational Physics and Fluid Dynamics

High/Efficiency Targets for High-Gain Inertial Confinement Fusion
John H. Gardner and Stephen E. Bodner[3]

---

[1] Radar Division
[2] Laboratory for Computational Physics and Fluid Dynamics
[3] Plasma Physics Division

Condensed Matter and Radiation Sciences Division

Handbook of the Band Structure of Elemental Solids
Dimitri A. Papaconstantopoulos

Effects of Target Constituent Mass Difference on Collision Cascade Induced Composition Changes in Binary Alloys
Mervine Rosen, George P. Mueller, Marvin L. Roush*,
Tim D. Andreadis,* and Omer F. Goktepe*

Plasma Physics Division

Physics of Laser-Produced Interstreaming Plasmas
Barrett H. Ripin, Abdul W. Ali, Hans R. Griem, Jacob Grun,
Charles K. Manka, Edgar A. McLean, Andrew N. Mostovych, Stephen P. Obenschain,
John A. Stamper and Steve T. Kacenjar*

Numerical Simulations of Comets: Predictions for Comet Giacobini–Zinner
Joel A. Fedder, John G. Lyon, and John L. Giuliani, Jr.

Acoustics Division

Principles and Applications of Harmonic–Correlation Processing
Albert A. Gerlach

The Geology of North America, Vol. M, The Western North Atlantic Region
Peter R. Vogt and Brian E. Tucholke*

Radar Division

DDG-51 Radar Cross Section Analysis
Dale A. Zolnick and Harold L. Toothman

An Experimental NATO IFF Radar Mode Transponder Receiver
Lawrence M. Leibowitz, Richard J. Blume, Tuan A. Mai,
and Leonard A. Mastrofini

Information Technology Division

Error–Resistant Narrowband Voice Encoder
George S. Kang and Wayne M. Jewett

Advanced Development Model Broadband Linear Power Amplifier
Adrian S. Eley, Edward E. Barr, Richard K. Royce,
and Charles E. Hobbis

Tactical Electronic Warfare Division

Dynamic Field Test Measurements of IR Chaff for A-10 Decoy Protection
John A. LaFemina, William E. Howell, Mary Ann Snapp,
and Paul Huffman*

Maximizing the Miss Distance of Cruise Missiles by Means of Angle Deception Countermeasures
Sheldon I. Wolk

Underwater Sound Reference Detachment

Extensional-Wave and Flexural-Wave Contributions to the Sound Field Radiated by a Fluid-Loaded Infinite Plate
Anthony J. Rudgers, Pieter S. Dubbelday, and Lisa A. Fagerstrom

Effect of Cure Systems and Reinforcing Fillers on Dynamic Mechanical Properties of Chlorobutyl Elastomers for Potential Vibration-Control Applications
Rodger N. Capps

Laboratory for the Structure of Matter

Image Reconstruction Using Electron Microdiffraction Patterns from Overlapping Regions
John H. Konnert and Peter D'Antonio

Chemistry Division

Proton Fermi-Contact Coupling Constants from Local-Density-Functional Theory: Application to the Soliton in Polyacetylene
Carter T. White, Frank W. Kutzler,* and Michael Cook*

Correlation of Surface Acoustic Wave Device Coating Responses with Solubility Properties and Chemical Structure Using Pattern Recognition
David S. Ballantine, Jr.*, Susan L. Rose-Pehrsson, Jay W. Grate, and Henry Wohltjen*

Material Science and Technology Division

Void Formation at Phase Boundaries and Ductile Fracture of Copper-Aluminum Alloy
Virgil Provenzano and Charles M. Gilmore*

Annealing Twins in f.c.c. Metals and Alloys
Chandra S. Pande, Mohammed A. Imam, and Bhakta B. Rath

Optical Sciences Division

Parametric Raman Gain Suppression in D_2 and H_2
Michael D. Duncan, Rita Mahon*, John F. Reintjes and Lawrence L. Tankersley*

Photoemitter Membrane Light Modulator
Arthur D. Fisher, Lai-Chang Ling,* John N. Lee, and Robert C. Fukuda*

Electronics Technology Division

Identification of the Ga Interstitial in $Al_xGa_{1-x}As$ Optically Detected Magnetic Resonance
Thomas A. Kennedy and Michael G. Spencer*

In Situ, Real-Time Diagnostics of OMVPE Using IR-Diode Laser Spectroscopy
Joseph E. Butler, Nicholas Bottka, Roger S. Sillmon and David K. Gaskill*

Naval Center for Space Technology

Utility Analysis for a Space-Based Infrared Surveillance System
Joseph V. Michalowicz, Stephen Angyal, and William H. Hair*

Some Research Toward the Development of a Hologram Laser Beam Corrector-Collimator for Use in a Satellite Data Link
Charmaine Gilbreath, William H. Carter, and James W. Wagner*

CAPT Allen Miller presents the Annual Research Publication Awards to 83 authors of the 30 publications selected. The authors are recognized for superior scientific accomplishments in the field of Naval research and excellence in research and in its documentation. From the top: Susan L. Rose-Pehrsson, Chemistry Division; Dale A. Zolnick, Radar Division; Charmaine Gilbreath, Naval Center for Space Technology; and John F. Reintjes, Optical Sciences Division.

The Naval Research Laboratory has established many programs for the professional and personal development of its employees and for non-NRL professionals who choose to work at the Laboratory. Through these programs, NRL stimulates the exchange of ideas, meets critical short-term technical requirements, and provides a source of new, dynamic scientists and engineers who may better serve the needs of the Navy.

PROGRAMS FOR PROFESSIONAL DEVELOPMENT

223 **Programs for NRL People** — University education and scholarships, continuing education, professional development, and other activities

232 **Programs for Non-NRL People** — Fellowships, exchange programs, and cooperative employment

PROGRAMS FOR NRL PEOPLE

During 1986, NRL employees participated in 3300 individual training events. Many of these were presented as either video taped or on-site instructed courses on diverse technical subjects, management techniques, and enhancement of such personal skills as efficient use of time, speed reading, memory improvement, and interpersonal communications.

One common study procedure is for employees to work full-time at the Laboratory while taking job-related scientific courses at universities and schools in the Washington area. The training ranges from a single course to full graduate and postgraduate programs. Tuition for training is paid by NRL. The formal programs offered at NRL are described here.

GRADUATE PROGRAMS

- The **Advanced Graduate Research Program** (formerly the Sabbatical Study Program) enables selected professional employees to devote full time to research or pursue work in their own or a related field for one academic year at an institution of their choice without the loss of regular salary, leave, or fringe benefits. NRL pays all education costs, travel, and moving expenses for the employee and dependents. Criteria for eligibility include professional stature consistent with the applicant's opportunities and experience, a satisfactory program of study, and acceptance by the institution selected by the applicant. The program is open to paraprofessional (and above) employees who have completed 6 years of Federal Service, 4 of which are required at NRL. Since the program began in 1964, 157 employees have participated.

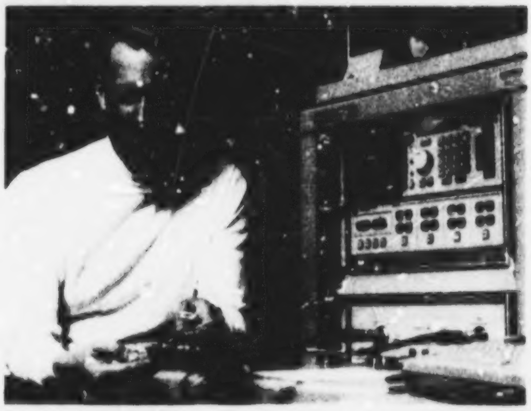

Dr. Christen Rausher of the Electronic Technology Division participated in the Advanced Graduate Research Program for one year at the Los Alamos National Laboratory, New Mexico.

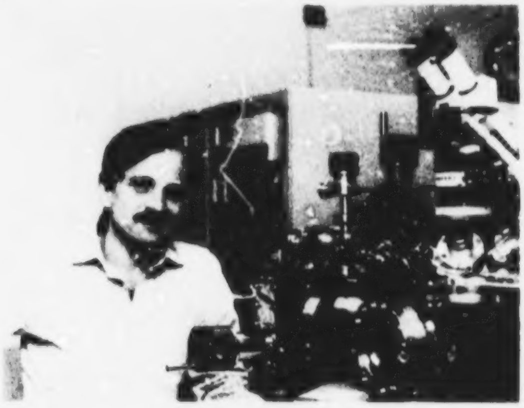

Dr. Irwin L. Singer of the Chemistry Division spent one year in England at Cambridge University doing research under the Advanced Graduate Research Program. Dr. Singer says of the occasion: "Marvelous opportunity to learn and to interact with mature scientists at Cambridge University."

- The **Edison Memorial Graduate Training Program** enables employees to pursue advanced studies in their fields at local universities. Participants in this program work 24 hours each workweek and pursue their studies during the other 16 hours. The criteria for eligibility include a minimum of 1 year of service at NRL, a bachelor's or master's degree in an appropriate field, and professional standing in keeping with the candidate's opportunities and experience.

Charmaine Gilbreath of the Naval Center for Space Technology is continuing her studies at John Hopkins University, under the Edison Memorial Training Program. In two years she hopes to receive a PhD in electrical engineering.

- To be eligible for the **Select Graduate Student Program**, employees must have a college degree in an appropriate field and must have maintained at least a B average in undergraduate study. Students accepted in this program devote a full academic year to graduate study. While attending school, they receive one half of their salary, and NRL pays for tuition, books, and laboratory expenses. During the summer, they work at the Laboratory and receive normal pay and fringe benefits. Thirty-seven staff members have enrolled in the program since it began in 1967.

- Research conducted at NRL may be used as thesis material for an advanced degree. This original research is supervised by a qualified employee of NRL who is approved by the graduate school. The candidate should have completed the required course work and should have satisfied the language, residence, and other requirements of the graduate school from which the degree is sought. NRL provides space, research facilities, and supervision but leaves decisions on academic policy to the cooperating schools.

- The **Alfred P. Sloan Fellows Program** is designed for competent young executives whose job performance indicates senior management potential. The Sloan Fellows spend 1 year with the Massachusetts Institute of Technology faculty and with policymakers in industry and government. They study the theory and practice of effective and responsible management in a rapidly changing society.

- The **Education for Public Management Program** serves the training needs of individuals who are at midcareer level and who have the talent to assume increasing responsibilities to direct agency programs and policies.

- The **Education Program for Federal Officials** is directed to the needs of a small group of Federal employees who have demonstrated high competence and unusual promise. The Woodrow Wilson School of Princeton University has developed this program to enable selected midcareer officials to enlarge their knowledge in particular disciplines, to relate their fields of specialization to the broader concerns of government, and to sharpen their capacity for objective analysis of governmental problems.

- Federal Executive fellowships are available, each year, to employees who want to study in the **Brookings Institute Advanced Study Program**. In the program, the fellow is exposed to and participates in planning, developing, and conducting educational conferences on public policy issues for leaders in public and private life.

- The **Fellowship in Congressional Operations for Executives** provides an opportunity for some of the most promising young, technically oriented Federal executives to participate in a variety of assignments designed to develop their knowledge and understanding of Congressional operations.

- The **Maxwell Midcareer Development Program** of the Maxwell Graduate School of Citizenship and Public Affairs, Syracuse, New York, is designed to increase the managerial knowledge, ability, and skills of experienced Government officials who have been identified by their agencies as having potential for advancement to positions demanding progressively greater managerial and executive responsibilities.

- The **Practicing Engineer Advanced Study Program** of the M.I.T. Center for Advanced Engineering, Cambridge, Massachusetts, enables experienced engineers and applied scientists to work in-depth in technological areas pertinent to their professions.

- The **Science and Technology Fellowship Program**, a subsidiary of the Commerce Science Program, includes a variety of special events, lectures, seminars, visits, conferences, field trips, and interactions with key persons from both the public and private sectors. Participants spend one week on Capitol Hill in an intensive, congressional orientation, and one week at the Brookings Institute Science Policy Conference. They also take two week-long field trips for on-site inspection of scientific institutions and industrial complexes.

- The **Stanford-Sloan Program of the Graduate School of Business**, Stanford, California, offers exceptional young executives an opportunity to make an intensive study of new concepts in business, to develop a top management perspective, and to broaden their intellectual horizons.

- The **Naval Postgraduate School** (NPS) in Monterey, California, provides advanced graduate study to selected Federal civilian employees who meet NPS academic requirements for the program in which they are interested, and whose employing agency is willing to act as sponsor.

CONTINUING EDUCATION

- Local colleges and universities offer **undergraduate and graduate courses** at NRL for employees interested in improving their skills and keeping abreast of current developments in their fields. These courses are also available at many other DoD installations in the Washington, DC area.

- The Employee Development Branch at NRL offers to all employees **short courses** in certain areas that are not available at local schools. Laboratory employees may attend these courses at nongovernment facilities as well. Interagency courses in management, personnel, finance, supervisory development, and clerical skills are also available.

For further information on any of the above programs, contact the Employee Development Branch (202) 767-2956.

TECHNOLOGY TRANSFER

- The **Navy Science Assistance Program** establishes an information loop between the Fleet and the R&D shore establishments to expedite technology transfer to the user. The program addresses operational problems, focuses resources to solve specific technical problems, and develops a nucleus of senior scientific personnel familiar with the impact of current research and system performance on military operations.

- The **Office of Research and Technology Applications Program** ensures the full use of the results of the Nation's Federal investment in research and development by transferring federally owned or originated technology to state and local governments and the private sector.

Inquiries concerning NRL's technology transfer programs should be made to Mr. Richard Fulper at (202) 767-3744.

PROFESSIONAL DEVELOPMENT

NRL has several programs, professional society chapters, and informal clubs that enhance the

Women in Science and Engineering (WISE)

Gwen VanHoosier, NRL's former Federal Women's Program manager, was asked what role her office played in helping to set up the WISE chapter at NRL. She answered: "I have been trying to find a way to bring the Laboratory women scientists and engineers together to share ideas and mutual concerns and to become familiar with the professional achievements of NRL women. So when informal discussions about WISE began to take place at the Laboratory, I was pleased and eager to pursue the establishment of a chapter at NRL."

Dr. Tang Hui of the Plasma Theory Branch, Plasma Physics Division, who among others was instrumental in establishing the local WISE chapter at NRL, said when asked what is the purpose of WISE: "...To provide opportunities for professional contact among women in science and engineering, to recognize the achievements of women in science and engineering, and to encourage women to seek careers in science and engineering."

Dr. Isabella Karle, right, recipient of the 1986 Women in Science and Engineering (WISE) Lifetime Achievement Award, proudly shows her awards. Dr. Martha Farmer of the Chemistry Division stands in the background.

Dr. Debra Rolison of the Surface Chemistry Branch, Chemistry Division, when asked what she likes most about WISE answered: "Our strong point is the promotion of communication among the women professionals Lab-wide. NRL has few channels for information exchange across division and directorate lines among the researchers actively creating the science and engineering. I believe the most effective channels are informal, and WISE has fostered such channels for NRL's women professionals."

Dr. Martha Farmer of the Biomolecular Engineering Branch, Chemistry Division, when asked how she has benefited from her association with WISE, said: "I believe I have benefited by having the opportunity of meeting regularly with other women professionals at the Laboratory, and obtaining and sharing knowledge of "the ropes" and how to get things done. Another benefit I see is that WISE has focused more attention on NRL women scientists and engineers and their contributions. I believe that all of us have benefited from that."

professional growth of employees. Some of these are listed below.

- The **Counseling Referral Service** (C/RS) helps employees to define short- and long-range career goals, to improve their job-seeking skills, and to deal with issues affecting job productivity. The C/RS provides individual counseling, career development, and training workshops on such topics as stress management, relaxation techniques, substance abuse, and weight control. Additionally, the C/RS is available to help employees with any kind of personal problems that may be interfering with job performance. (Contact Dr. V. Hampson at (202) 767-6857.)

- A chartered chapter of **Women in Science and Engineering** (WISE) was established at NRL in 1983. Informal monthly luncheons and seminars are scheduled to inform scientists and engineers of women's research at NRL and to provide an informal environment for members to practice their presentations. Recently, WISE initiated a colloquium series to feature outstanding women scientists. Guest speakers for the 1986 WISE colloquia were Dr. Vera Rubin of the Department of Terrestrial Magnetism, Carnegie Institution of Washington and Dr. Joanne Simpson, Laboratory for Atmospheres, NASA/Goddard Space Flight Center. (Contact Dr. Wendy Fuller at (202) 767-2793, Dr. Debra Rolison at (202) 767- 3617, or Dr. Cha-mei Tang Hui at (202) 767-4148.)

- **Sigma Xi**, the Scientific Research Society, encourages original investigation in pure and applied science. The society honors individuals who have demonstrated ability to perform original research by conferring membership and by conducting an active program in support of original research. The NRL chapter, compiled of approximately 450 members, presents annual awards in pure and applied science to outstanding NRL staff members. The chapter also sponsors lectures on a wide range of scientific topics of interest to both the scientific and government communities. Each spring the chapter sponsors an Edison Day Memorial Lecture in honor of the founder of the Laboratory. A distinguished scientist, usually a Nobel laureate, is invited to speak for the occasion. (Contact Dr. C. H. Tsao at (202) 767-2803 or Mr. Ronald Beard at (202) 767-2595.)

- Employees interested in developing effective self expression, listening, thinking, and leadership potential are invited to join either of two NRL chapters of **Toastmasters International**. Members of these clubs, who possess diverse career backgrounds and talents, meet three times a month in an effort to learn to communicate not by rules but by practice in an atmosphere of understanding and helpful fellowship. (Contact Mrs. Kathleen Parrish at (202) 767- 2782.)

Kathy Parrish, immediate past president of the Thomas Edison Toastmasters Club, awards the Able Toastmasters (ATM) badge to bulletin editor, Dr. Wade Miner

- The **Federal Executive Professional Association** (FEPA) provides testimony, recommendations, and constructive criticism of the policies of the Executive Branch on existing proposed legislation and on regulatory actions. It also assists various advisory boards and commissions concerned with professional employee relations and benefits. The FEPA meets monthly for seminars given by NRL management. (Contact Dr. Louis Beach at (202) 767-5692.)

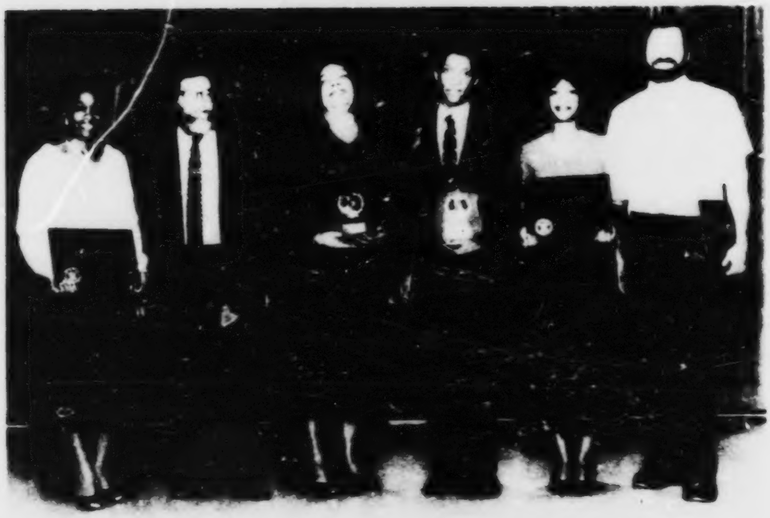

NRL's 1985 EEO Award recipients Loretta Johnson and Dr. George Carruthers (center) display their plaques. They are flanked (from left by Dr. Brenda Holmes, Dr. Joel Schnur, Gladys Stuart, and Alan Pezzulich, who received certificates of commendation.

EQUAL EMPLOYMENT OPPORTUNITY (EEO) PROGRAMS

Equal employment opportunity is a fundamental NRL policy for all persons, regardless of race, color, sex, religion, national origin, age, or physical/mental handicap. The EEO Office's major functions include affirmative action in employment; discrimination complaint process; community outreach program; EEO training for supervisors, managers, and EEO collateral duty personnel; advice and guidance to management on EEO policy; and special emphasis programs such as:

- The **Federal Women's Program** (FWP) which aims at improving employment and advancement opportunities for women in the Federal Service. The FWP provides guidance and assistance to NRL managers and supervisors in their efforts to reduce underrepresentation of women in NRL's work force.

  The FWP also sponsors awareness programs during the year to highlight concerns and issues that affect women in the workplace. A three-day program is held annually to observe the Federal Women's Week.

- The **Hispanic Employment Program** provides guidance and assistance on recruiting and ensuring equal employment opportunity to Hispanic Americans. The program is involved with Hispanic community organizations, such as "El Ingeniero" (The Engineer) that encourages Hispanic youth to pursue a career in engineering.

- The **Handicap Program** provides technical assistance to management to ensure a safe and comfortable environment for handicapped employees. It also sponsors a Handicap Summer Employment Program that places disabled college and high school students in the paraprofessional and technical positions at the Laboratory.

Special programs are held during the year to promote an awareness of the contributions and capabilities of women and minorities.

El Ingeniero paves the way to exciting careers. As part of NRL's Community Outreach Program, the Hispanic Employment Program Subcommittee sponsored a tour of the Laboratory; LT. John McEwan talks to touring students.

Julian Cummings, a mobility-impaired student, builds a computer program. Julian, a physics and astronomy major with a 4.0 average from the University of California-Berkley, came East to NRL to participate in the Handicap Summer Employment Program.

Howard "Rocky" Stone, a retired CIA officer, was the guest speaker at NRL's Handicap Awardness Day Program. He recalled his days as a CIA agent and the special problems he faced because of his hearing impairment. Here he is demonstrating a listening device used by hard-of-hearing individuals. Toni Pineau signed for hearing impaired audience members.

A Black History Month Art and Essay Contest is conducted annually for students from nearby communities. Awards are presented to the winners at the Black History Month commemorative program.

The EEO Committee sponsors a Christmas party for local school children. (Contact Ms. Sol del Ande Eaton, Deputy EEO Officer, at (202) 767-2486 for all EEO programs.)

- Other programs that enhance the development of NRL employees include computer clubs (Edison, Atari, Edison Commodore, and the NRL-IBM PC) and the Amateur Radio Club. The Recreation Club accommodates the varied interests of NRL's employees with its numerous facilities, such as a 25 -yard, 6-lane indoor swimming pool; a gymnasium with basketball, volleyball, and badminton courts; a weight room and exercise area; ping pong; meeting rooms; softball and basketball leagues; jacuzzi whirlpool; sauna; classes in karate, aerobics exercise, swimming and swimnastics; and specialized sports clubs (running, skiing, biking, golfing). The Showboaters, a nonprofit drama group that presents live theater for the enjoyment of NRL and the community, performs in two major productions each year, in addition to occasional performances at Laboratory functions and benefits for local charities. The most recent productions include "Man of La Mancha" with its famous arias "The Impossible Dream" and "Harvey." Though based at NRL, membership in Showboaters is not limited to NRL employees.

PROGRAMS FOR NON–NRL PEOPLE

Several programs have been established for non–NRL professionals. These programs encourage and support the participation of visiting scientists and engineers in research of interest to the Laboratory. Some of the programs may serve as stepping–stones to federal careers in science and technology. Their objective is to enhance the quality of the Laboratory's research activities through working associations and interchanges with highly capable scientists and engineers and to provide opportunities for outside scientists and engineers to work in the Navy laboratory environment. Along with enhancing the Laboratory's research, these programs acquaint participants with Navy capabilities and concerns.

RECENT Ph.D., FACULTY MEMBER, AND COLLEGE GRADUATE PROGRAMS

- The **National Research Council (NRC)/ NRL Cooperative Research Associateship Program** selects associates who conduct research at NRL in their chosen fields in collaboration with NRL scientists and engineers. The tenure period is 2 years. Following their tenure, the Office of Naval Research offers the associate posttenure research grants tenable at an academic institution. In 1985, 31 associates were appointed to 9 NRL divisions. In 1986, 29 associates chose appointments at NRL.

- The American Society for Engineering Education (ASEE) administers the **Office of Naval Technology (ONT) Postdoctoral Fellowship Program** which aims to increase the involvement of highly trained scientists and engineers in disciplines necessary to meet the evolving needs of naval technology. Appointments are for 1 year (renewable for a second and sometimes a third year). These competitive appointments are made jointly by ONT and ASEE.

- The American Society for Engineering Education also administers the Navy/ASEE **Summer Faculty Research Program** for university faculty members to work for 10 weeks with professional peers in participating Navy laboratories on research of mutual interest. NRL hosted 52 of these faculty participants in 1986.

- The **NRL/United States Naval Academy (USNA) Cooperative Program for Scientific Interchange** allows faculty members of the U.S. Naval Academy to participate in NRL research. This collaboration benefits the Academy by providing the opportunity for USNA faculty members to work on research of a more practical or applied nature. In turn, NRL's research program is strengthened by the available scientific and engineering expertise of the USNA faculty.

- The **Office of Naval Research Graduate Fellowship Program** helps U.S. citizens obtain advanced training in disciplines of science and engineering critical to the U.S. Navy. The 3–year program awards fellowships to recent outstanding graduates to support their study and research leading to doctoral degrees in specified disciplines such as electrical engineering, computer sciences, material sciences, applied physics, and ocean engineering. Award recipients are encouraged to continue their study and research in a Navy laboratory during the summer. Eight ONR graduate Fellows chose NRL for their summer work in 1986.

For further information about the above five programs, please contact Mrs. Jessica Hileman at (202) 767-3865.

- The **United States Naval Academy Ensign Program** assigns Naval Academy graduates to NRL to work in areas of their own choosing commensurate with their academic qualifications. These graduates provide a fruitful summer of research assistance, while gaining valuable experience in the Navy's R&D program. (Contact CDR Tom Frazier at (202) 767-2103.)

PROFESSIONAL APPOINTMENTS

- **Faculty Member Appointments** use the special skills and abilities of faculty members for periods of short duration to fill positions of a scientific, engineering, professional, or analytical nature.

- **Consultants and experts** are employed because they are outstanding in their fields of specialization, or because they possess ability of a rare nature and could not normally be employed as regular civil servants.

- **Intergovernmental Personnel Act Appointments** temporarily assign personnel from the state or local government or educational institution to the Federal Government (or vice versa) to improve public services rendered by all levels of government.

UNDERGRADUATE COLLEGE
STUDENT PROGRAMS

Several programs are tailored to the undergraduate that provide employment and work experience in naval research. These are designed to attract applicants for student and full professional employment in the Laboratory's shortage category positions, such as engineers, physicists, mathematicians, and computer scientists. The student employment programs build an understanding of NRL job opportunities among students and educational personnel so that educators can provide students who will meet NRL's occupational needs. The employment programs for college students include the following:

- The **Cooperative Education Program** alternates periods of work and study for students pursuing bachelor degrees in engineering, computer science, or the physical sciences. Several universities participate in this program.

- The **Federal Junior Fellowship Program** hires students entering college to be assistants to scientific, professional, or technical employees.

- The **Summer Employment Program** employs students for the summer in paraprofessional and technician positions in engineering, physical sciences, and computer sciences.

- The **Student Volunteer Program** helps students gain valuable experience by allowing them to voluntarily perform educationally related work at NRL.

- The **1040-Hour Appointment** employs students on a halftime basis to assist in scientific work related to their academic program.

Fred Hellrich, Associate Director, Naval Space Technology Center, gives a demonstration in the payload checkout facility to engineering students from Lincoln University, PA, during a tour of NRL.

For additional information, contact Mrs. Cathy Downing at (202) 767-3030.

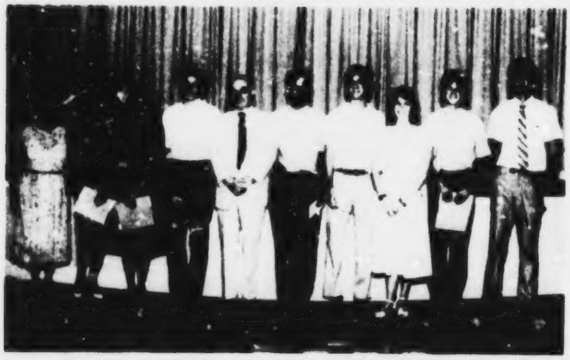

NRL's DoD science and engineering research apprentices are pictured with guest speaker Dr. Jerome Karle and program coordinator Nancy Lowry at the Sixth Annual Awards luncheon. They are, from left, Nancy Lowry; Erica Webber, Washington Academy of Science Award; Holly Stewart, Dave Venezky Award; Michael Davis, Armed Forces Communication and Electronics Association (AFCEA) Educational Fund Award; Dr. Jerome Karle; George Thomas, AFCEA Educational Award; Christopher Monsour, AFCEA Educational Award; Jodi Lowry, AFCEA Educational Award; John Rinko, AFCEA Educational Award; and Thomas Jordan, Washington Academy of Science Award.

Neicko Williams, an NRL summer intern student working in the Condensed Matter and Radiation Sciences Division, won first place in undergraduate competition in a student symposium at the 58th Annual National Technical Association Conference held at the National Aeronautics and Space Administration (NASA) Goddard Space Flight Center. His paper, "The Effects of Electron Irradiation on Vertical Junction Solar Cells," was judged most outstanding in its category. Neicko is a graduate of John F. Kennedy High School in Silver Spring, MD and is currently majoring in physics and aerospace engineering at Morehouse College in Atlanta.

HIGH SCHOOL PROGRAMS

- The **Gifted and Talented Internship Program** provides a meaningful part-time employment experience for high school graduates who plan to pursue a bachelor's degree in engineering, computer science, or the physical sciences.

- The **DoD Science & Engineering Apprentice Program** employs high school juniors and seniors to serve for 8 weeks as junior research associates. Under the direction of a mentor, students gain a better understanding of research, its challenges, and its opportunities through participation in scientific programs. Criteria for eligibility are based on science and mathematics courses completed and grades achieved; scientific motivation, curiosity, and capacity for sustained hard work; a desire for a technical career; teacher recommendations; and achievement test scores.

For additional information on these programs, please contact the Employee Development Branch at (202) 767-2956.

The Navy continues to be a pioneer in initiating new developments and a leader in using them in military operations. The primary means of informing the scientific community and the general population of the advances made at NRL is through publication of research as journal articles, reports, and conference proceedings. This chapter identifies NRL's numerous unclassified scientific publications so that their detailed information may be readily accessible to other scientists and engineers within or outside of NRL.

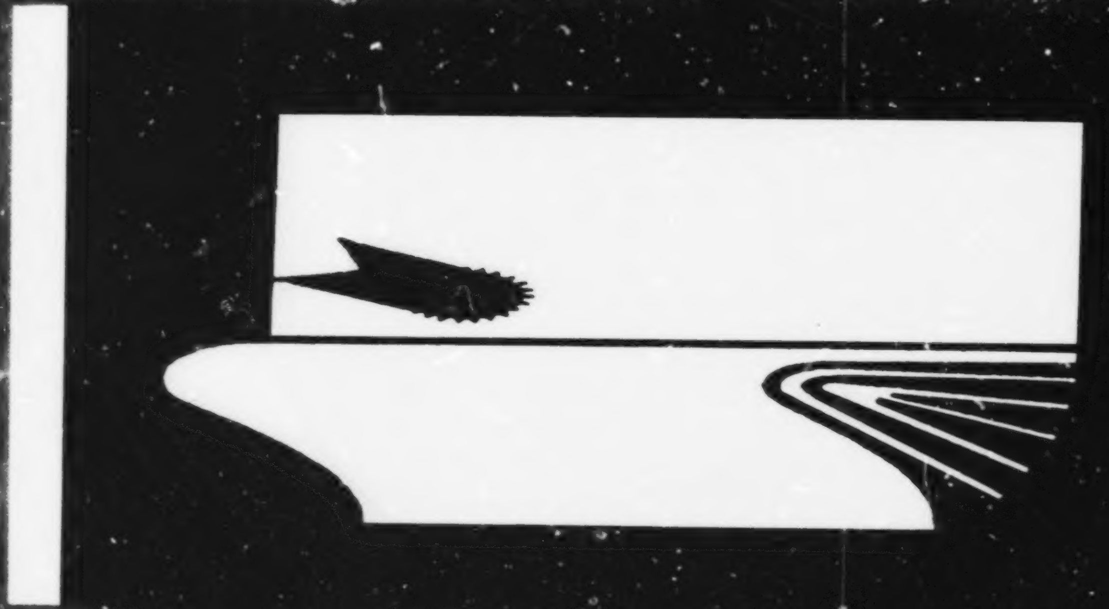

PAPERS, REPORTS, & PATENTS

PAPERS,
REPORTS,
AND
PATENTS

239 Papers in Journals, Books, and Proceedings of Meetings

278 Formal Reports

279 Patents

PAPERS IN JOURNALS, BOOKS, AND PROCEEDINGS OF MEETINGS

In several respects, NRL is like a factory–the input ingredients are the talents and ideas of the people and research funds, and the output product is information. This product is packaged in the form of reports; articles in science journals and books; papers presented to scientific societies and topical conferences; and patents.

This section lists a portion of NRL's output for 1986. The omitted parts are oral presentations, reports that carry a military security classification, and letter reports to sponsors. In the following bibliography, an asterisk identifies a coauthor who is not a member of the NRL staff.

Type of Contribution	Unclass.	Class.	Total
Papers in periodicals, books, and proceedings of meetings	583	0	583
NRL Reports	53	25	78
NRL Memorandum Reports	124	35	159
Books			6
Patents granted			62
SIRs			14

ACOUSTICS

A Multibounce Single-Scatter Ray-Theoretic Model, by Tolstoy, A , Berman, D.H., Wright, E.B., and Baer, R.N., *Journal of the Acoustical Society of America* **80**:622–632

A VAX-11/750 Based Ocean Acoustic Data Acquisition and Processing System for Shipboard and Laboratory Use, by Decina, B.A. and Padgett, J.S., *Proceedings 1986 Working Symposium on Oceanographic Data Systems*, IEEE, NY, pp. 137–144

A VAX-Based Data Acquisition and Processing System for Multi-Channel Acoustic Data, by Padgett, J.S. and Dundore, D.M., *Proceedings 1986 Working Symposium on Oceanographic Data Systems*, IEEE, NY, pp. 130–136

A Vector Parabolic Equation Model for Elastic Propagation, by Wales, S.C., *Ocean Seismo-Acoustics: Low Frequency Underwater Acoustics*, Plenum Press, NY, pp.57–66

Acoustic Reflection from Surfaces and Shapes, by Neubauer, W.G., *Naval Research Laboratory*, Washington, DC, 398pp.

Acoustic Ringing Response of the Individual Resonances of an Elastic Cylinder, by Numrich. S.K., Howell, W.E., Subrahmanyan, J.V.,* and Uberall, H., *Journal of the Acoustical Society of America* **80**:1161-1169

An Acoustic Model for Bathymetric Scattering with Low-Frequency Applications, by Baer, R.N., Perkins, J.S., Wright, E.B., and Adams, B.B., *Ocean Seismo-Acoustics: Low-Frequency Underwater Acoustics*, Plenum Press, NY, pp. 345-353

An Analysis of the Loss of Sensitivity in Porous Ceramic Hydrophones, by Rittenmyer, K.M., Dubbelday, P.S., and Ting, R.Y., *Journal of Wave-Material Interaction* 1:69-78

An Analytical Technique for Reducing the Influence of Edge Diffraction in Reflection Measurements Made on Thin Acoustical Panels, by Piquette, J.C., *Journal of the Acoustical Society of America* **80**:19-27

Application of a Neumann-Series Method to Two Problems in Acoustic Radiation Theory that are Formulated in Terms of Green's Functions, by Rudgers, A.J., *Journal of the Acoustical Society of America* **79**:1211-1222

Coherence Propagation and Geometric Acoustics, by Berman, D.H. and McCoy, J.J.,* *Journal of the Acoustical Society of America* **79**:635-643

Effect of Cure Systems and Reinforcing Fillers on Dynamic Mechanical Properties of Chlorobutyl Elastomers for Potential Vibration-Control Applications, by Capps, R.N., *Rubber Division, American Chemical Society in: Rubber Chemistry and Technology* **59**:103-122

Effects of Upper Crustal Geoacoustic Parameters on Low Frequency Sound, by Diachok, O.I., Dicus, R.L., and Wales, S.C., *Ocean Seismo-Acoustics: Low Frequency Underwater Acoustics*, Plenum Press, NY, pp. 711-720

Evaluation of New Piezoelectric Composite Materials for Hydrophone Applications, by Ting, R.Y., *American Ceramic Society Meeting in: Ferroelectrics* **67**:143-157

Experimental Confirmation of Horizontal Refraction of Sound Propagation in a Wedge-Like Ocean, by Doolittle, R., Tolstoy, A., and Buckingham, M.,* *Ocean Seismo-Acoustics: Low Frequency Underwater Acoustics*, Plenum Press, NY, pp. 169-178

Extensional-Wave and Flexural-Wave Contributions to the Sound Field Radiated by a Fluid-Loaded Infinite Plate, by Rudgers, A.J., Dubbelday, P.S., and Fagerstrom, L.A.,* *Journal of the Acoustical Society of America* **80**:932-950

Failure Analysis of Acoustic Transducer Recovered After 2351 Days (6.4 Years) in Seawater at a Depth of 494 Meters, by Hugus, G.D. and Sandwith, C.J.,* *Current Practices and New Technology in Ocean Engineering, OED* Vol 11, American Society of Mechanical Engineers, NY, pp. 259-265

Fiber Optic Acoustic Sensors, by Bucaro, J.A., Cole, J.H.,* Dandridge, A., Giallorenzi, T.G., and Lagakos, N., *Optical Testing and Metrology*, SPIE Vol. 661, SPIE-The International Society of Photo-Optical Instrumentation Engineers, Bellingham, WA, pp. 182-188

Hot-Film Anemometry Measurement of Hydroacoustic Particle Motion, by Dubbelday, P.S., *Journal of the Acoustical Society of America* **79**:2060-2066

Imaging of Long-Range Reverberation from Ocean Basin Topography, by Erskine, F.T., Bernstein, G.M., Franchi, E.R., and Adams, B.B., *Marine Geodesy* **10**:69-78

Interactions Between Acoustics and Vortex Structures in a Central Dump Combustor, by Kailasanath, K., Gardner, J., Boris, J., and Oran, E., *AIAA/ASME/ASEE 22nd Joint Propulsion Conference, Paper AIAA-86-1609*, American Institute of Aeronautics and Astronautics, NY, pp. 1-9

Linear and Nonlinear Ocean Acoustic Propagation Models, by Kuperman, W.A. and McDonald, B.E.,* *Ocean Seismo-Acoustics: Low Frequency Underwater Acoustics*, Plenum Press, NY, pp. 115-128

Mapping of Structure-Borne Intensity Using Nearfield Acoustical Holography, by Williams, E.G., Dardy, H.D., and Washburn, K.B.,* *1986 International Conference on Noise Control Engineering, Inter-Noise 86*, pp. 1247-1250

Piezoelectric Properties of Calcium-Modified Lead Titanate and its Application in Underwater Transducers, by Rittenmyer, K.M., Ting, R.Y., and Henriquez, T.A., *Journal of the Acoustical Society of America* **79**:2073- 2076

Reverberation Mapping for Basin-Wide Bathymetric Surveys, by Schifter, D.E., Franchi, E.R., Griffin, J.M., and Adams, B.B., *Marine Geodesy* **10**:1-33

Rough Surface Elastic Wave Scattering in a Horizontally Stratified Ocean, by Kuperman, W.A. and Schmidt, H.,* *Journal of the Acoustical Society of America* **79**:1767-1777

Seamount Height Estimation from Long-Range, Low Frequency Acoustic Backscatter, by Erskine, F.T., Franchi, E.R., and Adams, B.B., *Ocean Seismo-Acoustics: Low Frequency Underwater Acoustics*, Plenum Press, NY, pp. 335- 344

Spherical Wave Scattering by an Elastic Solid Cylinder of Infinite Length, by Piquette, J.C., *Journal of the Acoustical Society of America* **79**:1248-1259

Statistical Characterization of Small Scale Bottom Topography as Derived from Multibeam Sonar Data, by Czarnecki, M. and Bergin, J., *Proceedings 1986 Working Symposium on Oceanographic Data Systems*, IEEE, NY, pp. 15-24

The Sound-Speed Structure, by Hurdle, B.G., *The Nordic Seas*, Springer-Verlag, NY, pp. 155-181

ARTIFICIAL INTELLIGENCE

Globally Connected Network Models for Computing Using Fine-Grained Processing Elements, by Szu, H., *Proceedings of the International Conference on Lasers '85, Society for Optical and Quantum Electronics*, McLean, VA, pp. 92-97

Independence and Bayesian Updating Methods, by Johnson, R.W., *Uncertainty in Artificial Intelligence*, Elsevier Science Publishers B.V. (North Holland), NY, pp. 197-201

Relative Entropy, Probabilistic Inference and AI, by Shore, J.E., *Artificial Intelligence*, Elsevier Science Publishers B.V.(North Holland), NY, pp. 211-215

ATMOSPHERIC SCIENCE

Atmospheric Electricity in the Planetary Boundary Layer, by Hoppel, W.A., Anderson, R.V., and Willett, J.C., *The Earth's Electrical Environment*, National Academy Press, Washington, DC, pp. 149-165

Climatology, by Gathman, S.G., *The Nordic Seas*, Springer-Verlag, NY, pp. 1-20

Comments on the Paper "Heterogeneous Nucleation of Water Vapor on Monodisperse Ag and NaCl Particles with Diameters Between 6 and 18 nm," by Hoppel, W.A. and Alofs, D.J.,* *Aerosol Science and Technology* **5**:487-490

Down Looking Lidar Inversion Constrained by Ocean Reflection and Forward Scatter of Laser Light, by Hooper, W.P. and Gerber, H., *Applied Optics* **25**:689-697

Effect of Nonprecipitating Clouds on the Aerosol Size Distribution in the Marine Boundary Layer, by Hoppel, W.A., Frick, G.M., and Larson, R.E., *Geophysical Research Letters* **13**:125–128

Ion–Aerosol Attachment Coefficients and the Steady–State Charge Distribution on Aerosols in a Bipolar Ion Environment, by Hoppel, W.A. and Frick, G.M., *Aerosol Science and Technology* **5**:1–21

BIOSCIENCES

Adaptive Invariant Novelty Filters, by Szu, H.H. and Messner, R.A.,* *Proceedings of the IEEE* **74**:518–519

CERAMICS, PLASTICS, AND GLASSES

A Quantitative Explanation of the Difference in the Temperature Dependence of the Viscoelastic Softening and Terminal Dispersions of Linear Amorphous Polymers, by Ngai, K.L. and Plazek, D.J.,* *Journal of Polymer Science Part B: Polymer Physics* **24**:619–632

Effect of Fiber Coatings and Composite Processing on Properties of Zirconia–Based Matrix SiC Fiber Composites, by Bender, B., Shadwell, D., Bulik, C., Incorvati, L., and Lewis, D., *American Ceramic Society Bulletin* **65**:363–369

Effects of Self–Propagating Synthesis Reactant Compact Character on Ignition, Propagation and Resultant Microstructure, by Rice, R.W.,* Richardson, G.Y., Kunetz, J.M., Schroeter, T., and McDonough, W.J., *Ceramic Engineering and Science Proceedings* **7**:737–750

Frequency and Temperature Dependence of Elastic Moduli of Polymers, by Lagakos, N., Jarzynski, J.,* Cole, J.H., and Bucaro, J.A., *Journal of Applied Physics* **59**:4017–4031

Grain Size Dependence of SbSI with Oriented Grains, by Yon, K., Kahn, M., Rice, R.W.,* and Spann, J.R.,* *86th Annual Meeting of the American Ceramic Society in: Advanced Ceramic Materials* **1**:64–67

Hot Rolling of Ceramics Using Self–Propagating High Temperature Synthesis, by Rice, R.W.,* McDonough, W.J., Richardson, G.Y., Kunetz, J.M., and Schoeter, T., *American Ceramic Society 87th Annual Meeting in: Ceramic Engineering and Science Proceedings* **7**:751–760

Hot–Pressing of Ceramics Using Self–Propagating Synthesis, by Richardson, G.Y., Rice, R.W.,* McDonough, W.J., and Schroeter, T., *10th Annual Conference on Composites and Advanced Ceramic Materials in: Ceramic Engineering and Science Proceedings* **7**:761– 770

Interpretation of Differences in Temperature and Pressure Dependences of Density and Concentration Fluctuations in Amorphous Poly(phenylmethyl siloxane), by Ngai, K.L. and Fytas, G., *Journal of Polymer Science: Part B: Polymer Physics* **24**:1683–1694

Lattice Parameters and Density for Y_2O_3–Stabilized ZrO_2, by Ingel, R.P. and Lewis, D., *Journal of the American Ceramic Society* **69**:325–332

Low–Frequency Vibrational Modes and the Far Infrared Dielectric Loss in Glasses, by Strom, U., *Physical Review Letters* **56**:2110

Mechanical Failure Characteristics of Ceramic Multilayer Capacitors, by McKinney, K.R., Rice, R.W.,* and Wu, C.C., *Journal of the American Chemical Society* **69**:C-228–C-230

Nonlinear Viscoelasticity and Yield of Glassy Polymers: A New Approach, by Ngai, K.L., Rendell, R.W.,* Yee, A.F.,* and Bankert, R.J.,* *International Symposium on Non- Linear Deformation, Fracture and Fatigue of Polymeric Materials in: Polymer Preprints* **27**:83

Novel Ceramic Microstructures and Nanostructures from Advanced Processing, by Bender, B.A., Ingel, R.P., McDonough, W.J., and Spann, J.R., *Advanced Ceramic Materials* **1**:137–144

Oxidation Resistant C–C Composites, by Markels, J.H., Beyers, S.A., Wu, C.C., and Spann, J.R.,* *Metal Matrix, Carbon and Ceramic Matrix Composites*, NASA CP-2445, pp. 261–276

Raman Scattering and Electron Spin Resonance Studies of Fluorozirconate Glasses, by Freitas, J.R.,* Strom, U., and Tran, D.C., *Journal of Non-Crystalline Solids* **81**:303–317

Rapid EDXD Studies of Isothermal Crystallization of Metallic Glasses, by Qadri, S.B.,* Elam, W.T., Ayers, J.D., Vold, C.L., Skelton, E.F., and Webb, A.W., *Proceedings of the International Conference on X-Ray and VUV Synchrotron Radiation Instrumentation in: Nuclear Instruments and Methods in Physics Research* **A246**:817–819

Stabilized Zirconia–Alumina Thin Films, by Gilmore, C.M.,* and Quinn, C.,* Skelton, E.F., Gossett, C.R., Qadri, S.B.,* *13th International Conference on Metallurgical Coatings in: Journal of Vacuum Science and Technology A* **4**:2598–2600

CHEMISTRY

A Calorimetric and Infrared Spectroscopic Study of the Stabilizing Solute Proline, by Rudolph, A.S. and Crowe, J.H.,* *Biophysical Journal* **50**:423–430

A Comparison of the One-Dimensional Band Structures of Ni Tetrabenzoporphyrins and Phthalocyanine Conducting Polymers, by Kutzler, F.W. and Ellis, D.E.,* *Journal of Chemical Physics* **84**:1033–1038

A General Method for the Synthesis of Diacetylenic Acids, by Singh, A.* and Schnur, J.M., *Synthetic Communications* **16**:847–852

A Polymeric Solid-State Electrochromic Cel, by Calvert, J.M.,* Manuccia, T.J., and Nowak, R.J., *Journal of the Electrochemical Society* **135**:951–953

A Revised Rydberg Formula for Two-Electron Systems: I. (core)ns^2, by Wang, H.T., *Journal of Physics B. Atomic and Molecular Physics* **19**:3401–3410

A Stable Intrinsically Conductive Polymer, by Keller, T.M., *Journal of Polymer Science: Part C: Polymer Letters* **24**:211–214

Activation Energies for Thermal Desorption of Hydroxyl Radicals from Single-Crystal Platinum (111) and Polycrystalline Platinum Foil Surfaces, by Hsu, D.S.Y., Hoffbauer, M.A.,* and Lin, M.C., *Langmuir* **2**:302–304

Amidoxime-Functionalized Coatings for Surface Acoustic Wave Detection of Simulant Vapor, by Jarvis, N.L.,* Lint, J., Snow, A.W., and Wohltjen, H.,* *Fundamentals and Applications of Chemical Sensors, ACS Symposium Series 309*, American Chemical Society, Washington, DC, pp. 309–319

An Equilateral Triangle of Spin-1/2 Nuclei in a Uniaxial System: NMR Spectra, Molecular Motions, Order Parameter and Potential Energy Function for AsF_3 Intercalated in $C_{40}AsF_6 . 2CH_3NO_2$, by Miller, G.R.,* Moran, M.J.,* Resing, H.A., and Tsang, T.,* *Langmuir* **2**:194–203

Applications of the LCGTO-$X\alpha$ Method to Transition Metal Carbonyls, by Rosch, N.,* Jorg, H.,* and Dunlap, B.I., *Quantum Chemistry: The Challenge of Transition Metals and Coordination Chemistry*, NATO ASI Series C, Vol. 176, D. Reidel Publishing Co., Boston, MA, pp. 179–187

Atomic Data and Spectral Line Intensities for the Beryllium Isoelectronic Sequence (Ar XV Through Kr XXXIII), by Bhatia, A.K.,* Feldman, U., and Seely, J.F., *Atomic Data and Nuclear Data Tables* **35**:449–472

Autoxidation of Nitrogen Heterocycles. 3. Solvent Effects in the Autoxidation of 2,

5–Dimethylpyrrole, by Beaver, B.D., Cooney, J.V., and Watkins, J.M.,* *Journal of Heterocyclic Chemistry* **23**:1095–1097

Characterization and Stability Properties of Polar Extracts Derived from a Recent Shale Liquid, by Mushrush, G.W., Cooney, J.V., Beal, E.J., and Hazlett, R.N., *Fuel Science Technology International* 4:103–125

Charge Transfer, Polarization, and Relaxation Effects on the Auger Line Shape of Si, by Ramaker, D.E.,* Hutson, F.L.,* Turner, N.H., and Mei, W.N.,* *Physical Review B* **33**:2574–2588

Correlation of Surface Acoustic Wave Device Coating Response with Solubility Properties and Chemical Structure Using Pattern Recognition, by Ballantine, D.S.,* Rose, S.L., Grate, J.W., and Wohltjen, H.,* *ACS National Meeting in*: *Analytical Chemistry* **58**:3058–3066

Dehydrogenation of Isobutane by Oxygen–Deficient Cobalt/Oxygen Cluster Ions, by Freas, R.B. and Campana, J.E.,* *Journal of the American Chemical Society* **108**:4659–4661

Derivatives of Phthalocyanines Prepared for Deposition as Thin Films by the Langmuir–Blodgett Technique, by Barger, W.R., Snow, A.W., Wohltjen, H.,* and Jarvis, N.L.,* *Second International Conference on Langmuir– Blodgett Films in*: *Thin Solid Films* **133**:197–206

Detection of Hazardous Gases and Vapors: Pattern Recognition Analysis of Data from an Electrochemical Sensor Array, by Stetter, J.R.,* Jurs, P.C.,* and Rose, S.L., *Analytical Chemistry* **58**:860–866

Diode Laser Spectroscopy of Chemical Moieties at Surfaces, by Butler, J.E., Bermudez, V.M., and Rubinovitz, R.L., *Laser Applications in Chemistry*, SPIE Vol. 669, SPIE–The International Society of Photo–Optical Instrumentation Engineers, Bellingham, WA, pp. 125–127

Direct Fatty Acid Profiling of Complex Lipids in Intact Algae by Fast–Atom–Bombardment Mass Spectrometry, by Ross, M.M., Neihof, R.A., and Campana, J.E., *Analytica Chimica Acta* **181**:149–157

Effect of Covalent Attachment of Immunoglobulin Fragments on Liposomal Integrity, by Bredehorst, R.,* Ligler, F.S., Kusterbeck, A.W.,* Chang, E.L., Gaber, B.P., and Vogel, C.W., *Biochemistry* 25:5693

Effect of Water on the Strength of Filled Polychloroprene Vulcanizates, by Hinkley, J.A.* and Holmes, B.S., *Journal of Applied Polymer Science* 32:4873–4881

Effects of Three Stabilizing Agents – Proline, Betaine, and Trehalose – on Membrane Phospholipids, by Rudolph, A.S., Crowe, J.H., and Crowe, L.M., *Archives of Biochemistry and Biophysics* **245**:134–143

Electric Discharge–Induced Oxidation of Hydrogen Cyanide, by Fraser, M.E.* and Sheinson, R.S., *Plasma Chemistry and Plasma Processing* **6**:27– 38

Electrodeposition of Tantalum Silicide Coatings from Molten Salts, by Stern, K.H. and Williams, C.E., *Electrochemical Society Meeting – Electrodeposition Symposium in*: *Journal of the Electrochemical Society* **133**:2157– 2160

Electronic Detection of Synthetic Lubricant Oxidative Breakdown, by Bolster, R.N. and Wohltjen, H., *40th Annual Meeting of ASLE in*: *ASLE Transactions* **29**:377–382

Evidence for a Sedimentary Siloxane Horizon, by Pellenbarg, R.E. and Tevault, D.E., *Environmental Science and Technology* **20**:743–744

Fabrication of an Integrated Optical Waveguide Chemical Vapor Microsensor by Photopolymerization of a Bifunctional Oligomer, by Giuliani, J.F., Kim, K.H., and Butler, J.E., *Applied Physics Letters* **48**:1311–1313

Fast-Atom Bombardment and Chemical Ionization/Fast-Atom Bombardment Mass Spectrometry of Lubricants, by Freas, R.B. and Campana, J.E.,* *Analytical Chemistry* **58**:2434–2438

Fluoroepoxy Resin for Moisture Vapor Barrier Coating and Other Applications, by Lee, S.Y.* and Griffith, J.R., *Industrial and Engineering Chemistry Product Research and Development* **25**:572–577

Friction and Surface Chemistry of Implantation Modified Metal/Carbide Composite, by Dillich, S.A.* and Singer, I.L., *International Conference on Surface Modifications and Coatings in: Surface and Coatings Technology* **29**:207–220

Geometry Optimization Using Local Density Functional Methods, by Dunlap, B.I., *Symposium on the Applications of Density Functional Theory to Chemistry in: Journal of Physical Chemistry* **90**:5524–5529

Heteroatom Effects in Heterocyclic Ring Chain Polymers, by Mintmire, J.W., White, C.T., and Elert, M.L.,* *Synthetic Metals* **16**:235–243

Influence of Complete Enclosure on Liquid Pool Fires, by Tatem, P.A., Williams, F.W., Ndubizu, C.C.,* and Ramaker, D.E.,* *Combustion Science and Technology* **45**:185

Infrared Absorption of Solid Nitrogen Activated by CO_2, H_2O and C_2N_2, by DiLella, D.P.,* and Tevault, D.E., *Chemical Physics Letters* **126**:38–42

Infrared Diode Laser Spectroscopy of the SCl Radical in the $X^2\Pi_{3/2}$ State, by Yamada, C.,* Butler, J.E., Kawaguchi, K.,* Kanamori, H.,* and Hirota, E.,* *Journal of Molecular Spectroscopy* **116**:108–111

Inhibition of Dehydration-Induced Fusion Between Liposomal Membranes by Carbohydrates as Measured by Fluorescence Energy Transfer, by Womersly, C., Uster, P., Rudolph, A.S., and Crowe, J.H., *Cryobiology* **23**:245–255

Ion-Molecule Reaction Studies of Mass Selected Carbon Cluster Ions Formed by Laser Vaporization, by McElvaney, S.W., Creasy, W.R., and O'Keefe, A., *Journal of Chemical Physics* **85**:632–633

Kinetic Study of the Reaction $CH(X^2\pi) + H_2$ ($\rightleftharpoons$) $CH_2(X^3B_1) + H$ in the Temperature Range 372 to 675 K, by Zabarnick, S., Fleming, J.W., and Lin, M.C., *Journal of Chemical Physics* **85**:4373–4376

Kinetics and Mechanism of the Thermal Decomposition of Dimethylnitrosamine at Low Temperatures, by Lloyd, S.A., Umstead, M.E., and Lin, M.C., *Journal of Energetic Materials* **3**:187

Kinetics of the Reaction of CH_3S with NO, NO_2 and O_2, by Balla, R.J., Nelson, H.H., and McDonald, J.R. *Chemical Physics* **109**:101–107

LCAO-Xα Calculations of Rotational Energy Barriers – Prototypes of Chemical Reaction, by Dunlap, B.I. and Cook, M., *5th International Congress on Quantum Chemistry in: International Journal of Quantum Chemistry* **29**:767–777

Laser Photolysis of 2, 6 Dinitrotoluene in Solution, by Atherton, S.J.* and Craig, B.B., *Chemical Physics Letters* **127**:7–12

Laser-Induced Reactions of NO_2 in the Visible Region. II. Kinetics and Mechanistic Study of the NO_2–CO System, by Umstead, M.E., Lloyd, S.A., and Lin, M.C., *Applied Physics* **B39**:55–59

Laser-Induced Reactions of NO_2 in the Visible Region. III. Adamantane Nitration in the Liquid Phase, by Umstead, M.E. and Lin, M.C., *Applied Physics* **B39**:61–63

Liposome-Encapsulated Hemoglobin as a Red Cell Surrogate: Preparation Scale-Up, by Beissinger, R.L.,* Farmer, M.C., and Gossage, J.L.,* *Transactions of American Society for Artificial Internal Organs* **32**:58–63

Mechanisms of Synfuel Degradation. 3. Interactive Effects in Nitrogen Compound Induced Storage Instability in Shale Derived Diesel Fuel, by Cooney, J.V.. Beal, E.J., and Beaver, B.D., *Fuel Science and Technology International* **4**:1–18

Methyl Production from Trimethylgallium Decomposition and the Effect of Added Hydrazine, by Squire, D.W., Dulcey, C.S., and Lin, M.C., *Thin Films – Interfaces and Phenomena, Materials Research Society Symposia Proceedings Vol. 54*, Materials Research Society, Pittsburgh, PA, p. 709

Microscopic Model for Propagation of Shock–Induced Detonations in Energetic Solids, by Peyrard, M.,* Odiot, S.,* Oran, E., Boris, J., and Schnur, J., *Physical Review B* **33**:2350–2363

Microsensor Vapor Detectors Based on Coating Films of Phthalocyanine and Several of its Metal Complexes, Mixed $MgSO_4$–Na_2SO_4 Effects in the 973 K Hot Corrosion of CoCrAlY, by Jones, R.L. and Williams. C.E., *Journal of the Electrochemical Society* **133**:217–223

Microsensor Vapor Detectors Based on Coating Films of Phthalocyanine and Several of Its Metal Complexes, by Barger, W.R., Wohltjen, H.,* Snow, A.W., Lint, J., and Jarvis, N.L.,* *Fundamentals and Applications of Chemical Sensors, ACS Symposium Series 309*, American Chemical Society, Washington, DC, pp. 155–165

Modeling of Nonlinear Longitudinal Instability in Solid Rocket Motors, by Baum, J.D. and Levine, J.N.,* *36th Congress of the International Astronautical Federation in: Acta Astronautica* **13**:339–348

Molecular Modeling of the Phospholipid Bilayer, by Gaber, B.P., Chandrasekar, I., and Lowery, A.H., *American Chemical Society, Polymer Symposium in: Polymer Preprints* **27**:31

Molecular Theory and Cooperative Mechanism of Shock Waves – Induced Detonations in Energetic Molecular Crystals, by Odiot, S., Peyrard, M., Schnur, J., and Oran, E., *International Journal of Quantum Chemistry* **29**:1625–1634

Molten Salt Solution Chemistry in Low Temperature Hot Corrosion, by Jones, R.L., *The Interaction of Molten Salts and Metals. Current Understanding of Hot Corrosion and New Approaches to Practical Problems, Molten Salts Discussion Group*, Leeds University, Leeds, U.K., pp. 129–133

Multiphoton Ionization Spectroscopy and Vibrational Analysis of a 3p Rydberg State of the Hydroxymethyl Radical, by Dulcey, C.S. and Hudgens, J.W.,* *Journal of Chemical Physics* **84**:5262– 5270

Multiphoton–Ionization/Mass Spectrometric Detection of Gallium Atom During the Trimethylgallium CVD Reaction, by Squire, D.W., Dulcey, C.S.,* and Lin, M.C., *Chemical Physics Letters* **131**:112–117

Multiple–Quantum NMR Study of Clustering in Hydrogenated Amorphous Silicon, by Baum, J.,* Gleason, K.K.,* Pines, A.,* Garroway, A.N., and Reimer, J.A.,* *Physical Review Letters* **56**:1377–1380

NMR Images of Solids, by Chingas, G.C.,* Miller, J.B., and Garroway, A.N., *Journal of Magnetic Resonance* **66**:530–535

Nitration of 4–Nitro–N, N– dimethylbenzylamine. Formation of 2–Methyl–6–nitroindazole, by Boyer, J.H.,* Pagoria, P.F.,* Pillai, T.P.,* Pace, M.D., and Stec, D., *Journal of Chemical Research(S) Issue 11*:416–417

Nonlinear UV Excitation: Neutral vs. Ionic Channels of Molecular Fragmentation, by Craig, B.B.. Faust, W.L., and Chattopadhyay, S.K.,* *Journal of Chemical Physics* **85**:4995–4996

Numerical Simulations of the Cellular Structure of Detonations in Liquid Nitromethane – Regularity of the Cell Structure, by Guirguis, R.,* Oran, E.S., and Kailasanath, K., *Combustion and Flame* **65**:339–365

On the Importance of the Reaction $CH_2+N_2 \rightarrow HCN+NH$ as a Precursor for Prompt NO Formation, by Sanders, W.A.,* Lin, C.Y.,* and Lin, M.C., *Combustion Science and Technology* **51**:103

Oxygen Absorption by 2,5- Dimethylpyrrole Doped Fuel. Measurement Under Conditions of Accelerated Storage, by Cooney, J.V. and Wechter, M.A.,* *Fuel* **65**:433–436

Pattern Generation at the Solidification Front as Examined from Traces in the Solid: Forbidden Cells, by Resing, H.A. and Nachtrieb, N.H.,* *Journal of Crystal Growth* **78**:69–84

Prevention of Fusion and Leakage in Freeze-Dried Liposomes by Carbohydrates, by Crowe, L.M., Womersley, C., Crowe, J.H., Reid, D., Appel, L., and Rudolph, A.S., *Biochimica et Biophysica Acta* **861**:131–140

Production and Reactions of the Isopropoxy Radical, by Balla, R.J., Nelson, H.H., and McDonald, J.R., *Proceedings of the Seventeenth International Symposium on Free Radicals, NBS Special Publication 716*, National Bureau of Standards, Gaithersburg, MD, pp. 30–31

Production of Large Carbon Cluster Ions by Laser Vaporization, by O'Keefe, A., Ross, M.M., and Baronavski, A.P., *Chemical Physics Letters* **130**:17–19

Production of OH from the Collision-Free Photodissociation of Nitromethane at 266 nm, by Zabarnick, S., Fleming, J.W., and Baronavski, A.P., *Journal of Chemical Physics* 85:3395–3400

Properties of Graphitized Carbon Fiber-Halogen Residue Compounds, by Dominguez, D.D., Murday, J.S., Ehrlich, A.C., and Gillespie, D.J., *Carbon* **24**:1–13

Proton Fermi-Contact Coupling Constants from Local Density-Functional Theory: Application to the Soliton in Polyacetylene, by White, C.T., Kutzler, F.W., and Cook, M., *Physical Review Letters* **56**:252–255

Quantitative Analysis of Mixtures by Auger Electron Spectroscopy, by Turner, N.H. and Lee, W.W.,* *Applied Surface Science* **25**:345–354

Quantitative Determination of Corrosion Inhibitors in Middle Distillate Jet Fuels by Gel Permeation Chromatography, by Hardy, D.R., Black, B.H.,* and Wechter, M.A.,* *Journal of Chromatography* **366**:351–361

Radiative Lifetimes and Kinetic Studies of Metastable $NO^+(a^3\Sigma^+)$ and $O_2(a^4\Pi u)$, by O'Keefe, A. and McDonald, J.R., *Chemical Physics* **103**:424–436

Reaction Dynamics of NC_2 Decomposition on Ge: An Example of Dissociative Desorption, by Modl, A.,* Robota, H.,* Segner, J.,* Vielhaber, W.,* Lin, M.C., and Ertl, G., *Surface Science* **169**:L341– L347

Reaction Dynamics of $O(^1D_2)+H_2$, HD, D_2:OH, $OD(X^2\Pi i)$ Product Internal Energy Distributions, by Butler, J.E., Jursich, G.M.,* Watson, A.,* and Wiesenfeld, J.R.,* *Journal of Chemical Physics* **84**:5365–5377

Reaction Kinetics of OH with Nitromethane Dimethylnitrosamine and 1, 3, 5-Trioxane: Photolytic Production of OH from Nitromethane at 266 nm, by Zabarnick, S.S., Fleming, J.W., Baronavski, A.P., and Lin, M.C., *Proceedings of the Seventeenth International Symposium on Free Radicals, NBS Special Publication 716*, National Bureau of Standards, Gaithersburg, MD, pp. 731–756

Reaction of Vanadium Compounds with Ceramic Oxides, by Jones, R.L., Williams, C.E., and Jones, S.R., *Journal of the Electrochemical Society* **133**:227–230

Removal of Static Field Inhomogeneity and Chemical Shift Effects in NMR Imaging, by Miller, J.B. and Garroway, A.N., *Journal of Magnetic Resonance* **67**:575–579

Residual Depth Profile in the Evaluation of Granular Adsorbent, by Deitz, V.R., *Nuclear Technology* **73**:96–101

Resonance Raman Spectra of Langmuir–Blodgett Monolayers, by DiLella, D.P., Barger, W.R., Snow, A.W., and Smardzewski, R.R., *Second International Conference on Langmuir–Blodgett Films in: Thin Solid Films* **133**:207–217

Reversible Thermochromism in Photopolymerized Phosphatidylcholine Vesicle, by Singh, A.,* Thompson, R.B., and Schnur, J.M., *Journal of the American Chemical Society* **108**:2785–2787

Rotational Energy Accomodation in OH Radicals Desorbing from a Polycrystalline Pt Foil and a Pt(111) Single Crystal, by Hoffbauer, M.A.,* Hsu, D.S.Y., and Lin, M.C., *Journal of Chemical Physics* **84**:532–534

Ru and Os Film Deposition from Metal Carbonyls, by Berry, A.D., Brown, D.J.,* Kaplan, R., and Cukauskas, E.J., *Journal of Vacuum Science and Technology A* **4**:215–218

Second Harmonic Generation of the Silver Electrode Interface in the Presence of Phthalazine, by Voss, D.F., Nagumo, M., Goldberg, L.S., and Bunding, K.A., *Journal of Physical Chemistry* **90**:1834–1838

Second International Symposium on Analysis and Detection of Explosives, by Garroway, A.N., *European Science Notes* **40**:459–461

Secondary Ion Mass Spectrometry: Polyatomic and Molecular Ion Emission, by Colton, R.J., Ross, M.M., and Kidwell, D.A., *Proceedings of the 11th International Conference on Atomic Collisions in Solids in: Nuclear Instruments and Methods in Physics Research* **B 13**:259–277

Selective Responses of Polymeric–Film–Coated Optical Waveguide Devices to Water and Toxic Volatile Compounds, by Giuliani, J.F., Jarvis, N.L.,* and Snow, A., *Fundamentals and Applications of Chemical Sensors, ACS Symposium Series 309, American Chemical Society, Washington, DC pp. 320-329*

Shock–Moderated Chemistry: Diffusion–Controlled Quenching in Solutions at kbar Pressures, by Justus, B.L., Huston, A.L., and Campillo, A.J., *Chemical Physics Letters* **128**:274–279

Simultaneous Electrical Conductivity and Piezoelectric Mass Measurements on Iodine–Doped Phthalocyanine Langmuir–Blodgett Film, by Snow, A.W., Barger, W.R., Klusty, M., Wohltjen, J.,* and Jarvis, N.L.,* *Langmuir* **2**:513–519

Single–Photon IR Laser Photochemistry of 2–Chloroethanol in Solid Rare Gases, by Hoffman, W.F.,* Aspiala, A.,* and Shirk, J.S., *Journal of Physical Chemistry* **90**:5706–5710

Soliton Defects in Polyacetylene: Local–Density Functional Results, by Kutzler, F.W., White, C.T., and Mintmire, J.W., *International Journal of Quantum Chemistry* **29**:793–797

Spectrum and Energy Levels of Br XXV, Br XXIX, Br XXX and Br XXXI, by Feldman, U., Seely, J.F., Brown, C.M., Ekberg, J.O.,* Richardson, M.C.,* Behring, W.E.,* and Reader, J.,* *Journal of the Optical Society of America B* **3**:1605–1608

Summary Abstract: Multicomponent Quantitative Analysis by Auger Electron Spec-

troscopy, by Turner, N.H., *Journal of Vacuum Science and Technology A* **4**:1565–1567

Surface Analysis: X-Ray Photoelectron Spectroscopy and Auger Electron Spectroscopy, by Turner, N.H., *Analytical Chemistry* **58**:153R–165R

Systematic Development of Reduced Reaction Mechanisms for Dynamic Modeling, by Frenklach, M.,* Kailasanath, K., and Oran, E.S., *Dynamics of Reactive Systems, Part II. Modeling and Heterogeneous Combustion. Progress in Astronautics and Aeronautics* **105**:365–376

Temperature Dependence of the CN Radical Reactions with C_2H_2 and C_2H_4, by Lichtin, D.A.* and Lin, M.C., *Chemical Physics* **104**:325–330

Temperature–Reversible Oxidation of Carbon Monoxide by New and Weathered Whetlerite, by Deitz, V.R. and Poziomek, E.J.,* *Carbon* **24**:463–468

The Combination Reaction of CH_3 and C_6H_5O, by Lin, C.Y.* and Lin, M.C., *Australian Journal of Chemistry* **39**:723-734

The Effect of Pressure on Vesicle Fusion, by Chang, E.L., *Xth AIRAPT International High Pressure Conference in: Physica* **139–140 B+C**:885–889

The Magic Number Nine - Atom Alkali Halide Cluster Ion. Is the Nine - Atom Planar Structure Most Stable?, by Dunlap, B.I. and Campana, J.E., *Organic Mass Spectrometry* **21**:221–224

The Photodissociation of ClCN: A Theoretical Determination of the Rotational State Distribution of the CN Fragment, by Waite, B.A.* and Dunlap, B.I., *Journal of Chemical Physics* **84**:1391- 1396

The Role of Alternative Geometries in Alkali-Halide Clusters, by Dunlap, B.I., *Journal of Chemical Physics* **84**:5611–5616

The Secondary Structure of Calcium Pump Proteins in Light Sarcoplasmic Reticulum and Reconstituted in a Single Lipid Component as Determined by Raman Spectroscopy, by Williams, R.W., McIntyre, J.O.,* Gaber, B.P., and Fleischer, S.,* *Journal of Biological Chemistry* **261**:14520-14524

Theoretical Photoelectron Spectra Using Local-Density Function Results, by Mintmire, J.W., Kutzler, F.W., and White, C.T., *International Journal of Quantum Chemistry: Quantum Chemistry Symposium* **19**:745

Thermal Decomposition and Reduction of Carbonate Ion in Fluoride Melt, by Deanhardt, M.L.,* Stern, K.H., and Kende, A., *Journal of the Electrochemical Society* **133**:1148–1152

Thermal Decomposition of Methyl Phenyl Ether in Shock Waves: The Kinetics of the Phenoxy Radical Decomposition Reaction, by Lin, C.Y.* and Lin, M.C., *Journal of Physical Chemistry* **90**:425–431

Tribology Research at the Metal Research Institute of TNO, by Singer, I.L., *European Science Notes* **40**:429–433

Tubule Formation by Hetero Bifunctional Polymerizable Lipids: Synthesis and Characterization, by Singh, A.,* Price, R.,* Schoen, P.E., Yager, P., and Schnur, J.M., *ACS Conference in: Polymer Preprints* **27**:393–394

Zinc Sulfate Reactions in Hot Corrosion, by Jones, R.L. and Williams, C.E., *Journal of the Electrochemical Society* **133**:1742–1746

COMMUNICATIONS

A Layered Approach to Simulating Communication Systems Simula, by Hauser, J.P. and Baker, D.J., *MILCOM'86, Communications–Computers: Teamed for the '90s*, IEEE, NY, pp. 36.2.1–36.2.7

A More Efficient Cryptographic Matchmaking Protocol for Use in the Absence of a Continuously Available Third Party, by Meadows, C., *1986 IEEE Symposium on Security and Privacy*, IEEE, NY, pp. 134- 137

Discrimination Against Partially Overlapping Interference – Its Effect on Throughput in Frequency Hopped Multiple Access Channels, by Wieselthier, J.E. and Ephremides, A.,* *IEEE Transactions on Communications* **COM-34**:136-142

Performance of Coded FH/MFSK with a Quantizer-Limiter in a Worst-Case Partial Band Gaussian Interference Channel, by Crepeau, P.J., *MIL- COM'86, Communications- Computers: Teamed for the '90s*, Vol. 1, IEEE, NY, pp. 12.2.1-12.2.6

Precise Timing as a System, by Murray, J.A., *MILCOM'86, Communications-Computers: Teamed for the '90s*, IEEE, NY, pp. 29.6.1-29.6.5

Recognition of Previously Unfamiliar Speakers as a Function of Narrow-Band Processing and Speaker Selection, by Schmidt-Nielsen, A. and Stern, K.R.,* *Journal of the Acoustical Society of America* **79**:1174-1177

Sounder Updates for Statistical Model Predictions of Maximum Usable Frequency for HF Sky Wave Paths, by Reilly, M.H. and Daehler, M., *Radio Science* **21**:1001-1008

Sounder Updates Statistical Model Predictions of Maximum Usable Frequencies on HF Sky Wave Paths, by Reilly, M.H. and Daehler, M., *MILCOM'86, Communications-Computers: Teamed for the '90s*, Vol. 1, IEEE, NY, pp. 14.3.1-14.3.6

COMPUTER SCIENCE

A Modular Software for Image Information Systems, by Chang, S.K.* and Yang, C.C., *Statistical Image Processing and Graphics*, Marcel Dekker, Inc., NY, pp. 127-144

A Visual Programming Environment for Designing User Interfaces, by Jacob, R.J.K., *Visual Languages*, Plenum Publishing Corp., NY, pp. 87-107

Digital Imaging of Ocean Temperature Finestructure Patches, by Rosenblum, L.J., *Proceedings 1986 Working Symposium on Oceanographic Data Systems*, IEEE, NY, pp. 208-210

Direct Manipulation, by Jacob, R.J.K., *Proceedings of the IEEE International Conference on Systems, Man and Cybernetics*, IEEE, NY, pp. 384-388

Edge Detection by Partitioning, by Lee, J.S., *Statistical Image Processing and Graphics*, Marcel Dekker, Inc., NY, pp. 59-69

Embedded Expert Systems, by Shumaker, R.P., *Expert Systems in Government Symposium*, IEEE, NY, p 456

On Access Checking in Capability-Based Systems, by Kain, R.Y.* and Landwehr, C.E., *1986 IEEE Symposium on Security and Privacy*, IEEE, NY, pp. 95-100

Software Engineering for Rulebased Systems, by Jacob, R.J.K. and Froscher, J.N., *Fall Joint Computer Conference*, IEEE, NY, pp. 185-189

What Search Algorithm Gives Optimal Average-Case Performance When Search Resources are Highly Limited, by Mutchler, D., *27th Annual IEEE Symposium on Foundations of Computer Science*, IEEE Computer Society, Washington, DC, pp. 71-76

COSMIC RAYS

Nuclear Cross Sections, Cosmic Ray Propagation and Source Composition, by Silberberg, R., Tsao, C.H., and Letaw, J.R.,* *Cosmic Radiation in Contemporary Astrophysics*, D. Reidel Publishing Co., Boston, MA, pp. 113-133

The Composition, Propagation and Origin of High Energy ($E > 10^{12}$ eV/u) Cosmic Rays, by Silberberg, R., *Cosmic Radiation in Contemporary Astrophysics*, D. Reidel Publishing Co., Boston, MA, pp. 99-111

ELECTRONICS AND ELECTRICITY

A Ka-Band Circular Polarization Analyzer, by Gold, S.H., *Review of Scientific Instruments* 57:36-38

An Evaluation of Nonlinear Resistors for Pulse Power Switching, by Ford, R. and Kahn, M., *Proceedings of the 5th IEEE Pulse Power Conference*, IEEE, NY, pp. 652–655

Analysis of Helical Waveguide, by Ahn, S. and Ganguly, A.K., *IEEE Transactions on Electron Devices* **ED– 33**:1348–1355

Charge Transport by the Ion Shunt Effect, by Knudson, A.R., Campbell, A.B., Hauser, J.R.,* Jessee, M.,* Stapor, W.J., and Shapiro, P.,* *1986 Annual Conference on Nuclear and Space Radiation Effects in: IEEE Transactions on Nuclear Science* **NS–33**:1560–1564

Defense Electronics: A Balance of Functionality, Finance and Form, by Spielman, B.E., *Microwave Journal* **29**(9):26– 39

Gyroklystron Amplifier Phase Noise Measurements, by McAdoo, J.,* Bollen, W.M.,* McCurdy, A.,* Granatstein, V.L.,* and Parker, R.K., *International Journal of Electronics, Special Issue on Gyrotrons* **61**:1025–1028

Hot Electron Effect on MOSFET Terminal Capacitances, by Yao, C.T., Peckerar, M., Friedman, D., and Hughes, H., *Proceedings of the IEEE Custom Integrated Circuits Conference*, IEEE, NY, pp. 208–211

Improved Oscillator Phase Locking by Use of a Modulated Electron Beam in a Gyrotron, by McCurdy, A.H.,* Armstrong, C.M., Bollen, W.M.,* Parker, R.K., and Granatstein, V.L.,* *Physical Review Letters* **57**:2379–2382

Ionizing Radiation in Microelectronics Processing, by Dozier, C.M., *Solid State Technology* **29**(10):105–108

Models of Kohlrausch Relaxations, by Ngai, K.L., Rajagopal, A.K., Rendell, R.W.,* and Teitler, S., *IEEE Transactions on Electrical Insulation* **EI–21**:313–318

Particle Damage Effects in GaAs JFET Test Structures, by Campbell, A.B., Knudson, A.R., Stapor, W.J., Summers, G., Xapsos, M.A., Jessee, M.,* Palmer, T.,* Zuleeg, R.,* and Dale, C.J., *1986 Annual Conference on Nuclear and Space Radiation Effects in: IEEE Transactions on Nuclear Science* **NS–33**:1435– 1441

Self–Oscillating GaAs FET Demodulator and Downconverter for Microwave Modulated Optical Signals, by Rauscher, C., Goldberg, L., and Yurek, A.M., *1986 IEEE MTT–S International Microwave Symposium Digest*, IEEE, NY, pp. 721– 724

"Signal Flow" – AVLSI Fault Tolerant Architecture for Signal Processing, by Wu, Y.S. and Wu, L.J., *VLSI 85. VLSI Design of Digital Systems*, North–Holland, NY, pp. 229–238

Solid State Monolithic Variable Phase Shifter with Operation into the Millimeter Wave Wavelength Regime, by Krowne, C.M. and Neidert, R.E., *International Journal of Infrared and Millimeter Waves* **7**:715–728

The Poisoning and Reactivation Kinetics of Uncoated Tungsten–Based Dispenser Cathodes Exposed to Water Vapor, by Marrian, C.R.K. and Shih, A. *IEEE Transactions on Electron Devices* **ED–33**:1874–1882

The Phenomenon of Electron Rollout for Energy Deposition and Defect Generation in Irradiated MOS Devices, by Brown, D.B., *IEEE Transactions on Nuclear Science* **NS–33**:1240–1244

Use of the Subthreshold Behavior to Compare X–Ray and Co–60 Radiation–Induced Defects in MOS Transistors, by Dozier, C.M., Brown, D.B., Freitag, R.K., and Throckmorton, J.L.,* *IEEE Transactions on Nuclear Science* **NS–33**:1324–1329

GEOSCIENCES

Geophysical and Geochemical Signatures and Plate Tectonics, by Vogt, P.R., *The Nordic Seas*, Springer–Verlag, NY, pp. 413–662

Heat Conduction Within an Elastic Earth, by Lanzano, P., *Earth, Moon, and Planets* **36**:157–166

Seafloor Topography, Sediments, and Paleoenvironments, by Vogt, P.R., *The Nordic Seas*, Springer–Verlag, NY, pp. 237–410

Thermoelastic Deformations of the Earth's Lithosphere: A Mathematical Model, by Lanzano, P., *Earth, Moon, and Planets* **34**:283–304

INSTRUMENTATION

A Novel Instrument for High–Pressure Research at Ultra–High Temperatures, by Schiferl, D.,* Katz, A.I.,* Mills, R.L.,* Schmidt, L.C.,* Vanderborgh, C.,* Skelton, E.F., Elam, W.T., Webb, A.W., Qadri, S.B.,* and Schaefer, M.,* *Xth AIRAPT International High Pressure Conference in*: *Physica* **139–140 B+C**:897–899

DC Fiber Optic Accelerometer with Sub–μg Sensitivity, by Bucholtz, F., Kersey, A.D.,* and Dandridge, A., *Electronics Letters* **22**:451–452

Electronics Package for Rugged HPGe Detectors, by Beach, L.A. and Phillips, G.W., *IEEE 1986 Nuclear Science Symposium in*: *IEEE Transactions on Nuclear Science* **NS–33**:664–667

Improvements in Real–Time Data Acquisition for Gas Electron Diffraction, by Ewbank, J.D.,* Schafer, L.,* Paul, D.W.,* Monts, D.L.,* and Faust, W.L., *Review of Scientific Instruments* **57**:967–972

Magnetoelastic Amorphous Metal Fluxgate Magnetometer, by Mermelstein, M.D.,* *Electronics Letters* **22**:525–526

Magnetic Stirrer for Diamond–Anvil Cells, by Skelton, E.F., Elam, W.T., Webb, A.W., and Qadri, S.B.,* *Xth AIRAPT International High Pressure Conference in*: *Physica* **139–140 B+C**:919–921

Maximum Entropy and Reliability Distribution, by Teitler, S., Rajagopal, A.K., and Ngai, K.L., *IEEE Transactions on Reliability* **R–35**:391–395

Optimization of Layered Synthetic Microstructures for Narrowband Reflectivity at Soft X–Ray and EUV Wavelengths, by Meekins, J.F., Cruddace, R.G., and Gursky, H., *Applied Optics* **25**:2757–2763

Temperature Measurements of Shocked Water Using a Fluorescence Probe, by Justus, B.L., Huston, A.L.,* and Campillo, A.J., *Shock Waves in Condensed Matter*, Plenum Publishing Corp., NY, pp. 249–254

The Far UV Cameras (NRL–803) Space Test Program Shuttle Experiment, by Carruthers, G.R., *Ultraviolet Technology*, SPIE Vol 682, SPIE–The International Society of Photo–Optical Instrumentation Engineers, Bellingham, WA, pp. 11–27

Use of a Magnetic Spectrometer for Profiling Light Elements by Elastic Recoil Detection, by Gossett, C.R., *7th International Conference on Ion Beam Analysis in*: *Nuclear Instruments and Methods in Physics Research* **B15**:481–485

LASER SCIENCE

Absolute Line Intensities for Photon Pumping of X–Ray Lasers, by Elton, R.C., Lee, T.N., and Molander, W.A., *Physical Review A* **33**:2817–2820

Angioplasty with a Laser and Fiber Optics at 2.94 μm, by Esterowitz, L., Hoffman, C.A., Tran, D.C., Levin, K.,* Storm, M.,* Bonner, R.F.,* Smith, P.,* and Leon, M.,* *Optical and Laser Technology in Medicine*, SPIE Vol. 605, SPIE–The International, Society of PhotoOptical Instrumentation Engineers, Bellingham, WA, pp. 32–36

Beam Cleanup with Stimulated Raman Scattering in the Intensity–Averaging Regime, by Reintjes, J., Lehmberg, R.H., Chang, R.S.F.,* Duignan, M.D.,* and Calama, G., *Journal of the Optical Society of America B* **3**:1408–1427

Effect of Beam Quality on the Free-Electron Laser, by Freund, H.P.* and Ganguly, A.K., *Physical Review A* **34**:1242–1246

Frequency Modulation Characteristics of Coupled Stripe Laser Diode Array, by Goldberg, L., Taylor, H.F., and Weller, J.F., *IEEE Journal of Quantum Electronics* **QE-22**:513–516

Generation and Use of Spontaneous X-Ray Emission from Laser-Heated Plasmas, by Nagel, D.J., *High Intensity Laser Processes*, SPIE Vol. 664, SPIE–The International Society of Photo-Optical Instrumentation Engineers, Bellingham, WA, pp. 142–150

High-Efficiency Targets for High-Gain Inertial Confinement Fusion, by Gardner, J.H. and Bodner, S.E., *Physics of Fluids* **29**:2672–2678

High-Gain, Long-Pulse FreeElectron-Laser Oscillator, by Mathew, J.* and Pasour, J.A., *Physical Review Letters* **56**:1805–1808

Illumination Uniformity of Laser-Fusion Pellets Using Induced Spatial Incoherence, by Schmitt, A.J. and Gardner, J.H., *Journal of Applied Physics* **60**:6–13

Injection-Locked Operation of a 20-Element Coupled-Stripe Laser Array, by Goldberg, L. and Weller, J.F., *Electronics Letters* **22**:858–859

Laser Processing of High-Tech Materials at High Irradiance, by Whitlock, R.R., *Laser Welding, Machining and Materials Processing, Proceedings of the International Congress on the Applications of Lasers and Electro-Optics*, IFS (Publications), Ltd., NY

Mid-IR Solid State Laser with Fiber Optics as an Ideal Medical Scalpel, by Esterowitz, L., Hoffman, C.A., Levin, K.,* and Storm, M.,* *Proceedings of the International Conference on Lasers 85*, Society for Optical and Quantum Electronics, McLean, VA, pp. 68–71

Nonlinear Analysis of Efficiency Enhancement in Free-Electron-Laser Amplifiers, by Freund, H.P.* and Ganguly, A.K., *Physical Review A* **33**:1060–1072

Parametric Behavior of a High Gain 35 GHz Free Electron Laser Amplifier with Guide Magnetic Field, by Gold, S.H., Ganguly, A.K., Freund, H.P.,* Fliflet, A.W., Granatstein, V.L.,* Hardesty, D.L., and Kinkead, A.K., *Seventh International Conference on Free Electron Lasers in: Nuclear Instruments and Methods in Physics Research* **A250**:366–368

Polarizaton-Resolved Low-Frequency Noise in GaAlAs Lasers, by Dandridge, A., Miles, R.W., and Taylor, H.F., *Journal of Lightwave Technology* **LT-4**:1311–1316

Proposal for FEL Experiments Driven by the National Bureau of Standards CW Microtron, by Tang, C.M., Sprangle, P., Penner, S.,* Kincaid, B.M.,* and Freeman, R.R.,* *Seventh International Conference on Free Electron Lasers in: Nuclear Instruments and Methods in Physics Research* **A250**:278–282

Reflective Probing of Laser Generated Multikbar Compressional Shocks in Water, by Campillo, A.J., Griffin, R.D., and Schoen, P.E., *Optics Communications* **57**:301–306

SBS with an HF Laser, by Whitney, W.T., Duignan, M.T.,* and Feldman, B.J., *Proceedings of the International Conference on Lasers '85*, Society for Optical and Quantum Electronics, McLean, VA, pp. 42–43

Short Wavelength Laser Calculations in the Be I, B I and C I Isoelectronic Sequences, by Feldman, U., Seely, J.F., and Doschek, G.A., *International Colloquium on X-Ray Lasers in: Journal de Physique, Colloque C6* **47**:C6- 187–C6-202

Simultaneous Amplification and Compression of Continuous-Wave Mode-Locked Nd: YAG Laser Pulses, by Voss, D.F. and Goldberg, L.S., *Optics Letters* **11**:210–212

Some Characteristics of a Droplet Whispering-Gallery-Mode Laser, by Lin, H.B., Huston, A.L., Justus, B.L., and Campillo, A.J., *Optics Letters* **11**:614-616

Spontaneous Radiation of an Electron Beam in a Free-Electron Laser with a Quadrupole Wiggler, by Levush, B.,* Antonsen, T.M.,* and Manheimer, W.M., *Journal of Applied Physics* **60**:1584-1590

Strongly Inhibited Rayleigh Taylor Growth with 0.25μm Lasers, by Emery, M.H., Gardner, J.H., and Bodner, S.E., *Physical Review Letters* **57**:703-706

MAGNETISM

Ferrimagnetic Resonance Linewidth in Single Crystal MnZn-Ferrite, by Vittoria, C. and Williams, C.M., *International Conference on Magnetism in: Journal of Magnetism and Magnetic Materials* **54-57**:1193-1194

Magnetic Resonance Investigations of MBE-Grown Fe/Ag/Fe Sandwiches, by Krebs, J.J., Vittoria, C., Jonker, B.T., and Prinz, G.A., *International Conference on Magnetism 1985 in: Journal of Magnetism and Magnetic Materials* **54-57**:811-813

Magnetization of $(Y_{0.9}R_{0.1})_2Fe_{14}B$ Single Crystals, by Koon, N.C. and Das, B.N., *ICM 85 in: Journal of Magnetism and Magnetic Materials* **54-57**:523-524

Some Approaches to the Study of Realistic Forms of the Landau-Lifshitz Equations, by Zachary, W.W., *14th International Colloquium on Group Theoretical Methods in Physics*, World Scientific Publishing Co., Singapore, pp. 417-420

MATHEMATICS

An Analytical Expression for Coefficients Arising when Implementing a Technique for Indefinite Integration of Products of Special Functions, by Piquette, J.C., *SIAM Journal on Mathematical Analysis* **17**:1033-1035

An Inverse Scattering Formalism for Higher-Order Differential Operators, by Zachary, W.W., *Journal of Mathematical Analysis and Applications* **117**:449-495

Local and Global Methods of Nonlinear Dynamics, by Saenz, A.W., ed, Zachary, W.W., ed, and Cawley, R.,* ed, *Lecture Notes in Physics 252*, Springer-Verlag, NY, 263 pp.

Rigorous Results on Crystal Channeling via Canonical Maps, by Saenz, A.W., *Local and Global Methods of Nonlinear Dynamics, Lecture Notes in Physics 252*, Springer-Verlag, NY, pp. 231-237

Sequential Dynamics for a Family of Master Equations, by Rajagopal, A.K.,* Ngai, K.L., and Teitler, S., *Physica* **137A**:359-366

The Discrete Variable-Finite Basic Approach to Quantum Scattering, by Lill, J.V., Parker, G.A.,* and Light, J.C.,* *Journal of Chemical Physics* **85**:900-910

MECHANICS

A Richardson Criterion for Compressible Swirling Flows in a Toroidal Magnetic Field, by Fung, Y.T., *Journal of Fluid Mechanics* **29**:1326-1328

Constrained-Layer Model Investigation Based on Exact Elasticity Theory, by Dubbelday, P.S., *Journal of the Acoustical Society of America* **80**:1097-1102

Numerical Simulations of the Initiation of Gaseous Detonations in Shock Tubes, by Kailasanath, K., Oran, E.S., and Boris, J.P., *Shock Waves and Shock Tubes*, Stanford University Press, Stanford, CA, pp. 367-373

Rayleigh Wave Propagation in Deformed Orthotropic Materials, by Delsanto, P.P. and Clark, A.V.,* *Review of Progress in Quantitative Nondestructive Evaluation*, Vol. 5B, Plenum Publishing Corp, NY, pp. 1407-1414

Rotational Motion Generated by Shock Propagation Through a Nonuniform Gas, by

Picone, J.M., Boris, J.P., Oran, E.S., and Ahearne, R.,* *Shock Waves and Shock Tubes*, Stanford University Press, Stanford, CA, pp. 523-529

METALLURGY

ASTM and the Department of Defense as Standards Partners, by Steele, L.E., *DOD/SAE/ASTM Conference on the Adoption of Non-Government Standards – An Equal Partner Approach*, Society of Automotive Engineers, NY, pp. 19-23

An Impression Method for Characterization of the Flow Behavior of Superplastic Material, by Yu, H.Y.,* Imam, M.A., and Rath, B.B., *Materials Science and Engineering* **79**:125-132

Analysis of Sub-Critical Cracking in a Ti-5Al-2.5Sn Liquid Hydrogen Control Valve, by Meyn, D.A. and Bayles, R.A., *Corrosion Cracking*, American Society for Metals, Metals Park, Ohio, pp. 103-112

Assessment of J-R Curves Obtained from Precracked Charpy Specimens, by Kapp J.A.* and Jolles, M.I., *Fracture Mechanics*, Seventeenth Volume, ASTM STP 905, American Society for Testing and Materials, Philadelphia, PA, pp. 401-411

Composition Profiles at Graphite-Aluminum Interphases by Rutherford Backscattering, by Everett, R., Henshaw, W., Simons, D.G.,* and Land, D.J.,* *Composite Interfaces, Proceedings of the First International Conference*, North-Holland, NY, pp. 231-240

Corrosion Behavior of Laser-Surface Melted and Laser-Surface Alloyed Steels, by McCafferty, E. and Moore, P.G., *Journal of the Electrochemical Society* **133**:1090-1096

Corrosion Behavior of a Graphite Fiber/Magnesium Metal Matrix Composite in Aqueous Chloride Solution, by Trzaskoma, P.P., *Corrosion* **42**:609-613

Cracking Resistance in a 4.5- inch (114.mm) Plate of 7075-T 7351 Aluminum Alloy, by Yoder, G.R., Cooley, L.A., Watson, T.J.,* and Crooker, T.W., *Structures, Structural Dynamics and Materials Conference*, AIAA-86-0985-CP, American Institute of Aeronautics and Astronautics, NY, pp. 585- 594

Degradation in Strength of Laminated Composites Subjected to Intense Heating and Mechanical Loading, by Griffis, C.A., Nemes, J.A., Stonesifer, F.R., and Chang, C.I., *Journal of Composite Materials* **20**:216-235

Dispersion Toughening, by Li, J.C.M.* and Sanday, S.C., *Acta Metallurgica* **34**:537-543

Effect of Environment on Fatigue Crack Propagation Behavior of Alloy 718 at Elevated Temperatures, by Smith, H.H. and Michel, D.J., *1984 TMS-AIME Fall Meeting in: Metallurgical Transactions A* **17A**:370-374

Electrochemical Behavior of Laser Processed Metal Surfaces, by McCafferty, E. and Moore, P.G., *Laser Surface Treatment of Metals*, Martinus Nijhoff, the Netherlands, p. 263

Friction and Wear Properties of Ion Implanted and Ion Beam Enhanced Vapor Deposited Surfaces, by Sartwell, B.D., *Proceedings of the Conference on the Applications of Ion Plating and Implantation to Materials*. American Society for Metals, Metals Park, Ohio, pp. 1-8

Growing Sophistication in Dealing with Structural Integrity, by Steele, L., *Nuclear Engineering International* **31**:378:21-22

High Power Laser Beam Welding in Production, by Metzbower, E.A., *Electron and Laser Beam Welding*, Pergamon Press, NY, pp. 271-279

High Temperature Crack Propagation Under Cyclic and Static Loads, by Sadananda, K., *International Conference on Creep*, Tokyo, Japan, pp. 283-290

Ionic Current Densities in the Nearfield of a Corroding Iron–Copper Galvanic Couple, by Crowe, C.R. and Kasper, R.G.,* *Journal of the Electrochemical Society* **133**:879–887

Laser–Formed Protective Coatings, by Moore, P.G., Ayers, J.D., and McCafferty, E., *Encyclopedia of Materials Science and Engineering*, Vol. 4, Pergamon Press, NY, pp. 2502–2505

Morphological Stability of Second Phase Particles Under Creep Conditions, by Sadananda, K., Louat, N.,* and Imam, M.A., *Structure and Deformation of Boundaries Proceedings*, AIME, Warrendale, PA, pp. 229–316

Morphological Stability of γ' Precipitates in Nickel–Base Superalloys, by Louat, N.,* Sadananda, K., and Imam, M.A.,* *Phase Boundary Deformation Conference*, AIME, Warrendale, PA, pp. 299–316

Plastic Energy Dissipation as a Parameter to Characterize Crack Growth, by Watson, T.J. and Jolles, M.I., *Fracture Mechanics: Seventeenth Volume*, ASTM STP 905, American Society for Testing and Materials, Philadelphia, PA, pp. 542–555

Quantitative Electron Channeling Measurement of Ion Implantation Damage in Aluminum, by Vardiman, R.G., *Proceedings of the Symposium on Irradiation Effects Associated with Ion Implantation in: Nuclear Instruments and Methods in Physics Research* **B16**:143–147

Surface Modification by Laser or Ion Beams, by McCafferty, E., *Critical Issues in Reducing the Corrosion of Steels*, NACE, Houston, Texas, p. 224

Temperature Measurements of a Molten Weld Pool Along the Keyhole in Laser Beam Welding, by Moon, D.W. and Metzbower, E.A., *Welding for Challenging Environments*, Pergamon Press, NY, pp. 41–50

The Beta–to–Alpha Phase Transformation in a Uranium Alloy, by Vandermeer, R.A., *Metallurgical Transactions A* **17A**:1717–1723

The Effect of Anodic Coatings on the Pitting of Silicon Carbide/Aluminum Metal Matrix Composites, by Trzaskoma, P.P. and McCafferty, E., *Aluminum Surface Treatment Technology*, Electrochemical Society, Pennington, NJ, p.171

The Effect of pH of Zero Charge on the Pitting Potential, by Natishan, P.M., McCafferty, E., and Hubler, G.K., *Journal of the Electrochemical Society* **133**:1061–1062

The Effects of Sulfur and Nickel on the Mechanical Properties of HY–Steel Laser Weldments, by Moon, D.W., Phillips, R.H.,* and Metzbower, E.A., *Laser Welding, Machining and Materials Processing, Proceedings of the International Conference on Applications of Lasers and Electro–Optics*, IFS (Publications) Ltd., NY, pp. 3–10

The Modification of Fatigue Properties by Ion Implantation, by Vardiman, R.G., *Conference on the Application of Ion Plating and Ion Implantation to Materials*, American Society for Metals, Metals Park, OH, pp. 1–7

The Pitting Behavior of Ion Implanted Aluminum, Natishan, P.M., McCafferty, E., and Hubler, G.K., *The Electrochemical Society*, Pennington, NJ, p.437

Thermal Effects on Polymer Composite Structures, by Chang, C.I., *Theoretical and Applied Fracture Mechanics* **6**:113–120

Void Formation at Phase Boundaries and Ductile Fracture of Copper–Aluminum Alloy, by Provenzano, V. and Gilmore, C.M.,* *Proceedings of Phase Boundary Deformation Conference*, AIME, Warrendale, PA, pp. 141–158

NUCLEAR PHYSICS

Development of a Rugged HPGe Detector, by Beach, L.A. and Phillips, G.W., *Sixth Symposium on X- and Gamma-Ray Sources and Applications in: Nuclear Instruments and Methods in Physics Research* **A242**:520–524

Hyperspherical Techniques – A Summary and Outlook, by Haftel, M.I., *Few Body Methods: Principles and Applications*, World Scientific Publishing Co., Singapore, pp. 793–802

OCEANOLOGY

A Numerical Study of the Frequency and the Energetics of Nonlinear Internal Gravity Waves, by Shen, C.Y. and Holloway, G.,* *Journal of Geophysical Research* **91**:953–973

A Two-Scale Model of Short Wind-Generated Waves, by Plant, W.J., *Journal of Geophysical Research* **91**:10735–10749

Bathymetry, by Perry, R.K., *The Nordic Seas*, Springer-Verlag, NY, pp. 211–235

Estimating Absolute Current Velocities by Merging Shipboard Doppler Current Profiler Data with Loran-C Data, by Trump, C.L., *Proceedings of the IEEE Third Working Conference on Current Measurement*, IEEE, NY, pp. 177–183

Horizontal Variability of Microstructure in the Vicinity of a Sargasso Sea Front, by Marmorino, G.O., Dugan, J.P.,* and Evans, T.E., *Journal of Physical Oceanography* **16**:967–980

Horizontal Wave Number Distribution of Potential Energy in the Ocean, by Dugan, J.P.,* Morris, W.D., and Okawa, B.S.,* *Journal of Geophysical Research* **91**:12993–13000

Naval Research Laboratory 1982 Phelps Bank Experiment, by Chen, D.T., Valenzuela, G.R., Garrett, W.D., and Kaiser, J.A.C., *Current Practices and New Technology in Ocean Engineering OED* **11**:43–53

Observation of Breaking Ocean Waves with Coherent Microwave Radar, by Keller, W.C., Plant, W.J., and Valenzuela, G.R., *Wave Dynamics and Radio Probing of the Ocean Surface*, Plenum Press, NY, pp. 285–293

Observations of an Anticyclonic Eddy of 18°C Water in the Sargasso Sea, by Brundage, W.L. and Dugan, J.P.,* *Journal of Physical Oceanography* **16**:717–727

Rapid Alternating Vertical Temperature Gradients in the East China Sea, by Burt, W.V.,* Neshybu, S.,* and Trump, C.L., *Continental Shelf Research* **6**:449–458

Richardson Criteria for Stratified Vortex Motions Under Gravity, by Fung, Y.T. *Physics of Fluids* **29**:368–371

The Effect of Inaccuracies in Weather-Ship Data on Bulk-Derived Estimates of Flux Stability and Sea-Surface Roughness, by Blanc, T.V., *Journal of Atmospheric and Oceanic Technology* **3**:12–26

The Mesoscale Spatial Structure and Evolution of Dynamical and Scalar Properties Observed in the Northwestern Atlantic Ocean During the Polymode Local Dynamics Experiment, by Shen, C.Y., McWilliams, J.C.,* Taft, B.A.,* Ebbesmeyer, C.C.,* and Lindstrom, E.J.,* *Journal of Physical Oceanography* **16**:454–482

The Nordic Seas, by Hurdle, B.C., ed., Springer-Verlag, NY, 777 pp

OPTICS

FA Centers in Additively Colored KI:Li Crystals, by Foster, D.R.* and Schneider, I., *Physical Review B* **33**:8779–8781

(F_2)A Centers in Additively Colored Lithium-Doped KI and KBr, by Foster, D.R.* and Schneider, I., *Optics Letters* **11**:213–215

A Combinatorial Approach for Classification of Patterns with Missing Information and Random Orientation, by Flick, T.E. and Jones, L.K.,* *IEEE Transactions on Pattern*

Analysis and Machine Intelligence **PAMI-8**:482–490

A Compact, Molecular, Mirror Bending and Positioning System, by Kirkland, J.P.,* Neiser, R.A.,* and Elam, W.T., *Nuclear Instruments and Methods in Physics Research* **A246**:203–206

A New Sampling Detection Scheme for High Sensitivity Fiber Optic Magnetometer, by Koo, K.P.,* Bucholtz, F., and Dandridge, A., *International Conference on Optical Fiber Sensors, OFS'86, Technical Digest*, pp. 77–80

A Synchronous Sampling Demodulation Scheme for Nonlinear Fiber Optic Sensors, by Koo, K.P.,* Bucholtz, F., and Dandridge, A., *Optics Letters* **11**:683–685

All-Fiber Polarimetric Sensor, by Mermelstein, M.D.,* *Applied Optics* **25**:1256–1258

Amorphous Metal-Fiber Optic Magnetometer Response-Dipole Rotation Model, by Mermelstein, M.,* *1985 International Conference on Magnetism – (Part III) in: Journal of Magnetism and Magnetic Materials* **54–57**:1473– 1474

An Optical Space Domain Reflectometer Based on the Faraday Effect, by Frigo, N.J., Dandridge, A., and Villarruel, C.A., *Journal of Lightwave Technology* **LT-4**:256–258

Applications of Wigner and Ambiguity Functions to Optics, by Szu, H.H., *Proceedings of the IEEE International Symposium on Circuits and Systems*, IEEE, NY, pp. 46–49

Broadly Tunable Infrared-Parametric Oscillator Using AgGaSe$_2$, by Eckardt, R.C.,* Fan, Y.X.,* Byer, R.L.,* Storm, M.E.,* Marquardt, C.L., and Esterowitz, L., *Applied Physics Letters* **49**:608–610

Characterization of Ti:LiNbO$_3$ Deep Waveguides Diffused in Dry and Wet Oxygen Ambient, by Eknoyan, O.,* Greenblatt, A.S., Burns, W.K., and Bulmer, C.H., *Applied Optics* **25**:737–739

Color Centers in Glass Optical Fiber Waveguides, by Friebele, E.J. and Griscom, D.L., *1985 Materials Research Society Symposium*, Vol. 61, Materials Research Society, pp. 319–331

Coupled Mode Analysis for Magnetoelastic Amorphous Metal Sensors, by Mermelstein, M.D.,* *INTERMAG'86, International Magnetics Conference in: IEEE Transactions on Magnetics* **MAG-22**:442–444

Current Sensing Utilizing Heterodyne Detection of the Faraday Effect in Single-Mode Optical Fiber, by Kersey, A.D.* and Jackson, D.A.,* *Journal of Lightwave Technology* **LT-4**:640–644

Detection of Deep-Red Low-Level Light Pulses, by Burnham, R. and Scarl, D., *Applied Optics* **25**:1514–1518

Electrical and Optical Properties of Sputtered TiNx Films as a Function of Substrate Deposition Temperature, by Thorpe, T.P., Qadri, S.B.,* Wolf, S.A., and Claassen, J.H., *Applied Physics Letters* **49**:1239–1241

Enhanced Species Selectivity in Opto-Acoustic Detection, by Seaver, M.,* Mannuccia, T.J., and McDonald, J.R., *Chemical Physics Letters* **123**:164–168

FA Centers in Additively Colored KI:Li Crystals, by Foster, D.R.* and Schneider, I., *Physical Review B* **33**:8779–8781

Features and Initial Performance Tests of the Grating/Crystal Monochromator, by Rife, J.C., Hunter, W.R.,* and Williams, R.T.,* *Proceedings of the National Conference on Synchrotron Radiation Instrumetation in: Nuclear Instruments and Methods in Physics Research* **A246**:252–255

Fiber Optic Feed for Phased Array Antennas, by Stilwell, D., Goldberg, L., Parent, M., Czaplak, D.,* Sherman, G.,* Weller, J.F., and Collins, W., *AP-S International Sympo-*

sium 1986. Antennas and Propagation Symposium Digest 1, 345–346

Fiber Optic Sensors, by Dandridge, A. and Miles, R.O.,* *Chemical Engineering Progress* **82**:51–52

Fiber–Optic Polarimetric DC Magnetometer Utilizing a Composite Metallic Glass Resonator, by Mermelstein, M.D.,* *Journal of Lightwave Technology* **LT–4**:1376–1380

Field Correlations Within a Completely Incoherent Primary Spherical Source, by Foley, J.T.,* Carter, W.H., and Wolf, E.,* *Journal of the Optical Society of America A* 3:1090–1096

Formation and Properties of Optical Waveguides in Strontium Barium Niobate (SBN:60), by Bulmer, C.H., Eknoyan, O.,* Taylor, H.F., Greenblatt, A.S., and Bleach, L.A., *American Ceramic Society Meeting, Proceedings*, p. 15

GaAs FET Demodulator and Down–Converter for Optical–Microwave Links, by Rauscher, C., Goldberg, L., and Yurek, A.M., *Electronics Letters* **22**:705–706

Guided–Wave Electro–Optic Modulator in $Ti:LiNbO_3$ at $\lambda=2.6\mu m$, by Eknoyan, O.,* Bulmer, C.H., Moeller, R.P., Burns, W.K., and Levin, K.H.,* *Journal of Applied Physics* **59**:2993–2995

High–Birefringence Fiber Optic Polarimeter and the Detection of DC Magnetic Fields, by Mermelstein, M.D.,* *Conference on Optical Fiber Communications '86, Technical Digest*, Optical Society of America, Washington, DC, pp. 24–25

High–Birefringence Fiber–Optic Polarimeter with Submicroradian Phase Delay Detectability, by Mermelstein, M.D.,* *Journal of Lightwave Technology* **LT–4**:449

High–Sensitivity DC Measurand Sensing Using Single–Mode Optical–Fibre Interferometry, by Kersey, A.D.,* Bucholtz, F., and Dandridge, A., *Fibre Optics '86*, SPIE Vol. 630, SPIE–The International Society of Photo–Optical Instrumentation Engineers, Bellingham, WA, pp. 266–269

Implementations of Adaptive Associative Optical Computing Elements, by Fisher, A.D., Fukuda, R.C.,* and Lee, J.N., *Optical Instrumentation Computing*, SPIE Vol. 625, SPIE–The International Society of Photo–Optical Instrumentation Engineers, Bellingham, WA, pp. 196–204

Infrared Power Spectral Density Diurnal Variations and Clutter Rejection Scaling Laws for Focal Plane Arrays, by Szu, H., *Hybrid Image Processing*, SPIE Vol. 638, SPIE–The International Society of Photo–Optical Instrumentation Engineers, Bellingham, WA, pp. 148–165

Light Scattering in Heavy–Metal Fluoride Glasses in the Infrared Spectral Region, by Tran, D.C., Levin, K.H., Ginther, R.J., Sigel, G.H., and Bruce, A.J.,* *Electronics Letters* **22**:117–118

Loss Mechanisms in Single–Mode Fiber Tapers, by Burns, W.K., Abebe, M.,* Villarruel, C.A., and Moeller, R.P., *Journal of Lightwave Technology* **LT–4**:608–613

Low–Temperature Behaviour of High–Birefringence Fibres, by Marrone, M.J. and Davis, M.A., *Electronics Letters* **21**:703–704

Microbend Fiber–Optic Phase Shifter, by Czaplak, D.S.,* Rashleigh, S.C.,* Taylor, H.F., and Weller, J.F., *Journal of Lightwave Technology* **LT–4**:50–54

New Nonlinear Phase Transduction Method for DC Measurand Interferometric Fibre Sensors, by Kersey, A.,* Bucholtz, F., and Dandridge, A., *Electronics Letters* **22**:75–76

New Optical Systems for the Measurement of Diffuse Reflectance, by Snail, K.A., *Infrared, Adaptive, and Synthetic Aperture Optical Systems*, SPIE Vol. 643, SPIE– The International Society of Photo–Optical Instrumentation Engineers, Bellingham, WA, pp. 84–92

Nonlinear Responses of Picosecond Photodetectors to Photogenerated Carriers, by Carruthers, T.F. and Weller, J.F., *Ultrafast Phenomena V*, Springer-Verlag, NY, pp. 131-133

Optical Design and Calibration of an Integrating Sphere Fourier Transform Spectrophotometer Emissometer, by Snail, K. and Carr, K.F.,* *Infrared, Adaptive, and Synthetic Aperture Optical Systems*, SPIE Vol. 643, SPIE-The International Society of Photo-Optical Instrumentation Engineers, Bellingham, WA, pp. 75-83

Optical Fiber Waveguides for Spacecraft Applications, by Friebele, E.J., Dorsey, K.L.,* and Gingerich, M.E., *Fiber Optics in Adverse Environments III*, SPIE Vol. 721, SPIE-The International Society of Photo-Optical Instrumentation Engineers, Bellingham, WA, pp. 98-103

Optical Implementation of a Time-Domain Beam Former, by Rolsma, P.B., Griffin, R.D., and Lee, J.N., *Optics Letters* **11**:821-823

Optical and Electronic Reduction of Rayleigh Backscatter Noise in Fibre-Coupled Semiconductor Diode Lasers, by Yurek, A. and Dandridge, A., *Electronics Letters* **22**:645-646

Parametric Raman Gain Suppression in D_2 and H_2, by Duncan, M.D., Mahon, R.,* Reintjes, J., and Tankersley, L.L.,* *Optics Letters* **11**:803-805

Phase Error Bounds of Fiber Gyro with Polarization Holding Fiber, by Burns, W.K., *Journal of Lightwave Technology* **LT-4**:8-14

Phase-Noise Reduction in Coherence-Multiplexed Interferometric Fiber Sensors, by Kersey, A.D.* and Dandridge, A., *Electronics Letters* **22**:616-618

Photoemitter Membrane Light Modulator, by Fisher, A.D., Lee, J.N., Ling, L.C.,* and Fukuda, R.C.,* *Optical Engineering* **25**:261-268

Picosecond Optical Mixing in Fast Photodetectors, by Carruthers, T.F. and Weller, J.F., *Applied Physics Letters* **48**:460-462

Point Defects in Amorphous SiO_2: What Have We Learned from 30 Years of Experimentation?, by Griscom, D.L., *Materials Research Society Symposium Proceedings*, Vol. 61, Materials Research Society, pp. 213-221

Preparation and Properties of High Optical Quality IR Transmitting Glasses and Fibers Based on Metal Fluorides, by Tran, D.C., Levin, K.H., Burk, M.J., Fisher, C.F., and Brower, D., *Infrared Optical Materials and Fibers IV*, SPIE Vol. 618, SPIE-The International Society of Photo-Optical Instrumentation Engineers, Bellingham, WA, pp. 48-50

Proposal for FEL Experiments Driven by the National Bureau of Standards CW Microtron, by Borsuk, G.M., Anderson, G.W., and Kub, F., *Optical Information Processing II*, SPIE Vol. 639, SPIE-The International Society of Photo-Optical Instrumentation Engineers, Bellingham, WA, pp. 2-10

Pyroelectric Effects in $LiNbO_3$ Channel-Waveguide Devices, by Bulmer, C.H., Burns, W.K., and Hiser, S.C.,* *Applied Physics Letters* **48**:1036-1038

Quantum Noise in Superluminescent Diodes, by Yurek, A.M., Taylor, H.F., Goldberg, L., Weller, J.F., and Dandridge, A., *IEEE Journal of Quantum Electronics* **QE-22**:522-527

Radiation Damage in Optically Transmitting Crystals and Glasses, by Williams, R.T.* and Friebele, E.J., *CRC Handbook of Laser Science and Technology, Vol. III, Optical Materials, Part 1 – Nonlinear Optical Properties/Radiation Damage*, CRC Press, Boca Raton, FL, pp. 299-449

Radiation Effects and Defect Centers in Fiber Optic Materials, by Friebele, E.J., Griscom, D.L., Dorsey, K.L.,* and Gingerich, M.E., *OPTO'86 Conference Proceedings*, ESI Publications, Paris, France, pp. 436–439

Radiation Response Prediction of Single Mode Optical Fiber Waveguides, by Askins, C.G., Shaw, C.M.,* and Friebele, E.J., *Fiber Optics in Adverse Environments III*, SPIE Vol. 721, SPIE–The International Society of Photo-Optical Instrumentation Engineers, Bellingham, WA, pp. 57–62

Rotation of Polarization Axes in High-Birefringence Fibers, by Marrone, M.J., Frigo, N.J., and Dandridge, A., *International Conference on Optical Fiber Sensors, OFS'86, Technical Digest*, pp. 247–250

Selective Two-Step Photoionization of F-Aggregate Centers Using 1.06-μm Radiation, by Schneider, I. and Foster, D.R.,* *Optics Letters* **11**:700–702

Simple Intensity-Modulation Based Fiber Displacement Sensor with Closed Loop Operation, by Kersey, A.D.,* Bucholtz, F., and Dandridge, A., *International Conference on Optical Fiber Sensors, OFS'86, Technical Digest*, pp. 295–298

Some Research Toward the Development of a Hologram Laser Beam Corrector-Collimator for Use in a Satellite Data Link, by Gilbreath-Frandsen, C., Carter, W.H., and Wagner, J.W.,* *Progress in Holographic Applications*, SPIE Vol. 600, SPIE–The International Society of Photo-Optical Instrumentation Engineers, Bellingham, WA, pp. 87–88

Stability of a Fiber-Optic Magnetometer, by Koo, K.P.,* Bucholtz, F., Dandridge, A., and Tveten, A.B., *IEEE Transactions on Magnetics* **MAG- 22**:141–144

Tandem Operation of Mach-Zehnder and Polarimetric Fiber Optic Interferometers: Sensor Applications, by Mermelstein, M.D.,* Kersey, A.D.,* and Dandridge, A. *International Conference on Optical Fiber Sensors, OFS'86, Technical Digest*, pp. 279–281

The Origin of Radiation-Induced Loss Increases in Optical Fiber Waveguides, by Friebele, E.J. and Griscom, D.L., *Proceedings of the Topical Conference on Optical Fiber Communications, OFC'86*, Optical Society of America, Washington, DC, pp. 38–40

Transitions of the Type 2s-sp in Oxygenlike Y, Zr, and Nb, by Behring W.E.,* Brown, C.M., Feldman, U., Seely, J.F., Reader, J.,* and Richardson, M.C.,* *Journal of the Optical Society of America B* **3**:1113–1115

Transmission Properties of 2.55μm Fluoride Glass Fibre, by Eknoyan, O.,* Moeller, R.P., Burns, W.K., Tran, D. C., and Levin, K.H.,* *Electronics Letters* **22**:752–753

Two-Wavelength Fibre Gyroscope with Wide Dynamic Range, by Kersey, A.D.,* Dandridge, A., and Burns, W.K., *Electronics Letters* **22**:935–936

Vapor Diffused Optical Waveguides in Strontium Barium Niobate (SBN:60), by Eknoyan, O.,* Bulmer, C.H., Taylor, H.F., Burns, W.K., Greenblatt, A.S., Beach, L.A., and Neurgaonkar, R.R.,* *Applied Physics Letters* **48**:13–15

Vapor Diffused Optical Waveguides in Strontium Barium Niobate (SBN:60), by Eknoyan, O.,* Bulmer, C.H., Taylor, H.F., Burns, W.K., Greenblatt, A.S., Beach, L.A., and Neugaonkar, R.R.,* *Topical Meeting on Integrated and Guided-Wave Optics, Digest*, Optical Society of America, Washington, DC, Paper THBB1, pp. 24–25

PHYSICS

3s-3p Laser Gain and X-Ray Line Ratios for the Carbon Isoelectronic Sequence, by Feldman, U., Seely, J.F., Doschek, G.A., and Bhatia, A.K.,* *Journal of Applied Physics* **59**:3953–3957

A Generalized Geometrical Representation of Coupled Mode Theory, by Frigo, N.J., *IEEE Journal of Quantum Electronics* **QE-22**:2131–2140

Analysis of X-Ray Diffraction Data from Nitrogen Implanted Polycrystalline Mo and Nb Films: Single Defects, by Rao,* S.E.,* Houska, C.R.,* and Grabowski, K.S., *Nuclear Instruments and Methods in Physics Research* **B18**:47–53

Characterization of a 3 cm Kaufman Ion Source with Nitrogen Feed Gas, Van Vechten, D.,* Hubler, G.K., and Donovan, E.P., *Low Energy Ion Beams IV in: Vacuum* **36**:841–845

Heisenberg Uncertainty and Kullback-Leibler Information, by Rajagopal, A.K.* and Teitler, S., *Physics Letters A* **115**:313–314

Inelastic Electric Lifetime in Niobium Films, by Dalrymple, B.J., Wolf, S.A., Ehrlich, A.C., and Gillespie, D.J., *Physical Review B* **33**:7514– 7519

Multiple Ionization and X-Ray Line Emission Resulting from Inner-Shell Electron Ionization, by Jacobs, V.L. and Rozsnyai, B.F.,* *Physical Review A* **34**:216–226

New Approach to the Solution of Quantum Problems, by Cummings, F.W.* and Rajagopal, A.K., *Physical Review A* **34**:3950–3953

Niobium and Niobium Alloy Wires for Electronic Applications, by LeTourneau, V., Wolf, S.A., Claassen, J.H., and Gubser, D.U., *Proceedings of the 11th International Cryogenic Engineering Conference*, Butterworths, Berlin, West Germany, pp. 699–704

Spectrum of Sodiumlike Selenium: Se XXIV, by Brown, C.M., Seely, J.F., Feldman, U., Richardson, M.C.,* Behring, W.E.,* and Cohen, L.,* *Journal of the Optical Society of America B* **3**:701– 703

Theoretical Computer Profiles Due to Valence Electrons of Ti and TiH_2, by Bacalis, N.C.,* Papanicolaou, N.I.,* and Papaconstantopoulos, D.A., *Journal of Physics F: Metal Physics* **16**:1471–1483

PLASMA PHYSICS

A New Mechanism for Excitation of Waves in a Magnetoplasma I. Linear Theory, by Ganguli, G.,* Lee, Y.C.,* and Palmadesso, P., *Ion Acceleration in the Magnetosphere and Ionosphere, Geophysical Monograph 38*, American Geophysical Union, Washington, DC, pp. 297–300

A New Mechanism for Excitation of Waves in a Magnetoplasma II. Wave-Particle and Nonlinear Aspects, by Palmadesso, P., Ganguli, G.,* and Lee, Y.C.,* *Ion Acceleration in the Magnetosphere and Ionosphere, Geophysical Monograph 38*, American Geophysical Union, Washington, DC, pp. 301–306

A New Mechanism for the Excitation of Kinetic Waves in a Magnetoplasma: Nonlinear Aspects and Applications, by Palmadesso, P.J., Ganguli, G. * and Lee, Y.C.,* *Chapman Conference on Ion Acceleration in the Magnetosphere and Ionosphere (sic)*

A Quasi-Local Theory of the ExB Instability in the Ionosphere, by Fu, Z.F.,* Lee, L.C.,* and Huba, J. D., *Journal of Geophysical Research* **91**:3263–3269

A $TE_{1,3}$ Gyrotron at 85 GHz, by Rhinewine, M. and Read, M.E., *International Journal of Electronics* **61**:729–733

Atomic Data and Spectral Line Intensities for the Boron Isoelectronic Sequence (Ar XIV Through Kr XXXII), by Bhatia, A.K.,* Feldman, U., and Seely, J.F., *Atomic Data and Nuclear Data Tables* **35**:319–343

Beam Trapping in High-Current Cyclic Accelerators with Strong Focusing Fields, by Sprangle, P. and Kapetanakos, C.A., *Particle Acclerators* **18**:203–213

Boundary Integral Method for Computing Eigenfunctions in Slotted Gyrotron Cavities of Arbitrary Cross-Sections, by McDonald, S.W.,* Finn, J.M.,* Read, M.E., and Manheimer, W.M., *International Journal of Electronics* **61**:795–822

Chaos and Nonlinear Dynamics of Single-Particle Orbits in a Magnetotaillike Magnetic Field, by Chen, J. and Palmadesso, P.J., *Journal of Geophysical Research* **91**:1499–1508

Control of Ion-Velocity Distributions in Laser-Target Interaction Experiments, by Grun, J., Stellingwerf, H.,* and Ripin, B.H., *Physics of Fluids* **29**:3390–3393

Convective Stabilization of Ionospheric Plasma Clouds, by Drake, J.F.* and Huba, J.D., *Journal of Geophysical Research* **91**:10108–10116

Current Density Monitor for Intense Relativistic Electron Beams, by Fiorito, R.B.,* Raleigh, M., and Seltzer, S.M.,* *Review of Scientific Instruments* **57**:2462–2470

Current Enhancement for Hose-Unstable Electron Beams, by Fernsler, R.F., Hubbard, R.F., Bui, B., Joyce, G., Lampe, M., and Lau, Y.Y., *Physics of Fluids* **29**:3056–3073

Dynamics of Imploding Neon Gas-Puff Plasmas, by Clark, R.W., Davis, J., and Cochran, F.L.,* *Physics of Fluids* **29**:1971–1978

Effect of AC and DC Transverse Self-Fields in Gyrotrons, by Antonsen, T.M.,* Manheimer, W.M., and Levush, B.,* *International Journal of Electronics* **61**:823–854

Effect of Finite Current Channel Width on the Collisional Ion Cyclotron Instability, by Huba, J. D. and Chaturvedi, P.K., *Planetary and Space Science* **34**:835–840

Effect of Pulse Sharpening on Imploding Neon Z-Pinch Plasmas, by Stephanakis, S.J., Apruzese, J.P., Burkhalter, P.G., Davis, J., Meger, R.A., McDonald, S.W.,* Mehlman, C.G.,* Ottinger, P.F., and Young, F.C., *Applied Physics Letters* **48**:829–831

Electron Orbits in Combined Rotating Quadrupole and Dipole Magnetic Fields, by Levush, R.,* Antonsen, T.M.,* and Manheimer, W.M., *Journal of Applied Physics* **59**:2634–2637

Filtered X-Ray Diodes for Imploding Plasma Experiments, by Young, F.C., Stephanakis, S.J., and Scherrer, V.E., *Proceedings of the 6th Topical Conference on High Temperature Plasma Diagnostics in: Review of Scientific Instruments* **57**:2174–2176

Formation of Highly Charged Ions of Ambient Gas Near Laser-Heated Targets, by Lee, T.N., Molander, W.A., and Elton, R.C., *Physical Review A* **33**:1202–1208

High Gain Free Electron Laser Oscillators, by Marable, W.P.,* Sprangle, P., and Tang, C.M., *Seventh International Free Electron Laser Conference in: Nuclear Instruments and Methods in Physics Research* **A250**:159–167

High-Current Simulation Codes, by Haber, I., *High-Current, High-Brightness, and High-Duty Factor Ion Injectors, AIP Conference Proceedings 139*, American Institute of Physics, NY, pp. 107–131

High-Power Microwave Plasma Pulse Compression, by Manheimer, W.M. and Ripin, B.H., *Physics of Fluids* **29**:2283–2291

High-Power Modulated Intense Relativistic Electron Sources with Applications to RF Generation and Controlled Thermonuclear Fusion, by Friedman, M., Serlin, V., Drobot, A.,* and Mondelli, A.,* *IEEE Transactions on Plasma Science* **PS-14**:201–214

Identification of Lines of Ions Belonging to the FI Isoelectronic Sequence for Rubidium, Strontium, and Yttrium, by Zigler, A.,* Feldman, U., and Doschek, G.A., *Journal of the Optical Society of America B* **3**:1221–1222

Induced Resonance Electron Cyclotron (IREC) QuasiOptical Maser, by Sprangle, P., Tang, C.M., and Serafim, P.,* *Proceedings of the Seventh International Conference on Free Electron Laser in: Nuclear Instru-*

ments and Methods in Physics Research **A250**:361–365

Induced Resonance Electron Cyclotron Quasi-Optical Maser in an Open Resonator, by Sprangle, P., Tang, C.M., and Serafim, P.,* *Applied Physics Letters* **49**:1154–1156

Inner-Shell X-Ray Line Spectra of Highly Ionized Titanium, Chromium, Iron and Nickel and Their Application to Laboratory Plasmas, by Lemen, J.R.,* Phillips, K.J.H.,* Doschek, G.A., and Cowan, R.D.,* *Journal of Applied Physics* **60**:1960–1973

Interferometric Studies of the Pressure of a Confined Laser Heated Plasma, by Griffin, R.D., Justus, B.L., Campillo, A.J., and Goldberg, L.S., *Journal of Applied Physics* **59**:1968–1971

K-Shell Aluminum Resonance Line Ratios for Plasma Diagnosis Using Spot Spectroscopy, by Apruzese, J.P., Duston, D.,* and Davis, J., *Journal of Quantitative Spectroscopy and Radiative Transfer* **36**:339–344

Laser Interaction in Long-Scale-Length Plasmas, by Gardner, J.H., Herbst, M.J., Young, F.C., Stamper, J.A., Obenschain, S.P., Manka, C.K., Kearney, K.J., Grun, J., Duston, D., and Burkhalter, P.G., *Physics of Fluids* **29**:1305–1320

Laser-Target Interaction Using Induced Spatial Incoherence, by Obenschain, S.P., Grun, J., Herbst, M.J., Kearney, K.J., Manka, C.K., McLean, E.A., Mostrovych, A.N., Stamper, J.A., Whitlock, R.R., Bodner, S.E. Gardner, J.H., and Lehmberg, R.H., *Physical Review Letters* **56**:2807–2810

Linear Effects of Varying Ion Composition on Perpendicularly-Driven Flute Modes: Comparison to Rocket Observations, by Walker, D.N., *Ion Acceleration in the Magnetosphere and Ionosphere, Geophysical Monograph 38*, American Geophysical Union, Washington, DC, pp. 311–316

Linear and Non-linear Theory of the Doppler-Shifted Cyclotron Resonance Maser Based on TE and TM Waveguide Modes, by Fliflet, A.W., *International Journal of Electronics* **61**:1049–1080

Long Conduction Time Plasma Erosion Opening Switch Experiment, by Hinshelwood, D.D.,* Boller, J.R., Commisso, R.J., Cooperstein, G., Meger, R.A., Neri, J.M., Ottinger, P.F., and Weber, B.V.,* *Applied Physics Letters* **49**:1635–1637

Magnetic Field Compression and Evolution in Laser-Produced Plasma Expansions, by Kacenjar, S., Hausman, M.,* Keskinen, M., Ali, A.W., Grun, J., Manka, C.,* McLean, E., and Ripin, B.H., *Physics of Fluids* **29**:2007–2012

Nonlinear Analysis of Efficiency Enhancement in Free-Electron-Laser Amplifiers, by Freund, H.P.* and Ganguly, A.K., *Physical Review A* **33**:1060–1072

Nonlinear Analysis of a Relativistic Beam-Plasma Cyclotron Instability, by Sprangle, P. and Vlahos, L.,* *Physical Review A* **33**:1261–1269

Numerical Simulation of a Low-Density Plasma Erosion Opening Switch, by Grossmann, J.M., Ottinger, P.F., Neri, J.M., and Drobot, A.T.,* *Physics of Fluids* **29**:2724–2735

One Dimensional Models for Relativistic Electron Beam Diode Design, by Finn, J.M.,* Fliflet, A.W., and Manheimer, W.M., *International Journal of Electronics* **61**:985–1003

Particle Accelerators Powered by Modulated Intense Relativistic Electron Beams, by Friedman, M. and Serlin, V., *Applied Physics Letters* **49**:596–598

Perpendicular Ion Beam-Driven Instability in a Multicomponent Plasma: Effects of Varying Ion Composition on Linear Flute Mode Oscillations, by Walker, D.N., *Journal of Geophysical Research* **91**:3305–3310

Projections of Cloud Structures and Their Spectra, by Zabusky, N.J.,* Hyman, E.,* and Mulbrandon, M., *Journal of Geophysical Research* **91**:5851–5858

Quantitative X-Ray Spectroscopy of Neon Z-Pinch Plasmas, by Mehlman, G.,* Burkhalter, P.G., Stephanakis, S.J., Young, F.C., and Nagel, D.J., *Journal of Applied Physics* **60**:3427–3432

Radiation Cooling and Gain Calculation for C VI 182-A° Line in Carbon-Selenium Plasmas, by Nam, C.H.,* Valeo, E.,* Suckewer, S.,* and Feldman, U., *Journal of the Optical Society of America B* **3**:1199–1205

SIMM1: A Linearized Particle Code, by Joyce, G. and Lampe, M., *Journal of Computational Physics* **63**:398–415

Saha Decrements and Collisional-Radiative Recombination and Ionization Coefficients for a Nonequilibrium Nitrogen Plasma, by Taylor, R. D.* and Ali, A.W., *Journal of Quantitative Spectroscopy and Radiative Transfer* **35**:213–230

Saha Decrements and Collisional-Radiative Recombination and Ionization Coefficients for a Nonequilibrium Oxygen Plasma, by Taylor, R. D.* and Ali, A.W., *Journal of Quantitative Spectroscopy and Radiative Transfer* **36**:373–383

Soft X-Ray Emission from Gas Puff Implosions, by Burkhalter, P.G., Mehlman, G.,* Young, F.C., Stephanakis, S.J., Scherrer, V.E., and Newman, D.A.,* *International Colloquium on X-Ray Lasers in Journal de Physique, Colloque* **C6**:C6-247–C6-252

Spectral Characteristics of Interchange Turbulence, by Hassam, A.B.,* Hall, W.,* Huba, J. D., and Keskinen, M.J., *Journal of Geophysical Research* **91**:13513–13522

Spectral Measurements from Laser-Produced Plasma in OMEGA, by Burkhalter, P.G., Newman, D.A.,* Rosen, D.L.,* Hudson, K.,* Richardson, M.,* and Audebert, P.,* *Proceedings of the 6th Topical Conference on High Temperature Plasma Diagnostics in: Review of Scientific Instruments* **57**:2171–2173

Spectrum Lines of Highly Ionized Zinc, Germanium, Selenium, Zirconium, Molybdenum, and Silver Injected into Princeton Large Torus and Tokamak Fusion Test Reactor Tokamak Discharges, by Hinnov, E.,* Boody, F.,* Cohen, S.,* Feldman, U., Hosea, J.,* Sato, K.,* Schwob, J.L.,* Suckewer, S.,* and Wouters, A., *Journal of the Optical Society of America B* **3**:1288–1294

Stochasticity of Particle Orbits in a Collective Particle Accelerator, by Ganguli, G.,* Mitchell, H.G.,* and Palmadesso, P., *Journal of Applied Physics* **59**:365–370

Sub-nanosecond Pulselength Millimeter Wave Generation with a Phase Modulated Quasi-Optical Gyrotron, by Manheimer, W.M. and Read, M.E. *International Journal of Electronics* **61**:1041–1048

Techniques and Initial Results from an X-Ray Laser Experiment Using Laser-Vaporized Copper Foil Plasmas, by Molander, W.A.,* Lee, T.N., Ford, J.L., and Elton, R.C., *High Intensity Laser Processes*, SPIE Vol. 664, SPIE–The International Society of Photo-Optical Instrumentation Engineers, Bellingham, WA, pp. 285–290

The Effect of Finite "Blob" Size on the Current Convective Instability in the Auroral Ionosphere, by Huba, J. D. and Chaturvedi, P.K., *Journal of Geophysical Research* **91**:7125–7130

The Two-Plasmon Instability for Low Temperature and Inhomogeneous Plasma, by Grebogi, C.* and Manheimer, W.M., *Plasma Physics and Controlled Fusion* **28**:439–451

Theory of the Orbitron Maser, by Burke, J.M., Manheimer, W.M., and Ott, E.,* *Physical Review Letters* **56**:2625–2628

X-Ray Spectroscopic Diagnostics of a Copper Plasma Produced by a Laser Line Focused

onto a Thin Foil, by Lee, T.N., Molander, W.A., Ford, J.L., and Elton, R.C., *Proceedings of the 6th Topical Conference on High Temperature Plasma Diagnostics in: Review of Scientific Instruments* **57**:2052–2054

RADAR

A Family of Curves for the Rough Surface Reflection Coefficient, by Miller, A.R. and Vegh, E., *IEE Proceedings* **133H**:483–489

Antennas, Propagation, and Radar Systems, by Skolnik, M.I., *AP–S International Symposium 1986, Antennas and Propagation Symposium Digest* Vol. 2, IEEE, NY, p. 497

Aspects of Radar Signal Processing, by Lewis, B.L., Kretschmer, F.K., and Shelton, W.K., Artech House, Inc., Norwood, MA, 554 pp.

Automatic Curve Fitting with Quadratic B–Spline Functions and its Application to Computer–Assisted Animation, by Yang, M.C.K.,* Kim, C.K.,* Cheng, K.Y.,* Yang, C.C., and Liu, S.S.,* *Computer Graphics and Image Processing* **33**:346–363

Exact Solution for Control Loop Adaptive Antenna Weights in Band–Limited Noise, by Gerlach, K. and Lang, R.H.,* *IEEE Transactions on Antennas and Propagation* **AP–34**:395–403

Fast Orthogonalization Networks, by Gerlach, K., *IEEE Transactions on Antennas and Propagation* **AP–34**:458–462

Grain Size Dependence of SbSI with Oriented Grains, by Yon, K., Kahn, M., Rice, R.W.,* and Spann, J.R.,* *86th Annual Meeting of the American Ceramic Society in: Advanced Ceramic Materials* **1**:64–67

HF Radar Measurements of Wave Spectral Development, by Trizna, D.B., *Wave Dynamics and Radio Probing of the Ocean Surface*, Plenum Press, NY, pp. 449–464

Mirror–Antenna Radar Concept, by Cross, D.C., Howard, D.D., and Titus, J.W., *Microwave Journal* **29**:323–335

MTI Target Visibility, by Kretschmer, F.F., *IEEE Transactions on Aerospace and Electronic Systems* **AES– 22**:216–218

On Microwave Scattering by Breaking Waves, by Wetzel, L., *Wave Dynamics and Radio Probing of the Ocean Surface*, Plenum Press, NY, pp. 273–284

Power Density and Threshold Control Strategies for Radar Track Initiation, by Cantrell, B.H., *IEEE 1986 National Radar Conference*, IEEE, NY, pp. 71–75

Pulse Compression Waveforms Using Huffman Codes, by Kretschmer, F.F., *IEEE 1986 National Radar Conference*, IEEE, NY, pp. 59–64

Remote Sensing of Directional Wave Spectra Using the Surface Contour Radar, by Walsh, E.J.,* Hancock, D.D.,* Hines, D.E.,* and Kenney, J.E., *Wave Dynamics and Radio Probing of the Ocean Surface*, Plenum Press, NY, pp. 449–464

Resonance Frequencies of Conducting Spheroids and the Phase Matching of Surface Waves, by Merchant, B.L., Nagl, A.,* and Uberall, H.,* *IEEE Transactions on Antennas and Propagation* **AP– 34**:1464–1467

Speckle Suppression and Analysis for Synthetic Aperture Radar Images, by Lee, J.S., *Optical Engineering* **25**:636–643

Using Spectral Estimation Techniques in Adaptive Processing Antenna Systems, by Gabriel, W., *IEEE Transactions on Antennas and Propagation* **AP–34**:291–300

RADIATION PHYSICS

Adaptation of a Program for Depth Distribution of Energy Deposition by Ion Bombardment: Better Stopping Powers, by Davisson, C.M. and Manning, I., *Computer Physics Communications* **42**:137–147

Analysis of Helium–Ion Scattering with a Desktop Computer, by Butler, J.W., *7th International Conference on Ion Beam Analysis in: Nuclear Instruments and Methods in Physics Research* **B15**:232–237

Calculation of Free-Bound Transition Strength in Channeling Radiation or Coherent Bremsstrahlung, by Saenz, A.W., Nagl, A.,* and Uberall, H.,* *11th International Conference on Atomic Collisions in Solids in: Nuclear Instruments and Methods in Physics Research* **B13**:23-26

Cascade Simulation of Crystal Orientation Dependence of Sputtering and Lattice Damage of Single Crystal Copper by Irradiation with 100 keV Copper Ions, by Mueller, G.P., Rosen, M., Fraser, W. Sprague, J.A., Malmberg, P.R., Lambert, J.M., Treado, P.A., and Reynolds, G.W., *Symposium on Sputtering in: Nuclear Instruments and Methods in Physics Research* **B13**:360-364

Characterization of the Absolute Photon Sensitivity of Gold Cathode Photoelectric Detectors, by Dozier, C.M., Freitag, R.F., and Fehl, D.L.,* *X-Ray Calibration: Techniques, Sources and Detectors*, SPIE Vol. 689, SPIE-The International Society of Photo-Optical Instrumentation Engineers, Bellingham, WA

Determination of the Quantum Density Matrix from Experiment: An Application to Position Annihilation, by Pecora, L.M., *Physical Review B* **33**:5987-5993

Effects of Target Constituent Mass Difference on Collision Cascade Induced Composition Changes in Binary Alloys, by Rosen, M., Mueller, G.P., Rousch, M.L.,* Andreadis, T.D., and Goktepe, O.F.,* *11th International Conference on Atomic Collisions in Solids in: Nuclear Instruments and Methods in Physics Research* **B13**:439-442

Energy Dependence of Proton Displacement Damage Factors for Bipolar Transistors, by Summers, G.P., Xapsos, M.A., Wolicki, E.A.,* Gehlhausen, M.A.,* Blicae, R.D.,* Marshall, P.,* and Dale, C.J., *1986 Annual Conference on Nuclear and Space Radiation Effects in: IEEE Transactions on Nuclear Science* **NS-33**:1282-1286

Friction and Wear Properties of Ion Implanted and Ion Beam Enhanced Vapor Deposited Surfaces, by Sartwell, B.D., *Ion Plating and Implantation Applications to Materials*, American Society for Metals, Metals Park, OH, pp. 81-89

IMPLNT-A Fortran Program to Calculate the Distribution of Implanted Ions Which Includes the Effects Due to Sputtering, by Davisson, C.M., *Proceedings of the International Conference on Atomic Collisions in Solids in: Nuclear Instruments and Methods in Physics Research* **B13**:421-425

In Situ Auger Electron Spectroscopy Applied to the Study of Chemisorption and Diffusion During Reactive Implantation of Titanium into Iron, by Baldwin, D.A.,* Sartwell, B.D., and Singer, I.L., *Applied Surface Science* **25**:364-379

Initial Tests of the NRL Ubitron, by Jackson, R.H. and Pershing, D.E.,* *1986 International Electron Devices Meeting*. IEEE, NY, pp. 342- 345

Modeling the Development of the Component Surface Fractions of Polycrystalline Metals During Ion Implantation, by Reynolds, G.W., *11th International Conference on Atomic Collisions in Solids in: Nuclear Instruments and Methods in Physics Research* **B13**:467-472

Single Event Upset Dependence on Temperature or an NMOS/Resistive-Load Static RAM, by Stapor, W.,* Johnson, R.L.,* Xapsos, M.A., Fernald, K.W.,* Campbell, A.B., Bhuva, B.L.,* and Diehl, S.E., *1986 Annual Conference on Nuclear and Space Radiation Effects in: IEEE Transactions on Nuclear Science* **NS-33**:1610-1615

Some Characteristics of a Droplet Whispering-Gallery-Mode Laser, by Lin, H.B., Huston, A.L., Justus, B.L., and Campillo, A.J., *Optics Letters* **11**:614–616

Spontaneous Radiation of an Electron Beam in a Free-Electron Laser with a Quadrupole Wiggler, by Levush, B.,* Antonsen, T.M.,* and Manheimer, W.M., *Journal of Applied Physics* **60**:1584–1590

Strongly Inhibited Rayleigh–Taylor Growth with 0.25μm Lasers, by Emery, M.H., Gardner, J.H., and Bodner, S.E., *Physical Review Letters* **57**:703–706

Synchrotron Radiation Beam Lines as X-Ray Calibration Sources, by Kirkland, J.P.,* Neiser, R.A.,* Elam, E.T., Rife, J.C., and Hunter, W.R.,* *X-Ray Calibration: Techniques, Sources and Detectors*, SPIE Vol. 689, SPIE–The International Society of Photo-Optical Instrumentation Engineers, Bellingham, WA, pp. 188–197

Temperature and Dose Dependence of an Amorphous Layer, by Richmond, E.D. and Knudson, A.R., *Materials Research Society Symposia Proceedings* Vol. 51, pp. 375–380

The Effect of the Choice of Response Matrix on Neutron Spectra Unfolded from Bonner Sphere Data, by Lowry, K.A. and Johnson, T.L., *Health Physics* **50**:543–547

The Role of Vibrational Excitations in Collision-Induced Dissociation Using Faddeev-AGS Theory, by Haftel, M.I. and Lim, T.K.,* *Journal of Chemical Physics* **84**:4407–4425

SOLID STATE

2Eg Transitions in GaSb–AlSb Quantum Well Structures, by Forchel, A.,* Cebulla, U.,* Trankle, G.,* Lach, E.,* Reinecke, T.L., Kroemer, H.,* Subbanna, S.,* and Griffiths, G.,* *Physical Review Letters* **57**:3217–3220

A Priori Predictions of Phase Transitions in KCaF$_3$ and RbCaF$_3$: Existence of a New Ground State, by Flocken, J.W.,* Guenther, R.A.,* Hardy, J.R.,* and Boyer, L.L., *Physical Review Letters* **56**:1738–1741

A Vacuum Field Effect Transistor Using Silicon Field Emitter Arrays, by Gray, H.F., Greene, R.F., and Campisi, G.J., *1986 IEDM Conference on Electron Devices*, IEEE, NY, p.331

Calculation of the Compton Profiles of Tantalum and Tungsten, by Papanicolaou, N.I.,* Bacalis, N.C.,* and Papaconstantopoulos, D.A., *Physica Status Solidi (b)* **57**:597–606

Characterization of Impurities in p-Type HgCdTe by PhotoHall Techniques, by Bartoli, F.J., Hoffman, C.A., and Meyer, J.R., *Workshop on the Physics and Chemistry of Mercury Cadmium Telluride in: Journal of Vacuum Science and Technology* **A4**:2047–2050

Comment on "The Growth of Fe Overlayers on Ag(100)" by G.C. Smith, H.A. Padmore and C. Norris, by Jonker, B.T. and Prinz, G.A., *Surface Science* **172**:L568–L570

Conductivity Relaxation and Spin Lattice Relaxation in Lithium and Mixed Alkali Borate Glasses: Activation Enthalpies, Anomalous Isotope-Mass Effect and Mixed Alkali Effect, by Ngai, K.L. and Jain, H.,* *Solid State Ionics–85 Conference in: Solid State Ionics* **18–19**:362–367

Defect Detection with a SQUID Magnetometer, by Weinstock, H.* and Nisenoff, M., *Review of Progress in Quantitative Nondestructive Evaluation* **5A**:699–704

Density Functionals in Solids II. Excitations, by Pickett, W.E., *Comments on Solid State Physics* **12**:57–68

Detection of Hydrogen in Nominally Pure GaP:Zn by Optically Detected Electron Nuclear Double Resonance, by Shiner, J.,* Kana-ah, A.,* Cavenett, B.C.,* Kennedy, T.A., and Wilsey, N., *Solid State Communications* **59**:653–656

Detection of Magnetic Fields Generated by Electrochemical Corrosion, by Bellingham, J.G.,* MacVicar, M.L.A.,* Nisenoff, M., and Searson, P.C.,* *Journal of the Electrochemical Society* **133**:1753–1754

Determination of the Green's Function in the Spectral Domain Using a Matrix Method: Application to Radiators or Resonators Immersed in a Complex Anisotropic Layered Medium, by Krowne, C.M., *IEEE Transactions on Antennas and Propagation* **AP-34**:247–253

Diagnostic Analysis of GaAs High-Electron-Mobility Devices and Integrated Circuits, by Christou, A. and Anderson, W.T., *Microbeam Analysis–1986*, San Francisco Press, Inc., San Francisco, CA, pp. 636–640

Direct Construction of Path Integrals in the Lattice-Space Multi-Band Dynamics of Electrons in a Solid, by Buot, F.A., *Physical Review A* **33**:2544–2562

Double-Crystal X-Ray Topographic Studies of Bulk and Epitaxially Grown $Zn_xCd_{1-x}Te$ ($0.0 < x < 0.06$), by Qadri S.B.,* Fatemi, M., and Divan, J.H.,* *Applied Physics Letters* **48**:239–241

Effect of Static Charge on the Infrared Spectrum of Amorphous Silicon, by Fong, C.Y.,* Nichols, C.S.,* Guttman, L.,* and Klein, B.M., *Physical Review B* **34**:2402–2406

Effective Hamiltonians for Phonon-Coupled and Spatially Confined Systems, by Kriman, A.M. *Physical Review B* **33**:6667–6674

Effects of Interface Charge on the Quantum Hall Effect, by Furneaux, J.E. and Reinecke, T.L., *Physical Review B* **33**:6897–6908

Effects of RF Bias on the Superconducting and Structural Properties of RF Magnetron Sputtered NbN, by Carter, W.L., Cukauskas, E.J., Qadri, S.B.,* Lewis, A.S.,* and Mattauch, R.J.,* *Journal of Applied Physics* **59**:2905– 2907

Effects of Various Implant Species and Post-Anneal Treatments on Si N-Channel MOSFETs, by Tseng, W.F., Hevey, R.H., Corazzi, R.J., Christou, A., and Davis, G.E., *Journal of Electronic Materials* **15**:1–6

Electrical and Optical Properties of Sputtered TiNx Films as a Function of Substrate Deposition Temperature, by Thorpe, T.P., Qadri, S.B.,* Wolf, S.A., and Claassen, J.H., *Applied Physics Letters* **49**:1239–1241

Electron-Phonon Coupling in UBe_{13}: Absence of Conventional Superconductivity, by Pickett, W.E., Krakauer, H.,* and Wang, C.S.,* *Physical Review B* **34**:6546–6549

Electron-Stimulated Desorption of Positive Ions from Hexagonal α-SiC, by Bermudez, V.M., Parrill, T.M.,* and Kaplan, R., *Surface Science* **173**:234–244

Electronic Characteristics of Quantum Well Electron Barrier Diodes, by Kirchoefer, S.W. and Newman, H.S., *Proceedings IEEE/Cornell Conference on Advanced Concepts in High Speed Semiconductor Devices and Circuits*, IEEE, NY, p. 246

Electronic Raman Scattering of the Negative Charge State of the 78-meV Double Acceptor in GaAs, by Shanabrook, B.V., Moore, W.J., and Bishop, S.G., *Physical Review B* **33**:5943–5945

Electronic Structure of the Carbon Vacancy in NbC, by Pickett, W.E., Klein, B.M., and Zeller, R.,* *Physical Review B* **34**:2517–2521

Electronic Structure of the Fe/Ge (110) Interface, by Pickett, W.E. and Papaconstantopoulos, D.A., *Physical Review B* **34**:8372–8378

Epitaxial Growth of Superconducting Niobium Thin Films by Ultrahigh Vacuum Evaporation, by Wolf, S.A., Claassen, J.H., Qadri, S.B., Dalrymple, B.J., and Francavilla, T.L., *Proceedings of the 32nd National Symposium of the American Vacuum Society in: Journal of Vacuum Science and Technology A* **4**:524–527

Exchange-Correlation Potentials for Spin-Polarized Systems at Finite Temperatures, by

Kanhere, D.G.,* Panat, P.V.,* Rajagopal, A.K., and Calloway, J.,* *Physical Review A* 35:490–497

Experimental Studies of Iron Impurity Centers in III–V Semiconductors, by Bishop, S.G., *Deep–Level Centers in Semiconductors*, Gordon and Breach, NY, p.541

First–Principles Theoretical Explanation of Incommensurate Behavior in Rb_2ZnCl_4, by Katkanant, V.,* Edwardson, P.J.,* Hardy, J.R.,* and Boyer, L.L., *Physical Review Letters* **57**:2033–2036

Formation of Charged N_1 Centers in KCl and KBr, by Schneider, I., *Journal of Applied Physics* **59**:1086–1091

Free–Exciton Diffusion and Decay in Zero–Stress Ge, by Culbertson, J.C., Westervelt, R.M.,* and Haller, E.E.,* *Physical Review B* **34**:6980–6986

Fundamental Radiation–Induced Defect Centers in Synthetic Fused Silicas: Atomic Chlorine, Delocalized E' Centers and Triplet State, by Griscom, D.L. and Friebele, E.J., *Physical Review* **34**:7524–7533

Growth of GaN Films Using Trimethylgallium and Hydrazine, by Gaskill, D.K., Bottka, N., and Lin, M.C., *Applied Physics Letters* **48**:1449–1451

Growth of Single Crystal bcc α–Fe on ZnSe via Molecular Beam Epitaxy, by Prinz, G.A., Jonker, B.T., Krebs, J.J., Ferrari, J.M., and Kovanic, F.,* *Applied Physics Letters* **48**:1756–1758

Handbook of the Band Structure of Elemental Solids, by Papaconstantopoulos, D.A., *Plenum Press*, NY, 410pp

High Dose Implantation of Nickel in Silicon, by Campisi, G.J., Dietrich, H.B., Delfino, M.,* and Sadana, D.K.,* *Materials Research Society Symposium Proceedings* **54**:747–752

High Power Pulse Reliability of GaAs Power FETs, by Anderson, W.T., Buot, F.A., Christou, A., and Anand, Y.,* *Reliability Physics 1986, 24th Annual Proceedings*, IEEE, NY, pp. 144–149

High Pressure Studies of $Hg_{0.8}Cd_{0.2}Te$, by Qadri, S.B., Skelton, E.F., Webb, A.W., and Dinan, J.,* *Journal of Vacuum Science and Technology* **A4**:1974–1976

Identification of the Ga Interstitial in $Al_xGA_{1-x}As$ by Optically Detected Magnetic Resonance, by Kennedy, T.A. and Spencer, M.G.,* *Physical Review Letters* **57**:2690–2693

In–Situ, Real–Time Diagnostics of OMVPE Using IR–Diode Laser Spectroscopy, by Butler, J.E., Bottka, N., Sillmon, R.S., and Gaskill, D.K., *Journal of Crystal Growth* **77**:163–171

Infrared Reflectance Evaluation of Chemically Vapor Deposited B–SiC Films Grown on Si Substrates, by Holm, R.T., Klein, P.H., and Nordquist, P.E.R., *Journal of Applied Physics* **60**:1479–1485

Interpretation of Differences in Temperature and Pressure Dependences of Density and Concentration Fluctuations in Amorphous Poly(phenylmethyl siloxane), by Ngai, K.L. and Fytas, G.,* *Journal of Polymer Science: Part B: Polymer Physics* **24**:1683–1694

Local Density Theory for Dynamical Correlation Corrections to Single Particle Excitations in Semiconductors, by Pickett W.E. and Wang, C.S.,* *International Symposium on Atomic, Molecular and Solid–State Theory, Scattering Problems, Many Body Phenomena, and Computational Quantum Chemistry in: International Journal of Quantum Chemistry, Quantum Chemistry Symposium* **20**:*299–311*

Low Frequency Raman Spectra of Chalcogenide Glasses, by Strom, U. and Freitas, J.A.,* *Solid State Communications* **59**:565–568

Metallic Epitaxy of Transition Metals on Semiconductors, by Prinz, G.A., *Materials Research Society Symposia Proceedings*, Vol. 56, Materials Research Society, pp. 139-144

Microwave and Millimeter-Wave Monolithic Integrated Circuits, by Spielman, B.E., *1986 IEEE Princeton Section Sarnoff Symposium*, IEEE, NY, pp. 1-5

Model for the 1.28-eV Double Acceptor Luminescence in GaAs, by Shanabrook, B.V., Moore, W.J., and Bishop, S.G., *Journal of Applied Physics* **59**:2535-2537

Multi-Ion Screening in Uncompensated Semiconductors, by Meyer, J.R. and Bartoli, F.J., *Physical Review Letters* **57**:2568-2571

Native Defects in Beta SiC, by Lin-Chung, P.J. and Li, Y.,* *Defects in Semiconductors III*, Trans Tech Publications, Switzerland, p.1247

New Materials Technology for Improving the Efficiency of Photovoltaic Solar Cells, by Statler, R.L. and Faraday, B.J., *Optical Materials Technology for Energy Efficiency and Solar Energy Conversion*, SPIE Vol. 653, SPIE-The International Society of Photo-Optical Instrumentation Engineers, Bellingham, WA, pp. 308-314

Nondestructive Evaluation of Metallic Structures Using a SQUID Magnetometer, by Weinstock, H.* and Nisenoff, M., *SQUID-85 Superconducting Quantum Interference Devices and Their Applications*, Walter de Gruyter and Co., Berlin, W.Germany, pp. 853-858

Novel Electrostatic Mechanism in the Thermal Instability of z-cut $LiNbO_3$ Interferometers, by Skeath, P.,* Bulmer, C.H., Hiser, S.C.,* and Burns, W.K., *Applied Physics Letters* **49**:1221-1223

Nuclear Magnetic Resonance in Al-rich Quasiperiodic Crystals, by Rubinstein, M., Stauss, G.H., Phillips, T.E.,* Moorjani, K.,* and Bennett, L.H., *Journal of Materials Research* **1**:243-246

Nuclear Magnetic Resonance Measurements of Lattice Distortions in GaAs:In, by Carlos, W.E., Bishop, S.G., and Treacy, D.J.,* *Applied Physics Letters* **49**:528-530

OMVPE of GaN and AlN Films by Metal Alkyls and Hydrazine, by Gaskill, D.K., Bottka, N., and Lin, M.C., *3rd International Conference on Metalorganic Vapor Phase Epitaxy in: Journal of Crystal Growth* **77**:418-423

Observation of and Bias-Dependent Annealing of a Paramagnetic Defect Possibly Unique to Thermally Grown SiO_2, by Carlos, W.E., *Applied Physics Letters* **49**:1767-1769

Off-Center Self-Trapped Excitons and Creation of Lattice Defects in Alkali Halide Crystals, by Williams, R.T.,* Song, K.S.,* Faust, W.L., and Leung, C.H.,* *Physical Review B* **33**:7232-7240

Ohmic Contact Control in Modulation-Doped Gallium Arsenide Field-Effect Transistors, by Christou, A., Efthimiopoulos, T.,* and Hatsopoulos, Z.,* *Applied Physics Letters* **49**:1077-1079

Photoreflectance Study of $Hg_{0.7}CD_{0.3}Te$ and $Cd_{1-x}Zn_xTe$: e_1 Transition, by Amirtharaj, P.M.,* Dinan, J.H.,* Kennedy, J.J.,* Boyd, P.R.,* and Glembocki, O.J., *Journal of Vacuum Science and Technology A* **4**:2028-2033

Photoreflectance of GaAs/GaAlAs Multiple Quantum Wells: Topographical Variations in Barrier Height and Well Width, by Parayanthal, P.,* Shen, H.,* Pollak, F.H.,* Glembocki, O.J., Shanabrook, B.V., and Beard, W.T., *Applied Physics Letters* **48**:1261-1263

Polarized-X-Ray Absorption Studies of Graphite Intercalated-Bromine Compounds, by Feldman, J.L., Elam, W.T., Ehrlich, A.C., Skelton, E.F., Dominguez, D.D., Chung, D.D.L.,* and Lytle, F.W.,* *Physical Review B* **33**:7961-7982

Potential-Induced Breathing Model for the Elastic Moduli and High-Pressure Behavior of the Cubic Alkaline-Earth Oxides, by

Mehl, M.J.,* Hemley, R.J.,* and Boyer, L.L., *Physical Review B* **33**:8685–8696

Radiation Induced Substrate Currents in a GaAs MMIC Amplifier, by Beall, J.M.* and Anderson, W.T., *GaAs IC Symposium, Technical Digest 1986*, IEEE, NY, pp. 133–140

Radiation Hardened ICs – Advanced Silicon and GaAs Integrated Circuits, by Killiany, J.M., Hughes, H.L., Anderson, W.T., and Lambert, R.J., *Journal of Electronic Defense* **9**:2:33–49

Reduction of SiC Surface Oxides by a Ga Molecular Beam: LEED and Electron Spectroscopy Studies, by Kaplan, R. and Parrill, T.M.,* *Surface Science* **165**:L45–L52

Semi-Insulating Behavior in Undoped LEC InP After Annealing in Phosphorus, by Klein, P.B., Henry, R.L., Kennedy, T.A., and Wilsey, N.D., *Defects in Semiconductors, Materials Science Forum*, Volume 10–12, Trans Tech Publications, Ltd, Switzerland, pp. 1259–1264

Shallow Donors in Semi-Insulating GaAs and Their Role in the Excitation of the 0.64-eV Photoluminescence, by Paget, D.* and Klein, P.B., *Physical Review B* **34**:971–978

Soft X-Ray Calibration of Diffracting Materials, by Burkhalter, P.G., Gilfrich, J.V., Brown, D.B., and Rosen, D.L.,* *X-Ray Calibration: Techniques, Sources, and Detectors*, SPIE Vol. 689, SPIE–The International Society of Photo-Optical Instrumentation Engineers, Bellingham, WA, pp. 121–127

Spin-Polarized Photoemission Study of Epitaxial Fe(001) Films on Ag(001), by Jonker, B.T., Walker, K.H.,* Kisker, E.,* Prinz, G.A., and Carbone, C.,* *Physical Review Letters* **57**:142–145

Streak and Framing Camera Designs Using Surface Acoustic Wave Charge – Transfer Devices, by Whitlock R.R. and Papanicolaou, N.A., *Optical Engineering* **25**:1267– 1277

Structural Studies of $Cd_{0.95}Zn_{0.05}Te$ and $Cd_{0.90}Mn_{0.10}Te$ Under Pressure, by Qadri, S.B., Skelton, E.F., Webb, A.W., and Kennedy, J.,* *Journal of Vacuum Science and Technology* **A4**:1971–1973

Structure of SiO_2 Films on Silicon as Revealed by Oxygen Transport, by Revesz, A.G.,* Mrstik, B.J., Hughes, H.L., and McCarthy, D., *Journal of the Electrochemical Society* 133:586–592

Studies of the Fractional Quantum Hall Effect in a Silicon MOSFET, by Furneaux, J.E., Syphers, D.A.,* Brooks, J.S.,* Schmiedeshoff, G.,* Wheeler, R.G.,* and Stiles, P.J.,* *Electronic Properties of Two-Dimensional Systems in: Surface Science* **170**:154–159

Superconducting and Structural Properties of RF Magnetron Sputtered Niobium Nitride for Josephson Junctions, by Cukauskas, E.J. and Carter, W.L., *Cryogenic Engineering Conference and International Cryogenic Materials Conference in: Advances in Cryogenic Engineering* **32**:643–650

Temperature Dependence of Photoreflectance in GaAs-AlGaAs Multiple Quantum Wells, by Glembocki, O.J., Shanabrook, B.V., and Beard, W.T., *Surface Science* **174**:206–210

The Properties of Hydrogen Donors Confined in GaAs-AlGaAs Multiple Quantum Wells, by Shanabrook, B.V., *Electronic Properties of Two-Dimensional Systems in: Surface Science* **170**:449–458

The Search for the Full Atomic Structure of EL2 in GaAs, by Kennedy, T.A., *Defects in Semiconductors I*, Trans Tech Publications, Switzerland, p.283

Theory of Electronic States in Disordered Alloy Hydrides, by Papaconstantopoulos, D.A., Laufer, P.M., and Switendick, A.C.,* *Hydrogen in Disordered and Amorphous Solids*, Plenum Publishing Corp., NY, pp. 139–152

Theory of Superconductivity in Palladium–Noble Metal Hydrides, by Laufer, P.M. and Papaconstantopoulos, D.A., *Physical Review B* **33**:5134– 5137

Thermal Bleaching of γ–Ray–Induced Defect Centers in High Purity Fused Silica by Diffusion of Radiolytic Molecular Water, by Griscom, D.L., *Structure and Bonding in Noncrystalline Solids*, Plenum Publishing Corp., NY, pp. 369–384

Transient Small–Polaron Hopping Motion, by Emin, D.* and Kriman, A.M., *Physical Review B* **34**:7278–7289

Triplet Spin ODMR from Phosphorus Antisites in Undoped InP, by Kennedy, T.A., Wilsey, N.D., Klein, P.B., and Henry, R.L., *Defects in Semiconductors I*, Trans Tech Publications, Switzerland, p.271

Unconventional Superconductivity and Normal–State Properties in the Heavy Fermion Superconductor UPt_3, by Wang, C.S.,* Krakauer, H.,* and Pickett, W.E., *Journal of Physics F: Metal Physics* **16**:L287–L293

Vibrational Properties of the Si(100) 2x1 Surface, by Tiersten, S.,* Ying, S.C.,* and Reinecke, T.L., *Physical Review B* **33**:4062–4076

Vibrational Spectroscopy at High External Pressure: The Diamond Anvil Cell, by John R Ferraro, Academic Press, New York, 1984, by Skelton, E.F., *Physics Today* **39**:4:62–64

Vibrational Spectroscopy of Adsorbates Using a Tunable Diode Laser, by Bermudez, V.M., Hylden, J.L., and Butler, J E., *Vibrations and Surfaces 1985 in: Journal of Electron Spectroscopy and Related Phenomena* **38**·143–152

X–Ray Diffraction Tools and Techniques for Solid State Devices, by Fatemi, M., *Review of Progress Quantitative Nondestructive Evaluation* **5B**:991–1000

SPACE SCIENCE

$2s^22p^5$ – $2s2p^6$Transitions in Fluorinelike Ions from Zr^{31}+ to Sn^{41}+d, by Reader, J.,* Brown, C.M., Ekberg, J.O.,* Feldman, U., Seely, J.F., and Behring, W.E.,* *Journal of the Optical Society of America B* **3**:1609–1611

A Siphon Mechanism for Supplying Prominence Mass, by Poland, A.I.* and Mariska, J.T., *Solar Physics* **104**:303–312

An IRAS Survey of IR Excesses in G–type Stars, by Odenwald, S.F., *Astrophysical Journal* **307**:711–722

Angular Momentum–Limited Degenerate and Semidegenerate Neutrino Halos, by Chubb, T.A., *Astrophysical Journal* **305**:609–622

Comment on the Paper "On the Influx of Small Comets Into the Earth's Upper Atmosphere I. Observations," by Chubb, T.A.,* *Geophysical Research Letters* **13**:1075–1077

Comparison of CREME Model LET Spectra with Spaceflight Dosimetry Data, by Letaw, J.R.* and Adams, J.H., *1986 Annual Conference on Nuclear and Space Radiation Effects in: IEEE Transactions on Nuclear Science* **NS–33**:1620– 1625

Coronal Mass Ejection Associated with the Stationary Post–Flare Arch of 21–22 May 1980, by McCabe, M.K.,* Svestka, Z.F.,* Howard, R.A., Jackson, B.V.,* and Sheeley, N.R., *Solar Physics* **103**:399–408

Correlated Observations of Impulsive UV and Hard X–Ray Bursts from the Solar Maximum Mission, by Cheng, C.C., *Highlights of Astronomy, Joint Scientific Discussion XIX IAU General Assembly*, IAU, pp. 739–742

Culgoora Radio and Skylab EUV Observations of Emerging Magnetic Flux in the Lower Corona, by Stewart, R.T.,* Brueckner, G.E., and Dere, K.P., *Solar Physics* **106**:107-130

Daily Observations of Radio Sources in 1983, by Waltman, E.,* Feldzahler, B.J.,* Johnston, K.J., Spencer, J.H., Angerhofer, P.E.,* Florkowski, D.R.,* Josties, F.J.,* McCarthy, D.D.,* and Matsakis, D.N.,* *Astronomical Journal* **91**:231–254

Dynamic Evolution of the Transition Zone Plasma in Solar Flares and Active Region Transients, by Cheng, C.C. and Tandberg-Hanssen, E.,* *Astrophysical Journal* **309**:421–434

Far-Infrared and Radio Observations of DR-6, DR-7, and DR-22, by Odenwald, S.,* Shivanandan, K., Campbell, M.,* Fazio, G.,* Schwartz, P., and Moseley, H.,* *Astrophysical Journal* **306**:122–129

Fast Timing Experiments on Black Holes and Gravitational Wave Sources, by Wood, K.S., *Proceedings of the Fourth Marcel Grossmann Meeting on General Relativity*, Elsevier Science Publishers B.V., NY, pp. 873–881

HEAO-2 X-Ray Observations of Clusters of Galaxies, by Ulmer, M.,* Kowalski, M.P., and Cruddace, R.G., *Astrophysical Journal* **303**:162–170

High Resolution X-Ray Spectra of Solar Flares, VIII. Mass Upflow in the Large Flare of 1980 November 7, by Karpen, J.T., Doschek, G.A., and Seely, J.F., *Astrophysical Journal* **306**:327–339

High-Resolution Telescope and Spectrograph Images of the Solar Chromosphere and Transition Zone, by Dere, K.P., Bartoe, J.D.F., and Brueckner, G.E., *Astrophysical Journal* **305**:947-953

Infrared Cirrus and High-Latitude Molecular Clouds, by Weiland, J.L.,* Blitz, L.,* Dwek, E.,* Hauser, M.G.,* Magnani, L.,* and Rickard, L.J., *Astrophysical Journal* **306**:L101-L104

Interplanetary Shocks Preceded by Solar Filament Eruptions, by Cane, H.V.,* Kahler, S.W.,* and Sheeley, N.R., *Journal of Geophysical Research* **91**:13321–13329

Luminosities of Sources Associated with Molecular Outflows, by Mozurkewich, D., Schwartz, P.R., and Smith, H.A., *Astrophysical Journal* **311**:371–379

Magnetic Energy Storage and Conversion in the Solar Atmosphere, by Spicer, D.S., Mariska, J.T., and Boris, J.P., *Physics of the Sun Volume II: The Solar Atmosphere*, D. Reidel Publishing Co., Boston, MA, pp. 181–248

Measured Wavelength for n = 4 to 2 Transitions in Fe XXIV and Fe XXIII, by Seely, J.F. and Feldman, U., *Physica Scripta* **33**:110–112

Measurement of Wavelengths and Lamb Shifts for Inner-Shell Transitions in Fe XVIII- XXIV, by Seely, J.F., Feldman, U., and Safronova, U.I.,* *Astrophysical Journal* **304**:838–848

Mg VII and Si IX Line Ratios in the Sun, by Keenan, F.P.,* Kingston, A.E.,* Aggarwal, K.M.,* and Widing, K.G., *Solar Physics* **103**:225–230

Modeling of Coronal X-Ray Emission from Active Cool Stars, by Stern, R.A.,* Antiochos, S.K., and Harnden, F.R.,* *Cool Stars, Stellar Systems, and the Sun*, Springer-Verlag, NY, pp. 216–218

Multispectral Observations of FIRSSE Sources. I Radio Observations of Optically Identified Objects, by Albert, C.E.,* Schwartz, P.R., Bowers, P.F.,* and Rickard, L.J.,* *Astronomical Journal* **92**:75–78

Numerical Simulations of Comets: Predictions for Comet Giacobini-Zinner, by Fedder, J.A., Lyon, J.G., and Giuliani, J.L., *EOS* **67**:17–19

On the Dividing Line for Stellar Coronae, by Antiochos, S.K., Haisch, B.M.,* and Stern, R.A.,* *Astrophysical Journal* **307**:L55–L59

On the Short Time Scale Variability of the Seyfert Galaxy NGC 6814, by Beall, J.H.,* Wood, K.S., and Yentis, D.J., *Astrophysical Journal* **308**:563–570

Outflows and Ejections in the Solar Transition Zone, by Dere, K.P., Bartoe, J.D.F., and Brueckner, G.E., *Astrophysical Journal* **310**:456–462

Radiation Effects on GaAs Charge Coupled Devices with High Resistivity Gate Structures, by Bellem, R.D.* and Jenkins, W.C., *IEEE Transactions on Nuclear Sciences* **NS-33**:1084–1089

Radio Studies of Extragalactic Supernovae, by Weiler, K.W., Sramek, R.A.,* and Panagia, N.,* *Science* **2 31**:1251–1254

Radio Supernovae, by Weiler, K.W., Sramek, R.A.,* Panagia, N.,* Van der Hulst, J.M.,* and Salvati, M.,* *Astrophysical Journal* **301**:790–812

Rapid Acceleration of Energetic Particles in the 1982 February 8 Solar Flare, by Kane, S.R.,* Chupp, E.L.,* Forrest, D.J.,* Share, G.H., and Rieger, E.,* *Astrophysical Journal* **300**:L95–L98

Reanalysis of Pioneer Orbiter Ultraviolet Spectrometer Data: OI 1304 Intensities and Atomic Oxygen Densities, by Paxton, L.J. and Meier, R.R., *Geophysical Research Letters* **13**:229–232

Response of an Emerging Flux Tube to a Current-Driven Instability, by Karpen, J.T. and Boris, J.P., *Astrophysical Journal* **307**:826–837

Simulations of the Gross Solar Magnetic Field During Sunspot Cycle 21, by Sheeley, N.R., DeVore, C.R., and Shampine, L.R.,* *Solar Physics* **106**:251–268

Solar Filament Eruptions and Energetic Particle Events, by Kahler, S.W.,* Cliver, E.W.,* Cane, H.V.,* McGuire, R.E.,* Stone, R.G.,* and Sheeley, N.R., *Astrophysical Journal* **302**:504–510

Spectral Evolution of Pulse Structures in Gamma-Ray Bursts, by Norris, J.P., Share, G.H., Messina, D.C.,* Dennis, B.R.,* Desai, U.D.,* Cline, T.L.,* Matz, S.M.,* and Chupp, E.L.,* *Astrophysical Journal* **301**:213–219

Subluminous, Radio Emitting Type I Supernovae, by Panagia, N.,* Sramek, R.A.,* and Weiler, K.W., *Astrophysical Journal* **300**:L55–L58

The Decay of the Mean Solar Magnetic Field, by Sheeley, N.R. and DeVore, C.R., *Solar Physics* **103**:203–224

The Effect of Different Resistivity Models on Magnetotail Dynamics, by Lyon, J.G., Fedder, J.A., and Huba, J.D., *Journal of Geophysical Research* **91**:8057–8064

The Extreme-Ultraviolet Spectrum (300–630 A) of an Erupting Prominence Observed from Skylab, by Widing, K.G., Feldman, U., and Bhatia, A.K.,* *Astrophysical Journal* **308**:982–992

The High-Resolution Solar Spectrum, 1175–1710, by Sandlin, G.D., Bartoe, J.D.F., Brueckner, G.E., Tousey, R., and VanHoosier, M.E., *Astrophysical Journal* **61**:801–898

The Origin of the 28- to 29-Day Recurrent Patterns of the Solar Magnetic Field, by Sheeley, N.R. and DeVore, C.R., *Solar Physics* **104**:425–429

The Quiet Solar Transition Region, by Mariska, J.T., *Annual Review of Astronomy and Astrophysics* **24**:23–48

The Role of Nonlocal Heat Conduction in Solar Flares, by Karpen, J.T. and DeVore, C.R., *The Lower Atmosphere of Solar Flares: Relationships Between Low Temperature Plasmas and High Energy Emissions*, National Solar Observatory, Sunspot, NM, pp. 416–427

The Solar Cycle Dependence of Coronal Mass Ejections, by Howard, R.A., Sheeley, N.R., Michels, D.J., and Koomen, M.J.,* *The Sun and the Heliosphere in Three Dimensions, Proceedings of the XIXth ESLAB Symposium*, D. Reidel Publishing Co., Boston, MA, pp. 107–111

The Structure of the Static Corona and Transition Region, by Antiochas, S.K. and Noci, G.,* *Astrophysical Journal* **301**:440–447

The T Tauri Radio Source II. The Winds of T Tauri, by Schwartz, P.R., Simon, T.,* and Campbell, R.,* *Astrophysical Journal* **303**:233–238

Theoretical NeV Emission Line Ratios Compared to Solar Observations, by Keenan, F.P.,* Aggarwal, K.M.,* and Widing, K.B., *Solar Physics* **105**:47–50

VLA Maps of Formaldehyde Absorption Toward NGC 2024, by Crutcher, R.M.,* Henkel, C.,* Wilson, T.L.,* Johnston, K.J., and Bieging, J.H.,* *Astrophysical Journal* **307**:302–312

STRUCTURE RESEARCH

3, 3–Bis(Methylnitraminomethyl) Oxetane(I) and 3, 3–Bis(Nitratomethyl)Oxetane(II), by George, C., and Gilardi, R., *Acta Crystallographica* **C42**:1161–1164

The Effect of Zn and Mn on CdTe Bond Strength in $Cd_{1-x}Zn_xTe$ (x = 0.04 + 0.001) and $Cd_{1-x}Mn_xTe$ (x = 0.1 + 0.005), by Qadri, S.B.,* Skelton, E.F., Webb, A.W., and Kennedy, J.,* *Xth AIRAPT International High Pressure Conference in: Physica* **139–140 B+C**:341–342

Alkaloids from Dendrobatid Poison Frogs: Trans–Decahydroquinolines and Indolizidines, by Tokuyama, T.,* Nishimori, N.,* Karle, I.L., Edwards, M.W.,* and Daly, J.W.,* *Tetrahedron* **42**:3453–3460

Baeyer–Villiger Oxidation of Pentacyclo $[5.4.0.0^{2,6}.0^{3,10}.0^{5,9}]$ Undecane-8, 11–Dione, by Rao Surapaneni, C.* and Gilardi, R., *Journal of Organic Chemistry* **51**:2382–2385

Comparison of (–)–Eseroline with (+)–Eseroline and Dihydroseco–Analogs in Antinociceptive Assays, by Schonenberger, G.,* Jacobson, A.E.,* Brossi, A., Streaty, R.,* Klee, W.A.,* Flippen–Anderson, J.L., Henderson, J.L., and Gilardi, R., *Journal of Medicinal Chemistry* **19**:2268–2273

Compressibility of Ni_3In, by Webb, A.W., Skelton, E.F., Qadri, S.B.,* and Cannon, J.F.,* *Xth AIRAPT International High Pressure Conference in: Physica* **139–140 B +C**:311–313

Conformational Changes in Cyclic Peptides Upon Complexation with Alkali and Alkaline Earth Metal Ions, by Karle, I.L., *Biomolecular Stereodynamics III. Proceedings of the Fourth Conversation in the Discipline Biomolecular Stereodynamics*. Adenine Press, Albany, NY, pp. 197–215

Energy Dispersive Diffraction at Elevated Pressures Using Synchrotron Radiation, by Skelton, E.F., *Transactions of the American Crystallographic Association* **21**:33–39

Energy Dispersive Spectroscopy Using Synchrotron Radiation: Intensity Considerations, by Skelton, E.F., Elam, W.T., Qadri, S.B., Webb, A.W., and Schiferl, D.,* *Xth AIRAPT International High Pressure Conference in: Physica* **139– 140 B +C**:499–504

From X-Ray Reflections to a Complete Molecular Structure, by Karle, I.L. *The Chemist* **63**:8–11

Image Reconstruction Using Electron Microdiffraction Patterns from Overlapping Regions, by Konnert, J. and D'Antonio, P., *Ultramicroscopy* **19**:267–278

Neurotoxins Producing Parkinson's Syndrome, by Flippen–Anderson, J.L., Gilardi, R., and George, C., *Acta Crystallographica* **C42**:1185–1189

Nonempirical Atom-Atom Potentials for Main Components of Intermolecular Interaction Energy, by Sokalski, W.A.,* Lowery, A.H., Roszak, S.,* Lewchenko, V.,* Blaisdell, J.,* Hariharan, P.C.,* and Kaufman, J.J.,* *Journal of Computational Chemistry* **7**:693-700

Novel Macrocyclic Trichothecenes from Myrothecium Roridum, by Jarvis, B.B.,* Comezoglu, F.T.,* Lee, Y.W.,* Flippen-Anderson, J.L., Gilardi, R.D., and George, C.F., *Bulletin des Societes Chimigues Belges* **95**:681-697

On the SiOSi Angle in 1, 2-Ditert-butyl-1, 1, 2, 2- tetraphenyldisiloxane, by Karle, I.L., Karle, J.M.,* and Nielsen, C.J.,* *Acta Crystallographica* **C42**:64-67

Parallel Packing of α-Helices in Crystals of n Boc-Trp-Ile-Ala-Aib-Ile-Val-Aib-Leu-Aib-Pro-OMe.2H$_2$O, by Karle, I.L., Sukumar, M.,* and Balaram, P.,* *Proceedings of the National Academy of Sciences* **83**:9284-9288

Preparation of Optically Active Secondary Amines by Thermal Decomposition of (Methylbenzyl)Urea Analogs: Absolute Configuration of (+) and (-)-Mecamylamine, by Schonenberger, B., *Helvetica Chimica Acta* **69**:283-287

Radial Distribution Function Analysis, by Konnert, J.H., Karle, J., and D'Antonio, P., *ASM Handbook on Materials Characterization*, Vol. 10, American Society for Metals, Metals Park, OH, pp. 393-401

Recovering Phase Information from Intensity Data - Nobel Lecture, 9 December 1985, by Karle, J., *Chemica Scripta* **26**:261-276

Recovering Phase Information from Intensity Data, by Karle, J., *Science* **232**:837- 843

Regiochemical Control in Intramolecular Photochemical Reactions of 1, 6- Heptadienes: Carbonyl-Substituted 1-(4-Alkenyl)- 1-Cyclopentenes, by Matlin, A.R.,* George, C.F., Wolff, S.,* and Agosta, W.C.,* *Journal of the American Chemical Society* **108**:3385- 3394

Sterospecificity of a New Reaction of L-Ascorbic Acid with Cis and Trans Olefinic 1, 4-Dicarbonyl Compounds, by Fodor, G.,* Sussangarn, K.,* Mathelier, H.,* Fang, K.*, Arnold, R.,* Karle, I., and Flippen-Anderson, J. *Journal of Organic Chemistry* **51**:3148-3150

Structure of Isororidin E, by Flippen-Anderson, J.L. and Gilardi, R., *Acta Crystallographica* **42**:1184-1185

Structure of N-(4-Amino-3- Furazanyl)-2, 2, 2- Trichloro-N'- Methoxyacetamidine, by George, C. and Gilardi, R., *Acta Crystallographica* **C42**:1457-1458

The 1985 Nobel Prize in Chemistry, by Hendrickson, W.A., *Science* **231**:362-364

Triplet Phase Invariants from Single Isomorphous Replacement on One-Wavelength Anomalous Dispersion Data, Given Heavy-Atom Information, by Karle, J., *Acta Crystallographica* **A42**:246- 253

Variability in the Backbone Conformation of Cyclic Pentapeptides: Crystal Structure of Cyclic (Gly-LPro-DPhe-Gly-LAla), by Karle, I.L., *International Journal of Peptide and Protein Research* **28**:420-427

Water Structure in [Phe^{4}VAL^6] Antamanide-12H$_2$O Crystallized from Dioxane, by Karle, I.L., *International Journal of Peptide and Protein Research* **26**:6-14

X-Ray Structure Determination of the Naturally Occurring Isomer of Cyanobacterin, by Gleason, F.K.,* Porwoll, J.,* Flippen-Anderson, J.L., and George, C., *Journal of Organic Chemistry* **51**:1615- 1616

FORMAL REPORTS

8839 **New Version of the Energy-Deposition Code E- DEP-1: Better Stopping Powers**, by Davisson, C.M., and Manning, I.

8917 **An Investigation of Dielectric Loaded Ridged Waveguide**, by Young, C.W.

8940 **Executing Trace Specifications Using Prolog**, by McLean, J.D., Weiss, D.M., and Landwehr, C.E.

8948 **Survey and Examples of Specification Techniques for User-Computer Interfaces**, by Jacob, R.J.K.

8952 **Biodeuterated Materials: High-Temperature Lubricants from Algae**, by Neihof, R.A., Ross, M.M., and Campana, J.E.

8967 **An Incomplete Lipschitz-Hankel Integral of Ko Part I.**, by Miller, A.R.

8968 **An Investigation of Expert Systems Usage for Software Requirements Development in the Strategic Defense Initiative Environment**, by Chien, Y.T. and Liebowitz, J.

8971 **Gaussian Arbitrarily Varying Channels**, by Hughes, B. and Narayan, P.

8972 **Tethered Balloon Measurements at San Nicholas Island (Oct. 1984): Instrumentation, Data Summary, Preliminary Data Interpretation**, by Gerber, H.

8973 **General Solutions to Maxwell's Equations for a Transverse Field**, by Gordon, W.B.

8981 **Adaptive Digital Processing Investigation of DFT Subbanding vs Transversal Filter Canceler**, by Gabriel, W.F.

8984 **Degradation in Performance of Adaptive Null-Steering Antennas**, by Kahn, W.K.

8989 **Layer 1: A SIMULA Context for Simulating the Operation of Communication Systems**, by Hauser, J.P., and Baker, D.J.

8990 **The Smoke Hazards Resulting from the Burning of Shipboard Materials Used by the U.S. Navy - Part II.**, by Williams, F.W., Zinn, B.T.,* Browner, R.F.,* and Powell, E.A.*

8995 **Analytical and Physical Aspects of Two-Dimensional Spectra Associated with Stationary Random Processes**, by Bergin, J.M.

8996 **Design and Operation of the Forward Scattering Meter**, by James, J.E. and Gerber, H.

9000 **Hardware Design for a Fixed-Wing Airborne Gravity Measurement System**, by Brozena, J.M., Eskinzes, J.G., and Clamons, J.D.

9005 **Superstructure Flow Distortion Corrections for Wind Speed and Direction Measurements Made from Tarawa Class (LHA1-LHA5) Ships**, by Blanc, T.V.

9007 **The Canted Spectral Transform and its Properties**, by Gerlach, A.A., Flowers. K.D., Anderson, W.L., and Kunz, E.L.

9015 **Radar Target Detection in Non-Gaussian**, Correlated Clutter, by Cantrell, B.

9018 **Error-Resistant Narrowband Voice Encoder**, by Kang, G.S. and Jewett, W.M.

9019 **Developing a Software Engineering Methodology for Knowledge-Based Systems**, by Jacob, R.J.K. and Froscher, J.N.

9022 **Characteristics of the Two-Dimensional Spectrum of Roughness on a Seamount**, by Czarnecki, M.F. and Bergin, J.M.

9027 **Improved Oscillator Phase Locking Using a Modulated Electron Beam in a Gyrotron**, by McCurdy, A.H., Armstrong, C.M., Bollen, W.M., Parker, R.K., and Granatstein, V.L.

PATENTS GRANTED

NRL scientists have made significant contributions in many areas of technology. One measure of the quality and quantity of these contributions is the number of patents received. In Fiscal Year 1986, NRL reseachers were awarded 62 patents bringing NRL's total to 3138 patents issued since 1923.

4,565,710-**Process for Producing Carbide Coatings,** January 21 to Irwin L. Singer and Russell A. Jeffries.

4,566,011-**Palindromic Polyphase Code Expander-Compressor,** January 21 to Bernard L. Lewis and Frank F. Kretschmer, Jr.

4,566,013-**Coupled Amplifier Module Feed Networks for Phased Array Antennas,** January 21 to Richard Steinberg and J. Paul Shelton.

4,567,401-**Wide-Band Distributed rf Coupler,** January 28 to Larry R. Barnett, Yue-Ying Lau, Kwo R. Chu, and Victor L. Granatstein.

4,568,189-**Apparatus and Method for Aligning a Mask and Wafer in the Fabrication of Integrated Circuits,** February 4 to John F. Bass, Nelson Saks, and Martin Peckerar.

4,568,396-**Wear Improvement in Titanium Alloys by Ion Implantation,** February 4 to Ronald G. Vardiman.

4,568,650-**Oxidation of Reduced Ceramic Products,** February 4 to William S. Coblenz and Roy W. Rice.

4,569,033-**Optical Matrix-Matrix Multiplier Based on Outer Product Decomposition,** February 4 to William C. Collins, P. Denzil Stilwell, Jr., and Ravindra A. Athale.

4,572,900-**Organic Semiconductor Vapor Sensing Method,** February 25 to Henry Wohltjen.

4,573,050-**Dual Scan Rate Radar,** February 25 to William M. Waters.

4,573,797-**Analog Fiber Gyro with Extended Linear Range,** March 4 to William K. Burns and Robert P. Moeller.

4,574,259-**High Switching Speed Electrically Tuned Microwave Magnetic Resonance Devices,** March 4 to George T. Rado, Carmine Vittoria, and James M. Ferrari.

4,574,287-**Fixed Aperture, Rotating Feed, Beam Scanning Antenna System,** March 4 to William M. Waters.

4,575,179-**Integrated Optical Signal Processor Using Diffraction of Light by Magnetostatic Waves,** March 11 to John N. Lee and Arthur D. Fisher.

4,578,614-**Ultra-Fast Field Emitter Array Vacuum Integrated Circuit Switching Device,** March 25 to Richard F. Greene.

4,578,677-**Range Doppler Coupling Magnifier,** March 25 to Bernard L. Lewis.

4,578,804-**Polynomial Grating,** March 25 to John F. Meekins and Herbert Gursky.

4,580,140-**Twin Aperture Phased Array Lens Antenna,** April 1 to Theodore C. Cheston.

4,582,724-**Chemical Bonding Agent for the Suppression of Rusty Bolt Intermodulation Interference,** April 15 to John C. Cooper.

4,584,710-**Coherent Receiver Phase and Amplitude Alignment Circuit,** April 22 to James P. Hansen.

4,587,325-**Processable and Stable Conductive Polymers from Diether-Linked Bisorthodinitrile Monomers,** May 6 to Teddy M. Keller.

4,589,772–**Pulsed Remote Gauge,** May 20 to Raymond A. Patten and Jerry A. Blodgett.

4,590,448–**Tunable Microwave Filters Utilizing a Slotted Line Circuit,** May 20 to Carmine Vittoria.

4,591,510–**Rusty Bolt Intermodulation Interference Reducer,** May 27 to Ramanathan Panayappan and John C. Cooper.

4,591,786–**Fiber–Optic Magnetic Gradiometer with Variable Magnetic Biasing Fields,** May 27 to Kee P. Koo and George H. Sigel, Jr.

4,592,056–**Resonant Photon Pumping Mechanisms for a Plasma X–ray Laser,** May 27 to Raymond C. Elton.

4,593,968–**Potting Techniques for Fiber Optical Couplers,** June 10 to Thomas G. Giallorenzi.

4,595,925–**Altitude Determining Radar Using Multipath Discrimination,** June 10 to James P. Hansen.

4,596,461–**In–Line, Concurrent Electromagnetic Beam Analyzer,** June 24 to John L. DeRosa and Terence J. Wieting.

4,596,986–**Sidelobe Canceller with Adaptive Antenna Subarraying Using a Weighted Butler Matrix,** June 24 to Grealie A. Andrews and Karl Gerlach.

4,597,666–**Apparatus for Determining the Liquid Water Content of a Gas,** July 1 to Hermann E. Gerber and Bernard G. Uifers.

4,597,933–**Radiative Opacity and Emissivity Measuring Device,** July 1 to Barrett H. Ripin and Robert R. Whitlock.

4,598,247–**Spectrum Analyzer and Analysis Method For Measuring Power and Wavelength of Electromagnetic Radiation,** July 1 to Frederick M. Mako, John A. Pasour, and Charles W. Roberson.

4,600,853–**SAW–CTD Serial to Parallel Imager and Waveform Recorder,** July 15 to Robert R. Whitlock and Nicolas A. Papanicolaou.

4,600,885–**Fiber Optic Magnetometer for Detecting DC Magnetic Fields,** July 15 to Kee P. Koo, Anthony Dandridge, Alan B. Tveten, and George H. Sigel.

4,603,295–**Two-Headed DC Magentic Target Proximity Sensor,** July 29 to Frank W. Heemstra.

4,603,296–**Fiber Optic DC Magnetometer Without Hysteresis Ambiguity,** July 29 to Kee P. Koo and George H. Sigel.

4,607,344–**Triple Matrix Product Optical Processors Using Combined Time–and–Space Integration,** August 19 to Ravindra A. Athale and John N. Lee.

4,607,912–**In–Line Optical Fiber Polarizer,** August 26 to William K. Burns and Carl A. Villarruel.

4,608,537–**Low Perturbation Electron Injector for Cyclic Accelerators,** August 26 to Frederick Mako, Wallace Manheimer, Christos A. Kapetanakos, and Frederick Sandel.

4,611,140–**SAW–CTD Parallel to Serial Imager,** September 9 to Robert R. Whitlock and Nicolas A. Papanicolaou.

4,612,642–**Operation of Transversely Excited N_2O Lasers,** September 16 to Wayne T. Whitney.

4,613,755–**Method of Mass Spectrometry,** September 23 to Jeffrey W. Hudgens.

4,614,672–**Liquid Phase Epitaxy (LPE) of Silicon Carbide,** September 30 to Arrigo Addamiano.

4,617,493–**Collective Interaction Klystron,** October 14 to Yue–Ying Lau.

4,618,453–**Conductive Heterocyclic Ladder Polymers,** October 21 to Oh–Kil Kim.

4,619,845–**Method for Generating Fine Sprays of Molten Metal for Spray Coating and Power Making,** October 28 to Jack D. Ayers and Iver E. Anderson.

4,619,986–**Epoxy Phthalonitrile Polymers,** October 28 to Teddy M. Keller.

4,620,942–**Electrically Conductive Ladder Polymers,** November 4 to Oh–Kil Kim.

4,621,896–**Optical Fibers with Reduced Pressure Sensitivity to High Frequency Acoustic Field,** November 11 to Nicholas Lagakos, James H. Cole, and Joseph A. Bucaro.

4,622,266–**Moldable Electrically Conductive Polymer Compositions,** November 11 to Oh–Kil Kim.

4,622,552–**Factored Matched Filter/FFT Radar Doppler Processor,** November 11 to Grealie A. Andrews and Samuel I. Sheller.

4,626,369–**Lead Zirconate Titanate Ceramics,** December 2 to Basil E. Walker.

4,626,854–**Method and Apparatus for Generating a Modified P_1 Code,** December 2 to Frank F. Kretschmer, Jr. and Bernard L. Lewis.

4,630,011–**Microwave and Millimeter Wave Phase Shifter,** December 16 to Robert E. Neidert and Clifford M. Krowne.

4,630,300–**Front–End Processor for Narrowband Transmission,** December 16 to George S. Kang, Stephanie S. Everett, and Alexander F. Thornhill.

4,630,883–**Optical Waveguide Apparatus and Method for Manufacturing,** December 23 to Henry F. Taylor, George H. Sigel, and Michael E. Gingerich.

4,631,447–**Ireb Converter to AC Pulses,** December 23 to Moshe Friedman and Victor Serlin.

4,631,500–**Microwave Frequency Divider Having Regenerative Oscillation,** December 23 to Christen Rauscher.

4,632,010–**Airboc Chaff Deployment System,** December 30 to Waymon Humphries, John Bryant, Richard C. Eklund, Donald C. Hayes, and Peter Ferko.

4,633,170–**Bragg Cell Spectrum Analyzer,** December 30 to William K. Burns.

4,633,255–**Method for Sea Surface High Frequency Radar Cross–Section Estimation Using Doppler Spectral Properties,** December 30 to Dennis B. Trizna.

STATUTORY INVENTION REGISTRATION

Recently Congress authorized a new form of patent protection known as the Statutory Invention Registration or "SIR". A SIR document provides all the protection generally needed by the Navy and carries all of the prestige of a standard patent but at a significantly lower cost. SIRs are generally used to protect significant mission–related inventions which are primarily of military value and have little commercial application. In Fiscal Year 1986, 14 SIR's were issued to NRL researchers.

These patents and SIR's ensure the Navy's control over, and free use of, the technology it has developed.

SIR Reg. No. H8–**Thermodynamic Waste Heat Transfer System,** January 7 to James E. Hays.

SIR Reg. No. H14–**Adaptive Doppler Filter Banks,** January 7 to Bernard L. Lewis.

SIR Reg. No. H28–**Chemical Vapor Deposition (CVD) of Cubic Silicon Carbide SIC,** February 4 to Arrigo Addamiano.

SIR Reg. No. H29–**Tunnett Diode and Method of Making,** March 4 to Aristos Christou and John E. Davey.

SIR Reg. No. H39–**Multilayer Super–Conducting Shield and Method of Manufacturing Same,** March 4 to Donald U. Gubser and Stuart A. Wolf.

SIR Reg. No. H57–**Partially Adaptive Array Using Bootlace Lens,** May 6 to William F. Gabriel and James K. Hsiao.

SIR Reg. No. H92–**Generalized Adaptive MTI System,** July 1 to Frank F. Kretschmer, Jr. and Bernard L. Lewis.

SIR Reg. No. H94–**High Stability Fiber Optic Magnetic Field Sensor with Enhanced Linear Range Using Magnetic Feedback Nulling,** July 1 to Kee P. Koo.

SIR Reg. No. H95–**Heterojunction D (OR A+) Millimeter and Submillimeter Wave Detector,** July 1 to Benjamin V. Shanabrook and William J. Moore.

SIR Reg. No. H96–**Intensity Modulated Light Source,** August 5 to Henry F. Taylor.

SIR Reg. No. H108–**Radar Doppler Processor Using a Fast Orthogonalization Network,** August 5 to Karl Gerlach.

SIR Reg. No. H125–**Etch and Polish for Metal Halides,** September 2 to Paul E. R. Nordquist, Jr.

SIR Reg. No. H170–**Self Aligned Notch for INP Planar Transferred Electron Oscillator,** December 2 to Steven G. Binari.

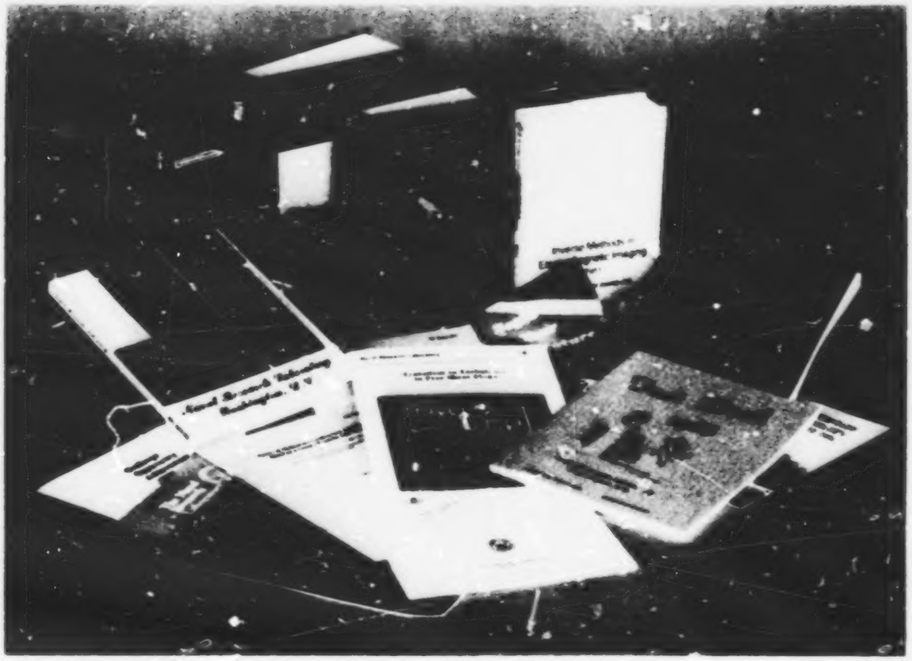

Some of the books, papers, and reports representing the Naval Research Laboratory's publications.

BEST COPY AVAILABLE

ORGANIZATIONAL CHART
APRIL 1987

COMMANDING OFFICER
Code 1000
CAPT W.C. Miller, USN

DIRECTOR OF RESEARCH
Code 1001
Dr. T. Coffey

DEPUTY EQUAL EMPLOYMENT OPPORTUNITY OFFICER
Code 1003
S. Eaton

PUBLIC AFFAIRS OFFICER
Code 2610
J.W. Gately, Jr.

SCIENTIFIC CONSULTANT TO THE DIRECTOR OF RESEARCH
Code 1004
Dr. P. Mange

OFFICE OF MANAGEMENT AND ADMINISTRATION
Code 1005
M. Oliver

COMMAND SUPPORT DIVISION
Code 1200
CAPT M.A. Howard, USN
- Operational Services
- Security
- Contracting
- Research Requirements & Applications
- NRL Flight Support Detachment

FINANCIAL MANAGEMENT DIVISION
Code 1300
R.W. Steinbeck
- Budget
- Accounting
- Disbursing
- Equipment Resource Management and Control

PROGRAM COORDINATION OFFICE
Code 1008
Dr. R.T. Swim

CIVILIAN PERSONNEL DIVISION
Code 1800
D.J. Blome
- Personnel Operations
- Employee Development
- Employee Relations

TECHNICAL SERVICES DIRECTORATE
Code 2000
J.D. Brown

GENERAL SCIENCE AND TECHNOLOGY DIRECTORATE
Code 4000
Dr. W.R. Ellis

WARFARE SYSTEMS AND SENSORS RESEARCH DIRECTORATE
Code 5000
R.R. Rojas

MATERIAL SCIENCE AND COMPONENT TECHNOLOGY DIRECTORATE
Code 6000
Dr. B.B. Rath

NAVAL CENTER FOR SPACE TECHNOLOGY
Code 8000
P.G. Wilhelm

BLANK PAGE

ORGANIZATIONAL CHART (Continued)

TECHNICAL SERVICES DIRECTORATE
Code 2000

ENGINEERING SERVICES DIVISION
Code 2300
M.A. Shimkus*
- Mechanical Engineering & Manufacturing
- Electronic Engineering & Fabrication

SUPPLY DIVISION
Code 2400
LCDR T.R. Lippert, USN
- Purchasing/Requisition Control
- Receipt Control
- Material
- Automated Inventory Management
- Technical

PUBLIC WORKS DIVISION
Code 2500
CDR T.R. Rampe, USN
- Engineering
- Maintenance, Utilities, & Transportation
- Contract Administration
- Maintenance Control
- Administrative
- Planning

TECHNICAL INFORMATION DIVISION
Code 2600
P. Imhof
- Information Services
- Technical Library
- Publications
- Graphic Design Services
- Systems/Photographic

CHESAPEAKE BAY DETACHMENT
Code 2700
CDR S. Kummer, USN
- Operations/Security
- Maintenance & Support

RESEARCH COMPUTATION DIVISION
Code 2800
R.F. Saenger
- User Support
- Systems Support

GENERAL SCIENCE AND TECHNOLOGY DIRECTORATE
Code 4000

SPACE SCIENCE DIVISION
Code 4100
Dr. H. Gursky
- Atmospheric Physics
- X-Ray Astronomy
- Radio & IR Astronomy
- Upper Atmospheric Physics
- Gamma & Cosmic Ray Astrophysics
- Solar Physics
- Solar Terrestrial Relationships
- Ionospheric Effects
- E.O. Hulburt Center for Space Research

LABORATORY FOR COMPUTATIONAL PHYSICS AND FLUID DYNAMICS
Code 4400
Dr. J.P. Boris
- Reactive Flow and Dynamical Systems
- Fluid Structure Interactions
- Hydrodynamic Developments
- Computational Physics Developments

CONDENSED MATTER AND RADIATION SCIENCES DIVISION
Code 4600
Dr. D.J. Nagel
- Radiation Survivability
- Metal Physics
- Radiation-Matter Interactions
- Materials Modification & Analysis
- Condensed Matter Physics

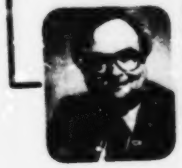

PLASMA PHYSICS DIVISION
Code 4700
Dr. S. Ossakow
- Plasma Radiation
- Laser Plasma
- High-Power Electromag. Radiation
- Experimental Plasma Physics
- Plasma Technology
- Geophysical & Plasma Dynamics
- Plasma Theory
- Advanced Beam Technologies
- Charged Particle Physics

WARFARE SYSTEMS AND SENSORS RESEARCH DIRECTORATE
Code 5000

ACOUSTICS DIVISION
Code 5100
Dr. D. Bradley
- Acoustics Media Characterization
- Applied Ocean Acoustics
- Physical Acoustics
- Software Systems Development
- Large Aperture Acoustics
- Ocean Dynamics
- Marine Systems

RADAR DIVISION
Code 5300
Dr. M.I. Skolnik
- Radar Analysis
- Radar Techniques
- Search Radar
- Target Characteristics
- Identification Systems
- Airborne Radar
- Electromagnetics
- Systems Control & Research

INFORMATION TECHNOLOGY DIVISION
Code 5500
Dr. J.R. Davis
- Navy Center for Applied Research in Artificial Intelligence
- Communication Systems Engineering
- Transmission Technology
- Integrated Warfare Technology
- Computer Science & Systems

TACTICAL ELECTRONIC WARFARE DIVISION
Code 5700
Dr. J.A. Montgomery
- Offboard Countermeasures
- EW Support Measures
- Airborne EW Systems
- Ships EW Systems
- Advanced Techniques

UNDERWATER SOUND REFERENCE DETACHMENT
Code 5980
Dr. J.E. Blue
- Technical Services
- Electronics
- Transducer
- Measurements
- Computer

MATERIAL SCIENCE AND COMPONENT TECHNOLOGY DIRECTORATE
Code 6000

LABORATORY FOR STRUCTURE OF MATTER
Code 6030
Dr. J. Karle

CHEMISTRY DIVISION
Code 6100
Dr. W.M. Tolles
- Chemical Dynamics and Diagnostics
- Polymeric Materials
- Surface Chemistry
- Navy Technology Center for Safety and Survivability
- Biomolecular Engineering

MATERIAL SCIENCE AND TECHNOLOGY DIVISION
Code 6300
Dr. B.B. Rath
- Environmental Effects
- Physical Metallurgy
- Ceramics
- Composite Materials
- Mechanics of Materials
- Thermostructural Materials
- Structural Integrity

OPTICAL SCIENCES DIVISION
Code 6500
Dr. T.G. Giallorenzi
- Advanced Concepts
- Applied Optics
- Laser Physics
- Electro-optical Technology
- Optical Techniques

ELECTRONICS TECHNOLOGY DIVISION
Code 6800
Dr. G.M. Borsuk
- Solid State Devices
- Electronic Material Technology
- Surface Physics
- Microwave & Millimeter Wave Tube Technology
- Microwave Technology
- Semiconductors

NAVAL CENTER FOR SPACE TECHNOLOGY
Code 8000

SPACE SYSTEMS DEVELOPMENT DEPARTMENT
Code 8100
R.E. Eisenhauer
- Spacecraft Engineering
- Advanced Systems Development
- Communication Systems Technology
- Terrestrial Systems

SPACECRAFT ENGINEERING DEPARTMENT
Code 8200
R.T. Beal
- Design, Manufacturing and Processing
- Systems Analysis and Test
- Control Systems
- Concept Development

SPACE SYSTEMS TECHNOLOGY DEPARTMENT
Code 8300
L.M. Hammarstrom
- Space Sensing
- Space Applications
- Systems Engineering and Analysis
- Advanced Concepts and Processing

*ACTING

--- ADDITIONAL DUTY

Code	Office	Key Personnel	Extension*
	EXECUTIVE DIRECTORATE		
1000	Commanding Officer	CAPT W.C. Miller, USN	73403
1001	Director of Research	Dr. T. Coffey	73301
1002	NRL Inspector General	CAPT M.A. Howard, USN†	73621
1004	Scientific Consultant	Dr. P. Mange	73724
1005	Head, Office of Management and Admin.	Ms. M. Oliver	73086
1006	Head, Exploratory Development Program Office	Dr. S. Sacks	73666
2610	Public Affairs Officer	Mr. J.W. Gately, Jr.†	72541
1200	Chief Staff Officer	CAPT M.A. Howard, USN	73621
1208	NRL Counsel	Ms. S. Weldon	72244
1220	Head, Security Branch	Mr. M.B. Ferguson	73048
1300	Comptroller	Mr. R.W. Steinbeck	73405
1500	Head, Program Coordination Office	Dr. R.T. Swim	73314
1800	Head, Civ. Pers. Div.	Mr. D.J. Blome	73421
1803	Deputy EEO Officer	Ms. S. Eaton	72486
	TECHNICAL SERVICES DIRECTORATE		
2000	Associate Director of Research	Mr. J.D. Brown	72879
2010	Safety Officer	Mr. H.C. Kennedy, Jr.	72249
2020	Head, Administrative Services Office	Ms. L.V. Dabney	73858
2300	Engineering Services Officer	Mr. R. Perlut**	72300
2400	Supply Officer	LCDR T.R. Lippert	73446
2500	Public Works Officer	CDR T.R. Rampe, USN	73371
2600	Head, Tech. Info. Div.	Mr. P.H. Imhof	73388
2700	Chesapeake Bay Detachment Officer	CDR S. Kummer	301-257-4002
2800	Head, Research Computation Division	Mr. R.F. Saenger	72751
	GENERAL SCIENCE AND TECHNOLOGY DIRECTORATE		
4000	Associate Director of Research	Dr. W.R. Ellis	73324
4070	Health Physics Group	Mr. J.N. Stone	72232
4100	Supt., Space Science Div.	Dr. H. Gursky	76343
4400	Dir., Lab. for Computational Physics and Fluid Dynamics	Dr. J.P. Boris	73055
4600	Supt., Condensed Matter & Radiation Sciences Div.	Dr. D.J. Nagel	72931
4700	Supt., Plasma Physics Div.	Dr. S. Ossakow	72723
	WARFARE SYSTEMS AND SENSORS RESEARCH DIRECTORATE		
5000	Associate Director of Research	Mr. R.R. Rojas	73294
5100	Supt., Acoustics Div.	Dr. D.L. Bradley	73482
5300	Supt., Radar Div.	Dr. M.I. Skolnik	72936
5500	Supt., Information Technology Div.	Dr. J. Davis	72903
5700	Supt., Tactical Elec. Warfare Div.	Dr. J.A. Montgomery	76278
5900	Supt., Underwater Sound Reference Det.	Dr. J.E. Blue	305-859-5120
	MATERIAL SCIENCE AND COMPONENT TECHNOLOGY DIRECTORATE		
6000	Associate Director of Research	Dr. B.B. Rath	73566
6030	Head, Lab. for Structure of Matter	Dr. J. Karle	72665
6100	Supt., Chemistry Div.	Dr. W.M. Tolles	73026
6300	Supt., Mat. Sci. & Tech. Div.	Dr. B.B. Rath**	72926
6500	Supt., Optical Sciences Div.	Dr. T.G. Giallorenzi	73171
6800	Supt., Electronics Tech. Div.	Dr. G.M. Borsuk	73525
	NAVAL CENTER FOR SPACE TECHNOLOGY		
8000	Director	Mr. P.G. Wilhelm	76547
8100	Supt., Space Systems Development Dept.	Mr. R.E. Eisenhauer	72611
8200	Supt., Spacecraft Engineering Dept.	Mr. R.T. Beal	76407
8300	Supt., Space Systems Technology Dept.	Mr. L.M. Hammarstrom	73920

---

*Direct-in-Dialing (202) 76-; AUTOVON 29-

**Acting

†Additional duty

NRL REVIEW STAFF

The *NRL Review* is a result of the collaboration of the scientific, engineering, and support staff with the Technical Information Division (TID). In addition to the scientists and engineers who provided material for the *Review*, the following have also contributed to its publication.

Senior Science Editor: Dr. Bob Fox
Senior TID Editor: Irene Barron

Head, Technical Information Division: Peter H. Imhof

Graphic design: T. Phillips

Mission Page by: T. Phillips, Photography by: M. Savell

Photographic production: G. Blakes, D. Boyd, G. Bennett, R. Bussey, W. Griffith, G. Campbell, H. Hill, C. Morrow, B. Horton, J. Marshall, B. Horton J. Marshall, M. Savell, and W. Wiggins

Computerized composition production: J. Kogok, D. Wilbanks

Editorial assistance: R. Barlow, R. Baturin, R. Duley, L. Hurst, M. Long, and D. Nelson

Computerized composition assistance: M. Bray, C. Cain, J. Craze, J. Hays, P. Lore, D. Mitchell, C. Williams, S. Schrock, C. Sims, C. Johnson, D. Stewart, C. Petit-Frere, and D. Gloystein

Graphic services assistance: L. Jackson, J. Morrow, and B. Zevgolis

Production coordination: T. Calderwood, M. Peevy

Production consultants: J.A. Kaiser, K. Parrish

Distribution: J. Harris

Valuable assistance in other matters was given by: J.A. Kaiser, J. Boris, E. Oran, R. Löhner, E. Williams, E. Stone, B. Sweeney, J. Davis, R. Clark, T. Giallorenzi, R. Meier, and R. McCoy.

EMPLOYMENT OPPORTUNITIES FOR ENTRY-LEVEL AND EXPERIENCED PERSONNEL

This *Review* illustrates some of the exciting science and engineering carried out at NRL as well as the potential for new personnel.

The Naval Research Laboratory offers a wide variety of challenging positions that involve the full range of work from basic and applied research to equipment development. The nature of the research and development conducted at NRL requires professionals with experience. Typically, there is a continuing need for electronics, mechanical aerospace, ceramic, and materials engineers; metallurgists with bachelor's and/or advanced degrees; and physical and computer scientists with Ph.D. degrees. Opportunities exist in the areas described below.

Ceramic and Materials Scientists/Engineers. These employees work on the mechanical properties, coating and materials processing, and materials research.

Electronics engineers. These engineers work in the following areas; communication satellite design, analog and digital signal processing, information processing, strategic and tactical communication systems design, instrumentation, microcomputer design, satellite attitude-control systems, image processing, IR sensors, focal plane arrays, radar, inverse scattering phenomena, statistical communication theory, electro-optics, hardware/software interfacing, artificial intelligence, electromagnetic (EM) scattering, digital electronics, fiber optics, optical information processing, semiconductor device processing, microwave tubes, threat systems analysis, electroacoustic optics, RF measurement design, EM propagation, EM theory, HF radar propagation analysis, electronic warfare simulation, pulsed power technology, vacuum electronics, microwave technologies, networking techniques, speech processing, Navy C^3I, electronic countermeasure systems design, spacecraft attitude controls, and orbitology.

Mechanical and Aerospace Engineers. These employees may be assigned to satellite thermal design, structural design, propulsion, experimental fluid mechanics, experimental structural mechanics, solid mechanics, elastic/plastic fracture mechanics, materials characterization of composites, finite element methods, nondestructive elevation, characterization of fracture resistance of structural alloys, and combustion.

Computer Science Graduates. Employees in this field are involved with artificial intelligence, software engineering, software systems specifications, computer design/architecture, systems analysis, and command information systems.

Chemists. Chemists are recruited to work in the areas of inorganic and organometallic synthesis, solution kinetics and mechanisms, surface analysis, organic chemistry, combustion, colloid/surface chemistry, fire suppression, and nuclear decay.

Physicists. Physics graduates may concentrate on such fields as electromagnetics, image processing, inverse scattering phenomena, acoustics, inversion theory, mathematical modeling of scattering processors, radar system development, electro-optics, focal plane arrays, signal processing, plasma physics, astrophysics, semiconductor technology, relativistic electronics, beam/wave interactions, low-temperature physics, superconductivity, physical/chemical vapor disposition of thin and thick coatings, wave propagation, ionospheric physics, computational hydrodynamics, computational atomic physics, and supersonic, gas-dynamic numerical modeling.

FOR FOREIGN NATIONALS

U.S. citizenship is required for employment at NRL.

APPLICATION AND INFORMATION

Interested applicants should submit a resume or a Federal Employment Application Form (OPM 1282), which can be obtained from local officers of the Office of Personnel Management and Personnel Offices of Federal agencies, to the address below.

Direct inquires to:

Naval Research Laboratory
Civilian Personnel Division, Code 1813 RV 86
Attn: Marguerite Luck
Washington, DC 20375-5000
202-767-3030

CONTRIBUTIONS BY DIVISIONS AND LABORATORIES

Space Science Division (4100)

- Far Ultraviolet Imagery of Comet Halley from Sounding Rockets
- Heavy Ions in the Inner Magnetosphere
- XLA—The X-Ray Large Array for the Space Station
- Detection of Anti-Matter in the Galaxy
- Dividing Line for Stellar Coronal
- Renormalized Inverse Scattering Theory for Dielectric Profiles

Laboratory for Computational Physics and Fluid Dynamics (4400)

- Active/Adaptive Noise Cancellation in a Liquid-Filled Pipe
- Steep and Breaking Deep Water Waves
- Quantum Chemical Calculation of Chemical Reaction Paths: MeO
- Direct Numerical Simulation of Turbulent Channel Flow
- Vortex Motions in Stratified Wakes

Plasma Physics Division (4700)

- Soft X-Ray Laser Generation
- Modulated Intense Relativistic Electron Beams
- Charged Particle Beam Propagation
- Free Electron Lasers

Acoustics Division (5100)

- Rapid Three-Dimensional Ocean Acoustic Computations
- Inertial Wave Dynamics
- Nonlinear Salt Finger Instability Simulation
- Ship Wake/Film Experiment

Radar Division (5300)

- Radar Target Detection in Non-Gausaian, Correlated Clutter
- Speckle in Space Based Radar Images
- Open Ocean Shipboard Radar Sea-Scatter Experiments
- Mark XV IFF Radar Mode
- Designing Systems with VHSIC Components

Information Technology Division (5500)

- Integrated Battle Group Communication Networks
- Single Board Digital Signal Processor for Voice and Data Applications
- SID Mid-Course Battle Management

Tactical Electronic Warfare Division (5700)

- Computer-Controlled Emissivity Measurement System
- Synthetic Line-of-Sight Simulations

Underwater Sound Reference Detachment (5900)

- Constrained-Layer Damping of Structure-Borne Sound
- Analytic Representations of Viscoelastic Moduli

Laboratory for Structure of Matter (6030)

- Atomic Resolution Images

Chemistry Division (6100)

- Liposome-Encapsulated Hemoglobin, A Potential Blood Surrogate
- Two-Dimensional NMR Images in Solids
- Laser Studies of Flame Chemistry
- Advanced Fluorinated Polymers Meeting Navy Needs
- Surface Chemistry in Semiconductor Processing Using Laser Ionization

Material Science and Technology Division (6300)

- Measurement of Undercooling Effects in Gas-Atomized Metal Powders
- Surface Modification for Improved Corrosion Resistance
- Processing of High T_c Ceramic Superconductors
- Computer Modeling of Anisotropic Elasticity and Piezoelectric Effects in Ceramics
- Mechanisms of Interdiffusion in Coated Superalloys

Optical Sciences Division (6500)

- Optical Studies of Aerosols
- Photoemitter Membrane Light Modulator for Optical Processing
- Parametric Raman Gain Suppression
- Fiber-Optic Magnetic Sensors
- Development of Infrared Focal Plane Arrays for Advanced Navy Sensors

Electronics Technology Division (6800)

- IR-Diode Laser Spectroscopy in the Study of the Vapor Phase Epitaxy Process
- Ga Interstitials in AlGaAs Epitaxial Layers
- Phase-Controlled Gyrotron Oscillators
- Beta Silicon Carbide Transistor Development
- Kinetic Inductance Microstrip Lines

Space Systems Development Department (8100)

- Holograms Made with Laser Diodes for Use in a Satellite Communications Link

INDEX

Accelerator
  electron beam, 17, 143
  particle, 17, 147
  plasma, 147
  RF, 130
Acoustic noise acceleration, 51
Acoustics
  active/adaptive, 51
  modeling, 56
  ocean computations, 56
  sound damping, 85
Active/adaptive acoustics, 51
Administration, NRL, 6
Advanced Graduate Research Program, 223
Aircraft, 24, 25
Alan Berman Publication Awards
Alfred P. Sloan Fellows Program, 224
Aluminum coatings, 102
Aluminum-Gallium-Arsenide, 128
Amateur Radio Club, 230
Analysis, mathematical, 179
Anti-matter, 41
Anti-sound techniques, 51
Appointments,
  consultants, 233
  experts, 232
  faculty, 232
Apprentice programs, 235
Arrays, focal plane, 165
Atomic resolution, 104
Atomization, metal powders, 89
Attenuation, structure-borne sound, 85
Awards
  Alan Berman Publication
  special
Ballistic objects, tracking of, 190
Battle group communications, 185
Battle management, SDI, 190
Beams
  charged particle, 145
  electron, 145, 143, 130
  propagation, 145
Beta silicon carbide transistor, 133
Blood
  surrogate, 74
  see also hemoglobin
Books published
Career counceling, 228
Ceramic superconductor, 95
Ceramics
  high critical temperature, 95
  piezoelectric effect, 97
  processing of, 95
Channel flow, turbulent, 173
Charged particle beams, 145
Chesapeake Bay Detachment, 24
Chemical reaction pathways, 71
Chemistry
  flame, 78
  quantum, 71
  surface, 126
Clutter, radar, 111
Coatings
  aluminum, 102
  fluorinated polymers, 79
  high temperature, 102
Coherent sources, 130
Coma, gaseous, 35
Combustion, 78
Comet Halley, 35
Communications
  battle group, 185
  spacecraft, 45
Community outreach programs, 7
Composites, organic, 76
Computational fluid dynamics, 53
Computer clubs, 232
Computers, 20, 190
Constrained-layer damping, sound, 85
Consultants, 232
Convection
  salt finger, 62
  turbulent, 62
Cooperative education, 233
Cooperative Research Associateships, 232
Coronae, giant stars, 43
Corporate Facilities Investment Plan, 25
Corrosion
  hot, 102
  resistance, 92
Counciling Referral Service, 228
Cray X-MP/12 computer, 20
Critical temperature, high, 95
Crystal growth, 73
Damping, sound, 85
Dashpot models, viscoelasticity, 179
Decomposition, metal alkyl, 73
Defects, solid state, 128
Detection, radar theory, 111
DICOMED, 21
Dielectric properties, 171
Diffusion
  aluminum coatings, 102
  in flames, 62
Digital signal processing, 188
Droplets, diagnostics, 153
Dynamic modulus, 179
Edison Memorial Graduate, Training, 223
Education Programs, 224
Educational Opportunities, 7, 223-225, 232
Elasticity, anisotropic, 97
Elastomeric materials, 179
Electrochemistry, 92
Electron
  beams, 130, 143, 145
  cyclotron maser, 147
  paramagnetic resonance, 128
Electronic warfare, 175
Electro-optics laboratory, 26
Emissivity measurement system, 87
Employment Opportunities, 229, 230
Encapsulated hemoglobin, 74
Engineering Services, 21
Epitaxial layers and structures, 128, 133
Epitaxy, vapor phase, 73
Equal employment opportunities, 229-230
Extensional waves, 85
Facilities,
  optical, 16
  scientific, *see* scientific facilities
  support, 20
Faculty appointments, 232
Federal Executive Professional Association, 228
Federal Woman's Program, 229
Fellowship, 224
Fiber optic sensors, 162
Field stations, 22, 23
Films
  epitaxial, 128
  ocean surface, 64
  Fire I, 11
Flames
  diffusion in, 62
  free radicals, 62
Flexural waves, 85
Flows, gas, 153
Fluid dynamics, 173
  channel flow, turbulent, 173
  computational, 53, 173
  wave breaking, 53
Fluorinated polymers, 79
Focal plane arrays, 165
Free electron laser, 147
Free radicals, 78
Funding profile, NRL, 6
Future, NRL in the, 25
GAMBLE II, 17
Gamma rays, galactic, 41

Gas
  atomization, 89
  flows, 153
Gaseous coma, 35
Graduate Program, 223, 232
Gravitational instability, 62
Gyroklystron, 130
Gyrotron, 130
Halley comet, 35
Handicap program, 229
Hemoglobin, encapsulated, 74
High school programs, 235
High temperature
  coatings, 102
  mechanical properties at, 102
  optical properties at, 87
Hispanic employment program, 229
History, NRL, 3-7
Holography, infrared, 45
Honors, individual, 205
Hose instability, 145
Hot corrosion, 102
Hypervelocity impact facilities, 20
  line space
Identification Friend or Foe, 117
Image processing, optical, 155
Imaging, nuclear magnetic resonance, 76
Images, atomic resolution, 104
Individual honors, 205
Inductance, kinetic, 136
Inertial waves, ocean, 58
Infrared
  diode laser spectroscopy, 73
  focal plane arrays, 165
  holography, 45
Instability
  gravitational, 62
  hose, 145
  resistive, 145
Integrated circuits, 123
Intense electron beam, 143
Interdiffusion in superalloys, 102
Internetworking, battle group, 185
Interogrator, 117
Interstitials, 133
Inverse
  free electron laser, 147
  scattering theory, 171
Ion focused regime, particle beam, 145
Key personnel
Kinetic inductance, 136
Kinetics, flame, 78
Laser
  diagnostic, 78
  diodes for holograms, 45
  driven particle accelerator, 147
  produced plasma, 141
  spectroscopy, 73
Lasers
  and surfaces, 92, 153
  free electrons, 147
  in surface chemistry, 126
  x-ray generation, 141
Layers, epitaxial, 128, 133
Library, 21
Light modulator, 155
Line-of-sight simulation, 175
Lipids, 74
Locked oscillators, 130
Magnetic field facility, 11
Magnetic sensors, 162
Magnetostriction, 162
Marine Corrosion Test Facility, 24
Maser, electron cyclotron, 147
Materials, elastomeric, 179
Mathematical analysis, 179
Membrane, light modulator, 155
MESFET, 133
Metal alkyl decomposition, 73
Metallurgy, powder, 89
Microchannel plate, 155
Microcomputer, single board, 188
Microelectronics Processing Facility, 11
Microstrip, 136
Microstructures, epitaxial, 128
  dashpot, 179
Model, optical, 175
  spring, 179
Modeling
  acoustics, 56
  elasticity, 97
Modulus, dynamic, 179
Molecular beam epitaxy, 128
National Research Council Associateship, 232
Naval Academy
  Cooperative Program, 232
  Ensign Program, 233
Navy Center for Applied Research in Artificial Intelligence, 10
Network technology, unified, 185
Networking, battle group, 185
Nickel, superalloy substrate, 102
Noise cancellation, active adaptive, 51
Nondestructive evaluation, 76
NRL today, 6-25
Nuclear magnetic resonance, 76
Numerical simulation
  channel flow, turbulent, 173
Ocean
  radar sea-scatter, 114
  roughness, 64
  salt fingers, 62
  signatures, 64
  structure and sound, 56
  surface films, 64
Opportunities, educational employment and professional, *see* Programs
Optical
  aerosol studies, 153
  diagnostics, 153
  fiber sensor, 162
  light modulator membrane, 155
  processing, 155
  properties, high temperature, 87
Organic composites, 76
Organization, NRL, 6
Oscillations, inertial, 58
Oscillator, gyrotron, 130
Oscillators, locked, 130
Oxidation, 102
Particle accelerator, laser, 147
Particles, charged, 145
Personnel
  key
Personnel development, 7, 223-235
Piezoelectric effects, 97
PHAROS III, 17
Plasma
  accelerator, beat wave, 147
  laser produced, 141
Photoemitter membrane, 155
Photoluminescence, 128
Polymers, fluorinated, 79
Postdoctoral fellowships, 232
Powder metallurgy, 89
Probability density functions, 179
Processing
  ceramic superconductors, 95
  optical, 155
Professional appointments, 233
Professional development, 225
  opportunities, *see* Programs
Profiles, dielectric, 171
Programs
  Educational, 223, 224, 232
  Employment, 229, 231
  Equal Opportunity, 229
  Student, 233
Propagation, particle beams, 145
Publications
  awards, Alan Berman
  types and numbers
Publication services, 21
Quantum chemistry, 71
Radar
  gyrotron oscillator, 130
  Mark IV, 117
  mode, IFF, 117
  synthetic aperture, 112
  target detection in clutter, 111
  Radiation sources, 147
Radicals, free, 78
Raman scattering, simulated, 158
Random variables, elasticity, 179
Rapid solidification processing, 89
Rays, gamma, 41
Reaction
  pathways, chemical, 71
  unimolecular, 71
Recreation club, 230, 231
Reflectors, dielectric, 171
Rehabilitation of scientific facilities, 27

- Relativistic electron beams, 143
- Remote sensing
    - ship wakes, 64
    - waves, 53
- Reports published
- Research Associateships, 232
    - Platforms, 25
- Resistive instabilities, 145
- RF accelerator, 130
- Salt fingers, simulation, 62
- Scientific facilities, 8-24
- Sea-scatter, radar, 114
- Select Graduate Student Program, 223
- Semiconductors, 128
    - surface chemistry, 126
- Sensors
    - in space, 38
    - magnetic, 162
- Ship
    - hydrodynamics, 64
    - wakes, 64, 177
- Sigma Xi, 228
- Signal processing
    - digital, 188
    - optical, 155
    - radar, 111
    - VHSIC components, 123
- Silicon, beta, 133
- Simulation
    - numerical, salt fingers, 62
    - software, 175
- Single board microcomputer, 188
- Solids, NMR images of, 76
- Sonar, 56
- Sound, *see* Acoustics
- Sources, radiation, 147
- Space station, surveillance, 38
- Spacecraft communications, 45
- Speckle, radar, 112
- Spectroscopy
    - laser, 73
    - of flames, 78
    - UV, 35
- Spring models, viscoelasticity, 179
- Staff
    - key personnel
    - NRL Review
- Staff, NRL, 6
- Stars, giant, coronae, 43
- Strategic Defense Initiative (SDI), 190
- Structure-borne sound, attenuation of, 85
- Student Volunteer Program, 233
- Substrate, superalloy, 102
- Summer employment, 233
- Summer Faculty Research Program, 232
- Superalloy substrate, 102
- Superconductivity, 136
- Superconductors
    - ceramic, 95
    - high critical temperature, 95
- Support facilities, 20
- Synchrotron Radiation Facility, 20
- Surface
    - chemistry, 126
    - corrosion resistance, 92
- Surveillance from space, 38
- Synthetic aperture radar, speckle, 112
- Target detection, radar, 111
- Technical Information services, 21
- Technology transfer, 225
- Thin films, 128
- Toastmasters International, 228
- Tracking ballistic objects, 190
- Transistor development, 133
- Transition, turbulent, 62
- Transponder, IFF, 117
- Turbulence
    - channel flow, 173
    - convection, 62
    - ship wakes, 177
    - transition to, 62
- UV spectroscopy, 35
- Undercooling in metal powders, 89
- Undergraduate programs, 233
- Underwater Sound Reference Detachment, 24
- Unimolecular reaction, 71
- Unified Network Technology (UNT), 125
- Vapor phase epitaxy, 73
- Vesicules, blood, 74
- VHSIC components, 123
- Viscoelasticity, 179
- Vortex wakes, stratified, 177
- Wakes
    - ship and films, 64
    - stratified, 177
    - vortex, 177
    - turbulence in, 177
- Warfare, electronic, 175
- Waves
    - breaking, 53
    - extensional, 85
    - flexural, 85
    - inertial, 58
    - mean flow interactions, 58
    - steep, 53
- Women in Science and Engineering, 223, 228
- X-ray
    - giant stars, 43
    - large array in space (XLA), 38
    - laser generation, 141

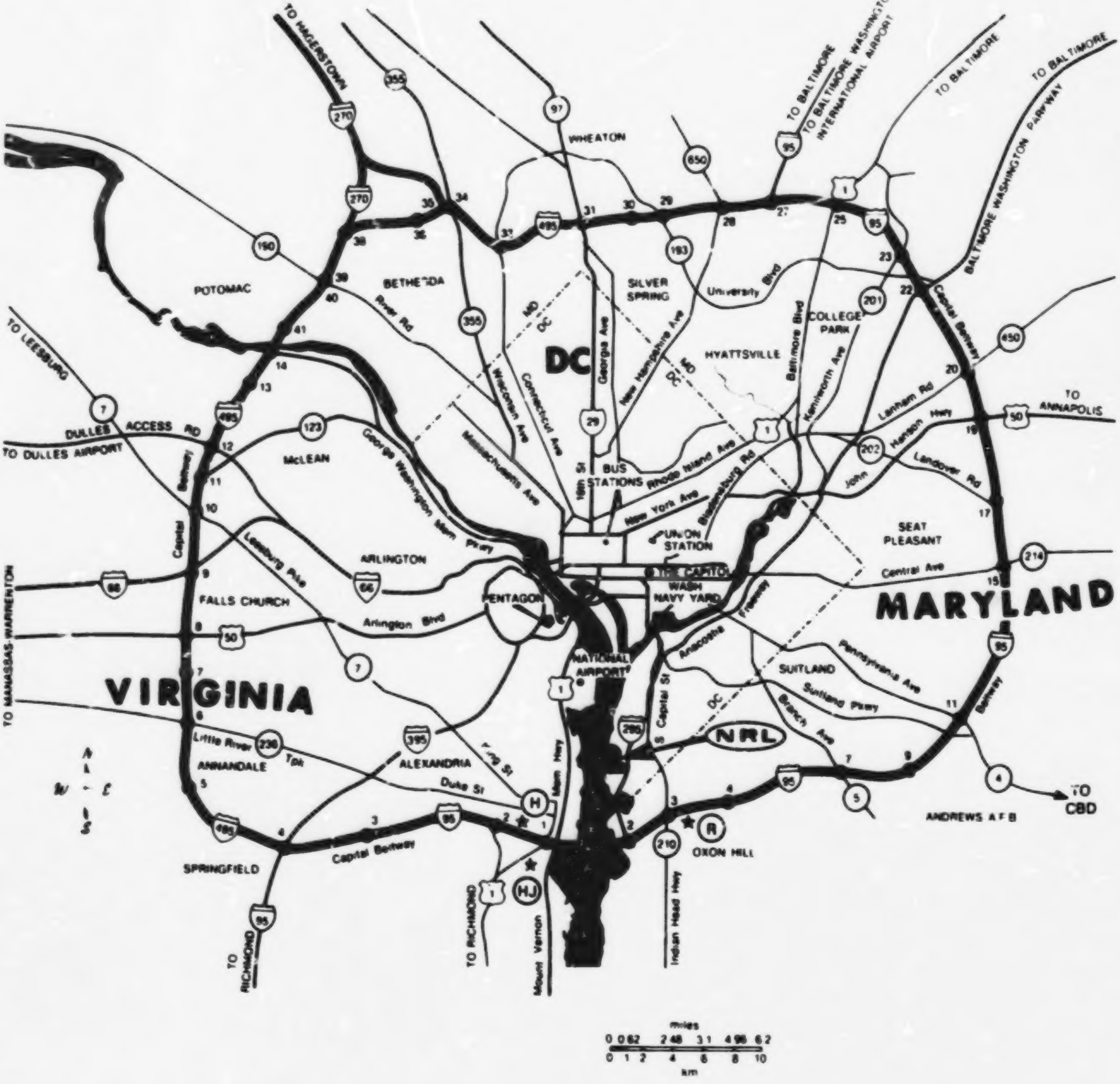
TO HAGERSTOWN
TO BALTIMORE
TO BALTIMORE WASHINGTON INTERNATIONAL AIRPORT
TO BALTIMORE
TO BALTIMORE
BALTIMORE WASHINGTON PARKWAY
WHEATON
POTOMAC
BETHESDA
SILVER SPRING
COLLEGE PARK
HYATTSVILLE
DC
TO LEESBURG
DULLES ACCESS RD
TO DULLES AIRPORT
McLEAN
ARLINGTON
FALLS CHURCH
PENTAGON
BUS STATIONS
UNION STATION
THE CAPITOL
WASH NAVY YARD
NATIONAL AIRPORT
SEAT PLEASANT
TO ANNAPOLIS
MARYLAND
VIRGINIA
SUITLAND
NRL
ANNANDALE
ALEXANDRIA
SPRINGFIELD
OXON HILL
ANDREWS A F B
TO CBD
TO MANASSAS-WARRENTON
TO RICHMOND
TO RICHMOND
Capital Beltway
George Washington Mem Pkwy
Massachusetts Ave
Connecticut Ave
Wisconsin Ave
Georgia Ave
New Hampshire Ave
Rhode Island Ave
New York Ave
Bladensburg Rd
Baltimore Blvd
Kenilworth Ave
University Blvd
Lanham Rd
John Hanson Hwy
Landover Rd
Central Ave
Pennsylvania Ave
Suitland Pkwy
Branch Ave
Anacostia Freeway
Capital St
Indian Head Hwy
Mount Vernon Mem Hwy
Arlington Blvd
Leesburg Pike
Little River Tpk
Duke St
King St
River Rd
H
HJ
R
miles
0 0.62 2.48 3.1 4.96 6.2
0 1 2 4 6 8 10
km

LOCATION OF NRL IN THE CAPITAL AREA